TECHNISCHE UNIVERSITÄT MÜNCHEN
Ingenieurfakultät Bau Geo Umwelt
Professur für Risikoanalyse und Zuverlässigkeit

Time-variant reliability of deteriorating structural systems conditional on inspection and monitoring data

Ronald Schneider

Vollständiger Abdruck der von der Ingenieurfakultät Bau Geo Umwelt der Technischen Universität München zur Erlangung des akademischen Grades eines

Doktor-Ingenieurs

genehmigten Dissertation.

Vorsitzender: Prof. Dr.-Ing. André Borrmann

Prüfer der Dissertation: 1.   Prof. Dr. Daniel Straub

                                          2.   Prof. Dr. Sebastian Thöns (Technical University of Denmark)

                                          3.   Prof. Dr. John Dalsgaard Sørensen (Aalborg University)

Die Dissertation wurde am 27.06.2019 bei der Technischen Universität München eingereicht und durch die Ingenieurfakultät Bau Geo Umwelt am 19.09.2019 angenommen.

Abstract

The current practice of operating and maintaining deteriorating structural systems ensures acceptable levels of structural reliability, but it is not clear how efficient it is. Changing the current prescriptive approach to a risk-based approach has great potential to enable a more efficient management of such systems. Risk-based optimization of operation and maintenance strategies identifies the strategy that optimally balances the cost for controlling deterioration in a structural system with the achieved risk reduction. Inspections and monitoring are essential parts of operation and maintenance strategies. They are typically performed to reduce the uncertainty in the structural condition and inform decisions on maintenance actions. In risk-based optimization of operation and maintenance strategies, Bayesian updating is used to include information contained in inspection and monitoring data in the prediction of the structural reliability. All computations need to be repeated many times for different potential inspection and monitoring outcomes. This motivates the development of robust and efficient approaches to this computationally challenging task.

The reliability of deteriorating structural systems is time-variant because the loads on them and their capacities change with time. In most practical applications, the reliability analysis of deteriorating structural systems can be approached by dividing their lifetime into discrete time intervals. The time-variant reliability problem can then be represented by a series of time-invariant reliability problems. Using this methodology as a starting point, this thesis proposes a novel approach to compute the time-variant reliability of deteriorating structural systems for which inspection and monitoring data are available. The problem is formulated in a nested way in which the prediction of the structural condition is separated from the computation of the structural reliability conditional on the structural condition. Information on the structural condition provided by inspections and monitoring is included in the reliability assessment through Bayesian updating of the system deterioration model employed to predict the structural condition. The updated system reliability is obtained by coupling the updated deterioration model with a probabilistic structural model utilized to calculate the failure probability conditional on the structural condition. This approach is the first main outcome of this thesis and termed nested reliability analysis (NRA) approach. It is demonstrated in two numerical examples considering inspected and monitored steel structures subject to high-cycle fatigue.

An alternative – recently developed – approach, which also follows the strategy of discretizing time, describes deteriorating structural systems with hierarchical dynamic Bayesian networks (DBN). DBN combined with approximate or exact inference algorithms also enable the computation of the time-variant reliability of deteriorating structural systems conditional on information provided by inspection and monitoring data. In this thesis – as a proof of concept – a software prototype is developed based on the DBN approach, which can be used to assess the reliability of a corroding concrete box girder for which half-cell potential measurements are available. This is the second main outcome of this thesis.

Both approaches presented in this thesis enable an integral reliability analysis of inspected and monitored structures that accounts for system effects arising from (a) the correlation among deterioration states of different structural elements, (b) the interaction between element deterioration and system failure, and (c) the indirect information gained on the condition of all unobserved structural elements from inspecting or monitoring the condition of some structural elements. Thus, both approaches enable a system-wide risk-based optimization of operation and maintenance strategies for deteriorating structural systems.

The NRA approach can be implemented relatively easily with subset simulation, which is a sequential Monte Carlo method suitable for estimating rare event probabilities. Subset simulation is robust and considerably more efficient than crude Monte Carlo simulation. It is, however, still sampling-based and its efficiency is thus a function of the number of inspection and monitoring outcomes, as well as the value of the simulated event probabilities. The current implementation of the NRA approach performs separate subset simulation runs to estimate the reliability at different points in time. The efficiency of the NRA approach with subset simulation can be significantly improved by exploiting the fact that failure events in different years are nested. The lifetime reliability of deteriorating structural systems can thus be computed in reverse chronological order in a single subset simulation run.

The implementation of the DBN approach is much more demanding than the implementation of the NRA approach but it has two main advantages. Firstly, the graphical format of the DBN facilitates the presentation of the model and the underlying assumptions to stakeholders who are not experts in reliability analysis. Secondly, it can be combined with exact inference algorithms. In this case, its efficiency neither depends on the number of inspection and monitoring outcomes, nor on the value of the event probabilities to be calculated. However, in contrast to the NRA approach with subset simulation, the DBN approach with exact inference imposes restrictions on the number of random variables and the dependence structure that can be implemented in the model.

Acknowledgements

Contents

1 Introduction

1.1 Motivation

Engineering structures are important parts of transport, water, energy and communication infrastructure systems. Bridges, tunnels, towers and retaining walls are typical examples of this class of structures. Generally, these structures are subject to deterioration processes such as corrosion and fatigue. Depending on the adopted design principles, the construction quality and the exposure to environmental factors, deterioration can have an adverse effect on the performance of engineering structures. To ensure an adequate performance throughout their service lives, it may be necessary to perform maintenance[1] actions.

On many structures, inspections and monitoring are performed to obtain information on the structural condition. Their outcomes can support the prediction of the future structural condition and performance and enable an improved (condition-based or predictive) planning of maintenance actions. It is common practice to perform visual inspections, which provide information on visible deterioration states such as rust staining on and cracking of concrete surfaces as well as concrete spalling. Non-destructive testing is often utilized if visual inspections are insufficient. For example, half-cell potential measurements are carried out to detect corroding reinforcement in concrete structures. In addition to performing inspections, more and more deteriorating structures are equipped with monitoring systems because of recent advances in sensor technology, data transmission and processing. Applications include corrosion sensors embedded in concrete structures to monitor the ingress of chlorides, and sensors recording vibration data, which can provide information on the structural condition.

The cost of operating and maintaining deteriorating structures can be substantial. For example, in 2016 the German federal government spent €4.64 billion on operating and maintaining the transregional road network, out of which €0.87 billion were spent on maintaining bridges and other types of engineering structures within the network (BMVI 2018). Since resources for operating and maintaining deteriorating structures are limited, they should be allocated efficiently. An efficient operation and maintenance strategy balances the cost of controlling deterioration in structural systems with the achieved risk reduction, and ensures that the given requirements regarding serviceability, safety of users and personnel as well as risk to the environment are fulfilled at any time. Identifying and adopting such strategies is of great importance to society as they affect the quality of life and safety of all members of society, the quality of the environment, and budgets of governments and industry.

---

[1] In this thesis, maintenance is understood to include repair, replacement and retrofitting actions, and operation is understood to include inspection, monitoring and services (see also Sørensen 2009).

To optimally plan operation and maintenance actions, a proper assessment and prediction of the condition and performance of deteriorating structures is essential. Inspection and monitoring results should be utilized when they become available to update the present knowledge on the current and future condition and performance. As an example of current practice, consider again the assessment of engineering structures within the German federal road network. These structures are regularly assessed by expert engineers after performing visual inspections (e.g. Vollrath and Tathoff 2002). The engineers determine location, type and extent of visible damages, and rate the condition of the affected structural components. The individual component ratings are then aggregated into a system condition rating based on empirical models (Haardt 1999). This approach has several limitations: (a) The assessment is subjective and qualitative. In addition, a study conducted in the United States of America found that the assessment by inspectors is subject to significant variability (Phares et al. 2001). (b) Uncertainties in the assessment are not treated formally. (c) There is no consistent basis for including information from past inspections in the assessment. (d) The future condition and performance of a structure cannot be predicted. For these reasons, decisions on operation and maintenance activities based on this approach may be inefficient.

As an alternative, deteriorating structures can be assessed using structural reliability analysis. In structural reliability, an engineering model consisting of physics-based deterioration and structural models is applied to predict the structural condition and behavior (Ditlevsen and Madsen 1996; Melchers 1999). Such predictions are uncertain. Uncertainty is, for example, present in the demand on the structure, material properties, geometrical dimensions, and the models themselves. To account for these uncertainties, the engineering model is combined with probabilistic models of the model parameters. By probabilistically modeling the uncertainties in the model parameters and propagating them through the engineering model, a probabilistic description of the structural condition and behavior is obtained. Based on the probabilistic engineering model, probabilities of rare system states (typically failure) can be computed with structural reliability methods. In structural reliability, these probabilities are applied to quantify the system performance. In particular, the probability of the complement of the system failure event (i.e. the probability of survival) is the system reliability.

In a probabilistic setting, Bayesian analysis can be applied to systematically and quantitatively include uncertain and incomplete (and possibly contradicting) inspection and monitoring data in the prediction of the condition and performance of deteriorating structures. Thereby, the posterior probabilistic model of the model parameters conditional on inspection and monitoring results is determined, which then forms the basis for updating the probabilities of the rare system states. In this way, the effect of inspection and monitoring results on the condition and performance of deteriorating structural systems can be quantified.

Probabilistic modelling and structural reliability analysis have high potential to enhance the management of deteriorating structures. The reasons are:

(a) An initial prediction of the condition and performance of deteriorating structures can be obtained based on the prior probabilistic engineering model. The uncertainties in the prediction are addressed through the prior probabilistic models of the model parameters, which are

derived from all relevant sources of information available prior to performing in-service inspection and monitoring. This includes, for example, design information, data from tests performed during construction, and expert knowledge.

(b)   Bayesian analysis can be applied to consistently include data available from in-service inspection and monitoring in the prediction of the structural condition and performance. It provides the means to fuse information from different sources in the same model and to account for the associated uncertainties. This process can be repeated each time new data become available.

(c)   Reliability analysis can be applied to demonstrate that deteriorating structures (in conjunction with inspection and monitoring data) comply with safety requirements if this cannot be demonstrated with standard semi-probabilistic approaches. Target reliabilities are, for example, defined in the Probabilistic Model Code (JCSS 2001) and ISO 2394 (2015).

(d)   Reliability analysis forms the basis for optimal planning of operation and maintenance actions using pre-posterior analysis from classical Bayesian decision theory (Raiffa and Schlaifer 1961; Benjamin and Cornell 1970). Pre-posterior analysis is a consistent framework for jointly optimizing decisions on collecting of information on deteriorating structures together with decisions on maintenance actions (e.g. Thoft-Christensen and Sørensen 1987; Faber et al. 2000; Straub and Faber 2006; Nielsen and Sørensen 2011; Luque and Straub 2019).

All this motivates the application of structural reliability analysis to assess the condition and performance of deteriorating structures. Such analyses are mainly performed at the structural element level because probabilistic deterioration models are typically available at this level. These models are primarily applied to estimate and update the probability of element deterioration states such as fatigue failure of welded connections (e.g. Tang 1973; Madsen 1987). However, deterioration processes at different locations in a structure are generally correlated due to spatial variability and common influencing factors (Hergenröder and Rackwitz 1992; Vrouwenvelder 2004; Malioka 2009; Luque et al. 2017). This correlation reduces the reliability of redundant structural systems (Gollwitzer and Rackwitz 1990; Straub and Der Kiureghian 2011) and has an effect on what can be learned about the overall system condition by inspecting and monitoring only parts of a structure (Vrouwenvelder 2004). For these reasons, the reliability of deteriorating structures should be analyzed and updated at the structural system level.

A number of publications consider modeling of spatial dependence among deterioration processes in structural systems by introducing correlations among the parameters of the models describing deterioration of structural elements by means of random field models (e.g. Stewart and Mullard 2007; Ying and Vrouwenvelder 2007; Straub 2011b; Papakonstantinou and Shinozuka 2013), hierarchical models (e.g. Faber et al. 2006; Maes and Dann 2007; Straub et al. 2009; Luque et al. 2017) and coefficients of correlation (e.g. Moan and Song 2000; Vrouwenvelder 2004; Maljaars and Vrouwenvelder 2014). Therein, the effect of inspection and monitoring outcomes on the probability of either corrosion states in reinforced concrete structures or fatigue failures in steel structures is quantified using Bayesian analysis. However, the impact of deterioration at different elements on the structural system reliability is not included in these works.

The reliability analysis of deteriorating structural systems requires the solution of time-variant reliability problems because the demand on and the capacity of the structure vary with time. Generally, the outcrossing approach is used to solve such problems (Rackwitz 2001). The main component of this approach is the computation of the expected number of outcrossings, which in turn is estimated from the corresponding outcrossing rate. Different methods for computing the time-variant reliability based on the outcrossing approach have been proposed (e.g. Schall et al. 1991; Andrieu-Renaud et al. 2004). The application of these methods to structural systems with many deteriorating elements subject to arbitrary load processes is, however, non-trivial. Additional challenges arise when inspection and monitoring data are included in the assessment.

The time-variant reliability analysis can also be approached by dividing the service life of a structure into discrete time intervals or occurrences of discrete load events (Melchers 1999). In this case, the reliability problem corresponds to the calculation of the probability that failure occurs in any time interval or during any load event leading up to a certain point in time. Various researchers adopt this approach to analyze the time-variant reliability of deteriorating structural systems (e.g. Mori and Ellingwood 1993; Stewart and Rosowsky 1998b; Enright and Frangopol 1999; Val et al. 2000; Stewart and Al-Harthy 2008; Li et al. 2015; Wang et al. 2017). In these works, the effect of correlation among element deterioration, and the effect of inspection and monitoring data on the system reliability is not considered.

While substantial progress has been made over the past decades, an integral framework for analyzing the reliability of deteriorating structural systems with inspection and monitoring data is not available. This motivates the development of novel modeling and computational strategies for this task. Ultimately, the modeling approach and the computational methods should lead to efficient and robust software that can be used by engineers who are not experts in structural reliability analysis. Only in this way can structural reliability analysis enhance the management of deteriorating structures in practice.

1.2   Scope

Motivated by the above, this thesis explores novel approaches to compute the time-variant reliability of deteriorating structural systems conditional information contained in inspection and monitoring data. Following Straub et al. (2020), the quantification of the time-variant reliability of deteriorating structures is reviewed, and situations in which the time-variant reliability problem can be transformed into a series of time-invariant problems are discussed. Based on this discussion and work published in (Schneider et al. 2017), the core of this thesis then proposes an approach to compute the time-variant reliability of deteriorating structural systems conditional on inspection and monitoring data. The problem is formulated as a nested reliability problem in which the computation of the system condition is decoupled from the computation of the system reliability conditional on the system condition. The approach is inspired by the work of Wen and Chen (1987) and called nested reliability analysis (NRA) approach in the following. This thesis provides a detailed presentation of the proposed NRA approach including:

- a description of a generic model for probabilistically representing deterioration in structural systems,

- a brief discussion on modeling dependence among deterioration processes at different locations in structural systems,

- a proposal for a classification of inspection and monitoring technologies, which provide information on the structural condition and the parameters influencing deterioration,

- a proposal for a formulation of the time-variant reliability of deteriorating structural systems conditional on inspection and monitoring results, and

- a proposal for an efficient method to evaluate the time-variant reliability.

The NRA approach is demonstrated through two numerical examples considering welded steel structures subject to high-cycle fatigue. The first example estimates – in analogy to an offshore structure – the reliability of an inspected jacket-type frame. It studies the effect of different inspection scenarios in terms of inspection coverage, times and outcomes. The second example considers a monitored Daniels system, which is an idealized redundant structural system. This example presents a concept for modeling global damage detection information and integrating this type of information in the reliability analysis of the deteriorating Daniels system.

In addition, this thesis applies a novel approach to analyze the time-variant reliability of deteriorating structural systems conditional on inspection and monitoring data, which has been originally proposed by Straub (2009) and extended by Luque and Straub (2016). The approach represents deteriorating structural systems with dynamic Bayesian networks (DBN) and is termed DBN approach in the following. In this thesis, a detailed summary of the DBN approach is provided including a description of:

- a generic DBN model for probabilistically representing element deterioration,

- an approach to describing dependence among element deterioration with DBN,

- a generic model for probabilistically representing inspection and monitoring results in DBN, which provide information on element deterioration states and the parameters influencing deterioration,

- a generic DBN model for probabilistically representing deteriorating structural systems, and

- an existing inference algorithm for evaluating the DBN of the deteriorating structural.

This thesis employs the DBN approach to analyze and update the time-variant reliability of a concrete box girder subject to spatially distributed reinforcement corrosion and demonstrates that it can be implemented in a software prototype. The software prototype was developed in collaboration with researchers from the Technische Universität München and the Technical University of Denmark (Schneider et al. 2014; Schneider et al. 2015a; Schneider et al. 2015b). The author's main contributions to the software prototype are the development and implementation of the deterioration and structural model of the box girder, as well as the implementation of an existing inference algorithm.

1.3 Outline

Section 2 introduces the theory and methods of time-invariant structural reliability. Section 3 then discusses how reliability estimates can be consistently updated with inspection and monitoring data using Bayesian analysis. In particular, the BUS (Bayesian updating with structural reliability methods) approach recently proposed in (Straub 2011a; Straub and Papaioannou 2015b; Straub et al. 2016) is presented. Thereafter, Section 4 reviews the quantification of the time-variant reliability of deteriorating structural systems. This section also discusses when the time-variant reliability can be approximated through a series of time-invariant reliability problems. Based on this discussion, Section 5 presents the NRA approach and demonstrates it through two numerical examples considering an inspected jacket-type steel frame and a monitored Daniels system. Both structures are subject to high-cycle fatigue. Subsequently, Section 6 presents the DBN approach and applies it in a numerical example considering an inspected concrete box girder subject to chloride-induced reinforcement corrosion. The numerical example first describes the model of the deteriorating box girder and its implementation in a software prototype. Subsequently, the prototype is applied to analyze and update the time-variant reliability of the deteriorating box girder. Finally, the findings of this thesis are discussed in Section 7, and concluding remarks are provided together with an outlook in Section 8.

2 Time-invariant structural reliability

The following sections introduce the theory and methods of time-invariant structural reliability. Section 2.1 formulates the general structural reliability problem, which can be solved with specialized methods called structural reliability methods (SRM). The overview on SRM provided in Section 2.2 is limited to the scope required for the remainder of this thesis. Subsequently, Section 2.3 introduces the system reliability problem. Finally, Section 2.4 discusses important aspects of structural systems reliability analysis. Comprehensive introductions to structural reliability can be found in standard textbooks (Ditlevsen and Madsen 1996; Melchers 1999). Throughout this section and the remainder of this thesis it will be assumed that the reader is familiar with the basic notions of probability theory. The notation used in this thesis follows Straub (2018a).

2.1 The structural reliability problem

Consider the case in which the demand on and the capacity of a structural system are time-invariant, i.e. the structure either fails when it is subject to the demand or it never fails. In this case, all stochastic parameters that influence the performance of a structural system can be modeled probabilistically by time-invariant random variables. These variables are often called the basic random variables and are collectively represented by the random vector $\mathbf{X}$. Realizations of $\mathbf{X}$ are denoted by $\mathbf{x}$. Each realization $\mathbf{x}$ corresponds to a point in the outcome space of $\mathbf{X}$. The (prior) knowledge on the stochastic parameters is characterized through the (prior) joint probability density function (PDF) $f_{\mathbf{X}}(\mathbf{x})$ of $\mathbf{X}$ which is typically derived from both data and expert knowledge.

In structural reliability, the failure event F of a structural system is described through a limit state function[2] $g(\mathbf{x})$ as a function of the random variables $\mathbf{X}$ (Ditlevsen and Madsen 1996; Melchers 1999). By convention, a negative value of the limit state function corresponds to failure of the system; hence the failure event F is defined as:

$$F = \{g(\mathbf{X}) \leq 0\} \tag{2.1}$$

The limit state function $g(\mathbf{x})$ includes the (possibly computationally expensive) engineering model of the structural system. Within this modeling framework, additional random variables are included in $\mathbf{X}$ to account for (a) model uncertainties arising from a simplified representation of the system behavior and from omitting parameters that also influence the structural performance, and (b) statistical uncertainties due to the limited data on the system parameters.

---

[2] Failure of a structural system is generally defined in terms of several limit state functions where each function represents a different failure mode (see Sections 2.3 and 2.4). The different limit state functions can be combined into a single limit state function as described in Section 2.3. Note that describing system failure by a single limit state function is not necessarily the computationally optimal approach.

The problem can be interpreted geometrically: The limit state function $g(\mathbf{x})$ describes a failure domain $\Omega_F = \{\mathbf{x} : g(\mathbf{x}) \leq 0\}$ in the outcome space of $\mathbf{X}$, and the failure probability is equal to the probability of $\mathbf{X}$ taking a value in the failure domain Ω_F. It can thus be calculated by integrating the joint PDF of $\mathbf{X}$ over the failure domain Ω_F:

$$\Pr(F) = \Pr[g(\mathbf{X}) \leq 0] = \int_{g(\mathbf{x}) \leq 0} f_{\mathbf{X}}(\mathbf{x}) \, \mathrm{d}\mathbf{x} \tag{2.2}$$

Equation (2.2) corresponds to the classical formulation of the (time-invariant) structural reliability problem. The problem is illustrated in Figure 2.1.

Note that in the context of system reliability the integral in Equation (2.2) is called a component reliability problem (see Section 2.3). Here, the term component refers to the fact that the failure event F is described in terms of a single limit state function $g(\mathbf{x})$. In this sense, a component does not necessarily correspond to a structural component (or element) of a structural system.

The probability of the complement of the failure event is the survival probability or the reliability of the structural system:

$$Rel = 1 - \Pr(F) \tag{2.3}$$

An alternative measure of structural reliability is the generalized reliability index β, which is related to the failure probability as follows (Ditlevsen and Madsen 1996):

$$\beta = -\Phi^{-1}[\Pr(F)] \tag{2.4}$$

where $\Phi^{-1}[\cdot]$ is the inverse standard normal cumulative distribution function (CDF).

2.2 Structural reliability methods

A variety of methods called structural reliability methods (SRM) are available to solve the integral in Equation (2.2). SRM typically transform the problem from the outcome space of the original random variables $\mathbf{X} = [X_1, X_2, \dots, X_n]^T$ to the outcome space of independent standard normal random variables $\mathbf{U} = [U_1, U_2, \dots, U_n]^T$ with joint PDF $\varphi_n(\mathbf{u}) = \prod_{i=1}^{n} \varphi(u_i)$ where $\varphi(\cdot)$ is the standard normal PDF (see, for example, Rackwitz 2001). This transformation is performed by applying a one-to-one mapping $\mathbf{U} = T(\mathbf{X})$. If all random variables $\mathbf{X}$ are statistically independent, each variable can be transformed individually as:

$$U_i = \Phi^{-1}[F_{X_i}(X_i)], \quad i = 1, \dots, n \tag{2.5}$$

where $F_{X_i}(x_i)$ is the marginal CDF of X_i. In most applications, the random variables will be correlated. If the joint distribution of $\mathbf{X}$ is known, the Rosenblatt transformation can be used (Hohenbichler and Rackwitz 1981). If the random variables $\mathbf{X}$ are defined by their marginal distributions and their stochastic dependencies are described in terms of coefficients of correlation, the Nataf transformation can be applied (Liu and Der Kiureghian 1986).
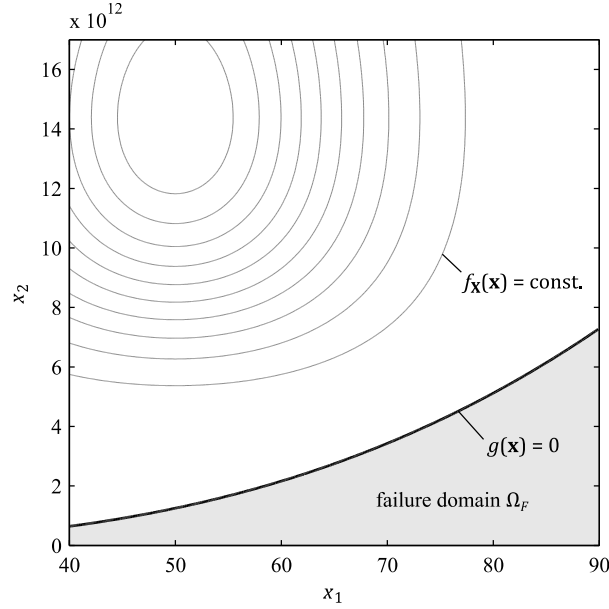
Figure 2.1: Illustration of the (time-invariant) structural reliability problem (adapted from Straub 2014a). In this example, fatigue of a metal component is modeled with the Palmgren-Miner damage accumulation rule and a single-slope SN curve with a negative inverse slope of 3. The component is subject to $n = 10^7$ fatigue load cycles with identical amplitude. The constant amplitude fatigue stress range is represented by a normal distributed random variable X_1. with mean $\mu_{X_1} = 50$ N/mm² and standard deviation $\sigma_{X_1} = 12.5$ N/mm². The intercept with the N-axis of the SN curve at a stress amplitude of 1 N/mm² is described by a lognormal distributed random variable X_2 with parameters $\mu_{\ln X_2} = 30.5 \ln[(N/mm^2)^{-3}]$ and $\sigma_{\ln X_2} = 0.45 \ln[(N/mm^2)^{-3}]$. X_1 and X_2 are independent. Fatigue failure of the component occurs if the accumulated damage $n \cdot X_2^{-1} \cdot X_1^3$ is greater than 1. The limit state function describing component fatigue failure is thus formulated as $g(\mathbf{x}) = 1 - n \cdot X_2^{-1} \cdot X_1^3$.

Using the inverse of the mapping $\mathbf{X} = T^{-1}(\mathbf{U})$, a transformed limit state function G describing the failure domain $\Omega_F^U = \{\mathbf{u} : G(\mathbf{u}) \leq 0\}$ in $\mathbf{U}$-space can now be defined as:

$$G(\mathbf{u}) = g[T^{-1}(\mathbf{u})] \tag{2.6}$$

Figure 2.2 illustrates the transformation of the structural reliability problem from the original outcome space to the standard normal space.

The mapping $\mathbf{U} = T(\mathbf{X})$ is probability preserving, i.e. $\Pr(F) = \Pr[g(\mathbf{X}) \leq 0] = \Pr[G(\mathbf{U}) \leq 0]$. Thus, the failure probability can be expressed in the transformed space as:

$$\Pr(F) = \Pr[G(\mathbf{U}) \leq 0] = \int_{G(\mathbf{u}) \leq 0} \varphi_n(\mathbf{u}) \, d\mathbf{u} \tag{2.7}$$

Two classes of methods exist for solving the integral in Equation (2.7): (a) methods based on the design point including the first-order reliability method (FORM) and (b) sampling-based methods such as Monte Carlo Simulation (MCS) and Subset Simulation (SuS). FORM, MCS and SuS are briefly introduced in the following.

2.2.1 First order reliability method

FORM approximates the failure domain $\Omega_F^U = \{\mathbf{u} : G(\mathbf{u}) \leq 0\}$ by a half-space. This is achieved by linearizing the limit state function $G(\mathbf{u})$ at the design point (or most likely failure point) $\mathbf{u}^*$
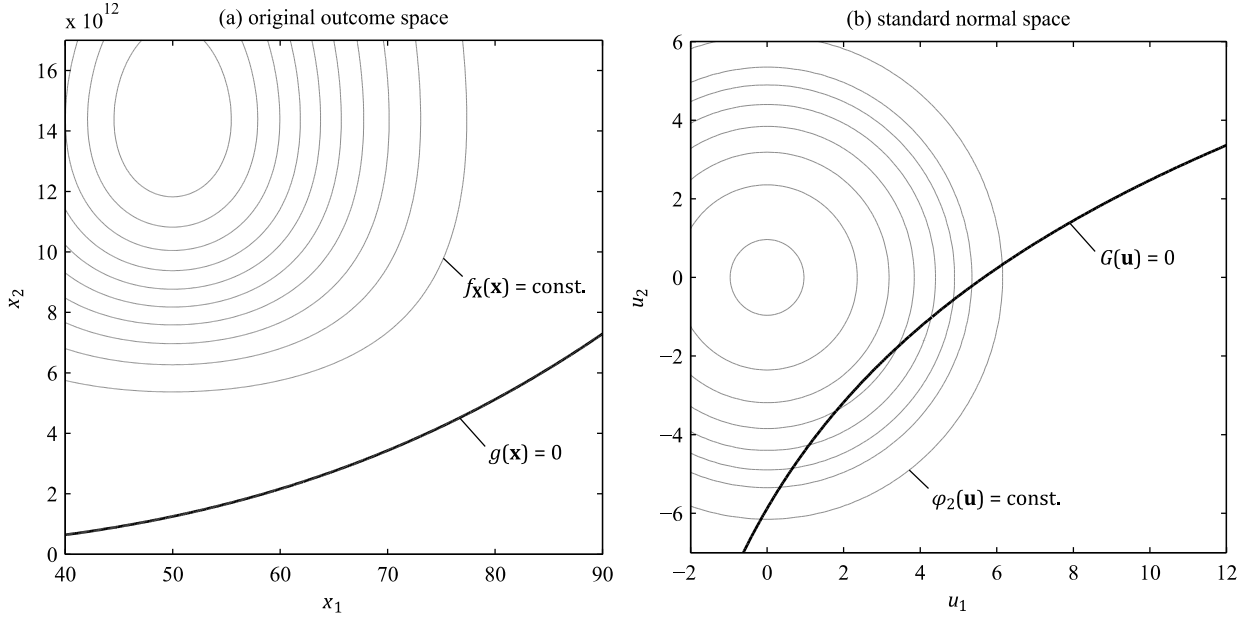
Figure 2.2: Illustration of the transformation of the component reliability problem from (a) the outcome space of the original random variables $\mathbf{X}$ to (b) the outcome space of independent standard normal random variables $\mathbf{U}$ (details of the example are described in the caption of Figure 2.1). In this example, which follows Straub (2014a), the random variables X_1 and X_2 are independent, and they can, therefore, be transformed separately. The inverse transformation from standard normal space is $X_1 = U_1 \cdot \sigma_{X_1} + \mu_{X_1}$ and $X_2 = \exp(U_2 \cdot \sigma_{\ln X_2} + \mu_{\ln X_2})$.

where the limit state surface $S = \{\mathbf{u} : G(\mathbf{u}) = 0\}$ is closest to the origin of the standard normal space. This is the point in the failure domain Ω_F^U with the maximum probability density. The failure probability is estimated by integrating $\varphi_n(\mathbf{u})$ over the resulting half-space. The simple result is (Hasofer and Lind 1974):

$$\Pr(F) \approx \Phi(-\beta_{FORM}) \tag{2.8}$$

where $\beta_{FORM} = \|\mathbf{u}^*\| = \sqrt{\mathbf{u}^{*T}\mathbf{u}^*}$ is the distance from the origin to $\mathbf{u}^*$, which is called the FORM reliability index and $\Phi(\cdot)$ is the standard normal CDF. The principle of FORM is illustrated in Figure 2.3.

The design point $\mathbf{u}^*$ can be identified by solving the following constrained optimization problem:

$$\mathbf{u}^* = \arg\min\|\mathbf{u}\| \quad \text{subjected to} \quad G(\mathbf{u}) \leq 0 \tag{2.9}$$

Several optimized algorithms are available for this task. The most widely applied algorithm is the Hasofer-Lind-Rackwitz-Fiessler algorithm (Hasofer and Lind 1974; Rackwitz and Fiessler 1978).

The accuracy of FORM can be verified and improved by applying a second-order approximation of the limit state function at the design point (Breitung 1984). This approach is known as second-order reliability method (SORM).

FORM and SORM have been successfully applied to a variety of structural reliability problems. However, identifying the design point may become difficult if the limit state function is formulated in terms of a numerical model or the dimension of the problem in terms of the number of random variables becomes large (Schuëller et al. 2004). Furthermore, in high dimensional problems or in
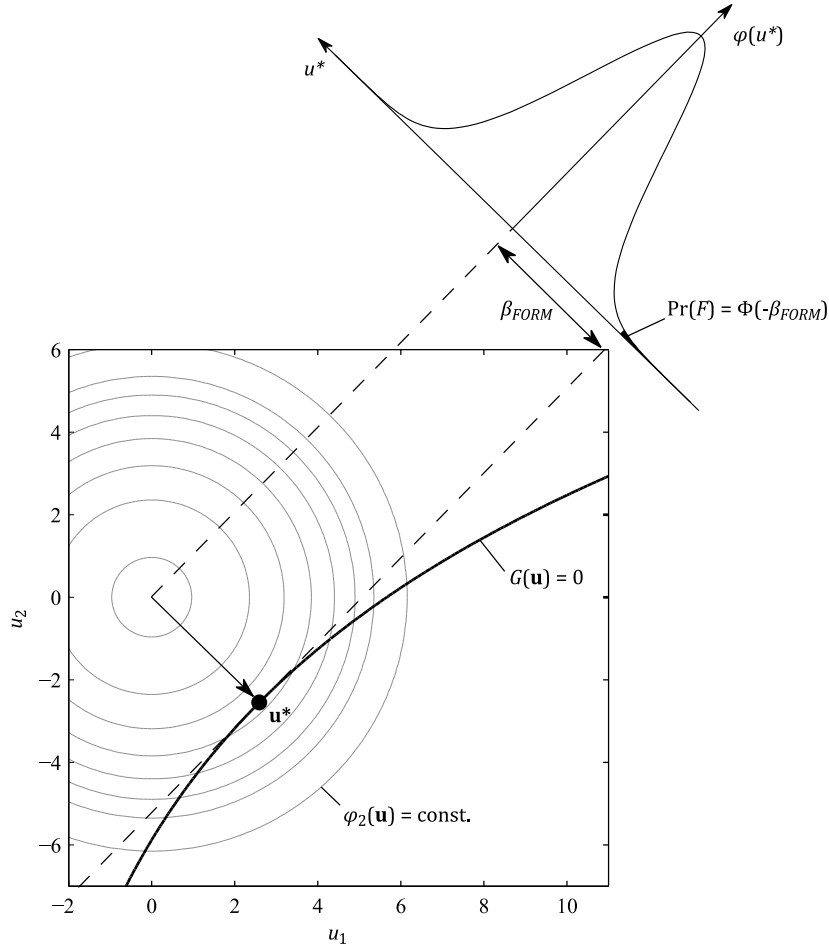
Figure 2.3: Illustration if the design point and the linear approximation of the limit state surface (adapted from Straub 2014a). The marginal PDF of **U** in the direction of the design point $\mathbf{u}^*$ is the standard normal PDF. Consequently, the FORM approximation of the failure probability is $\Pr(F) \approx \Phi(-\beta_{FORM})$.

problems with highly non-linear limit state surfaces FORM/SORM solutions may become inaccurate (Rackwitz 2001).

2.2.2 Monte Carlo simulation

MCS can be derived by rewriting the integral in Equation (2.7) in the following format:

$$\Pr(F) = \int_{G(\mathbf{u}) \leq 0} \varphi_n(\mathbf{u}) \, d\mathbf{u} = \int_{\mathbb{R}^n} \mathbb{I}[G(\mathbf{u}) \leq 0] \, \varphi_n(\mathbf{u}) \, d\mathbf{u} \tag{2.10}$$

where $\mathbb{I}[\cdot]$ is the indicator function, which is equal to 1 if its argument is true and 0 otherwise. Equation (2.10) corresponds to the expected value of $\mathbb{I}[G(\mathbf{U}) \leq 0]$. It follows that the failure probability can be estimated by generating N independent and identically distributed (i.i.d.) samples $\mathbf{u}^{(i)}$, $i = 1, \dots, N$ from $\varphi_n(\mathbf{u})$ and calculating the sample mean of $\mathbb{I}[G(\mathbf{U}) \leq 0]$:

$$\Pr(F) = \mathbb{E}\big[\mathbb{I}[G(\mathbf{U}) \leq 0]\big] \approx \hat{P}_{MC} = \frac{1}{N} \sum_{i=1}^{N} \mathbb{I}[G(\mathbf{u}^{(i)}) \leq 0] \tag{2.11}$$
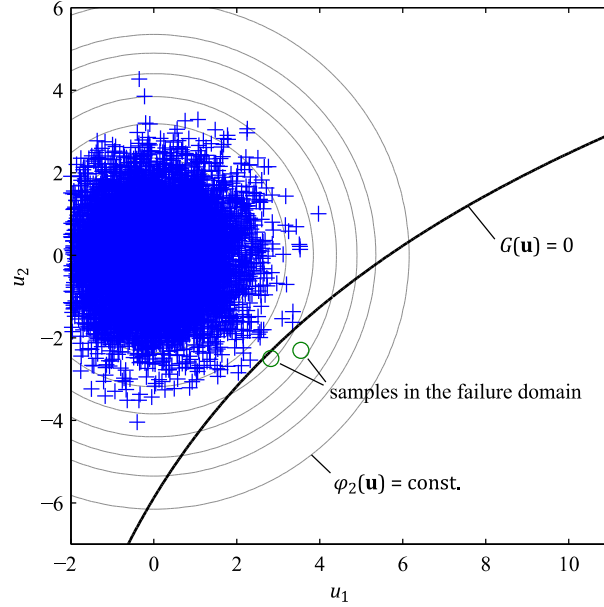
Figure 2.4: Illustration of Monte Carlo simulation with $N = 10^4$ samples (this example follows Straub 2014a). The blue crosses and green circles are i.i.d. samples $\mathbf{u}^{(i)}, i = 1, \ldots, N$ from $\varphi_2(\mathbf{u})$. Two samples – the green circles – are in the failure domain.

where $\hat{P}_{MC}$ denotes the MCS estimator of the failure probability, which provides an unbiased estimate of the failure probability (see, for example, Straub 2012). MCS is illustrated in Figure 2.4 for a two-dimensional problem.

The accuracy of the MCS estimator $\hat{P}_{MC}$ can be measured in terms of its coefficient of variation δ_{MC}, which is given by (see, for example, Straub 2012):

$$\delta_{MC} = \sqrt{\frac{1 - \Pr(F)}{N \, \Pr(F)}} \tag{2.12}$$

From Equation (2.12), two important conclusions can be drawn. (a) The accuracy of the MCS estimator does neither depend on the number of random variables nor on the shape of the limit state function. It is therefore a robust method. (b) If the failure probability to be estimated, $\Pr(F)$, is small, the number of samples N has to be large to achieve a reasonable accuracy of the estimate. In fact,

$$N = \frac{1 - \Pr(F)}{\delta_{MC}^2 \, \Pr(F)} \tag{2.13}$$

samples are required to achieve a coefficient of variation δ_{MC}. It follows that MCS is inefficient in estimating small failure probabilities.

Several methods have been developed to enhance the efficiency of standard MCS including importance sampling (IS) techniques. IS methods artificially increase the number of samples in the failure domain by sampling from an appropriately chosen sampling density commonly centered at the design point obtained from an initial FORM analysis (Schuëller and Stix 1987). Adaptive IS

schemes that do not require prior knowledge of the design point are also available (Bucher 1988; Au and Beck 1999; Kurtz and Song 2013; Papaioannou et al. 2016). An alternative importance sampling scheme is line sampling (Hohenbichler and Rackwitz 1988; Koutsourelakis et al. 2004). This method produces samples on a hyperplane orthogonal to a dominant direction pointing towards the limit state surface. The dominant direction is obtained from an initial FORM run. More recently, Bucher (2009) has developed asymptotic sampling, which is based on an asymptotic approximation of the failure probability (Breitung 1984; Gollwitzer and Rackwitz 1988) and estimates the failure probability in terms of the generalized reliability index based on initial MSC runs followed by a regression analysis. In recent years, subset simulation (SuS) proposed by Au and Beck (2001) has become popular. It expresses the failure probability as a product of conditional probabilities of nested intermediate failure events. With a suitable choice of the intermediate failure events, the conditional probabilities become large enough such that they can be estimated efficiently by simulation. SuS is presented in more detail in the following section.

2.2.3 Subset simulation

SuS proposed by Au and Beck (2001) is a sequential Monte Carlo method. The basic idea of SuS is to express the failure event as an intersection of a sequence of nested intermediate events.

$$F = E_0 \cap E_1 \cap \dots \cap E_M \tag{2.14}$$

where E_0 is the certain event and $E_0 \supset E_1 \supset \dots \supset E_M = F$. The events E_i are defined as:

$$E_i = \{G(\mathbf{U}) \leq b_i\} \tag{2.15}$$

where $b_0 = \infty > b_1 > b_2 > \dots > b_M = 0$. Applying the chain rule of probability and noting that $E_{i-1} = E_0 \cap E_1 \cap \dots \cap E_{i-1}$, the probability of failure can be written as:

$$
\begin{aligned}
\Pr(F) &= \Pr(E_0 \cap E_1 \cap \dots \cap E_M) \\
&= \Pr(E_0) \cdot \Pr(E_1|E_0) \cdot \Pr(E_2|E_0, E_1) \cdot \dots \cdot \Pr(E_M|E_0, \dots, E_{M-1}) \\
&= \prod_{i=1}^{M} \Pr(E_i|E_{i-1})
\end{aligned}
\tag{2.16}
$$

With a suitable choice of the thresholds b_i, the conditional probabilities $\Pr(E_i|E_{i-1})$ can be made much larger than $\Pr(F)$ such that they can be estimated efficiently with smaller sample sizes.

The conditional probability $\Pr(E_1|E_0) = \Pr(E_1)$ is computed using standard MCS. The estimator $\hat{P}_1$ of the probability $\Pr(E_1)$ is defined analogous to Equation (2.11):

$$\Pr(E_1) \approx \hat{P}_1 = \frac{1}{N} \sum_{j=1}^{N} \mathbb{I}[(G(\mathbf{u}_0^{(j)}) \leq b_1)] \tag{2.17}$$

where $\mathbf{u}_0^{(j)}$, $j = 1, \dots, N$ are i.i.d. samples from $\varphi_n(\mathbf{u}|E_0) = \varphi_n(\mathbf{u})$. The conditional probabilities $\Pr(E_i|E_{i-1})$, $i = 2, \dots, M$ are computed with an estimator like Equation (2.17), which requires

samples conditional on the events E_{i-1}. These samples are distributed according to the conditional PDFs:

$$\varphi_n(\mathbf{u}|E_{i-1}) = \frac{\varphi_n(\mathbf{u})\,\mathbb{I}[G(\mathbf{u}) \leq b_{i-1}]}{\Pr(E_{i-1})}, \quad i = 2, \dots, M \tag{2.18}$$

Samples from $\varphi_n(\mathbf{u}|E_{i-1})$ are generated by applying Markov Chain Monte Carlo (MCMC) sampling methods, which simulate states of a Markov chain whose stationary distribution is equal to the desired conditional distribution. Different MCMC algorithms for subset simulation are discussed in (Papaioannou et al. 2015). In this thesis, an algorithm called conditional sampling in **U**-space proposed by Papaioannou et al. (2015) is applied due to its simplicity and efficiency (see Appendix A for more details). Once samples $\mathbf{u}_{i-1}^{(j)}$, $j = 1, \dots, N$ from $\varphi_n(\mathbf{u}|E_{i-1})$ are available, an estimate of the conditional probabilities $\Pr(E_i|E_{i-1})$ can be computed as:

$$\Pr(E_i|E_{i-1}) \approx \hat{P}_i = \frac{1}{N}\sum_{j=1}^{N}\mathbb{I}[G(\mathbf{u}_{i-1}^{(j)}) \leq b_i], \quad i = 2, \dots, M \tag{2.19}$$

The samples $\mathbf{u}_{i-1}^{(j)}$, $j = 1, \dots, N$ are identically distributed according to $\varphi_n(\mathbf{u}|E_{i-1})$ but they are generally not statistically independent. The correlation among the MCMC samples has an effect on the efficiency and accuracy of SuS (see Papaioannou et al. 2015). It is important to adopt an MCMC sampling algorithm that produces samples with low correlation such that the conditional probabilities $\Pr(E_i|E_{i-1})$ can be estimated with a minimum number of samples (see also Appendix A).

Finally, an estimator $\hat{P}_{SuS}$ of the failure probability can be written as:

$$\Pr(F) \approx \hat{P}_{SuS} = \prod_{i=1}^{M}\hat{P}_i \tag{2.20}$$

The intermediate thresholds $b_1, b_2, \dots, b_{M-1}$ cannot be selected in advance as the actual failure probability $\Pr(F)$ and the shape of the limit state function $G(\mathbf{u})$ are not known in advance. Instead, the thresholds are chosen on the fly during subset simulation such that the conditional probabilities $\Pr(E_i|E_{i-1})$, $i = 1, \dots, M - 1$ are equal to a chosen value p_0. The first step of subset simulation simulates N i.i.d samples $\mathbf{u}_0^{(j)}$, $j = 1, \dots, N$ from $\varphi_n(\mathbf{u})$. The limit state function $G(\mathbf{u})$ is then evaluated for each sample and b_1 is set equal to the p_0-quantile of the N resulting values of the limit state function $G(\mathbf{u}_0^{(j)})$, $j = 1, \dots, N$. The second step of subset simulation then uses the N_0 samples for which $G(\mathbf{u}) \leq b_1$ as seeds to generate $N - N_0$ additional samples using MCMC sampling, making up a total of N conditional samples $\mathbf{u}_1^{(j)}$, $j = 1, \dots, N$ distributed according to $\varphi_n(\mathbf{u}|E_1)$. Subsequently, the limit state function $G(\mathbf{u})$ is evaluated for each conditional sample and b_2 is set equal to the p_0-quantile of the N resulting values of the limit state function $G(\mathbf{u}_1^{(j)})$, $j = 1, \dots, N$. The second step is repeated until the p_0-quantile becomes negative. At this stage, the failure event $E_M = F$ is reached, for which $b_M = 0$. The estimator $\hat{P}_{SuS}$ of the failure probability can now be rewritten as:

$$\Pr(F) \approx \hat{P}_{SuS} = p_0^{M-1} \hat{P}_M \tag{2.21}$$

where $\hat{P}_M$ is the estimator of the conditional probability $\Pr(E_M | E_{M-1})$, which is computed with Equation (2.19) with $i = M$. The SuS algorithm is summarized in Algorithm 2.1 and illustrated in Figure 2.5.

The value of the conditional probabilities p_0 and the number of samples per subset level N can be chosen freely. Au and Beck (2001) suggest a value $p_0 = 0.1$. N should be selected large enough to give accurate estimates of p_0. Following Equation (2.13), $N \approx 1000$ samples are required to obtain a coefficient of variation $\delta_{MC} = 0.1$ in estimating $p_0 = 0.1$ with standard MCS. Note that this estimate of N neglects the correlation among the samples generated with MCMC, which determines the number of effective samples at each subset level. Au and Beck (2001) provide an approximate expression for estimating N to achieve a certain accuracy in the estimate of the failure probability that considers the correlation among the MCMC samples.

The number of intermediate events E_i required to estimate a failure probability in the order of $\Pr(F) = 10^{-k}$ is $M = k$ if the value of the conditional probabilities is $p_0 = 0.1$. The total number of samples required to estimate $\Pr(F)$ with subset simulation is, therefore, proportional to $-\log_{10}[\Pr(F)]$ since the number of samples per subset level N is kept constant. In contrast, the total number of samples required to estimate $\Pr(F)$ with standard MCS is proportional to $1/\Pr(F)$ (see Equation (2.13)). Subset simulation is thus considerably more efficient in estimating small failure probabilities than standard MCS.

Algorithm 2.1: Subset simulation for estimating $\Pr(F) = \Pr(G(\mathbf{U}) \le 0)$ (Au and Beck 2001)

Input: p_0 (value of conditional probabilities), N (number of samples per subset level), and $G(\mathbf{u})$ (limit state function describing the failure event F in $\mathbf{U}$-space)

1. Generate N i.i.d. samples $\mathbf{u}_0^{(j)}$, $j = 1, \dots, N$ from $\varphi_n(\mathbf{u})$.

2. Set b_1 equal to the p_0-quantile of the samples $G(\mathbf{u}_0^{(j)})$, $j = 1, \dots, N$.

3. Initialize the counter $i = 1$.

4. While $b_i > 0$:

   a. Increase the counter $i = i + 1$.

   b. Use the N_0 samples for which $G(\mathbf{u}) \le b_{i-1}$ as seeds to generate $N - N_0$ additional samples using an MCMC sampling algorithm, making up a total of N conditional samples $\mathbf{u}_{i-1}^{(j)}$, $j = 1, \dots, N$ distributed according to $\varphi_n(\mathbf{u}|E_{i-1})$.

   c. Set b_i equal to the p_0-quantile of the samples $G(\mathbf{u}_{i-1}^{(j)})$, $j = 1, \dots, N$.

5. Evaluate $\hat{P}_M$ according to Equation (2.19) with $i = M$.

6. Return $\hat{P}_{SuS}$ as defined in Equation (2.21).

(a) MC sampling, identification of 1st intermediate threshold

(b) MCMC sampling at 1st intermediate failure level
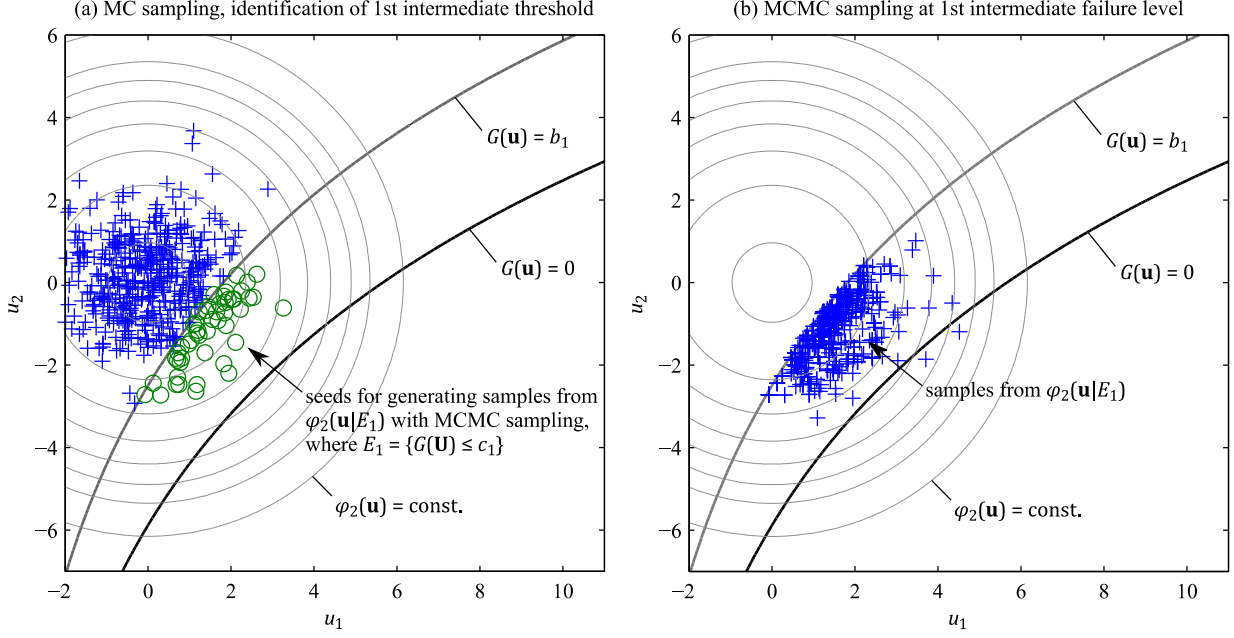
Figure 2.5: Illustration of subset simulation with $N = 500$ samples per subset level (this example follows Straub 2014a). (a) The blue crosses and green circles are i.i.d. samples $\mathbf{u}_0^{(i)}$, $i = 1, \dots, N$ from $\varphi_2(\mathbf{u})$. The threshold b_1 defining the first intermediate failure event $E_1 = \{G(\mathbf{U}) \leq b_1\}$ is set equal to p_0-quantile of the samples $G(\mathbf{u}_0^{(j)})$, $j = 1, \dots, N$. The samples for which $G(\mathbf{u}) \leq b_1$ – the green circles – are used as seeds for generating samples from $\varphi_2(\mathbf{u}|E_1)$ with MCMC. (b) The blue crosses are samples $\mathbf{u}_1^{(i)}$, $i = 1, \dots, N$ from $\varphi_2(\mathbf{u}|E_1)$.

2.3 The system reliability problem

A system reliability problem exists when the failure event F is defined by a combination of several limit state functions $g_i(\mathbf{x})$, $i = 1, \dots, M$. Each limit state function $g_i(\mathbf{x})$ describes a component failure event as $F_i = \{g_i(\mathbf{X}) \leq 0\}$ with corresponding failure domain $\Omega_{F_i} = \{\mathbf{x} : g_i(\mathbf{x}) \leq 0\}$ in the outcome space of $\mathbf{X}$. Two basic types of system reliability problems exist: the series and parallel system reliability problem. A series system fails as soon as one component fails. The failure probability of a series system can, therefore, be written as (Hohenbichler and Rackwitz 1983).

$$\Pr(F) = \Pr\left(\bigcup_{i=1}^{M} F_i\right) = \Pr\left(\bigcup_{i=1}^{M} \{g_i(\mathbf{X}) \leq 0\}\right) \tag{2.22}$$

If the component failure events F_i are statistically independent, the failure probability of a series system is computed as:

$$\Pr(F) = \Pr\left(\bigcup_{i=1}^{M} F_i\right) = 1 - \Pr\left(\bigcap_{i=1}^{M} \bar{F}_i\right) = 1 - \prod_{i=1}^{M} [1 - \Pr(F_i)] \tag{2.23}$$

Generally, the component failure events F_i are statistically dependent. In this case, knowledge of the component failure probabilities $\Pr(F_i)$ is not enough to compute the failure probability of a series system. However, simple bounds on the failure probability of a series system can be derived based on the extreme cases of fully dependent and mutually exclusive component failure events (e.g. Madsen et al. 1986):

$$\max_{i\in\{1,\dots,M\}} \Pr(F_i) \leq \Pr(F) \leq \sum_{i=1}^{M} \Pr(F_i) \tag{2.24}$$

If the statistical dependence among the component failure events F_i is positive (i.e. $\Pr(F_i \cap F_j) \geq \Pr(F_i) \cdot \Pr(F_j)$), a narrower upper bound can be defined based on statistically independent component failure events (see also Thoft-Christensen and Murotsu 1986):

$$\max_{i\in\{1,\dots,M\}} \Pr(F_i) \leq \Pr(F) \leq 1 - \prod_{i=1}^{M} [1 - \Pr(F_i)] \tag{2.25}$$

A parallel system fails if all components fail. Consequently, the failure probability of a parallel system can be expressed as (Hohenbichler and Rackwitz 1983):

$$\Pr(F) = \Pr\left(\bigcap_{i=1}^{M} F_i\right) = \Pr\left(\bigcap_{i=1}^{M} \{g_i(\mathbf{X}) \leq 0\}\right) \tag{2.26}$$

If the component failure events F_i are statistically independent, the failure probability of a parallel system is:

$$\Pr(F) = \Pr\left(\bigcap_{i=1}^{M} F_i\right) = \prod_{i=1}^{M} \Pr(F_i) \tag{2.27}$$

In analogy to Equation (2.24), simple bounds on the failure probability of a parallel system can be found based on mutually exclusive and fully dependent component failure events:

$$0 \leq \Pr(F) \leq \min_{i\in\{1,\dots,M\}} \Pr(F_i) \tag{2.28}$$

The two basic types of system reliability problems are illustrated in Figure 2.6.

A general system can be defined by a cut-set formulation, which describes the system as a series system of parallel sub-systems (Hohenbichler and Rackwitz 1983). In this formulation, each parallel sub-system is called a cut-set representing a set of component failure events whose joint occurrence represents failure of the system. The corresponding failure probability is written as:

$$\Pr(F) = \Pr\left[\bigcup_{k=1}^{K} \left(\bigcap_{i\in C_k} F_i\right)\right] = \Pr\left[\bigcup_{k=1}^{K} \left(\bigcap_{i\in C_k} \{g_i(\mathbf{X}) \leq 0\}\right)\right] \tag{2.29}$$

where K is the number of cut-sets and $C_k \subseteq \{1, \dots, M\}$ denotes the index set of the kth cut-set.

A general system can also be defined by a link-set formulation, which describes the system failure event F by the intersection of the unions of component failure events (Hohenbichler and Rackwitz 1983):

$$\Pr(F) = \Pr\left[\bigcap_{k=1}^{K} \left(\bigcup_{i\in L_k} F_i\right)\right] = \Pr\left[\bigcap_{k=1}^{K} \left(\bigcup_{i\in L_k} \{g_i(\mathbf{X}) \leq 0\}\right)\right] \tag{2.30}$$
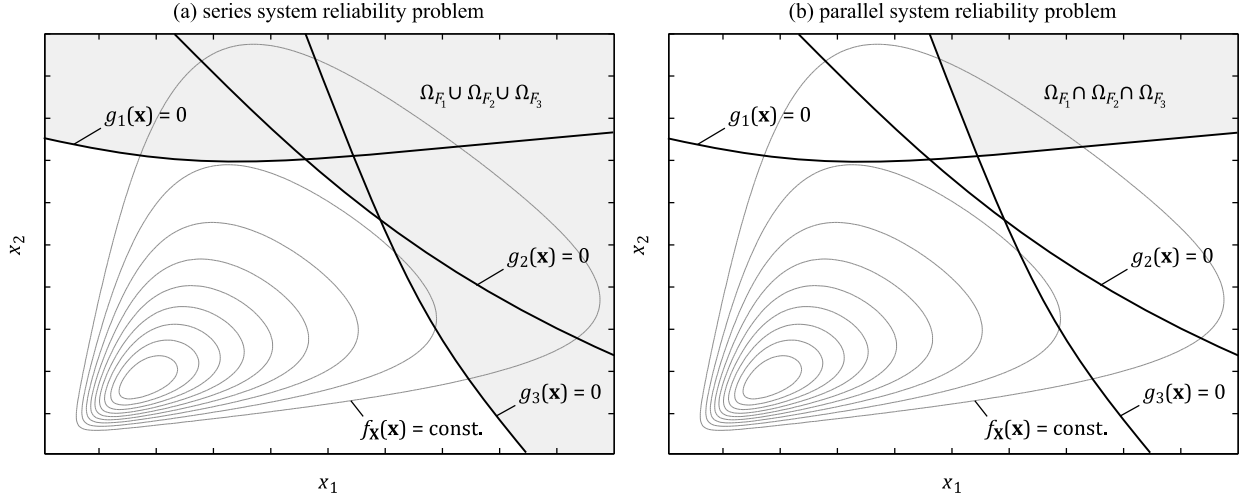
Figure 2.6: Illustration of the (a) series and (b) parallel system reliability problem.

where K is the number of link-sets and $L_k \subseteq \{1, \dots, M\}$ is the index set of the kth link-set. A link-set is a set of components whose joint survival corresponds to survival of the system.

Different methods are available for solving system reliability problems including first-order solutions for series and parallel system problems (Hohenbichler and Rackwitz 1983; Enevoldsen and Sørensen 1992) and for general systems defined as series systems of cut-sets (Enevoldsen and Sørensen 1993). More recently, the matrix-based system reliability method (Kang et al. 2008; Song and Kang 2009) and the sequential compounding method (Kang and Song 2010) have been proposed to solve the general system reliability problem. In addition, Song and Der Kiureghian (2003) show that linear programming can be applied to compute bounds on the system failure probability of any type of system.

Alternatively, the component limit state functions $g_i(\mathbf{x}), i = 1, \dots, M$ can be combined into a single equivalent limit state function $g(\mathbf{x})$. As an example, the equivalent limit state function $g(\mathbf{x})$ for a general system defined by a cut-set formulation reads (Madsen 1987):

$$g(\mathbf{x}) = \min_{k \in \{1, \dots, K\}} \left[\max_{i \in C_k} g_i(\mathbf{x}) \right] \tag{2.31}$$

Series and parallel systems are special cases of a general system. A series system consists of K cut-sets with a single component. Thus, the equivalent limit state function for a series system can be written as $g(\mathbf{x}) = \min[g_1(\mathbf{x}), \dots, g_K(\mathbf{x})]$. A parallel system consists of a single cut-set with M components, and the equivalent limit state function is defined as $g(\mathbf{x}) = \max[g_1(\mathbf{x}), \dots, g_M(\mathbf{x})]$.

Once an equivalent limit state function $g(\mathbf{x})$ is formulated, the system failure probability can be computed by integrating the joint PDF $f_{\mathbf{X}}(\mathbf{x})$ of $\mathbf{X}$ over the domain $\Omega_F = \{\mathbf{x} : g(\mathbf{x}) \leq 0\}$. This problem is equivalent to a component reliability problem defined in Equation (2.2). Note that the equivalent limit state function $g(\mathbf{x})$ defined by Equation (2.31) is generally not differentiable. Hence, the resulting component reliability problem must be solved using sampling-based methods (see Section 2.2).

2.4 Reliability of structural systems

Structures can be understood as systems of structural elements such as braces, columns, joints, bearings and foundations. Each structural element can fail in several different ways. A beam may, for example, fail in bending or lateral torsional buckling. Most structural systems can sustain failure of more than one structural element before system failure occurs. However, the degree of extra reliability due to structural redundancy depends on the post-failure behavior of the structural elements, as well as the functional and stochastic dependence among individual element failure events. These aspects must be considered when evaluating the failure probability of structural systems. In the following sections, the basic theory of time-invariant structural system reliability is presented. Section 2.4.1 describes a model suitable for evaluating the failure probability of statically determinate structures. Subsequently, some important aspects of modeling statically indeterminate structures are discussed in Section 2.4.2. Section 2.4.3 concludes with an analysis of an idealized redundant structural system to illustrate the influence of post-failure behavior of structural elements and dependence among element failure events on the system reliability. A more detailed introduction to the underlying theory can, for example, be found in (Thoft-Christensen and Murotsu 1986; Melchers 1999).

2.4.1 Statically determinate structures

Statically determinate structures do not exhibit any redundancy with respect to element failures. Such structural systems fail as soon as one structural element fails. They can, therefore, be modeled as a series system of M component failure events F_i (Thoft-Christensen and Murotsu 1986) where each component failure event F_i corresponds to an element failure mode. The failure probability of statically determinate structures is thus defined by Equation (2.22).

As an example, consider the statically determinate steel truss illustrated in Figure 2.7(a) with N structural elements subject to external loading. The truss is here assumed to lose its load carrying capacity as soon as one structural element fails either due to section yielding in tension or buckling in compression. Therefore, the truss has $M = 2N$ failure modes.

Depending on the structural system, the reliability assessment of statically determinate structures must also consider possible global instability modes. Such modes can be included as component failure events in the series system model.

2.4.2 Statically indeterminate structures

Statically indeterminate structures such as the truss shown in Figure 2.7(b) do not necessarily fail as soon as one structural element fails since the applied loads may still be sustained due to a redistribution of the load effects within the structural system. Failure of a statically indeterminate structure usually requires the joint and/or sequential formation of more than one element failure mode such that a system failure mode forms. Let M denote the number of component failure events F_i representing the different element failure modes. Each system failure mode k of a statically indeterminate structure can be modeled by a parallel system of component failure events F_i, $\forall i \in C_k$ where $C_k \subseteq \{1, \ldots, M\}$ denotes the index set of kth system failure mode. Most statically indeterminate structures have a large number of possible system failure modes, and overall system failure
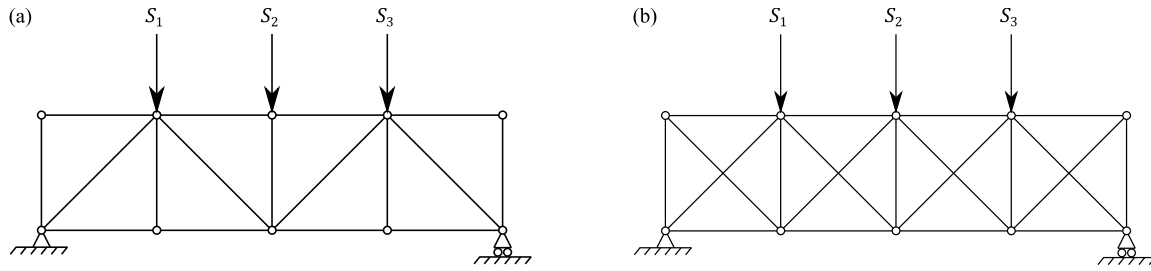
Figure 2.7: Statically (a) determinate and (b) indeterminate truss (adapted from Thoft-Christensen and Murotsu 1986).

takes place when the weakest system failure mode forms (Thoft-Christensen and Murotsu 1986). Statically indeterminate structures can, therefore, be modeled as a series system of K parallel systems or cut-sets of component failure events F_i where K denotes the number of possible system failure modes. The corresponding failure probability is defined by Equation (2.29).

Load effects must be redistributed within a statically indeterminate structure when an element failure mode occurs. It is, therefore, important to correctly model the mechanical behavior of element failure modes. Two important types of element failure modes are "ideal elastic - ideal brittle" and "ideal elastic - ideal plastic" failure modes as illustrated in Figure 2.8. In the following, "ideal elastic - ideal brittle" behavior will be called brittle behavior and "ideal elastic - ideal plastic" behavior will be called ductile behavior.

An element failure mode is brittle if there is no load-bearing capacity left in the structural element after failure has taken place. As an example, consider a welded connection in an offshore steel structure weakened due to fatigue crack growth. Such a connection may fail in a brittle mode under storm conditions because of rupture. After failure, the welded connection can no longer transfer any load effects. Another example is buckling of a compression member, which may also be idealized as a brittle failure mode.

An element failure mode is ductile if the structural element can sustain the maximum load effect after failure while deformation occurs. Therefore, the failed element still contributes to the load carrying capacity of the structural system. When considering ductile failure modes, it is important to ensure that enough plastic deformation capacity exists. For example, the plastic rotation capacity of a steel member may be limited due to the occurrence of local section buckling.

The effect of residual load-carrying capacity and load redistribution must be described in each step of a failure sequence leading to the formation of a system failure mode. Thus, the limit state func-
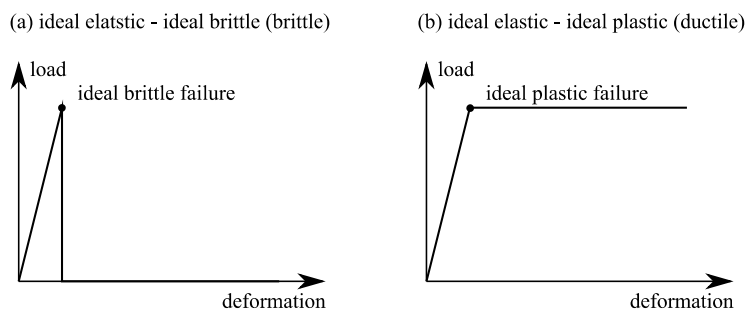
Figure 2.8: (a) Ideal elastic - ideal brittle (brittle) and (b) ideal elastic - ideal plastic (ductile) element failure mode behavior.

tions $g_i(\mathbf{x})$ describing the component failure events F_i of a parallel sub-system have to be formulated sequentially (Thoft-Christensen and Murotsu 1986). The first limit state function describes the occurrence of the first element failure mode without failure in any other structural elements. The second limit state function describes the formation of the second element failure mode given that the first element failure mode has occurred, i.e. after redistribution of the load effects. This process is continued until a system failure mode is completely described.

As an example, consider the continuous girder with two spans illustrated in Figure 2.9(a) (see Faber 2009 for a similar example). Each span has length a. A point load S is applied at the center of the left span. Assuming ductile material behavior, the girder has one system failure mode under the applied load as shown in Figure 2.9(b). The system failure mode may form in two different ways: (a) the first plastic hinge forms at location 1 followed by the formation of a plastic hinge at location 2 or (b) the plastic hinges form in reverse order. Let R_1 and R_2 denote the plastic moment capacities of the girder at locations 1 and 2. The random variables of the current problem are $\mathbf{X} = [R_1, R_2, S]^T$.

The limit state functions describing the formation of the initial plastic hinges at locations 1 and 2 can be written as:

$$g_1(\mathbf{x}) = r_1 - m_1 = r_1 - \frac{13}{64} s \cdot a \tag{2.32}$$

$$g_2(\mathbf{x}) = r_2 + m_2 = r_2 - \frac{3}{32} s \cdot a \tag{2.33}$$

where m_1 and m_2 are the bending moments at locations 1 and 2 determined by linear elastic analysis of the undamaged girder.

Suppose the first plastic hinge forms at location 1. The structural model is modified by introducing a corresponding hinge and fictitious bending moments to counteract the rotation. The modified structural model is shown in Figure 2.9(c).
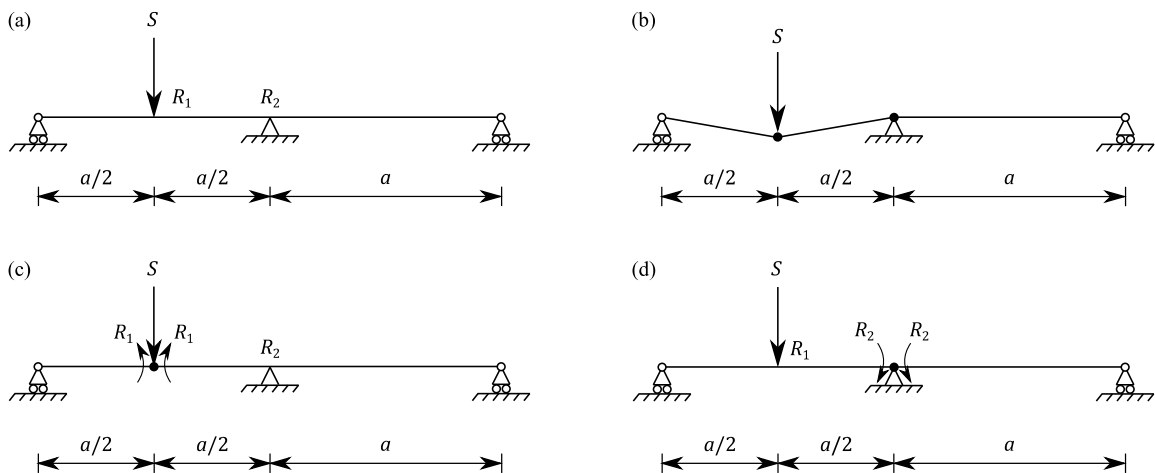
Figure 2.9: (a) Continuous girder with point load, (b) system failure mode of the girder, formation of a plastic hinge and fictitious bending moments at (c) location 1 and (d) location 2. The fictitious bending moments are introduced to counteract the rotation.

The limit state function describing the formation of a plastic hinge at location 2 given that a plastic hinge has formed at location 1 can now be defined as:

$$g_{2|1}(\mathbf{x}) = r_2 + m_{2|1} = r_2 - \frac{s \cdot a}{2} + 2r_1 \tag{2.34}$$

where $m_{2|1}$ is the bending moment at location 2 computed by linear elastic analysis of the modified structural model.

The modified structural model corresponding to the case in which the first plastic hinge forms at location 2 is shown in Figure 2.9(d). The conditional limit state function describing the formation of a plastic hinge at location 1 after the formation of a plastic hinge at location 2 is defined as:

$$g_{1|2}(\mathbf{x}) = r_1 - m_{1|2} = r_1 - \frac{s \cdot a}{4} + \frac{r_2}{2} \tag{2.35}$$

where $m_{1|2}$ is the bending moment at location 1 resulting from an linear elastic analysis of the modified structural model. This limit state function is equivalent to the one defined in Eq. (2.34).

The girder can now be modeled as a series system of two cut-sets where each cut-set represents a failure sequence leading to the formation of the system failure mode of the girder. The corresponding system failure probability is defined as:

$$\Pr(F) = \Pr\left[\left\{g_1(\mathbf{X}) \leq 0 \cap g_{2|1}(\mathbf{X}) \leq 0\right\} \cup \left\{g_2(\mathbf{X}) \leq 0 \cap g_{1|2}(\mathbf{X}) \leq 0\right\}\right] \tag{2.36}$$

Based on Equation (2.31), an equivalent limit state function describing failure of the girder can be formulated as:

$$\begin{aligned}
g(\mathbf{x}) &= \min\left[\max\left[g_1(\mathbf{x}), g_{2|1}(\mathbf{x})\right], \max\left[g_2(\mathbf{x}), g_{1|2}(\mathbf{x})\right]\right] \\
&= \min\left[g_{2|1}(\mathbf{x}), g_{1|2}(\mathbf{x})\right]
\end{aligned} \tag{2.37}$$

Since $g_{2|1}(\mathbf{x})$ and $g_{1|2}(\mathbf{x})$ are equivalent, it is sufficient to describe the event of system failure of the girder with ductile material behavior by either of these functions.

Now suppose the girder behaves brittle, i.e. it suddenly loses its rotation resistance after failure. To describe the brittle failure mode behavior, the conditional limit state functions must be modified as follows:

$$g_{1|2}(\mathbf{x}) = r_1 - m_{1|2} = r_1 - \frac{s \cdot a}{4} \tag{2.38}$$

$$g_{2|1}(\mathbf{x}) = r_2 + m_{2|1} = r_2 - \frac{s \cdot a}{2} \tag{2.39}$$

The above example demonstrates that the sequential definition of the limit state functions requires a reanalysis of the structure after the formation of each new element failure mode. The applied structural model has to be capable of correctly describing the mechanical behavior of each step in the failure sequence.

In structural systems with a low degree of redundancy, redistribution of load effects following the occurrence of a brittle failure mode typically leads to sudden overloading of the remaining structural elements. This effect is known as progressive collapse. Such structural systems are typically modeled as series systems of element failure events (Thoft-Christensen and Murotsu 1986; Melchers 1999). When assessing the reliability of structures with brittle and instability failure modes, it is also important to accurately model the sequence in which external loads are applied. This problem is known as load-path-dependence (Melchers 1999).

Ductile structural systems can also be modeled at mechanism level (Thoft-Christensen and Murotsu 1986). This approach considers each event $F_i = \{$formation of collapse mechanism $i\}$ as a component failure event defined in terms of a limit state function $g_i(\mathbf{x})$. System failure occurs when any of the possible collapse mechanism forms. It can, thus, be modeled as a series system of K component failure events F_i where K is the total number of possible system collapse mechanisms. The system failure probability is then given by Equation (2.22). As an example, consider the portal frame shown in Figure 2.10 (see also Madsen et al. 1986). The frame is subject to a horizontal point load H and a vertical point load V. It behaves ductile and $R_1, ..., R_5$ are the plastic moment capacities at the locations where plastic hinges are likely to form. Thus, the random variables of the current problem are $\mathbf{X} = [R_1, ..., R_5, H, V]^T$. The three dominant collapse mechanisms of the frame are also shown in Figure 2.10.

The limit state functions describing all three collapse mechanisms can be derived using the principle of virtual work (Madsen et al. 1986):

$$g_1(\mathbf{x}) = r_1 + r_2 + r_4 + r_5 - h \cdot a \tag{2.40}$$

$$g_2(\mathbf{x}) = r_2 + 2r_3 + r_4 - v \cdot a \tag{2.41}$$

$$g_3(\mathbf{x}) = r_1 + 2r_3 + 2r_4 + r_5 - h \cdot a - v \cdot a \tag{2.42}$$
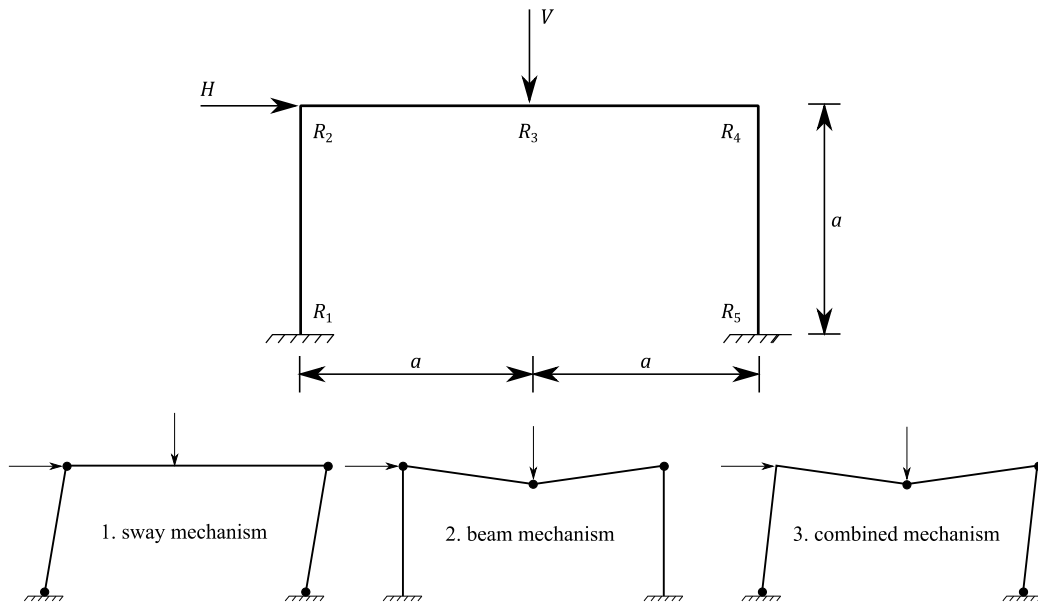
Figure 2.10: Frame with three dominant collapse mechanisms (adapted from Madsen et al. 1986).

33

The frame fails if any of the three collapse mechanisms forms. Its failure probability is, therefore, defined as:

$$\Pr(F) = \Pr(F_1 \cup F_2 \cup F_3) = \Pr(\{g_1(\mathbf{X}) \leq 0\} \cup \{g_2(\mathbf{X}) \leq 0\} \cup \{g_3(\mathbf{X}) \leq 0\}) \qquad (2.43)$$

The girder with ductile material behavior shown in Figure 2.9(a) can also be modeled at mechanism level. The limit state function describing the system failure mode is also found by the principle of virtual work:

$$g(\mathbf{x}) = 2r_1 + r_2 - \frac{s \cdot a}{2} \qquad (2.44)$$

As expected, this limit state function is equivalent to limit state functions given in Equations (2.34) and (2.35).

An important aspect of system reliability analysis is the dependence among the individual component failure events F_i, $i = 1, \ldots, M$ as well as the dependence among the K different system failure modes. The dependence among the individual component failure events F_i exists because the corresponding limit state functions $g_i(\mathbf{x})$ contain common and/or correlated random variables. As an example, consider the limit state functions in Equations (2.32) to (2.35) describing the component failure events of the girder shown in Figure 2.9(a). The load S is contained in each limit state function. The component failure events are, therefore, functionally dependent. In addition, the limit state functions contain the capacities R_1 and R_2. These capacities may have different realizations, but they are likely to be correlated. The component failure modes are, therefore, also stochastically dependent. Furthermore, dependence among the K different system failure modes exists as they often share common and/or stochastically dependent component failure events.

In theory, all possible system failure modes should be considered in the system reliability assessment. However, the total number of possible failure modes of real structures can be intractably large. For this reason, only the dominant system failure modes with the highest probability of occurrence are typically considered in structural system reliability analyses (see, for example, Murotsu et al. 1984; Thoft-Christensen and Murotsu 1986). Several methods are available that identify dominant failure modes and estimate the failure probability of structural systems (see Shao and Murotsu 1999 for an overview). Among existing methods the branch-and-bound technique (Murotsu et al. 1984) and simulation-based methods (Ditlevsen and Bjerager 1989; Melchers 1994) are considered theoretically rigorous but computationally expensive. Alternative methods such as the incremental loading method (Moses 1982), the β-unzippng method (Thoft-Christensen and Murotsu 1986), techniques employing linear programming in combination with simulation methods (Corotis and Nafday 1989) and methods utilizing heuristics (Shetty 1994; Xiao and Mahadevan 1994) are computationally efficient but they do not guarantee to find all dominant system failure modes. As a compromise, Shao and Murotsu (1999) and Kim et al. (2013) employ a simulation-based selective search technique utilizing a genetic algorithm to identify dominant system failure modes, and subsequently apply the matrix-based system reliability method (Kang et al. 2008; Song and Kang 2009) to compute the system failure probability.

2.4.3 Daniels system

Consider the idealized structural system with n_E elements shown in Figure 2.11. Such a system is known as a Daniels system (Daniels 1945). The elements of a Daniels system are equally elongated under the applied load S and each element can fail in tension. Daniels (1945) assumes that all elements have the same axial stiffness, and independent and identically distributed axial capacities $R_i, i = 1, \dots, n_E$. When the load S is applied, the weakest structural element fails first, followed by the second weakest element and so on. After failure of one element, the load redistributes among the remaining elements. At some point, the applied load cannot be sustained by the remaining elements and the system fails. It follows that a Daniels system has exactly one system failure mode. Note that Daniels (1945) neglects any dynamic effects during load redistribution.

To illustrate the influence of mechanical failure mode behavior on the system reliability of redundant structures, the reliability of the Daniels system is computed for brittle and ductile element behaviors following a parameter study presented by Gollwitzer and Rackwitz (1990). The element capacities $R_i, i = 1, \dots, n_E$ are modeled as i.i.d. normal random variables with mean μ_R and standard deviation σ_R. The coefficient of variation of the element capacities R_i is chosen to be $\delta_R = \sigma_R/\mu_R = 0.2$. The applied load is modeled as a deterministic variable $S = s$. Its value is selected such that the reliability index of each element i is $\beta_e = 2$, i.e. $s = n_E(\mu_R - \beta_e\sigma_R)$. The random variables of the current problem are $\mathbf{X} = [R_1, \dots, R_{n_E}]^T$.

If the elements behave brittle, the maximum capacity R_b of the Daniels system is given by (Gollwitzer and Rackwitz 1990):

$$R_b = \max_{i \in \{1, \dots, n_E\}} \{(n_E - i + 1)\hat{R}_i\} \tag{2.45}$$

where $\hat{R}_i$ are the ordered element capacities R_i such that $\hat{R}_1 \leq \hat{R}_2 \leq \dots \leq \hat{R}_{n_E}$. Daniels (1945) provides an exact recursive expression for the distribution of R_b. Gollwitzer and Rackwitz (1990) note that the system failure probability of a brittle Daniels system is given by:

$$\Pr(F) = \Pr\left[\bigcap_{i=1}^{n_E} \{(n_E - i + 1)\hat{R}_i \leq s\}\right] \tag{2.46}$$

This expression corresponds to a parallel system problem. Gollwitzer and Rackwitz (1990) solve the problem using first/second-order methods. However, the problem is here simply solved using
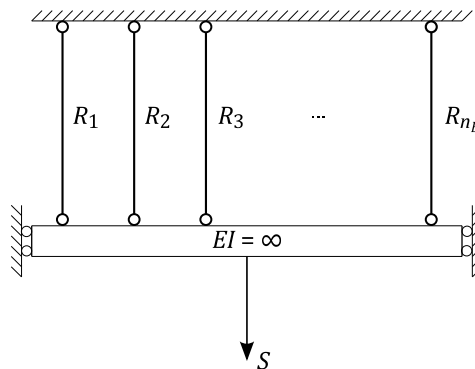
Figure 2.11: Daniels system with n_E elements. EI is the flexural rigidity.

MSC with 10^6 samples. The corresponding limit state function defining the system failure event is $g(\mathbf{x}) = r_b - s$.

If the members behave ductile, the maximum capacity of the Daniels system R_d is simply given by the sum of the normal distributed capacities, i.e. $R_d = \sum_{i=1}^{n_E} R_i$. Consequently, R_d is also normal distributed with mean $n_E \mu_R$ and standard deviation $\sqrt{n_E} \sigma_R$. It follows that the failure probability of the ductile Daniels system is given by:

$$\Pr(F) = \Pr(R_d \leq s) = \Phi\left(\frac{s - n_E \mu_R}{\sqrt{n_E} \sigma_R}\right) \tag{2.47}$$

The parallel system and series system configuration are also considered as bounding cases. In the current example, the component failure events F_i are independent since the element capacities R_i are independent. The system failure probability of the parallel system is thus defined as (see also Equation (2.27)):

$$\Pr(F) = \prod_{i=1}^{n_E} \Pr(F_i) \tag{2.48}$$

where $\Pr(F_i) = \Phi(-\beta_e), i = 1, \ldots, n_E$. The failure probability of the series system is given by (see also Equation (2.23)):

$$\Pr(F) = 1 - \prod_{i=1}^{n_E} [1 - \Pr(F_i)] \tag{2.49}$$

Note that the parallel system has no plausible mechanical meaning since load redistribution after element failure is not considered in this system configuration.

Figure 2.12 shows the system reliability index $\beta = -\Phi^{-1}[\Pr(F)]$ of the Daniels system as a function of the number of structural elements n_E for different mechanical failure mode behaviors.

The reliability of the series system decreases with n_E whereas the reliability of the parallel system significantly increases with n_E. When load redistribution is considered, the system reliability strongly depends on the mechanical behavior of the element failure modes. The reliability of the ductile system is considerably higher than the reliability of the brittle system. The reliability of the brittle system initially decreases below the reliability level of a single element $\beta_e = 2$. In a brittle system with a small number of elements, it is unlikely that the extra load can be sustained by the remaining members after the weakest element fails. Brittle systems with a low degree of indeterminacy behave like a series system. Only for a larger number of elements, the reliability of the brittle system exceeds the element reliability level.

As discussed in Section 2.4.2, the dependence among element failure modes also influence the reliability of structural systems. To demonstrate this effect, a Daniels system with $n_E = 5$ elements is considered. The same probabilistic model is applied as in the previous example. However, the element capacities $R_i, i = 1, \ldots, n_E$ of the Daniels system are now modeled as equi-correlated normal random variables with common correlation coefficient ρ_R among all pairs R_i and $R_j, i, j =$
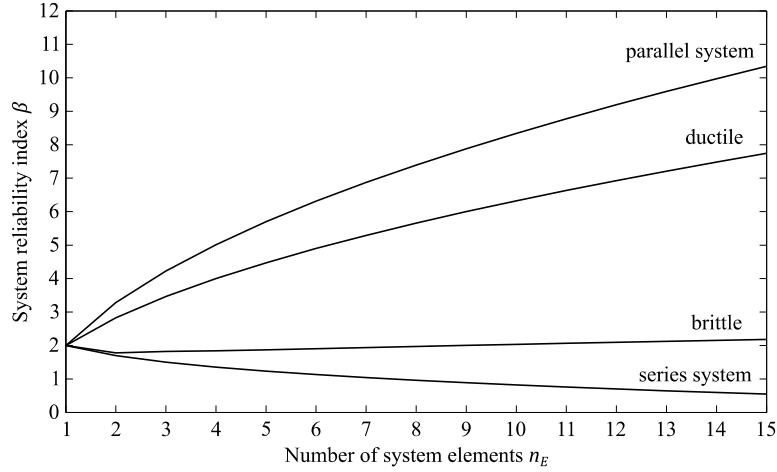
Figure 2.12: System reliability index $\beta = -\Phi^{-1}[\Pr(F)]$ of the Daniels system as a function of the number of elements n_E for different mechanical failure mode behaviors (see also Gollwitzer and Rackwitz 1990).

$1, \ldots, n_E, i \neq j$. Ductile and brittle element behavior, and the series system configuration are considered.

For the ductile case, it can be shown that the mean value and variance of the normal distributed maximum capacity $R_d = \sum_{i=1}^{n_E} R_i$ are $\mu_{R_d} = n_E \mu_R$ and $\sigma_{R_d}^2 = n_E \sigma_R^2 (1 + (n_E - 1)\rho_R)$. The failure probability of the ductile Daniels system is thus given by:

$$\Pr(F) = \Pr(R_d \leq s) = \Phi\left(\frac{s - n_E \mu_R}{\sqrt{n_E[1 + (n_E - 1)\rho_R]}\,\sigma_R}\right) \qquad (2.50)$$

The system failure probability of the brittle Daniels system is again estimated using MSC with 10^6 samples, and the first-order solution given in (Hohenbichler and Rackwitz 1983) is applied to compute the system failure probability of the series system. The results are shown in Figure 2.13.

The largest redundancy exists if the structural members behave ductile and their resistances are uncorrelated. In case of full positive correlation, the reliability of the ductile system is equal to the
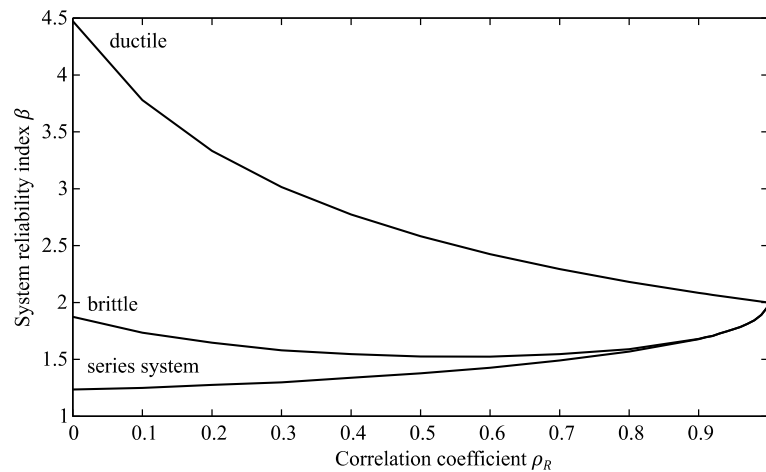
Figure 2.13: System reliability index $\beta = -\Phi^{-1}[\Pr(F)]$ of the Daniels system with $n_E = 5$ elements as a function of the common correlation coefficients ρ_R among all pairs of element capacities R_i and R_j for different mechanical failure mode behaviors (see also Gollwitzer and Rackwitz 1990).

reliability of a single structural member. In this case the ductile system has no redundancy. Medium positive correlations reduce the reliability of a small brittle system even further when compared to the zero-correlation case. For $\rho_R = 1$ the reliability of the brittle system is also equal the member reliability. The reliability of the series system increases with increasing positive correlation.

3 Bayesian analysis

3.1 Introduction

For structural systems with large consequences of failure, target failure probabilities related to a one year reference period and ultimate limit states are in the order of 10^{-4} - 10^{-6} (JCSS 2001; ISO 2394 2015). As highlighted by Straub et al. (2016), an estimation of such small failure probabilities by means of probabilistic structural models corresponds to an extrapolation from the domain of observation, and the computed failure probabilities must be carefully interpreted (see also Melchers 1999). However, information on the demand and capacity of a structural system provided by inspection and monitoring can be applied to improve the probability estimates. Bayesian analysis is a consistent framework for this task (Tang 1973; Madsen 1987; Sindel and Rackwitz 1998; Straub 2011a).

Essentially, inspection and monitoring of structural systems provide information on the stochastic parameters **X** that influence their performance. The information is typically incomplete as inspection and monitoring do not provide information on all parameters in **X**. In addition, the information is subject to uncertainty. Bayesian analysis is the mathematical framework for updating the joint PDF of **X** with incomplete and uncertain information. As illustrated in Figure 3.1, the analysis corresponds to classical statistical inference if the joint PDF of **X** is updated with direct measurements or samples of one or more parameters in **X** (see, for example, Gelman et al. 2004). The analysis corresponds to a probabilistic inverse analysis if it is applied to update the joint PDF of **X** with measurements or observations of the structural performance. The updated joint PDF of **X** then forms the basis for updating the probability of the failure event F.
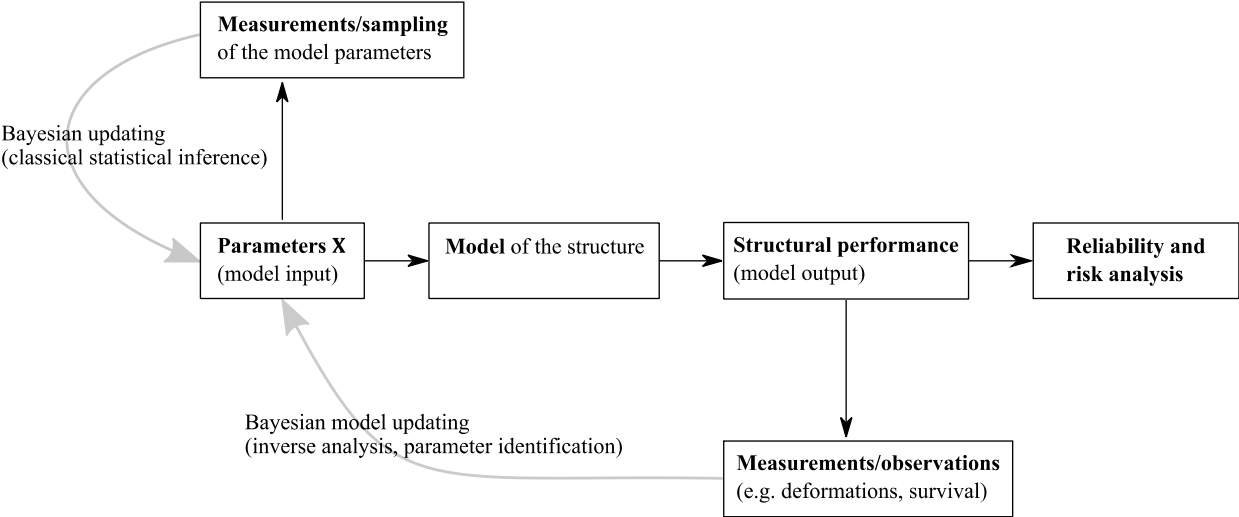
Figure 3.1: Illustration of Bayesian updating with direct or indirect information on the stochastic parameters **X** that influence the structural performance (adapted from Straub and Papaioannou 2015a). The information is direct if parameters in **X** are directly measured or sampled, and indirect if the relation between **X** and a measurement or observation is defined through a model.

An inspection or monitoring outcome can be modeled probabilistically by a random variable Z_i. Essentially, two cases can be distinguished: Z_i is a continuous random variable if it represents a measurement or sample of a continuous quantity, or it is a discrete random variable if it represents an inspection or monitoring outcome with discrete states. A typical example is an inspection or monitoring outcome with discrete states "indication" and "no indication" of damage.

All probabilistic inspection and monitoring outcomes are collectively represented by the random vector $\mathbf{Z} = [Z_1, \dots, Z_N]^T$. In a Bayesian setting, the relation between the joint observation $\mathbf{Z} = \mathbf{z}$ and the stochastic parameters $\mathbf{X}$ is modeled through the likelihood function $L(\mathbf{x}|\mathbf{z})$, which is proportional to the conditional probability of observing $\mathbf{Z} = \mathbf{z}$ when the stochastic parameters $\mathbf{X}$ take a value $\mathbf{x}$ (Straub and Papaioannou 2015b):

$$L(\mathbf{x}|\mathbf{z}) \propto \Pr(\mathbf{Z} = \mathbf{z}|\mathbf{X} = \mathbf{x}) \tag{3.1}$$

Bayes' theorem formalizes the process of updating the joint PDF of $\mathbf{X}$ with the observation $\mathbf{Z} = \mathbf{z}$:

$$f_{\mathbf{X}|\mathbf{Z}}(\mathbf{x}|\mathbf{z}) = \frac{L(\mathbf{x}|\mathbf{z}) \, f_{\mathbf{X}}(\mathbf{x})}{\int_{D_{\mathbf{X}}} L(\mathbf{x}|\mathbf{z}) \, f_{\mathbf{X}}(\mathbf{x}) \, \mathrm{d}\mathbf{x}} \tag{3.2}$$

where $D_{\mathbf{X}}$ denotes the domain of definition of $\mathbf{X}$, and $f_{\mathbf{X}}(\mathbf{x})$ and $f_{\mathbf{X}|\mathbf{Z}}(\mathbf{x}|\mathbf{z})$ are the prior and posteriors PDF of $\mathbf{X}$. As an example, Figure 3.2 illustrates the computation of the posterior PDF $f_{X|Z}(x|z)$ of a single random variable X, whose value is directly measured. The measurement is subject to an additive measurement error (this example follows Straub and Papaioannou 2015b).

Closed-form solutions of Equation (3.2) rarely exist, and Bayesian updating is typically performed using sampling methods. A popular class of methods for generating samples from the posterior PDF $f_{\mathbf{X}|\mathbf{Z}}(\mathbf{x}|\mathbf{z})$ are Markov chain Monte Carlo (MCMC) methods (Gilks et al. 1996; Gelman et al. 2004). These methods simulate states of a Markov chain whose unique stationary distribution is equal to the posterior PDF $f_{\mathbf{X}|\mathbf{Z}}(\mathbf{x}|\mathbf{z})$. A disadvantage of MCMC methods is the "burn-in problem", which means that it takes several initial samples before the marginal distribution of the generated
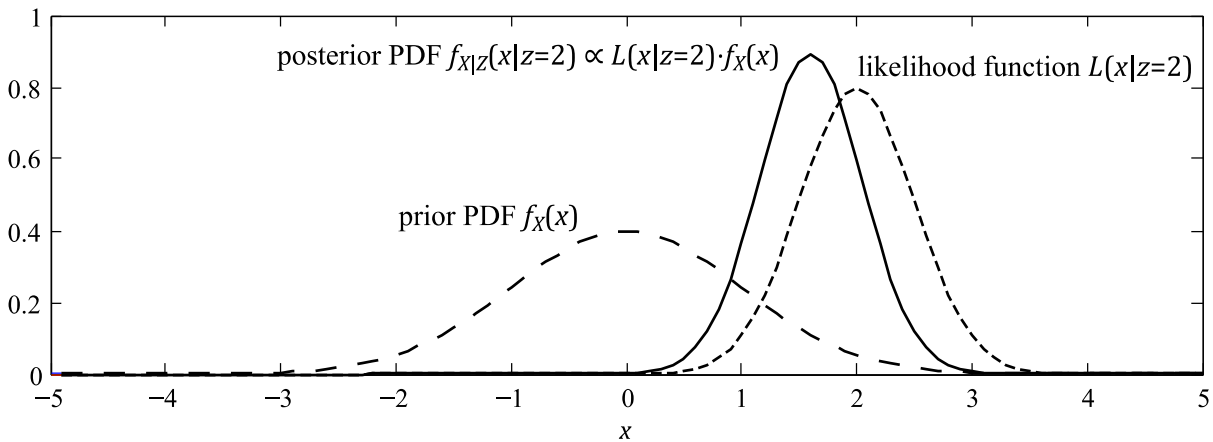
Figure 3.2: Bayesian updating of a random variable X, whose prior PDF is the standard normal PDF $f_X(x) = 1/\sqrt{2\pi} \cdot \exp(-x^2/2)$ (see also Straub and Papaioannou 2015b). X is measured to be 2. The measurement is subject to a normal distributed additive measurement error with zero mean and standard deviation 0.5. The likelihood function describing this measurement is therefore $L(x|z = 2) = 1/(0.5 \cdot \sqrt{2\pi}) \cdot \exp(-0.5 \cdot (2 - x)^2/0.5^2)$ (see also Section 3.2).

samples is sufficiently close to the chain's stationary distribution. In addition, it is difficult to choose an appropriate burn-in period, and hence it may be possible that the generated samples have not yet converged to the stationary distribution of the Markov chain after the chosen burn-in period (Plummer et al. 2006).

An alternative sampling method that does not suffer the "burn-in problem" is an implementation of BUS (Bayesian updating with structural reliability methods) with subset simulation. BUS proposed by Straub and Papaioannou (2015b) interprets the classical rejection sampling algorithm for Bayesian updating (Smith and Gelfand 1992) as generating samples in a "failure" domain defined in the outcome space of the stochastic system parameters augmented with an additional standard uniform random variable. This interpretation enables the application of existing structural reliability methods (SRM) to learn the posterior distribution of the stochastic system parameters. In addition, Straub et al. (2016) demonstrate that BUS can be adapted to directly perform Bayesian updating of failure probabilities.

The following sections present the BUS framework in more detail. First, Section 3.2 briefly describes how different types of inspection and monitoring outcomes are modeled with likelihood functions. Section 3.3 then introduces the basic idea behind BUS and its implementation with subset simulation. Finally, Section 3.4 shows how BUS can be applied to perform Bayesian updating of failure probabilities.

3.2 Likelihood functions

First, consider a single inspection or monitoring outcome $Z_i = z_i$ representing a measurement of a continuous quantity predicted by a model $q_i(\mathbf{X})$. If the measurement is subject to an additive measurement error E_i with PDF $f_{E_i}(\varepsilon_i)$, the following equality holds $Z_i = q_i(\mathbf{X}) + E_i$. It follows that $E_i = Z_i - q_i(\mathbf{X})$. In this special but common case, the likelihood of observing $Z_i = z_i$ given $\mathbf{X} = \mathbf{x}$ is equal to the probability density of the measurement error E_i taking the value $z_i - q_i(\mathbf{x})$. The likelihood function $L(\mathbf{x}|z_i) \propto \Pr(Z_i = z_i|\mathbf{X} = \mathbf{x})$ of the inspection or monitoring outcome $Z_i = z_i$ can thus be written as:

$$L(\mathbf{x}|z_i) = f_{E_i}[z_i - q_i(\mathbf{x})] \tag{3.3}$$

This example assumes that the model $q_i(\mathbf{x})$ predicts the true value of the measured quantity. In a probabilistic setting, this assumption is reasonable if the problem is formulated such that certain random variables are included in the model to explicitly represent model uncertainties (Ditlevsen 1982; JCSS 2001). These additional random variables are simply added to the random vector $\mathbf{X}$.

Probabilistic inspection and monitoring outcomes for which equalities like $Z_i = q_i(\mathbf{X}) + E_i$ can be formulated are said to provide equality information (Madsen 1987; Straub 2011a). The likelihood function for inspection and monitoring outcomes $Z_i = z_i$ providing this type of information is generically defined as (Straub and Papaioannou 2015b):

$$L(\mathbf{x}|z_i) = f_{Z_i|\mathbf{X}}(z_i|\mathbf{x}) \tag{3.4}$$

where $f_{Z_i|\mathbf{X}}(z_i|\mathbf{x})$ is the conditional PDF of the (continuous) inspection or monitoring outcome Z_i given $\mathbf{X} = \mathbf{x}$, which is typically defined in terms of the PDF of the associated measurement error (see also Betz 2017 for more details on formulating likelihood functions). Note that the likelihood function defined in Equation (3.4) includes the evaluation of the model, which predicts the measured quantity as in Equation (3.3).

Next, let $Z_i = 1$ represent the (discrete) inspection or monitoring outcome "a quantity predicted by the model $q_i(\mathbf{X})$ is larger than a threshold $q_{i,T}$", and let $Z_i = 0$ represent the complement. The inspection or monitoring outcome $Z_i = 1$ can be defined by the limit state function $h_i(\mathbf{x}) = q_{i,T} - q_i(\mathbf{x})$ as:

$$\{Z_i = 1\} = \{h_i(\mathbf{X}) \leq 0\} \tag{3.5}$$

In this formulation, measurement and model uncertainties are included as additional random variables in $\mathbf{X}$. An inspection or monitoring outcome of this type is said to provide inequality information (Madsen 1987; Straub 2011a). The conditional probability of observing $Z_i = 1$ given $\mathbf{X} = \mathbf{x}$ is:

$$\Pr(Z_i = 1|\mathbf{X} = \mathbf{x}) = \mathbb{I}[h_i(\mathbf{x}) \leq 0] \tag{3.6}$$

where $\mathbb{I}[\cdot]$ is the indicator function: $\mathbb{I}[\cdot] = 1$ if the condition $[\cdot]$ is true and $\mathbb{I}[\cdot] = 0$ otherwise. The likelihood function for the inspection or monitoring outcome $Z_i = z_i$ can thus be written as:

$$L(\mathbf{x}|z_i) = \begin{cases} 1 - \mathbb{I}[h_i(\mathbf{x}) \leq 0] & \text{if } z_i = 0 \\ \mathbb{I}[h_i(\mathbf{x}) \leq 0] & \text{if } z_i = 1 \end{cases} \tag{3.7}$$

More generally, the likelihood function for an inspection or monitoring outcome $Z_i = z_i$ providing inequality information is defined as:

$$L(\mathbf{x}|z_i) = p_{Z_i|\mathbf{X}}(z_i|\mathbf{x}) \tag{3.8}$$

where $p_{Z_i|\mathbf{X}}(z_i|\mathbf{x}) = \Pr(Z_i = z_i|\mathbf{X} = \mathbf{x})$ is the conditional probability mass function (PMF) of the (discrete) inspection or monitoring outcome Z_i given $\mathbf{X} = \mathbf{x}$.

When several inspection and monitoring outcomes $\mathbf{Z} = \mathbf{z}$ are available, the joint likelihood function $L(\mathbf{x}|\mathbf{z})$ must be formulated to describe the joint observation $\mathbf{Z} = \mathbf{z}$. If the probabilistic inspection and monitoring outcomes $\mathbf{Z}$ are statistically independent given $\mathbf{X} = \mathbf{x}$, a likelihood function $L(\mathbf{x}|z_i)$, $i = 1, \dots, N$ can be formulated for each inspection or monitoring outcome $Z_i = z_i$ separately, and the likelihood function for the joint observation $\mathbf{Z} = \mathbf{z}$ is computed as (Straub and Papaioannou 2015b):

$$L(\mathbf{x}|\mathbf{z}) = \prod_{i=1}^{N} L(\mathbf{x}|z_i) \tag{3.9}$$

If the probabilistic inspection and monitoring outcomes $\mathbf{Z}$ are statistically dependent for given values $\mathbf{X} = \mathbf{x}$, the combined likelihood function $L(\mathbf{x}|\mathbf{z})$ must be formulated such that the dependencies among the individual inspection and monitoring outcomes are modeled properly (e.g. Simoen et al. 2013). As an example (see also Straub and Papaioannou 2015b), consider measurements $\mathbf{z} = [z_1, \ldots, z_N]^T$ of quantities $\mathbf{q}(\mathbf{X}) = [q_1(\mathbf{X}), \ldots, q_N(\mathbf{X})]^T$. Suppose the measurements are subject to correlated, additive measurement errors $\mathbf{E} = [E_1, \ldots, E_N]^T$, which are probabilistically modeled by a joint normal PDF $f_{\mathbf{E}}(\boldsymbol{\varepsilon})$ with zero mean and covariance matrix $\boldsymbol{\Sigma}_{\mathbf{EE}}$. The corresponding observation is defined as $\{\mathbf{Z} = \mathbf{z}\} = \{\mathbf{q}(\mathbf{X}) + \mathbf{E} = \mathbf{z}\}$, and the likelihood function $L(\mathbf{x}|\mathbf{z})$ describing these measurements takes the following form:

$$L(\mathbf{x}|\mathbf{z}) = f_{\mathbf{Z}|\mathbf{X}}(\mathbf{z}|\mathbf{x}) = \frac{1}{\sqrt{(2\pi)^N \det(\boldsymbol{\Sigma}_{\mathbf{EE}})}} \exp\left[-\frac{1}{2}[\mathbf{z} - \mathbf{q}(\mathbf{x})]^T \boldsymbol{\Sigma}_{\mathbf{EE}}^{-1}[\mathbf{z} - \mathbf{q}(\mathbf{x})]\right] \qquad (3.10)$$

3.3 Bayesian updating with structural reliability methods (BUS)

3.3.1 Rejection sampling

Samples from the posterior PDF $f_{\mathbf{X}|\mathbf{Z}}(\mathbf{x}|\mathbf{z})$ can be generated with a simple rejection sampling algorithm described by Smith and Gelfand (1992). To derive this algorithm, it is first noted that the following relation holds for any likelihood function $L(\mathbf{x}|\mathbf{z})$:

$$cL(\mathbf{x}|\mathbf{z}) = F_P[cL(\mathbf{x}|\mathbf{z})] \qquad (3.11)$$

where P is an independent standard uniform random variable with PDF $f_P(p) = 1$ and CDF $F_P(p) = p$, and c is a positive constant that ensures $cL(\mathbf{x}|\mathbf{z}) \leq 1$ for all $\mathbf{x}$. The quantity $cL(\mathbf{x}|\mathbf{z})$ can now be expressed as:

$$
\begin{aligned}
cL(\mathbf{x}|\mathbf{z}) &= \int_0^{cL(\mathbf{x}|\mathbf{z})} f_P(p)\,\mathrm{d}p = \int_{p \leq cL(\mathbf{x}|\mathbf{z})} f_P(p)\,\mathrm{d}p \\
&= \int_0^1 \mathbb{I}[p \leq cL(\mathbf{x}|\mathbf{z})]\, f_P(p)\,\mathrm{d}p
\end{aligned}
\qquad (3.12)
$$

Consequently, the product $L(\mathbf{x}|\mathbf{z})\, f_{\mathbf{X}}(\mathbf{x})$ can be written as:

$$
\begin{aligned}
L(\mathbf{x}|\mathbf{z})\, f_{\mathbf{X}}(\mathbf{x}) &= \left[c^{-1} \int_0^1 \mathbb{I}[p \leq cL(\mathbf{x}|\mathbf{z})]\, f_P(p)\,\mathrm{d}p\right] f_{\mathbf{X}}(\mathbf{x}) \\
&= c^{-1} \int_0^1 \mathbb{I}[p \leq cL(\mathbf{x}|\mathbf{z})]\, f_{\mathbf{X}}(\mathbf{x})\, f_P(p)\,\mathrm{d}p
\end{aligned}
\qquad (3.13)
$$

Inserting Equation (3.13) into Equation (3.2) gives:

$$f_{\mathbf{X}|\mathbf{Z}}(\mathbf{x}|\mathbf{z}) = \frac{\int_0^1 \mathbb{I}[p \leq cL(\mathbf{x}|\mathbf{z})] \, f_{\mathbf{X}}(\mathbf{x}) \, f_P(p) \, \mathrm{d}p}{\int_{D_{\mathbf{X}}} \int_0^1 \mathbb{I}[p \leq cL(\mathbf{x}|\mathbf{z})] \, f_{\mathbf{X}}(\mathbf{x}) \, f_P(p) \, \mathrm{d}p \, \mathrm{d}\mathbf{x}} \tag{3.14}$$

The posterior cumulative distribution function (CDF) of $\mathbf{X}$ is obtained by integrating the posterior PDF of $\mathbf{X}$ (Straub and Papaioannou 2015b):

$$\begin{aligned} F_{\mathbf{X}|\mathbf{Z}}(\mathbf{x}_0|\mathbf{z}) &= \frac{\int_{-\infty}^{\mathbf{x}_0} \int_0^1 \mathbb{I}[p \leq cL(\mathbf{x}|\mathbf{z})] \, f_{\mathbf{X}}(\mathbf{x}) \, f_P(p) \, \mathrm{d}p \, \mathrm{d}\mathbf{x}}{\int_{D_{\mathbf{X}}} \int_0^1 \mathbb{I}[p \leq cL(\mathbf{x}|\mathbf{z})] \, f_{\mathbf{X}}(\mathbf{x}) \, f_P(p) \, \mathrm{d}p \, \mathrm{d}\mathbf{x}} \\[2mm] &= \frac{\int_{D_{\mathbf{X}}} \int_0^1 \mathbb{I}(\mathbf{x} \leq \mathbf{x}_0) \, \mathbb{I}[p \leq cL(\mathbf{x}|\mathbf{z})] \, f_{\mathbf{X}}(\mathbf{x}) \, f_P(p) \, \mathrm{d}p \, \mathrm{d}\mathbf{x}}{\int_{D_{\mathbf{X}}} \int_0^1 \mathbb{I}[p \leq cL(\mathbf{x}|\mathbf{z})] \, f_{\mathbf{X}}(\mathbf{x}) \, f_P(p) \, \mathrm{d}p \, \mathrm{d}\mathbf{x}} \end{aligned} \tag{3.15}$$

A Monte Carlo approximation of the posterior CDF $F_{\mathbf{X}|\mathbf{Z}}(\mathbf{x}_0|\mathbf{z})$ can be computed as:

$$F_{\mathbf{X}|\mathbf{Z}}(\mathbf{x}_0|\mathbf{z}) \approx \frac{\sum_{i=1}^N \mathbb{I}(\mathbf{x}^{(i)} \leq \mathbf{x}_0) \, \mathbb{I}[p^{(i)} \leq cL(\mathbf{x}^{(i)}|\mathbf{z})]}{\sum_{i=1}^N \mathbb{I}[p^{(i)} \leq cL(\mathbf{x}^{(i)}|\mathbf{z})]} \tag{3.16}$$

where $\mathbf{x}^{(i)}, i = 1, \dots, N$ are samples from $f_{\mathbf{X}}(\mathbf{x})$ and $p^{(i)}, i = 1, \dots, N$ are samples from the standard uniform PDF $f_P(p)$. It follows that all samples $\mathbf{x}^{(i)}$ from $f_{\mathbf{X}}(\mathbf{x})$ that fall into the domain

$$\Omega = \{(\mathbf{x}, p) : p \leq cL(\mathbf{x}|\mathbf{z})\} \tag{3.17}$$

are distributed according to the posterior PDF $f_{\mathbf{X}|\mathbf{Z}}(\mathbf{x}|\mathbf{z})$. Based on this, the rejection sampling algorithm summarized in Algorithm 3.1 for generating K samples from the posterior PDF of $\mathbf{X}$ can be defined. The principle of rejection sampling is illustrated in Figure 3.3.

The probability that a sample is accepted is equal to the denominator in Equation (3.14) (Straub and Papaioannou 2015b):

$$p_{acc} = \int_{D_{\mathbf{X}}} \int_0^1 \mathbb{I}[p \leq cL(\mathbf{x}|\mathbf{z})] \, f_{\mathbf{X}}(\mathbf{x}) \, f_P(p) \, dp \, d\mathbf{x} \tag{3.18}$$

This probability becomes very small if the number of observations and, consequently, the difference between the prior distribution and the likelihood function is large. In this situation, the rejection sampling algorithm is inefficient.

3.3.2 The BUS approach

Straub and Papaioannou (2015b) note that the denominator in Equation (3.14) corresponds to a structural reliability problem and interpret the domain $\Omega = \{(\mathbf{x}, p) : p \leq cL(\mathbf{x}|\mathbf{z})\}$ as a "failure" domain in the augmented outcome space of $\mathbf{X}$ and P. In agreement with structural reliability conventions, they define the domain Ω through a limit state function:

Algorithm 3.1: Rejection sampling algorithm for generating K samples from the posterior PDF $f_{\mathbf{X}|\mathbf{Z}}(\mathbf{x}|\mathbf{z})$ (Smith and Gelfand 1992; Straub and Papaioannou 2015b)

Input: K (number of required posterior samples), $f_{\mathbf{X}}(\mathbf{x})$ (prior PDF of $\mathbf{X}$), $L(\mathbf{x}|\mathbf{z})$ (likelihood function), and c (constant chosen such that $cL(\mathbf{x}|\mathbf{z}) \leq 1$ for all $\mathbf{x}$)

1. Initialize the counter $i = 1$.

2. While $i \leq K$:

   a. Generate a sample $\mathbf{x}^{(i)}$ from $f_{\mathbf{X}}(\mathbf{x})$.

   b. Generate a sample $p^{(i)}$ from the standard uniform PDF $f_P(p)$.

   c. If $p^{(i)} \leq cL(\mathbf{x}^{(i)}|\mathbf{z})$:

      i. Accept $\mathbf{x}^{(i)}$ as a sample of the posterior PDF $f_{\mathbf{X}|\mathbf{Z}}(\mathbf{x}|\mathbf{z})$

      ii. Increase the counter $i = i + 1$.

3. Return $\mathbf{x}^{(i)}$, $i = 1, \ldots, K$.
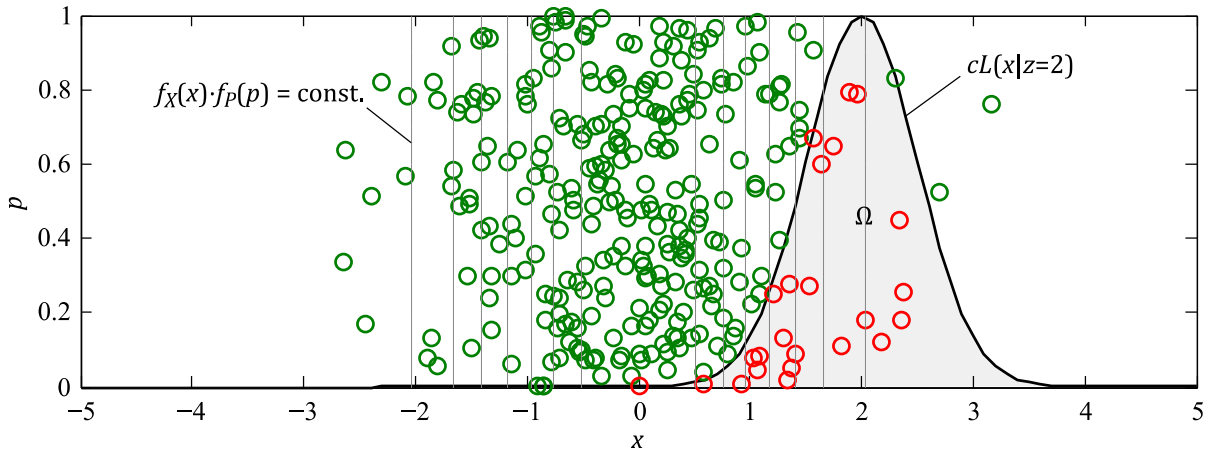
Figure 3.3: Illustration of rejection sampling (following Straub and Papaioannou 2015b). X is standard normal distributed and measured to be 2. The measurement is subject to a normal distributed additive measurement error with zero mean and standard deviation 0.5. The likelihood function describing this measurement is $L(x|z = 2) = 1/(0.5 \cdot \sqrt{2\pi}) \cdot \exp(-1/2 \cdot (2-x)^2/0.5^2)$. The constant c is selected as $c = 0.5 \cdot \sqrt{2\pi}$. The green and red circles are independent and identically distributed (i.i.d.) samples from $f_{X,P}(x,p) = f_X(x) \cdot f_P(p)$. The red circles are samples in the domain $\Omega = \{(x,p) : p \leq cL(x|z = 2)\}$ and are thus accepted.

$$h(\mathbf{x}, p) = p - cL(\mathbf{x}|\mathbf{z}) \tag{3.19}$$

as $\Omega = \{(\mathbf{x}, p) : h(\mathbf{x}, p) \leq 0\}$. The limit state function $h(\mathbf{x}, p)$ describes an observation event Z as:

$$Z = \{h(\mathbf{X}, P) \leq 0\} \tag{3.20}$$

The probability

$$\Pr(Z) = \Pr[h(\mathbf{X}, P) \leq 0] = \int_{D_{\mathbf{X}}} \int_0^1 \mathbb{I}[h(\mathbf{x}, p) \leq 0] \, f_{\mathbf{X}}(\mathbf{x}) \, f_P(p) \, \mathrm{d}p \, \mathrm{d}\mathbf{x} \tag{3.21}$$

is the "failure" probability of the equivalent reliability problem, which is equal to the potentially very small acceptance probability p_{acc} of the original rejection sampling algorithm defined in Equation (3.18).

The idea behind BUS is to (a) employ existing structural reliability methods to compute the probability $\Pr(Z)$, and (b) generate samples that lie in the "failure" domain Ω in a post-processing step. The simplest and most robust structural reliability method for computing $\Pr(Z)$ is Monte Carlo simulation (MCS). The advantage of MCS is that it directly generates samples located in Ω during the reliability analysis. In fact, an implementation of BUS with MCS is equivalent to the original rejection sampling algorithm. The disadvantage of MCS is that it is inefficient if $\Pr(Z)$ is small (see also Section 2.2.2). As an alternative, IS methods can be applied to compute $\Pr(Z)$ more efficiently. These methods produce weighted samples in the "failure" domain Ω and a re-sampling step is required to obtain unweighted samples (see, for example, Doucet et al. 2001). Another alternative to standard MCS is subset simulation (SuS), which is commonly applied to implement the BUS approach (Straub and Papaioannou 2015b; DiazDelaO et al. 2017; Giovanis et al. 2017; Betz et al. 2018b). This is because SuS is efficient in solving high-dimensional reliability problems (see also Section 2.2.3) and directly generates samples located in the "failure" domain Ω. The combination of BUS and SuS is presented in Section 3.3.4.

If the number of random variables $\mathbf{X}$ is limited and the domain Ω is similar to failure domains typically encountered in structural reliability, FORM can be used to implement BUS (Straub and Papaioannou 2015b; Straub et al. 2016). When applying FORM, the posterior distribution is approximated by a censored standard multivariate normal distribution in standard normal space (see also Section 2.2.1). Samples from this type of distribution can be generated (see, for example, Chopin 2012) and subsequently transformed into the outcome space of the original random variables.

3.3.3 The constant c in BUS

To apply the BUS approach, the constant c must be selected. As discussed in (Betz et al. 2018b), the optimal choice is $1/c = \sup[L(\mathbf{x}|\mathbf{z})]$ where $\sup[\cdot]$ is the supremum of the expression $[\cdot]$. Guidance on how to select c by inspecting the likelihood function is provided in (Straub and Papaioannou 2015b). In special cases, $\sup[L(\mathbf{x}|\mathbf{z})]$ can be readily selected. Consider, for example, a single measurement $Z_i = z_i$ subject to a measurement error E with PDF $f_E(\varepsilon)$. The supremum of the corresponding likelihood function is $\sup[L(\mathbf{x}|z_i)] = \max[f_E(\varepsilon)]$. Betz et al. (2018b) and DiazDelaO et al. (2017) demonstrate how c can be identified adaptively when BUS is combined with SuS. In addition, Betz et al. (2018a) propose a post-processing step for BUS, which returns an unbiased estimate of $\Pr(Z)$ and samples from the posterior distribution even if $1/c$ is selected smaller than the supremum of the likelihood function.

3.3.4 BUS with subset simulation

As discussed in Papaioannou et al. (2015), it is advantageous to perform SuS in standard normal space. To this end, the auxiliary random variable P and the system model parameters $\mathbf{X}$ are transformed to independent standard normal random variables $\mathbf{U} = [U_1, \dots, U_n, U_{n+1}]^T$ with joint PDF $\varphi_{n+1}(\mathbf{u}) = \prod_{i=1}^{n+1} \varphi(u_i)$ where $\varphi(\cdot)$ is the standard normal PDF. P and $\mathbf{X}$ are independent and can

be transformed separately. The inverse transformation from $\mathbf{U}$ to P and $\mathbf{X}$ is as follows (see also Straub and Papaioannou 2015b):

$$P = \Phi(U_{n+1}) \tag{3.22}$$

where $\Phi(\cdot)$ is the standard normal CDF, and

$$\mathbf{X} = T^{-1}(U_1, \dots, U_n) \tag{3.23}$$

$T(\cdot)$ is a probability preserving one-to-one mapping from the original outcome space of $\mathbf{X}$ to the standard normal space (see also Section 2.2). The limit state function $h(\mathbf{x}, p)$ defined in Equation (3.19) can now be expressed as:

$$h(\mathbf{x}, p) = H(\mathbf{u}) = \Phi(u_{n+1}) - cL(T^{-1}(u_1, \dots, u_n)|\mathbf{z}) \tag{3.24}$$

$H(\mathbf{u})$ describes the domain Ω_U in the standard normal space as $\Omega_U = \{\mathbf{u} : H(\mathbf{u}) \leq 0\}$.

In the context of BUS, SuS expresses the probability of the observation event Z as a product of conditional probabilities $\Pr(Z) = \prod_{i=1}^{M} \Pr(E_i | E_{i-1})$, where E_0 is the certain event and $E_0 \supset E_1 \supset \dots \supset E_M = Z$. The intermediate events E_i are defined in standard normal space as $E_i = \{H(\mathbf{U}) \leq b_i\}$, where $b_0 = \infty > b_1 > b_2 > \dots > b_M = 0$. The thresholds b_i are determined adaptively following the original SuS algorithm (see Section 2.2.3). By applying this procedure, the estimator $\hat{P}_{SuS}$ defined in Equation (2.21) provides an estimate of the probability $\Pr(Z)$.

Betz et al. (2018b) point out that the performance of BUS with SuS can be improved if the transition between the intermediate events is smooth. This can be achieved by applying an equivalent limit state function:

$$\hat{h}(\mathbf{x}, p) = \ln(p) - \ln[cL(\mathbf{x}|\mathbf{z})] \tag{3.25}$$

The corresponding limit state function in $\mathbf{U}$-space is then:

$$\hat{h}(\mathbf{x}, p) = \hat{H}(\mathbf{u}) = \ln[\Phi(u_{n+1})] - \ln[cL(T^{-1}(u_1, \dots, u_n)|\mathbf{z})] \tag{3.26}$$

where $\ln(\cdot)$ is the natural logarithm. The limit state function $\hat{h}(\mathbf{x}, p)$ describes the same "failure" domain as $h(\mathbf{x}, p)$ but the intermediate "failure" domains obtained with $\hat{h}(\mathbf{x}, p)$ converge smoothly to the final "failure" domain Ω (Betz et al. 2018b). In addition, the limit state function $\hat{h}(\mathbf{x}, p)$ avoids numerical problems when the likelihood function $L(\mathbf{x}|\mathbf{z})$ becomes very small for certain values $\mathbf{x}$.

The original SuS algorithm presented in Section 2.2.3 is adapted as summarized in Algorithm 3.2 such that K samples falling into domain Ω are return in addition to the probability of the observation event Z.

Algorithm 3.2: BUS with SuS in **U**-space (Straub and Papaioannou 2015b)

Input: p_0 (value of conditional probabilities), N (number of samples per subset level), K (number of required samples of the posterior distribution) and $\hat{H}(\mathbf{u})$ (equivalent limit state function defined in Equation (3.26) describing the observation event Z in **U**-space)

1. Generate N i.i.d. samples $\mathbf{u}_0^{(j)}$, $j = 1, \dots, N$ from $\varphi_{n+1}(\mathbf{u})$.

2. Set b_1 equal to the p_0-quantile of the samples $\hat{H}(\mathbf{u}_0^{(j)})$, $j = 1, \dots, N$.

3. Initialize the counter $i = 1$.

4. While $b_i > 0$:

   a. Increase the counter $i = i + 1$.

   b. Use the N_0 samples for which $\hat{H}(\mathbf{u}) \leq b_{i-1}$ as seeds to generate $N - N_0$ additional samples using an MCMC sampling algorithm, making up a total of N conditional samples $\mathbf{u}_{i-1}^{(j)}$, $j = 1, \dots, N$ distributed according to $\varphi_{n+1}(\mathbf{u}|E_{i-1})$.

   c. Set b_i equal to the p_0-quantile of the samples $\hat{H}(\mathbf{u}_{i-1}^{(j)})$, $j = 1, \dots, N$.

5. Evaluate $\hat{P}_M$ according to Equation (2.19) with $i = M$.

6. Evaluate $\hat{P}_{SuS} = \Pr(Z) = p_{acc}$ according to Equation (2.21)

7. Use the K_0 samples for which $\hat{H}(\mathbf{u}) \leq 0$ as seeds to generate $K - K_0$ additional samples using an MCMC sampling algorithm, making up a total of K conditional samples $\mathbf{u}^{(j)}$, $j = 1, \dots, K$ distributed according to $\varphi_{n+1}(\mathbf{u}|Z)$.

8. Transform the samples $\mathbf{u}^{(j)}$ to the original outcome space as $\mathbf{x}^{(j)} = T^{-1}(u_1^{(j)}, \dots, u_n^{(j)})$, $j = 1, \dots, K$ to obtain samples from the posterior distribution.

9. Return $\Pr(Z)$ and $\mathbf{x}^{(j)}$, $j = 1, \dots, K$.

3.4 BUS for failure probabilities

Straub (2011a) and Straub et al. (2016) apply BUS to perform Bayesian updating of failure probabilities. First, the posterior PDF $f_{\mathbf{X}|\mathbf{Z}}(\mathbf{x}|\mathbf{z})$ defined in Equation (3.14) is rewritten in terms of the limit state function $h(\mathbf{x}, p)$:

$$f_{\mathbf{X}|\mathbf{Z}}(\mathbf{x}|\mathbf{z}) = \frac{\int_0^1 \mathbb{I}[h(\mathbf{x}, p) \leq 0]\, f_{\mathbf{X}}(\mathbf{x})\, f_P(p)\, \mathrm{d}p}{\int_{D_{\mathbf{X}}} \int_0^1 \mathbb{I}[h(\mathbf{x}, p) \leq 0]\, f_{\mathbf{X}}(\mathbf{x})\, f_P(p)\, \mathrm{d}p\, \mathrm{d}\mathbf{x}} \tag{3.27}$$

The conditional probability of the failure event F given that $\mathbf{Z} = \mathbf{z}$ has been observed is obtained by integrating the posterior PDF $f_{\mathbf{X}|\mathbf{Z}}(\mathbf{x}|\mathbf{z})$ over the failure domain $\Omega_F = \{\mathbf{x} : g(\mathbf{x}) \leq 0\}$:

$$\Pr(F|\mathbf{Z} = \mathbf{z}) = \int_{g(\mathbf{x}) \leq 0} f_{\mathbf{X}|\mathbf{Z}}(\mathbf{x}|\mathbf{z}) \, d\mathbf{x} = \frac{\int_{g(\mathbf{x}) \leq 0} \int_0^1 \mathbb{I}[h(\mathbf{x}, p) \leq 0] \, f_{\mathbf{X}}(\mathbf{x}) \, f_P(p) \, dp \, d\mathbf{x}}{\int_{D_{\mathbf{X}}} \int_0^1 \mathbb{I}[h(\mathbf{x}, p) \leq 0] \, f_{\mathbf{X}}(\mathbf{x}) \, f_P(p) \, dp \, d\mathbf{x}} \tag{3.28}$$

Equation (3.28) can be rewritten to show that conditioning the failure probability on $\mathbf{Z} = \mathbf{z}$ is equivalent to conditioning it on the event Z defined by Equation (3.20):

$$\begin{aligned}
\Pr(F|\mathbf{Z} = \mathbf{z}) &= \frac{\int_{g(\mathbf{x}) \leq 0 \, \cap \, h(\mathbf{x}, p) \leq 0} f_{\mathbf{X}}(\mathbf{x}) \, f_P(p) \, dp \, d\mathbf{x}}{\int_{h(\mathbf{x}, p) \leq 0} f_{\mathbf{X}}(\mathbf{x}) \, f_P(p) \, dp \, d\mathbf{x}} \\[2mm]
&= \frac{\Pr[g(\mathbf{X}) \leq 0 \cap h(\mathbf{X}, P) \leq 0]}{\Pr[h(\mathbf{X}, P) \leq 0]} \\[2mm]
&= \Pr(F|Z)
\end{aligned} \tag{3.29}$$

$\Pr(F|Z)$ can be expressed in terms of the standard normal variables $\mathbf{U}$:

$$\Pr(F|Z) = \frac{\Pr[G(\mathbf{U}) \leq 0 \cap H(\mathbf{U}) \leq 0]}{\Pr[H(\mathbf{U}) \leq 0]} \tag{3.30}$$

The numerator of Equation (3.30) corresponds to a parallel system reliability problem and the denominator to a component reliability problem. Straub (2011a) and Straub et al. (2016) show how these problems can be solved with different structural reliability methods.

An illustration of BUS for failure probabilities is shown in Figure 3.4.
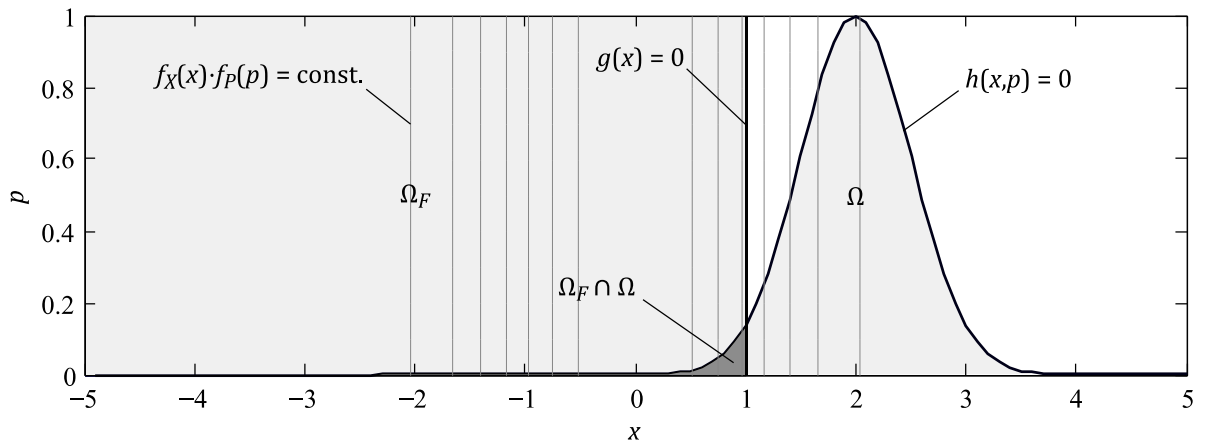
Figure 3.4: Illustration of BUS for failure probabilities (following Straub and Papaioannou 2015b). The limit state function describing failure is $g(x) = x - 1$. X is standard normal distributed and measured to be 2. The measurement is subject to a normal distributed additive measurement error with zero mean and standard deviation 0.5. The likelihood function describing this measurement $L(x|2) = 1/(0.5 \cdot \sqrt{2\pi}) \cdot \exp(-1/2 \cdot (2 - x)^2/0.5^2)$. The constant c is selected as $c = 0.5 \cdot \sqrt{2\pi}$.

4 Reliability of deteriorating structural systems

This section is adapted from Straub, D., Schneider, R., Bismut, E. and Kim, H.-J. (2020). Reliability analysis of deteriorating structural systems. *Structural Safety* **82**: 101877. Some passages and figures are directly taken from this reference.

4.1 Introduction

The demand on a structural system is generally time-variant, and its capacity also typically changes with time due to deterioration processes. In this case, failure of a structural system is described by a time-dependent limit state function[3] $g(\mathbf{x}, t)$ as a function of the stochastic parameters $\mathbf{X}$ that influence the system's condition and performance (Ditlevsen and Madsen 1996; Melchers 1999). Depending on the nature of these parameters, they are probabilistically modeled as random variables (e.g. non-ergodic parameters such as material strengths, model uncertainties and statistical uncertainties) or random processes (e.g. loads and environmental conditions randomly varying in time). The limit state function $g(\mathbf{x}, t)$ includes a physics-based engineering model of the structure and the deterioration processes. When the limit state function g depends on time t, the structural reliability problem is said to be time-variant.

As usual, a negative value of the limit state function $g(\mathbf{x}, t)$ corresponds to structural failure. It is thus possible to define a time-dependent failure event (of some sort) as:

$$F^*(t) = \{g(\mathbf{X}, t) \leq 0\} \tag{4.1}$$

This event is commonly called the point-in-time (or instantaneous) failure event. The corresponding point-in-time (or instantaneous) failure probability is given by:

$$\Pr[F^*(t)] = \Pr[g(\mathbf{X}, t) \leq 0] \tag{4.2}$$

$\Pr[F^*(t)]$ is often used as a metric for describing the reliability of deteriorating structural systems (e.g. Sarveswaran and Roberts 1999; Bastidas-Arteaga et al. 2009; Barone and Frangopol 2014; Schneider et al. 2015a; Schneider et al. 2017). However, this probability does not capture what happened before time t, and thus neglects the possibility that the structure might have already failed earlier. In time-variant structural reliability, one is instead interested in the event of failure at any time up to t, which can be written as:

$$F(t) = \{\exists \tau \in [0, t] : g(\mathbf{X}, \tau) \leq 0\} \tag{4.3}$$

or, equivalently,

---

[3] see also Footnote 2 on Page 17

$$F(t) = \left\{ \left(\min_{\tau \in [0,t]} g(\mathbf{X}, \tau) \right) \leq 0 \right\} \tag{4.4}$$

Applying the definition in Equation (4.4), the (cumulative) probability of failure within the time interval $[0, t]$ is:

$$\Pr[F(t)] = \Pr \left[\left(\min_{\tau \in [0,t]} g(\mathbf{X}, \tau) \right) \leq 0 \right] \tag{4.5}$$

This probability must be used to quantify the reliability of deteriorating structural systems. Importantly, all measures commonly utilized to describe the time-dependent reliability of engineering systems can be expressed as a function of $\Pr[F(t)]$ (Rausand and Høyland 2004; Straub 2018a). Four important measures are the cumulative distribution function (CDF) of the time to failure T_F

$$F_{T_F}(t) = \Pr(T_F \leq t) = \Pr[F(t)] \tag{4.6}$$

the corresponding probability density function (PDF)

$$f_{T_F}(t) = \frac{\mathrm{d}F_{T_F}(t)}{\mathrm{d}t} = \frac{\mathrm{d}\Pr[F(t)]}{\mathrm{d}t} \tag{4.7}$$

the reliability of the structure

$$Rel(t) = \Pr(T_F > t) = 1 - \Pr[F(t)] \tag{4.8}$$

and the failure rate or hazard function[4]

$$\lambda(t) = \frac{f_{T_F}(t)}{Rel(t)} = \frac{1}{1 - \Pr[F(t)]} \cdot \frac{\mathrm{d}\Pr[F(t)]}{\mathrm{d}t} \tag{4.9}$$

An additional quantity, which is relevant for decision making purposes in design as well as in operation and maintenance of deteriorating structural systems, is the risk associated with structural failure during the system's service life. The net-present value of the service life risk is computed as a function of the PDF of the time to failure $f_{T_F}(t)$ (Rackwitz 2000; Straub 2018a):

$$Risk(T_{SL}) = \int_0^{T_{SL}} c_F(t) \exp(-\gamma t) f_{T_F}(t) \, \mathrm{d}t \tag{4.10}$$

where T_{SL} is the (finite) service life of the structure, $c_F(t)$ is the cost associated with failure at time t and γ is the continuously compounded discount rate. The PDF $f_{T_F}(t)$ can be computed from $\Pr[F(t)]$ (see Equation (4.7)).

---

[4] The failure rate $\lambda(t)$ is the limit of the probability that failure occurs in the interval $(t, t + \Delta t]$ given that no failure has occurred prior to time t (Rausand and Høyland 2004), i.e. $\lim_{\Delta t \to 0} \Pr(t < T_F \leq t + \Delta t | T_F > t)/\Delta t = \lim_{\Delta t \to 0} [F_{T_F}(t + \Delta t) - F_{T_F}(t)]/[\Delta t \cdot Rel(t)] = f_{T_F}(t)/Rel(t)$.

It can be concluded that the reliability of a deteriorating structural system without maintenance is fully described by the failure probability $\Pr[F(t)]$. An estimation of $\Pr[F(t)]$ requires the solution of a time-variant reliability problem (Ditlevsen and Madsen 1996; Melchers 1999). Solving this type of problem is – in the general case – challenging. In most applications, however, deteriorating structural systems can be represented by a combination of deterioration and structural models, which allow a transformation of the time-variant reliability problem into a series of time-invariant reliability problems. The two classes of stochastic models for deteriorating structures that enable such a transformation are presented in Sections 4.2 and 4.3. The general case is briefly discussed in Section 4.4. Subsequently, the effect of inspection and monitoring as well as the effect of maintenance on the reliability of deteriorating structural systems is discussed in Sections 4.5 and 4.6.

4.2 Stochastic deterioration models resulting in monotonically decreasing limit state functions

The first common class of stochastic models for deteriorating structures – denoted as model class (a) – is illustrated Figure 4.1. Models of this class typically predict deterioration by a function $h_D(\mathbf{X}, t)$, which is monotonically increasing with time t for any realization of the stochastic input parameters $\mathbf{X}$. Failure is considered to occur when the accumulated damage due to deterioration exceeds a damage threshold D_{cr}, which – in the general case – is modeled by a random variable and included in $\mathbf{X}$. The resulting generic limit state function is:

$$g(\mathbf{x}, t) = d_{cr} - h_D(\mathbf{x}, t) \tag{4.11}$$

Limit state functions of this format are monotonically decreasing with time t for any value of $\mathbf{X}$. An example belonging to this class of models is fatigue crack growth modeled with Paris' law, when an equivalent stress range is applied to represent the random sequence of stress ranges, and when failure is defined as the exceedance of a critical crack size (see also Section 5.7.1.2). This class also includes deterioration models based on gamma processes, where failure occurs when the resistance falls below a threshold (see, for example, van Noortwijk 2009).

When the limit state function $g(\mathbf{x}, t)$ is a monotonically decreasing function, it will be negative at time t if it is negative at any time before t. As a consequence, all point-in-time failure events
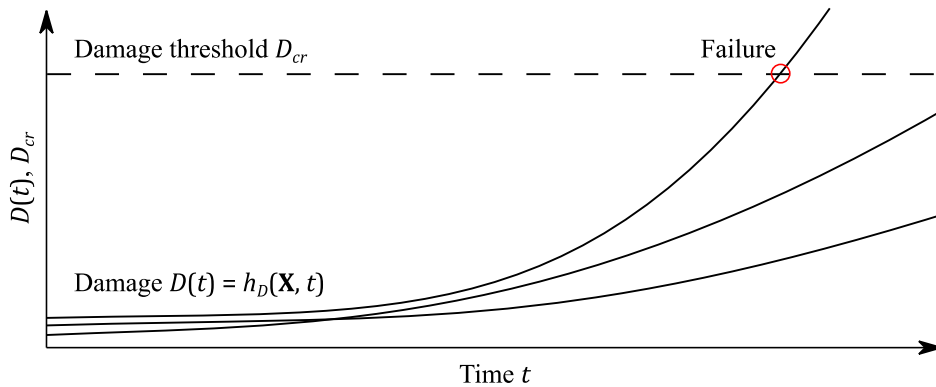
Figure 4.1: First common class of stochastic models for deteriorating structures (adapted from Straub et al. 2020). Models of this class lead to a monotonically decreasing limit state function with time t.

$F^*(\tau) = \{g(\mathbf{X}, \tau) \leq 0\}$ with $\tau < t$ are subsets of the failure event $F^*(t) = \{g(\mathbf{X}, t) \leq 0\}$, and the probability of failure in the time interval $[0, t]$ is equal to the point-in-time failure probability at time t:

$$
\begin{aligned}
\Pr[F(t)] &= \Pr\left[\left(\min_{\tau \in [0,t]} g(\mathbf{X}, \tau)\right) \leq 0\right] \\
&= \Pr[g(\mathbf{X}, t) \leq 0] \\
&= \Pr[F^*(t)]
\end{aligned}
\tag{4.12}
$$

From Equation (4.12) it follows that – in this special case – the computation of $\Pr[F(t)]$ simply involves the solution of a sequence of time-invariant reliability problems.

Note that this simplified formulation is invalid if the effect of maintenance (e.g. repair, exchange or retrofitting actions) is included in the reliability analysis because the limit state function $g(\mathbf{x}, t)$ will not be monotonically decreasing in this case (see also Section 4.6).

4.3 Deteriorating structures with separable demand and capacity parameters

The second common class of stochastic models for deteriorating structures – denoted by model class (b) – includes those models in which the random variables or processes $\mathbf{X}$ can be separated into a group $\mathbf{X}_R$ influencing the capacity of the structure and a group $\mathbf{X}_S$ determining the demand on the structure. In the simplest case, as illustrated in Figure 4.2, the demand on the structure can be characterized by a scalar random process $S(\mathbf{X}_S, t)$ and the capacity of the structure with respect to this demand is $R(\mathbf{X}_R, t)$. Depending on the formulation of the problem, the demand $S(\mathbf{X}_S, t)$ can be a load or a load effect. In the former case, $\mathbf{X}_S$ may represent the uncertainty in the parameters of the distribution of $S(\mathbf{X}_S, t)$. In the latter case, $\mathbf{X}_S$ may represent the uncertainty in structural properties. For the sake of simplicity, the dependence of S on $\mathbf{X}_S$ is dropped in the following. The
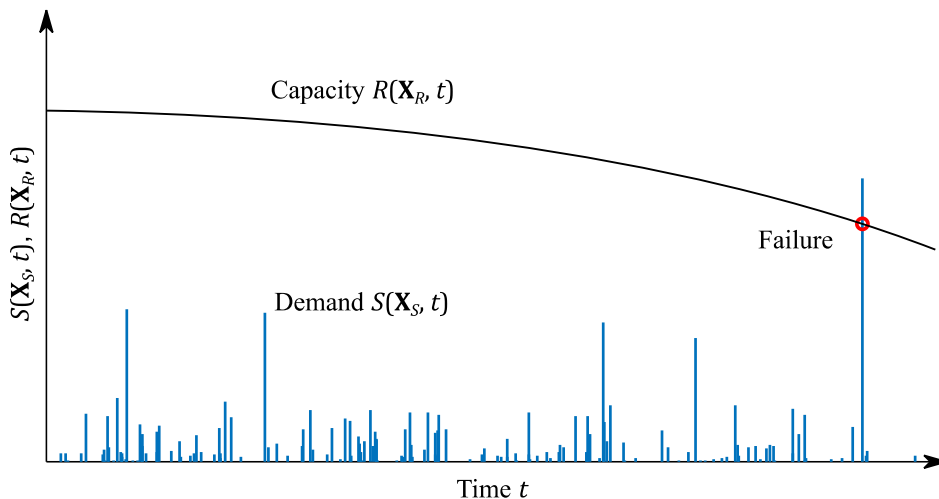
Figure 4.2: Illustration of the second common class of stochastic models for deteriorating structures. Models of this class include those in which the deteriorating capacity $R(\mathbf{X}_R, t)$ can be modeled statistically independent of the demand $S(\mathbf{X}_S, t)$.

capacity $R(\mathbf{X}_R, t)$ includes the deterioration processes and is a monotonically decreasing function of time t for any value of $\mathbf{X}_R$. The parameters of the deterioration model are included in $\mathbf{X}_R$.

The time-dependent reliability of deteriorating structures that can be represented by stochastic models of model class (b) can be approximated by a discrete-time approach. In this approach, time is divided into intervals $j = 1, \ldots, m$ such that the jth interval corresponds to $t \in (t_{j-1}, t_j]$. The length of the interval depends on the overall service life of the structure, on the length of inspection and maintenance intervals and on how fast deterioration progresses. A typical choice are yearly intervals.

An interval failure event F_j^* can now be defined as the event of failure in the interval $(t_{j-1}, t_j]$, without considering – like the point-in-time failure event $F^*(t)$ – the possibility that the structure may have failed earlier.

$$F_j^* = \{\exists \tau \in (t_{j-1}, t_j] : R(\mathbf{X}_R, \tau) \leq S(\tau)\} \tag{4.13}$$

An evaluation of the corresponding interval failure probability $\Pr(F_j^*)$ requires the solution of a first-passage problem (see Section 4.4). However, if $S(t)$ and $R(\mathbf{X}_R, t)$ are statistically independent, a conservative approximation of $\Pr(F_j^*)$ can be obtained as:

$$\Pr(F_j^*) \approx \Pr[R(\mathbf{X}_R, t_j) \leq S_{max,j}] \tag{4.14}$$

where $R(\mathbf{X}_R, t_j)$ is the capacity at the end of the jth interval, and

$$S_{max,j} = \max_{t \in (t_{j-1}, t_j]} S(t) \tag{4.15}$$

is the maximum demand in that interval (a statistic of $S(t)$). The distribution of $S_{max,j}$ can be obtained by performing an extreme value analysis. The probability $\Pr[R(\mathbf{X}_R, t_j) \leq S_{max,j}]$ can be computed by performing a time-invariant reliability analysis.

In most applications, the requirement of statistical independence among $S(t)$ and $R(\mathbf{X}_R, t)$ is (at least approximately) fulfilled. An example is high-cycle fatigue where fatigue damage is mainly caused by average load conditions, and only a minor portion of the damage is accumulated during extreme load events (see also Madsen et al. 1986). In contrast, the assumption of statistical independence among demand and capacity does not hold if a structure is subject to low-cycle fatigue. In this case, fatigue damage is mainly caused by stress cycles during extreme load events, and fatigue failure and structural failure can occur during the same load event.

Most structures are subject to the joint effect of several loads, and the demand on a structure is characterized by a vector $\mathbf{S}(t)$, which may again depend on additional random variables $\mathbf{X}_S$. If more than one load is time-variant, a load-combination problem must be considered in the computation of the interval failure probability $\Pr(F_j^*)$ (Melchers 1999). Several approximate solutions to the load combination problem are available (see, for example, Rackwitz and Fiessler 1978; Turkstra and Madsen 1980; Melchers 1999). Ditlevsen (2002) describes an approximate solution to this problem, which can be applied if one time-variant load is dominating. In this solution, the dominant time-variant load is represented by an extreme value distribution for the interval j and

the remaining time-variant loads are modeled by conditional distributions. The loads are then summarized in the vector $\mathbf{S}_{max,j}$ for the interval j. The interval failure probability $\Pr(F_j^*)$ is then computed as:

$$\Pr(F_j^*) \approx \Pr[g(\mathbf{X}_R, \mathbf{S}_{max,j}, t_j) \leq 0] \tag{4.16}$$

where $g(\mathbf{X}_R, \mathbf{S}_{max,j}, t_j)$ describes the interval failure event F_j^* in analogy to the simple expression in Equation (4.14), i.e. failure in interval j occurs if the maximum of the demand in the interval exceeds the capacity at the end of the interval. In the following, it is assumed that the limit state function $g(\mathbf{X}_R, \mathbf{S}_{max,j}, t_j)$ can be formulated.

Now consider the event of failure up to time t_j, which is denoted by $F(t_j)$. This event corresponds to the union of the interval failure events leading up to time t_j:

$$F(t_j) = F_1^* \cup F_2^* \cup \ldots \cup F_j^* \tag{4.17}$$

The corresponding probability of failure up to time t_j is

$$\Pr[F(t_j)] = \Pr(F_1^* \cup F_2^* \cup \ldots \cup F_j^*) \tag{4.18}$$

This corresponds to a series system reliability problem among the interval failure events leading up to time t_j. Hence, the following simple bounds can be defined for $\Pr[F(t_j)]$ (see also Equation (2.24)):

$$\max_{i \in \{1,\ldots,j\}} \Pr(F_i^*) \leq \Pr[F(t_j)] \leq \sum_{i=1}^{j} \Pr(F_i^*) \tag{4.19}$$

The statistical dependence among the interval failure events F_i^* will be positive, if the maximum demands $\mathbf{S}_{max,i}$ are statistically independent, or if their statistical dependence is positive[5]. In this case, a narrower upper bound can be defined (see also Equation (2.25)):

$$\max_{i \in \{1,\ldots,j\}} \Pr(F_i^*) \leq \Pr[F(t_j)] \leq 1 - \prod_{i=1}^{j} [1 - \Pr(F_i^*)] \tag{4.20}$$

Note that the failure probability $\Pr[F(t_j)]$ will be closer to the upper bound if the reliability is dominated by the uncertainty on the time-variant loads and if their maxima in different intervals are independent or weakly correlated. It will, however, be closer to the lower bound if the reliability is dominated (a) by the uncertainty on the capacity or the time-invariant loads; or (b) by the uncertainty on the time-variant loads and if their maxima in different intervals are strongly correlated.

The computation of the failure probability $\Pr[F(t_j)] = \Pr(F_1^* \cup F_2^* \cup \ldots \cup F_j^*)$ requires the solution of a series system problem, which is computationally more demanding than the evaluation of the individual interval failure probabilities $\Pr(F_i^*)$. In Section 5, a strategy for computing $\Pr[F(t_j)]$

---

[5] Note that the capacities $R(\mathbf{X}_R, t_i)$ will be positively correlated among different t_i.

is proposed, which can be applied when the structural system performance is described by the conditional probability of failure in any interval i given the structural condition at the end of the interval. Subsequently, Section 6 discusses how deteriorating structural systems that can be represented by model class (b) are modeled with hierarchical dynamic Bayesian networks (DBN). Based on the hierarchical DBN, the interval failure probabilities $\Pr(F_i^*)$ of the system are computed. The failure probability $\Pr[F(t_j)]$ is then approximated by the upper bound in Equation (4.20). Such an approximation has been frequently applied in the past (see, for example, Val et al. 2000; Stewart and Al-Harthy 2008).

Once the probabilities $\Pr[F(t_j)]$ for times t_j, $j = 1, \dots, m$ are available, the cumulative distribution function of the time to failure $F_{T_F}(t) = \Pr[F(t)]$ can be approximated by interpolation. The reliability $Rel(t)$ and the failure rate $\lambda(t)$ can subsequently be computed based on the approximation of $F_{T_F}(t)$ (see Section 4.1).

4.4 General case: the first-passage problem

In the general case, as illustrated in Figure 4.3, failure of a deteriorating structure is considered to occur when the time-dependent limit state function $g(\mathbf{x}, t)$ takes a negative value for the first time. The problem of estimating the cumulative distribution function $F_{T_F}(t) = \Pr[F(t)]$ of the time to failure T_F is known as the first-passage (or outcrossing) problem. The usual approach to solving this type of problem is the outcrossing approach (Rackwitz 2001). This approach has been used in the literature to compute the reliability of relatively simple deteriorating structures (see, for example, Schall et al. 1991; Andrieu-Renaud et al. 2004). However, challenges arise if it is applied to large deteriorating structures subject to arbitrary load processes. In addition, it is important to realize that available solutions to the outcrossing problem introduce approximation errors of their own. Consequently, the outcrossing approach should only be applied if the problem cannot be represented by model class (a) or (b).

For the sake of completeness, the main principles of the outcrossing approach are briefly summarized in the following. Let $N^+(t)$ be the random number of crossings of $g(\mathbf{X}, t)$ from a positive to a negative value in the time interval $(0, t]$. Failure in the time interval $[0, t]$ occurs if the structure fails at time $t = 0$ or if $N^+(t) > 0$. Hence, the failure probability $\Pr[F(t)]$ can also be written as:
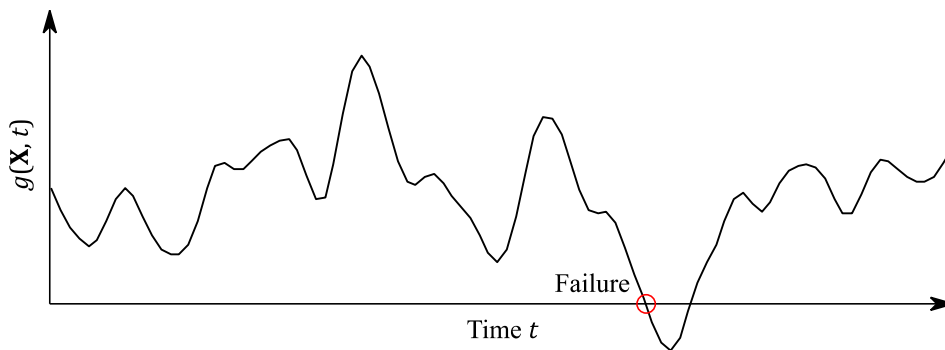
Figure 4.3: Illustration of the first-passage (or outcrossing) problem.

$$\Pr[F(t)] = \Pr[\{g(\mathbf{X}, 0) \leq 0\} \cup \{N^+(t) > 0\}] \tag{4.21}$$

Bounds on $\Pr[F(t)]$ can be found as (Shinozuka 1964; Bolotin 1981):

$$\max_{\tau \in [0,t]} \Pr[F^*(\tau)] \leq \Pr[F(t)] \leq \Pr[F^*(0)] + \mathbb{E}[N^+(t)] \tag{4.22}$$

where $\Pr[F^*(\tau)]$ is the point-in-time failure probability and $\mathbb{E}[N^+(t)]$ is the expected number of outcrossings in the time interval $(0, t]$. The upper bound in Equation (4.22) is typically applied as an approximation of the failure probability $\Pr[F(t)]$.

The expected number of outcrossings $\mathbb{E}[N^+(t)]$ is determined from the outcrossing rate $\nu^+(\tau)$, which is defined as (Rackwitz 2001):

$$\nu^+(\tau) = \lim_{\Delta\tau \to 0} \frac{\Pr[\{g(\mathbf{X}, \tau) > 0\} \cap \{g(\mathbf{X}, \tau + \Delta\tau) \leq 0\}]}{\Delta\tau} \tag{4.23}$$

if the point process of outcrossings is a regular process, i.e. if the probability of having more than one outcrossing in the time interval $[\tau, \tau + \Delta\tau]$ is negligibly small when $\Delta\tau \to 0$. Under this regularity condition, $\mathbb{E}[N^+(t)]$ can be computed as (Rackwitz 2001):

$$\mathbb{E}[N^+(t)] = \int_0^t \nu^+(\tau)\, d\tau \tag{4.24}$$

Analytical and asymptotic solutions for the outcrossing rate $\nu^+(\tau)$ are available in the literature for the case when the limit state function g only depends on sufficiently mixing random processes (see, for example, Ditlevsen and Madsen 1996; Melchers 1999; Rackwitz 2006).

When modeling deteriorating structures, the limit state function g typically depends on random processes and time-invariant random variables. In this case, an approach proposed by Schall et al. (1991) can be applied, which separates the stochastic parameters $\mathbf{X}$ into sufficiently mixing random processes $\mathbf{S}$, slowly mixing random processes $\mathbf{Q}$ having slow fluctuations compared to $\mathbf{S}$, and time-invariant random variables $\mathbf{R}$. The conditional outcrossing rate

$$\nu^+(\tau|\mathbf{Q} = \mathbf{q}, \mathbf{R} = \mathbf{r}) = \lim_{\Delta\tau \to 0} \frac{\Pr[\{g(\mathbf{S}, \mathbf{q}, \mathbf{r}, \tau) > 0\} \cap \{g(\mathbf{S}, \mathbf{q}, \mathbf{r}, \tau + \Delta\tau) \leq 0\}]}{\Delta\tau} \tag{4.25}$$

is then determined based on analytical and asymptotic solutions. Subsequently, the conditional expected number of outcrossings is evaluated as:

$$\mathbb{E}[N^+(t)|\mathbf{Q} = \mathbf{q}, \mathbf{R} = \mathbf{r}] = \int_0^t \nu^+(\tau|\mathbf{Q} = \mathbf{q}, \mathbf{R} = \mathbf{r})\, d\tau \tag{4.26}$$

Finally, the (unconditional) expected number of outcrossings is obtained by taking the expectation with respect to $\mathbf{Q}$ and $\mathbf{R}$:

$$\mathbb{E}[N^+(t)] = \mathbb{E}_{Q,R}\big[\mathbb{E}[N^+(t)|\mathbf{Q} = \mathbf{q}, \mathbf{R} = \mathbf{r}]\big] = \mathbb{E}_{Q,R}\left[\int_0^t \nu^+(\tau|\mathbf{Q} = \mathbf{q}, \mathbf{R} = \mathbf{r})\, d\tau\right] \qquad (4.27)$$

Alternatively, parallel system concepts can be applied, which directly solve Equation (4.23) to compute the outcrossing rate $\nu^+(\tau)$ (Andrieu-Renaud et al. 2004; Sudret 2008).

4.5 Deteriorating structures with inspection and monitoring data

Inspection and monitoring data contain information on the stochastic parameters $\mathbf{X}$ that influence the condition and reliability of deteriorating structural systems. In structural reliability, data obtained up to time t_Z is described by the event $Z(t_Z)$ and Bayes' rule is applied to learn the probability distribution of $\mathbf{X}$, i.e. the prior probability distribution $f_{\mathbf{X}}(\mathbf{x})$ of $\mathbf{X}$ is updated with $Z(t_Z)$ to the posterior probability distribution $f_{\mathbf{X}}[\mathbf{x}|Z(t_Z)]$ (see also Section 3.3). Consequently, the estimate of the failure probability is also updated. The updated failure probability is $\Pr[F(t)|Z(t_Z)]$ (see also Section 3.4). Note that the information obtained through inspections and monitoring does not change the actual condition and reliability of the structural system as it does not physically change the system. However, the information enables an improved estimation of the system condition and reliability and thus an improved decision-making regarding actions that physically change the system (e.g. repair and retrofitting actions).

For model class (a), the probability of failure at time t conditional on data obtained up to time t_Z is equal to the point-in-time failure probability at time t, i.e. $\Pr[F(t)|Z(t_Z)] = \Pr[F^*(t)|Z(t_Z)]$. In this case, it is sufficient to compute $\Pr[F^*(t)|Z(t_Z)]$.

For model class (b), the failure probability at time t_j conditional on $Z(t_Z)$ is given by:

$$\Pr[F(t_j)|Z(t_Z)] = \Pr[F_1^* \cup F_2^* \cup \dots \cup F_j^*|Z(t_Z)] \qquad (4.28)$$

Equation (4.28) implies that all interval failure events F_1^* to F_j^* must be considered in the computation of $\Pr[F(t_j)|Z(t_Z)]$. The updated failure probability $\Pr[F(t)|Z(t_Z)]$ is approximated by interpolation based on the updated failure probabilities $\Pr[F(t_j)|Z(t_Z)]$ for times t_j, $j = 1, \dots, m$.

When applying the outcrossing approach, the conditional point-in-time failure probability $\Pr[F^*(0)|Z(t_Z)]$ and the conditional expected number of outcrossings $\mathbb{E}[N^+(t)|Z(t_Z)]$ must be evaluated based on the conditional probability distribution of the stochastic parameters $\mathbf{X}$ given $Z(t_Z)$. $\Pr[F^*(0)|Z(t_Z)]$ and $\mathbb{E}[N^+(t)|Z(t_Z)]$ are then applied to compute an updated estimate of the upper bound of the updated failure probability $\Pr[F(t)|Z(t_Z)]$ (see Equation (4.22)).

Once the updated failure probability $\Pr[F(t)|Z(t_Z)]$ is available, the updated PDF of the time to failure $f_{T_F}[t|Z(t_Z)]$, the updated reliability $Rel[t|Z(t_Z)]$ and the updated failure rate $\lambda[t|Z(t_Z)]$ are computed by substituting $\Pr[F(t)]$ in Equations (4.7) to (4.9) with $\Pr[F(t)|Z(t_Z)]$.

In the literature, the updated probability of the failure event $F(t)$ is typically presented conditional on the inspection and monitoring data available up to time t, i.e. it is shown as $\Pr[F(t)|Z(t)]$. This process is known as filtering (Straub 2009) and illustrated in Figure 4.4(a), which shows the filtered failure probability of the welded jacket-type steel frame considered in the numerical example
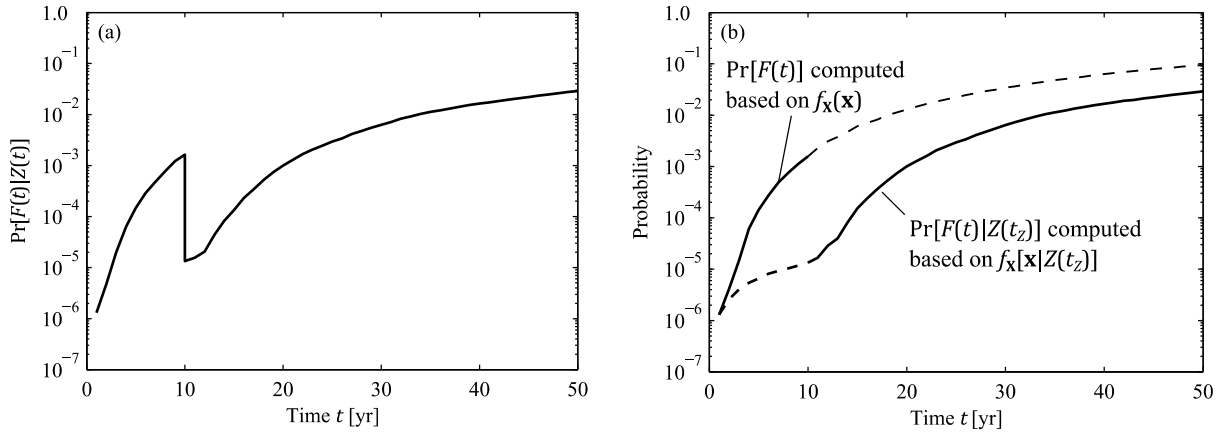
Figure 4.4: (a) Filtered failure probability $\Pr[F(t)|Z(t)]$ of the welded steel frame considered in Section 5.7.1 (the results are reproduced from Figure 5.14(b)). The frame is subject to high-cycle fatigue and some of its welded connections are inspected in year $t_Z = 10$ yr. No fatigue cracks are indicated. (b) Prior and posterior failure probability $\Pr[F(t)]$ and $\Pr[F(t)|Z(t_Z)]$ of the frame.

in Section 5.7.1. The frame is subject to high-cycle fatigue and some of its welded connections are inspected in year $t_Z = 10$ yr. The inspections do not indicate any fatigue cracks. The results in Figure 4.4(a) are reproduced from Figure 5.14(b) and demonstrate that conditioning the failure probability on data obtained at time t_Z can lead to a drop in that probability. Such a drop in the (cumulative) failure probability seems counterintuitive since it is a non-decreasing function of time. This effect can be explained by the fact that the failure probability before and after the updating is not based on the same data and thus not on the same probability distribution of the parameters $\mathbf{X}$ (see also Schneider and Straub 2020). In this example, the failure probability shown in Figure 4.4(a) for times $t \leq t_Z$ (before the updating) is computed based on the prior probability distribution $f_{\mathbf{X}}(\mathbf{x})$ whereas the failure probability for times $t \geq t_Z$ (after the updating) is estimated based on the posterior probability distribution $f_{\mathbf{X}}[\mathbf{x}|Z(t_Z)]$. To further illustrate this, Figure 4.4(b) separately shows the prior failure probability $\Pr[F(t)]$ computed based on $f_{\mathbf{X}}(\mathbf{x})$ and the posterior failure probability $\Pr[F(t)|Z(t_Z)]$ computed based on $f_{\mathbf{X}}[\mathbf{x}|Z(t_Z)]$ for times prior to and after t_Z. The results in Figure 4.4(b) also demonstrate that updating of the probability distribution of $\mathbf{X}$ with data obtained at time t_Z affects the reliability estimates before and after t_Z. The process of computing $\Pr[F(t)|Z(t_Z)]$ for times $t < t_Z$ is known as smoothing (see also Straub 2009).

Related to the above, it has been argued that if data are obtained at time t_Z, the period before t_Z can be neglected because the structure must have survived up to that time. However, the history prior to time t_Z cannot be neglected[6] since the observation of survival up to time t_Z contains valuable information, i.e. survival up to time t_Z is an indication that the structure has a certain minimum capacity and that the demand is not excessively large. In addition, the observation of survival up to the time of inspection and monitoring is not independent of the inspection and monitoring data. To formally include (a) the observation of survival up to time t_Z and (b) the inspection and monitoring data obtained up to that time in the prediction of the failure probability for times $t \geq$

---

[6] This issue is irrelevant for model class (a) because $\Pr[F(t)|Z(t_Z)] = \Pr[F^*(t)|Z(t_Z)]$.

t_Z, one must condition the probability of failure on the survival event $\bar{F}(t_Z)$ and the event $Z(t_Z)$ describing the data, i.e.:

$$
\begin{aligned}
\Pr[F(t)|Z(t_Z) \cap \bar{F}(t_Z)] &= \frac{\Pr[F(t) \cap \bar{F}(t_Z)|Z(t_Z)]}{\Pr[\bar{F}(t_Z)|Z(t_Z)]} \\
&= \frac{\Pr[F(t)|Z(t_Z)] - \Pr[F(t_Z)|Z(t_Z)]}{1 - \Pr[F(t_Z)|Z(t_Z)]}
\end{aligned}
\tag{4.29}
$$

As an alternative to the conditional failure probability $\Pr[F(t)|Z(t_Z) \cap \bar{F}(t_Z)]$, the more general failure rate λ at any time t can be computed conditional on $Z(t_Z)$ as described above. The conditional failure rate $\lambda[t|Z(t_Z)]$ corresponds to the PDF of the time to failure T_F at time t conditional on (a) survival up to that time and (b) the data obtained up to time t_Z.

4.6 Deteriorating structures with maintenance actions

Consider again the simplest case in which the structural capacity with respect to the demand can be described by a scalar process $R(t)$[7]. Maintenance actions such as repair, replacement and retrofitting of structural elements physically change the structural system and thus affect the probabilistic distribution of $R(t)$. An action performed at time t_M is modeled by adding new random variables and/or processes describing $R(t)$ for times $t \geq t_M$ (e.g. Madsen et al. 1991; RILEM 2001; Straub 2014b; Schneider 2019).

If the structural capacity after time t_M is statistically independent of the capacity before that time, and if the demand on the structure before and after time t_M is also independent, the events before t_M do not have to be considered in the subsequent reliability analysis. Otherwise, the entire history of the structure must be considered.

The modeling of maintenance is not further discussed in this thesis.

---

[7] The dependence of R on the stochastic parameters **X** is here omitted for readability.

5 Nested reliability analysis approach

This section revises and updates material originally published in Schneider, R., Thöns, S. and Straub, D. (2017). Reliability analysis and updating of deteriorating systems with subset simulation. *Structural Safety* **64**: 20-36. Some passages and figures are directly taken from this reference.

5.1 Introduction

Most deteriorating structural systems can be represented by model class (b) described in Section 4.3. For models of this class, an estimate of the failure probability $\Pr[F(t_j)] = \Pr(F_1^* \cup F_2^* \cup \ldots \cup F_j^*)$ involves the solution of a series system reliability problem among the different interval failure events F_i^*, $i = 1, \ldots, j$, where each interval failure event itself is described by a system reliability problem. This section proposes a strategy for computing $\Pr[F(t_j)]$, which is referred to as nested reliability analysis (NRA) approach in the following. It can be applied when the conditional probability of system failure in any time interval i conditional on the structural condition at the end of the interval, $\Pr(F_i^*|\mathbf{X}_R = \mathbf{x}_R)$, can be computed efficiently. In contrast to Section 4.3, all time-invariant random variables of the problem are included in $\mathbf{X}_R$ to ensure that the interval failure events F_i^*, $i = 1, \ldots, m$ are statistically independent given $\mathbf{X}_R = \mathbf{x}_R$. Such time-invariant random variables include, for example, uncertain permanent loads, model uncertainties and statistical uncertainties. If the interval failure events F_i^*, $i = 1, \ldots, m$ are independent given $\mathbf{X}_R = \mathbf{x}_R$, the conditional failure probability can be computed as:

$$\Pr[F(t_j)|\mathbf{X}_R = \mathbf{x}_R] = 1 - \prod_{i=1}^{m}[1 - \Pr(F_i^*|\mathbf{X}_R = \mathbf{x}_R)] \tag{5.1}$$

The total probability theorem is then applied to determine the unconditional failure probability of the structural system:

$$\Pr[F(t_j)] = \int_{\boldsymbol{D}_{\mathbf{X}_R}} \Pr[F(t_j)|\mathbf{X}_R = \mathbf{x}_R] f_{\mathbf{X}_R}(\mathbf{x}_R)\, \mathrm{d}\mathbf{x}_R \tag{5.2}$$

wherein $\boldsymbol{D}_{\mathbf{X}_R}$ is the domain of definition and $f_{\mathbf{X}_R}(\mathbf{x}_R)$ is the prior PDF of $\mathbf{X}_R$.

Deteriorating structures are usually inspected and monitored to reduce the uncertainty on the structural condition. Inspection and monitoring employed for this purpose provide information on the parameters of the deterioration model, which are included in $\mathbf{X}_R$. Let the random vector $\mathbf{Z}_{1:k}$ represent the probabilistic inspection and monitoring outcomes obtained in intervals 1 to k with $k = 1, \ldots, m$. The inspection and monitoring data $\mathbf{Z}_{1:k} = \mathbf{z}_{1:k}$ are used to update the prior PDF $f_{\mathbf{X}_R}(\mathbf{x}_R)$

of $\mathbf{X}_R$ to its posterior PDF $f_{\mathbf{X}_R|\mathbf{Z}_{1:j}}(\mathbf{x}_R|\mathbf{z}_{1:k})$. Subsequently, the posterior failure probability $\Pr[F(t_j)|\mathbf{Z}_{1:k} = \mathbf{z}_{1:k}]$ is obtained by inserting $f_{\mathbf{X}_R|\mathbf{Z}_{1:k}}(\mathbf{x}_R|\mathbf{z}_{1:k})$ into Equation (5.2):

$$\Pr[F(t_j)|\mathbf{Z}_{1:k} = \mathbf{z}_{1:k}] = \int_{D_{\mathbf{X}_R}} \Pr[F(t_j)|\mathbf{X}_R = \mathbf{x}_R] f_{\mathbf{X}_R|\mathbf{Z}_{1:k}}(\mathbf{x}_R|\mathbf{z}_{1:k}) \ \mathrm{d}\mathbf{x}_R \tag{5.3}$$

Following a discussion on modeling of deterioration, and on modeling of information provided by inspection and monitoring data in Sections 5.2 and 5.3, Sections 5.4 and 5.5 show how the integrals in Equations (5.2) and (5.3) can be transformed into component reliability problems. The resulting component reliability problems are potentially high-dimensional. They are here solved by means of subset simulation as discussed in Section 5.6. The NRA approach is demonstrated in two numerical examples in Section 5.7 considering an inspected steel frame and a monitored Daniels system subject to high-cycle-fatigue and time-variant loading.

5.2 Deterioration modeling

5.2.1 Generic system deterioration model

Deterioration in structural systems is modeled at the structural element level since probabilistic deterioration models are mainly available at this level. An element may be a structural member, a welded connection or a segment of a continuous surface (Straub and Der Kiureghian 2011). In a discrete-time approach, deterioration is evaluated at the end of each time interval. Let the random variable (or random vector) $D_{i,j}$ represent the condition of element i at the end of the jth interval. The relation between the deterioration model parameters and $D_{i,j}$ is described by a deterioration model $h_{D,i}$. Noting again that the capacity parameters $\mathbf{X}_R$ include those influencing deterioration, the deterioration model $h_{D,i}$ is written in generic form as:

$$D_{i,j} = h_{D,i}(\mathbf{X}_R, t_j) \tag{5.4}$$

In this formulation, additional random variables are included in $\mathbf{X}_R$ to account for (a) model uncertainties arising from a simplified representation of the actual deterioration phenomenon and from omitting parameters that also influence the deterioration process, and (b) statistical uncertainties due to the limited information on the deterioration model parameters.

All random variables describing the condition of the individual elements at the end of interval j are collected in a vector $\mathbf{D}_j = [D_{1,j}, \dots, D_{n_E,j}]^T$, where n_E is the number of deteriorating elements considered in the system reliability analysis. This vector represents the overall condition of the structural system at time t_j. The system condition $\mathbf{D}_j$ is described generically by a system deterioration model $\mathbf{h}_D$ as:

$$\mathbf{D}_j = \mathbf{h}_D(\mathbf{X}_R, t_j) = [h_{D,1}(\mathbf{X}_R, t_j), \dots, h_{D,n_E}(\mathbf{X}_R, t_j)]^T \tag{5.5}$$

Figure 5.1 illustrates the input-output relationship defined by the system deterioration model.
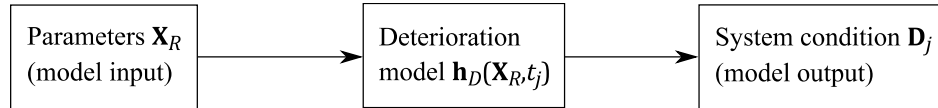
Figure 5.1: Illustration of the generic system deterioration model. The model describes the relation between the parameters $\mathbf{X}_R$ and the system condition $\mathbf{D}_j$.

5.2.2 Dependence modeling

Generally, deterioration of different elements in a structural system is interdependent. Such dependencies are in some cases caused by variability, but they mainly exist due to common influencing factors (Straub 2018b). As an example, in a welded steel structure constructed out of one steel grade by one contractor, using the same welding procedure and adopting the same quality standards, the correlation among fatigue deterioration of different welded connections due to common material properties and fabrication quality will be high. The correlation of deterioration influences the system reliability and is of relevance when optimizing the collection of information through inspection and monitoring.

Stochastic dependence of deterioration is modeled by introducing correlations among the parameters of the models describing the condition $D_{i,j}$ of the different elements i. Unfortunately, only a limited number of studies on dependence among deterioration processes exist (e.g. Li et al. 2004; Vrouwenvelder 2004; Malioka 2009; Luque et al. 2017). In most applications, correlation among the deterioration model parameters has to be estimated based at least partially on engineering judgment.

Hierarchical models and random field models are commonly applied to represent correlations among deterioration model parameters. The latter may be applied to model continuously distributed deterioration processes such as corrosion in reinforced concrete structures (e.g. Hergenröder and Rackwitz 1992; Stewart and Mullard 2007; Ying and Vrouwenvelder 2007; Malioka 2009; Straub 2011b; Papakonstantinou and Shinozuka 2013). The random field approach models a spatially varying parameter X as a random variable $X(z)$ at each location z, and describes the correlation structure of the different random variables $X(z)$ in terms of a suitable correlation function. Such random fields are typically discretized to enable their numerical representation (see, for example, Betz et al. 2014). Thus, a random field of a spatially varying parameter is defined by a discrete set of correlated random variables, which are part of $\mathbf{X}_R$. The joint distribution of the variables in a random field is commonly represented by a Gaussian copula, also known as the Nataf distribution model (Liu and Der Kiureghian 1986).

Hierarchical models are applied to model stochastic dependence of deterioration due to common influencing factors such as common environmental conditions, common material characteristics or joint model uncertainties. Such models define the parameters of the deterioration models conditional on random variables called hyperparameters (Faber et al. 2006; Maes and Dann 2007; Straub et al. 2009). Models with multiple hierarchies can also be defined (e.g. Luque et al. 2017). The additional random variables representing the common influencing factors in a hierarchical model are included in $\mathbf{X}_R$. Hierarchical models can be implemented through the Rosenblatt transformation (Hohenbichler and Rackwitz 1981).

Common influencing factors cannot always be modeled explicitly. As an alternative, statistical dependence among deterioration model parameters can be represented by correlation coefficients. As an example, statistical dependence of fatigue deterioration among welded connections due to common fabrication quality may be modeled by defining a correlation coefficient among the initial defect sizes at different hotspots (Moan and Song 2000; Vrouwenvelder 2004; Maljaars and Vrouwenvelder 2014). In this case, the Nataf model can be applied to model the joint distribution of the correlated deterioration model parameters.

Note that deterioration model parameters may also be time-variant. Such parameters are ideally modeled by random processes (see, for example, Lin and Yang 1985; Beck and Melchers 2004; Straub and Faber 2007; Altamura and Straub 2014). Like a random field, a random process represents a time-varying parameter X as a random variable $X(t)$ at each time t, and describes the correlation among the random variables $X(t)$ through a suitable correlation function. Continuous-time stochastic processes are discretized to facilitate their numerical representation. The resulting set of correlated random variables is included in $\mathbf{X}_R$. The joint distribution of the variables in a stochastic process may be represented by the Nataf model. In case a stochastic process has the Markov property, the Rosenblatt transformation may be applied (Altamura and Straub 2014).

5.3 Modeling of inspection and monitoring

5.3.1 Classification of inspection and monitoring techniques

To facilitate the modeling of information provided by in-service inspections and monitoring data, it is beneficial to classify inspection and monitoring techniques first. In the following, inspection and monitoring techniques are classified according to the:

1. **Inspected and monitored quantity**: Inspections and monitoring performed to reduce the uncertainty on the system condition $\mathbf{D}_j$ provide direct or indirect information on the deterioration model parameters included in $\mathbf{X}_R$ as illustrated in Figure 5.2. Thus, the inspected or monitored quantity associated with a certain inspection or monitoring technique can be a deterioration model parameter in $\mathbf{X}_R$ or an element condition $D_{i,j}$. For example, the concrete cover depth of reinforced concrete structures is a parameter of corrosion initiation models which can be measured with a cover meter. The size of a surface breaking fatigue crack in a welded connection – the output of fatigue crack growth models – can, for example, be determined based on eddy current testing. In many cases, however, only indicators of the element conditions $D_{i,j}$ or indicators of the system condition $\mathbf{D}_j$ can be measured or observed (Faber and Sørensen 2002). Indicators are related to the element conditions $D_{i,j}$ or to the system condition $\mathbf{D}_j$ through a (possibly stochastic) model, and thus provide indirect information on the deterioration model parameters in $\mathbf{X}_R$. For example, rust staining on the concrete surface is an indicator of reinforcement corrosion in concrete structures, which can be observed by visually inspecting the concrete surface (see, for example, Faber et al. 2006). As another example, modal parameters (modal frequencies, damping ratios and mode shapes) are often considered as indicators of the system condition $\mathbf{D}_j$. They can be derived from measured vibration response data (e.g. Farrar et al. 2001).
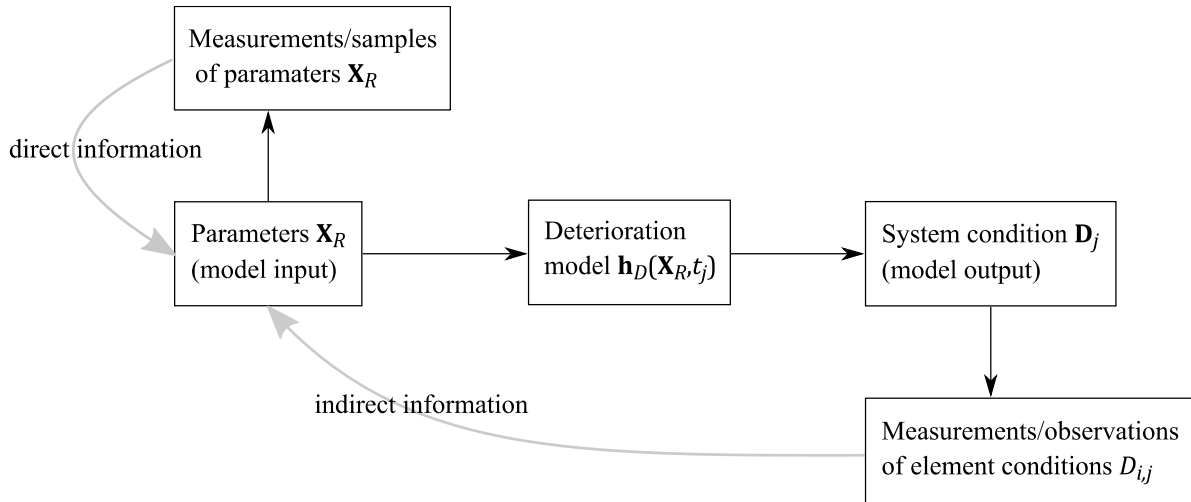
Figure 5.2: Inspection and monitoring techniques employed to reduce the uncertainty on the system condition $\mathbf{D}_j$ provide (a) direct information on the deterioration model parameters in $\mathbf{X}_R$ through direct measurements or samples of deterioration model parameters in $\mathbf{X}_R$, or (b) indirect information on the deterioration model parameters in $\mathbf{X}_R$ through measurements or observation of element conditions $D_{i,j}$. Indirect information on the deterioration model parameters in $\mathbf{X}_R$ is also obtained through measurements or observations of indicators of element conditions $D_{i,j}$ or indicators of the system condition $\mathbf{D}_j$.
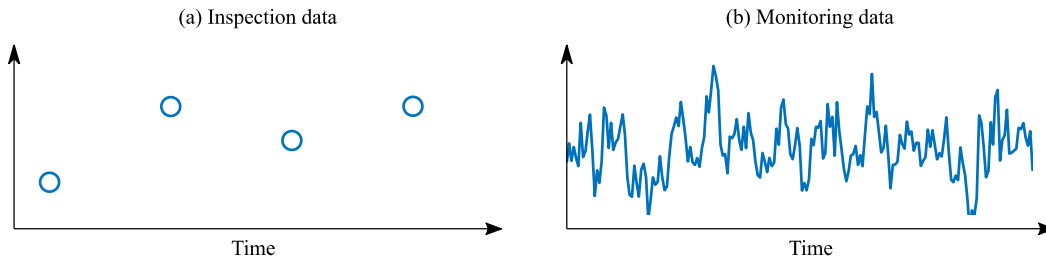
Figure 5.3: Illustration of the temporal characteristics of (a) inspections and (b) monitoring data.

2. **Type of information**: As discussed in Section 3.2, inspections and monitoring can provide equality or inequality information.

3. **Temporal characteristics**: Inspections are performed at discrete points in time, whereas monitoring is performed over a longer period. Monitoring can be performed continuously, periodically or following a triggering event. The temporal characteristics of inspection and monitoring are illustrated in Figure 5.3. Note that the datasets collected by monitoring systems are potentially large. To exploit these datasets, they are generally processed by suitable algorithms to derive summarizing statistics or to extract other meaningful features.

4. **Spatial characteristics**: Inspections generally cover large parts of a structure, while monitoring systems typically consist of multiple sensors installed at discrete locations in a structure. However, a clear distinction among inspection and monitoring due to their spatial characteristics is not necessarily possible since an inspection may only include a few discrete locations in a structural system and monitoring may cover continuous parts of a structural system.

The proposed classification scheme for information provided by inspections and monitoring performed to reduce the uncertainty on the structural condition is summarized in Table 5.1.

Table 5.1: Classification of inspection and monitoring techniques employed to reduce the uncertainty on the structural condition (adapted from Fischer et al. 2014).

Classification	Categories
Inspected/monitored quantity	• A parameter of the deterioration model (model input) • An element condition (model output) • An indicator related to an element condition • An indicator related to the condition of the system or subsystem
Type of information	• Equality information • Inequality information
Temporal characteristics	• Data collection at discrete points in time • Data collection over a longer period
Spatial characteristics	• Spatially discrete data collection • Spatially continuous data collection

5.3.2 Likelihood functions

The random vector $\mathbf{Z}_{1:k} = [\mathbf{Z}_1^T, \ldots, \mathbf{Z}_k^T]^T$ represents all probabilistic inspection and monitoring outcomes up to the end of the kth interval, where the different random vectors $\mathbf{Z}_k$ represent the probabilistic inspection and monitoring outcomes in the kth interval. Following Section 3, the relation between the joint inspection and monitoring outcome $\mathbf{Z}_{1:k} = \mathbf{z}_{1:k}$ and the deterioration model parameters in $\mathbf{X}_R$ is modeled by the joint likelihood function $L(\mathbf{x}_R|\mathbf{z}_{1:k})$, which is defined as (see also Equation (3.1)):

$$L(\mathbf{x}_R|\mathbf{z}_{1:k}) \propto \Pr(\mathbf{Z}_{1:k} = \mathbf{z}_{1:k}|\mathbf{X}_R = \mathbf{x}_R) \tag{5.6}$$

Under the common assumption that all inspection and monitoring outcomes $Z_{i,k}$ are statistically independent given $\mathbf{X}_R = \mathbf{x}_R$, the joint likelihood function $L(\mathbf{x}_R|\mathbf{z}_{1:k})$ is computed as (see also Equation (3.9)):

$$L(\mathbf{x}_R|\mathbf{z}_{1:k}) = \prod_k \prod_i L(\mathbf{x}_R|z_{i,k}) \tag{5.7}$$

where $L(\mathbf{x}_R|z_{i,k}) \propto \Pr(Z_{i,k} = z_{i,k}|\mathbf{X}_R = \mathbf{x}_R)$ is the likelihood function describing the ith inspection or monitoring outcome in the kth interval. The actual definition of the likelihood function $L(\mathbf{x}_R|z_{i,k})$ depends on the specific problem. Examples are presented in Section 5.7.1.3 (inspection of welded connections), Section 5.7.2.2 (global damage detection system) and Section 6.5.1.2 (inspection of reinforced concrete structures).

The assumption of conditional statistical independence does not always hold. As an example, spatial correlation among measurements exists if the sensors are closely spaced. In this case, the accuracy of the measurements is influenced by common influencing factors such as, for example, temperature. If inspection and monitoring outcomes $\mathbf{Z}_{1:k}$ are statistically dependent given $\mathbf{X}_R = \mathbf{x}_R$, the combined likelihood function $L(\mathbf{x}_R|\mathbf{z}_{1:k})$ must be formulated such that the spatial and/or

temporal dependencies among the individual inspection and monitoring outcomes are modeled correctly (e.g. Straub and Faber 2003; Simoen et al. 2013).

In general, the observation $\mathbf{Z}_{1:k} = \mathbf{z}_{1:k}$ does not provide information on all parameters in $\mathbf{X}_R$. These parameters cannot be learned. The likelihood function $L(\mathbf{x}_R|\mathbf{z}_{1:k})$ is defined such that it is constant with respect to those parameters.

5.4 Prior failure probability

The interval failure probability of a deteriorating structural system in any interval j is here assessed conditional on the capacity parameters $\mathbf{X}_R = \mathbf{x}_R$ (see also Equation (4.16)):

$$\Pr(F_j^*|\mathbf{X}_R = \mathbf{x}_R) \approx \Pr[g(\mathbf{x}_R, \mathbf{S}_{max,j}, t_j) \leq 0] \tag{5.8}$$

where $\mathbf{S}_{max,j}$ represents the maximum demand on the structure in interval j. Equation (5.8) corresponds a time-invariant (system) reliability problem (see Section 2). To solve this problem, the probabilistic structural model used in the reliability analysis is defined with element properties according to the system condition at end of interval j, i.e. $\mathbf{d}_j = \mathbf{h}_D(\mathbf{x}_R, t_j)$.

To ensure that the different interval failure events F_j^*, $j = 1, \dots, m$ are statistically independent given $\mathbf{X}_R = \mathbf{x}_R$, all time-invariant demand parameters are also included in $\mathbf{X}_R$. If the interval failure events are conditionally independent given $\mathbf{X}_R = \mathbf{x}_R$, the conditional probability of failure $\Pr[F(t_j)|\mathbf{X}_R = \mathbf{x}_R]$ can be computed according to Equation (5.1). To determine the probability of failure $\Pr[F(t_j)]$, the total probability theorem is then applied in Equation (5.2). Following an idea proposed by Wen and Chen (1987), it is now shown how the integral in Equation (5.2) can be transformed into a component reliability problem. To this end, an auxiliary standard uniform random variable P with PDF $f_P(p) = 1$ and CDF $F_P(p) = p$ is introduced. The conditional probability of failure can now be written as:

$$\Pr[F(t_j)|\mathbf{X}_R = \mathbf{x}_R] = F_P(\Pr[F(t_j)|\mathbf{X}_R = \mathbf{x}_R]) \tag{5.9}$$

It follows that (see also (3.12)):

$$\begin{aligned}
\Pr[F(t_j)|\mathbf{X}_R = \mathbf{x}_R] &= \int_0^{\Pr[F(t_j)|\mathbf{X}_R=\mathbf{x}_R]} f_P(p) \, \mathrm{d}p \\
&= \int_{p \leq \Pr[F(t_j)|\mathbf{X}_R=\mathbf{x}_R]} f_P(p) \, \mathrm{d}p \\
&= \int_0^1 \mathbb{I}[p \leq \Pr[F(t_j)|\mathbf{X}_R = \mathbf{x}_R]] f_P(p) \, \mathrm{d}p
\end{aligned} \tag{5.10}$$

Insertion Equation (5.10) into Equation (5.2) gives:

$$
\begin{aligned}
\Pr[F(t_j)] &= \int_{D_{\mathbf{X}_R}} \left[\int_0^1 \mathbb{I}\big[p \leq \Pr[F(t_j)|\mathbf{X}_R = \mathbf{x}_R] \big] f_P(p)\, \mathrm{d}p \right] f_{\mathbf{X}_R}(\mathbf{x}_R)\, \mathrm{d}\mathbf{x}_R \\
&= \int_{D_{\mathbf{X}_R}} \int_0^1 \mathbb{I}\big[p \leq \Pr[F(t_j)|\mathbf{X}_R = \mathbf{x}_R] \big] f_{\mathbf{X}_R}(\mathbf{x}_R) f_P(p)\, \mathrm{d}p\, \mathrm{d}\mathbf{x}_R
\end{aligned}
\tag{5.11}
$$

Equation (5.11) corresponds to a structural reliability problem in the augmented outcome space of $\mathbf{X}_R$ and P with limit state function:

$$
g_F(\mathbf{x}_R, p, t_j) = p - \Pr[F(t_j)|\mathbf{X}_R = \mathbf{x}_R]
\tag{5.12}
$$

The prior failure probability of the structural system up to time t_j can thus be written as:

$$
\Pr[F(t_j)] = \int_{g_F(\mathbf{x}_R, p, t_j) \leq 0} f_{\mathbf{X}_R}(\mathbf{x}_R) f_P(p)\, \mathrm{d}p\, \mathrm{d}\mathbf{x}_R = \Pr[g_F(\mathbf{X}_R, P, t_j) \leq 0]
\tag{5.13}
$$

All structural reliability methods can be used to solve this integral.

5.5 Posterior failure probability

The posterior failure probability up to time t_j, $\Pr[F(t_i)|\mathbf{Z}_{1:k} = \mathbf{z}_{1:k}]$, is computed according to Equation (5.3). In the following, the integral in Equation (5.3) is transformed into two component reliability problems using the approach presented in Sections 3.4 and 5.4. First, the posterior PDF of $\mathbf{X}_R$ given $\mathbf{Z}_{1:k} = \mathbf{z}_{1:k}$ is written as:

$$
f_{\mathbf{X}_R|\mathbf{Z}_{1:k}}(\mathbf{x}_R|\mathbf{z}_{1:k}) = \frac{L(\mathbf{x}_R|\mathbf{z}_{1:k}) f_{\mathbf{X}_R}(\mathbf{x}_R)}{\int_{D_{\mathbf{X}_R}} L(\mathbf{x}_R|\mathbf{z}_{1:k}) f_{\mathbf{X}_R}(\mathbf{x}_R)\, d\mathbf{x}_R}
\tag{5.14}
$$

Inserting Equation (5.14) in Equation (5.3) gives:

$$
\Pr[F(t_j)|\mathbf{Z}_{1:k} = \mathbf{z}_{1:k}] = \frac{\int_{D_{\mathbf{X}_R}} \Pr[F(t_j)|\mathbf{X}_R = \mathbf{x}_R] L(\mathbf{x}_R|\mathbf{z}_{1:k}) f_{\mathbf{X}_R}(\mathbf{x}_R)\, \mathrm{d}\mathbf{x}_R}{\int_{D_{\mathbf{X}_R}} L(\mathbf{x}_R|\mathbf{z}_{1:k}) f_{\mathbf{X}_R}(\mathbf{x}_R)\, \mathrm{d}\mathbf{x}_R}
\tag{5.15}
$$

The following relation holds for the conditional probability $\Pr[F(t_j)|\mathbf{X}_R = \mathbf{x}_R]$ and the likelihood function $L(\mathbf{x}_R|\mathbf{z}_{1:k})$:

$$
\Pr[F(t_j)|\mathbf{X}_R = \mathbf{x}_R] \cdot cL(\mathbf{x}_R|\mathbf{z}_{1:k}) = F_P\big[\Pr[F(t_j)|\mathbf{X}_R = \mathbf{x}_R] \cdot cL(\mathbf{x}_R|\mathbf{z}_{1:k}) \big]
\tag{5.16}
$$

where $F_P(p)$ is again the CDF of the standard uniform random variable P and c is a positive constant that ensures $cL(\mathbf{x}_R|\mathbf{z}_{1:k}) \leq 1$ for all $\mathbf{x}_R$ (see also Section 3.3). The product $\Pr[F(t_j)|\mathbf{X}_R = \mathbf{x}_R] \cdot L(\mathbf{x}_R|\mathbf{z}_{1:k})$ can thus be written as (see also Equations (3.12) and (5.10)):

$$\Pr[F(t_j)|\mathbf{X}_R = \mathbf{x}_R] \cdot L(\mathbf{x}_R|\mathbf{z}_{1:k})$$

$$= c^{-1} \int_0^1 \mathbb{I}\big[p \leq \Pr[F(t_j)|\mathbf{X}_R = \mathbf{x}_R] \cdot cL(\mathbf{x}_R|\mathbf{z}_{1:k})\big]\, f_P(p)\, \mathrm{d}p \tag{5.17}$$

In the same way, the likelihood function $L(\mathbf{x}_R|\mathbf{z}_{1:k})$ can be expressed as (see also Equation (3.12)):

$$L(\mathbf{x}_R|\mathbf{z}_{1:k}) = c^{-1} \int_0^1 \mathbb{I}\big[p \leq cL(\mathbf{x}_R|\mathbf{z}_{1:k})\big]\, f_P(p)\, \mathrm{d}p \tag{5.18}$$

Inserting Equation (5.17) into the numerator and Equation (5.18) into the denominator of Equation (5.15) leads to:

$$\Pr[F(t_j)|\mathbf{Z}_{1:k} = \mathbf{z}_{1:k}]$$

$$= \frac{\int_{D_{\mathbf{X}_R}} \int_0^1 \mathbb{I}\big[p \leq \Pr[F(t_j)|\mathbf{X}_R = \mathbf{x}_R] \cdot cL(\mathbf{x}_R|\mathbf{z}_{1:k})\big]\, f_{\mathbf{X}_R}(\mathbf{x}_R)\, f_P(p)\, \mathrm{d}p\, \mathrm{d}\mathbf{x}_R}{\int_{D_{\mathbf{X}_R}} \int_0^1 \mathbb{I}\big[p \leq cL(\mathbf{x}_R|\mathbf{z}_{1:k})\big]\, f_{\mathbf{X}_R}(\mathbf{x}_R)\, f_P(p)\, \mathrm{d}p\, \mathrm{d}\mathbf{x}_R} \tag{5.19}$$

The numerator in Equation (5.19) is a component reliability problem in the augmented outcome space of $\mathbf{X}_R$ and P with limit state function:

$$g_{F \cap Z}(\mathbf{x}_R, p, t_j, t_k) = p - \Pr[F(t_j)|\mathbf{X}_R = \mathbf{x}_R] \cdot cL(\mathbf{x}_R|\mathbf{z}_{1:k}) \tag{5.20}$$

The denominator in Equation (5.19) also corresponds to a component reliability problem in the augmented outcome space of $\mathbf{X}_R$ and P, which is described by the limit state function:

$$g_Z(\mathbf{x}_R, p, t_k) = p - cL(\mathbf{x}_R|\mathbf{z}_{1:k}) \tag{5.21}$$

The posterior probability of failure up to time t_k can now be written as:

$$\Pr[F(t_j)|\mathbf{Z}_{1:k} = \mathbf{z}_{1:k}] = \frac{\int_{g_{F \cap Z}(\mathbf{x}_R, p, t_j, t_k) \leq 0} f_{\mathbf{X}_R}(\mathbf{x}_R)\, f_P(p)\, dp\, d\mathbf{x}_R}{\int_{g_Z(\mathbf{x}_R, p, t_k) \leq 0} f_{\mathbf{X}_R}(\mathbf{x}_R)\, f_P(p)\, dp\, d\mathbf{x}_R}$$

$$= \frac{\Pr\big[g_{F \cap Z}(\mathbf{X}_R, P, t_j, t_k) \leq 0\big]}{\Pr\big[g_Z(\mathbf{X}_R, P, t_j) \leq 0\big]} \tag{5.22}$$

The denominator of Equation (5.22) can be interpreted as the probability of an observation event $Z(t_k) = \{g_Z(\mathbf{X}_R, P, t_k) \leq 0\}$ and the numerator corresponds to the probability of the joint event $F(t_j) \cap Z(t_k) = \{g_{F \cap Z}(\mathbf{X}_R, P, t_j, t_k) \leq 0\}$, i.e.:

$$\Pr[F(t_j)|\mathbf{Z}_{1:k} = \mathbf{z}_{1:k}] = \Pr[F(t_j)|Z(t_k)] = \frac{\Pr[F(t_j) \cap Z(t_k)]}{\Pr[Z(t_k)]} \tag{5.23}$$

Both the numerator and denominator in Equation (5.22) can be solved with structural reliability methods.

5.6 Computational aspects

The reliability problems in Equations (5.13) and (5.22) are high-dimensional since they include all (correlated) deteriorating elements of a structural system. Subset simulation, briefly introduced in Section 2.2.3, has been selected to solve these problems. It is robust and efficient in solving structural reliability problems with many random variables. In addition, it can be implemented relatively easily. In this thesis, the algorithm is implemented following Papaioannou et al. (2015).

To apply subset simulation, the reliability problems defined in Equations (5.13) and (5.22) are transformed to standard normal space following Section 3.3.4. The corresponding limit state functions G_F, $G_{F \cap Z}$ and G_Z are:

$$G_F(\mathbf{u}, t_j) = \ln[\Phi(u_{n+1})] - \ln\big[\Pr[F(t_j)|\mathbf{X}_R = T^{-1}(u_1, \dots, u_n)]\big],$$ (5.24)

$$\begin{aligned} G_{F \cap Z}(\mathbf{u}, t_j, t_k) = {} & \ln[\Phi(u_{n+1})] \\ & - \ln\big[\Pr[F(t_j)|\mathbf{X}_R = T^{-1}(u_1, \dots, u_n)] \cdot cL(T^{-1}(u_1, \dots, u_n)|\mathbf{z}_{1:k})\big] \end{aligned}$$ (5.25)

and

$$G_Z(\mathbf{u}, t_k) = \ln[\Phi(u_{n+1})] - \ln[cL(T^{-1}(u_1, \dots, u_n)|\mathbf{z}_{1:k})]$$ (5.26)

The prior and posterior probability of failure up to time t_j can now be defined in terms of the standard normal random variables $\mathbf{U}$:

$$\Pr[F(t_j)] = \Pr[G_F(\mathbf{U}, t_j) \leq 0]$$ (5.27)

$$\Pr[F(t_j)|Z(t_k)] = \frac{\Pr[G_{F \cap Z}(\mathbf{U}, t_j, t_k) \leq 0]}{\Pr[G_Z(\mathbf{U}, t_k) \leq 0]}$$ (5.28)

To compute $\Pr[F(t_j)]$ with subset simulation, the limit state function G_F defined in Equation (5.24) is used as input to Algorithm 2.1. Similarly, the limit state functions $G_{F \cap Z}$ and G_Z defined in Equations (5.25) and (5.26) are applied as input to Algorithm 2.1 to evaluate the probabilities $\Pr[F(t_j) \cap Z(t_k)]$ and $\Pr[Z(t_k)]$ with subset simulation. The conditional probability $\Pr[F(t_j)|Z(t_k)]$ is then simply the ratio of $\Pr[F(t_j) \cap Z(t_k)]$ to $\Pr[Z(t_k)]$ (see Equation (5.23)). Alternatively, $\Pr[F(t_j)|Z(t_k)]$ can be computed directly with a new subset simulation run following the estimation of $\Pr[Z(t_k)]$ (see also Schneider et al. 2013; Straub et al. 2016). For this purpose, a set of nested intermediate events $E_0 \supset E_1 \supset \cdots \supset E_M$ is defined where $E_0 = Z(t_k)$, $E_i = \{G_{F \cap Z}(\mathbf{U}, t_j, t_k) \leq b_i\}$, $i = 1, \dots, M$ and $b_1 > b_2 > \cdots > b_M = 0$. The conditional probability $\Pr[F(t_j)|Z(t_k)]$ can now be expressed as:

$$\Pr[F(t_j)|Z(t_k)] = \Pr(E_1 \cap E_2 \cap \dots \cap E_M|E_0) = \prod_{i=1}^{M} \Pr(E_i|E_{i-1})$$ (5.29)

The first threshold b_1 defining the intermediate event $E_1 = \{G_{F \cap Z}(\mathbf{U}, t_j, t_k) \leq b_1\}$ is determined from the samples conditional on $E_0 = Z(t_k)$, which are obtained as a by-product of estimating

$\Pr[Z(t_k)]$ with subset simulation (see also Algorithm 3.2). The remaining thresholds b_i, $i = 2, \ldots, M - 1$ are determined following the original subset simulation procedure. When applying this approach, the estimator $\hat{P}_{SuS}$ defined in Equation (2.21) provides an estimate of the conditional probability $\Pr[F(t_j)|Z(t_k)]$.

5.7 Numerical examples: steel structures subject to high-cycle fatigue

5.7.1 Zayas frame

Consider the two-dimensional welded steel frame shown in Figure 5.4, which is known as Zayas frame (Zayas et al. 1980). The frame is subject to gravity loads and a time-varying horizontal point load at the top to represent an environmental load. In addition, the frame is subject to fatigue loads throughout its service life of $T_{SL} = 50$ years. The effect of inspection outcomes on the reliability estimates of the structural system is studied.

5.7.1.1 System model

The Zayas frame consists of tubular steel elements with welded connections, which are especially vulnerable to fatigue deterioration due to material inhomogeneities, imperfections, high stress concentrations and residual stresses (Fricke 2003). Locations where fatigue cracks may develop are called hotspots. A welded connection may contain several hotspots.

Fatigue crack growth reduces the capacity of welded connections. In the current example, fatigue deterioration is assumed to occur at the welds connecting the braces with the legs and with the
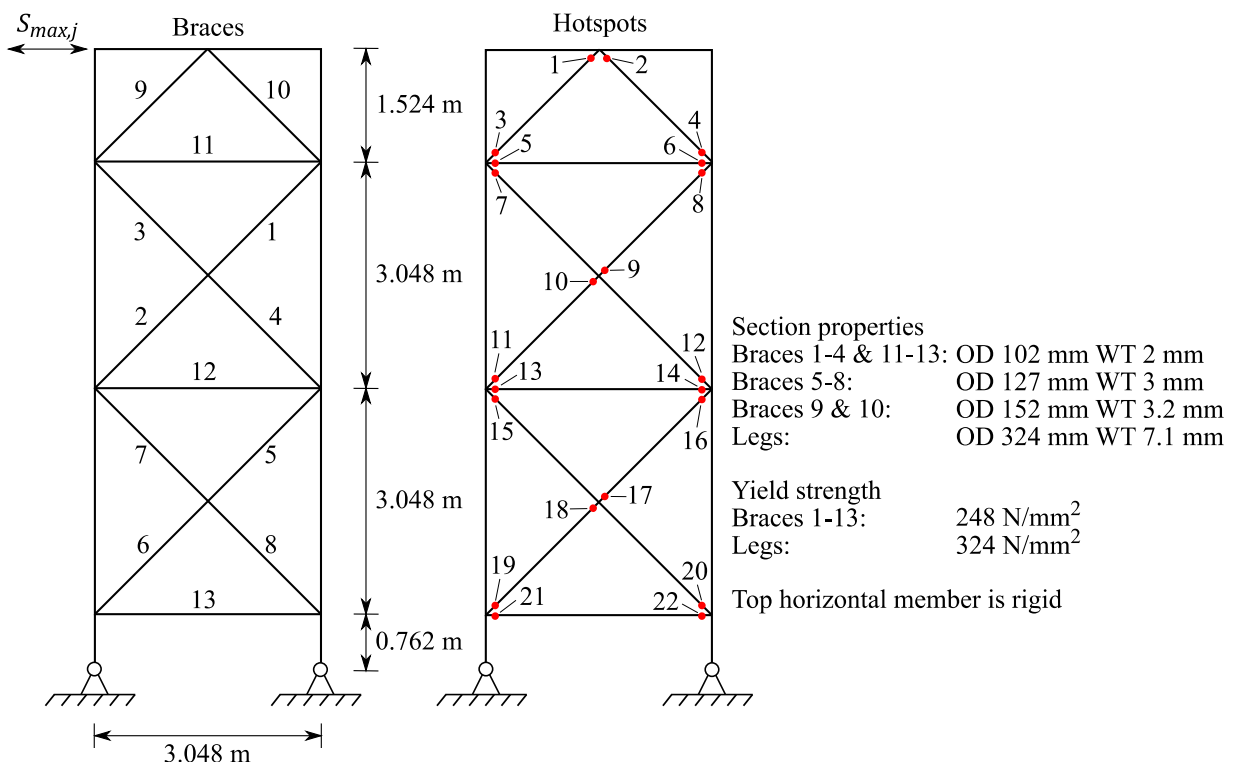
Figure 5.4: Zayas frame (Zayas et al. 1980). OD is the outer diameter and WT the wall thickness of the tubular steel members.

upper horizontal element as well as at the welds at the intersection of the X-braces. Furthermore, it is assumed that each deteriorating welded connection contains only one critical hotspot. Thus, there are $n_E = 22$ hotspots as indicated in Figure 5.4.

The approach of Straub and Der Kiureghian (2011) is adopted to determine the reliability of the welded steel structure subject to fatigue. At system level, no gradual degradation of the weld capacities is considered. At a given time t_j, a welded connection has either its full capacity or it has completely lost its capacity because of fatigue crack growth. In the current example, it is assumed that a welded connection loses its capacity if a fatigue crack at any of the associated hotspots grows beyond a critical size (see, for example, Madsen 1997). The condition of any hotspot i at time t_j is, therefore, modeled by a binary random variable $D_{i,j}$, where $D_{i,j} = 1$ is the hotspot fatigue failure event and $D_{i,j} = 0$ is the complement. The event of fatigue failure of hotspot i at time t_j is defined by a limit state function $g_i(\mathbf{x}_R, t_j)$ as $\{D_{i,j} = 1\} = \{g_i(\mathbf{X}_R, t_j) \leq 0\}$, where $\mathbf{X}_R$ represents the stochastic parameters influencing the capacity of the frame. $g_i(\mathbf{x}_R, t_j)$ is written as:

$$g_i(\mathbf{x}_R, t_j) = a_{c,i} - a_i(\mathbf{x}_R, t_j) \tag{5.30}$$

where $a_{c,i}$ is the critical crack size and $a_i(\mathbf{x}_R, t_j)$ is the realization of the fatigue crack size at hotspot i at time t_j given $\mathbf{X}_R = \mathbf{x}_R$. It is computed by means of a fatigue crack growth model presented Section 5.7.1.2. $a_{c,i}$ may be defined such that failure modes such as plastic collapse or unstable crack growth are approximately accounted for.

The function $h_{D,i}(\mathbf{X}_R, t_j)$ defining the relation between the capacity parameters $\mathbf{X}_R$ and the hotspot condition $D_{i,j}$ can now be written as:

$$D_{i,j} = h_{D,i}(\mathbf{X}_R, t_j) = \mathbb{I}[g_i(\mathbf{X}_R, t_j) \leq 0] \tag{5.31}$$

Using Equation (5.5), the system condition $\mathbf{D}_j = [D_{1,j}, \dots, D_{n_E,j}]^T$ of the Zayas frame can subsequently be calculated as a function of the capacity parameters $\mathbf{X}_R$. It follows that $\mathbf{D}_j$ is a binary random vector with 2^{n_E} possible states.

In the current example, fatigue deterioration is assessed at yearly intervals. The maximum of the environmental load in year j is denoted by $S_{max,j}$. The different $S_{max,j}$, $j = 1, \dots, T_{SL}$ are independent and identically Gumbel distributed with a coefficient of variation (c.o.v.) $\delta_{S_{max,j}} = 0.35$. The CDF of $S_{max,j}$ is denoted by $F_{S_{max,j}}(s)$. Material and geometry properties are modeled as deterministic parameters as listed in Figure 5.4. This simplification is reasonable since the uncertainties associated with these parameters are small compared to the uncertainties associated with the hotspot conditions $\mathbf{D}_j$ and the load $S_{max,j}$. It follows that $\mathbf{X}_R$ consists of the stochastic parameters influencing fatigue deterioration of all hotspots considered in the system reliability analysis.

Now let the random vector $\mathbf{B}_j = [B_{1,j}, \dots, B_{k,j}, \dots, B_{n_B,j}]^T$ represent the condition of the frame's braces at the end of interval j, where $n_B = 13$ is the number of braces (see Figure 5.4). The different $B_{k,j}$ are binary random variables modeling the condition of brace k at the end of interval j with states $B_{k,j} = 1$ (brace k is fully intact at time t_j) and $B_{k,j} = 0$ (brace k has completely lost its capacity at time t_j). A brace loses its capacity as soon as one of the associated hotspots (i.e. the

associated welded connections) fails. The relation between the hotspot conditions $\mathbf{D}_j$ and the condition of the braces $\mathbf{B}_j$ can be defined as follows:

$$\mathbf{B}_j = \mathbf{A} \cdot \mathbf{D}_j \tag{5.32}$$

where $\mathbf{A}$ is an adjacency matrix of size $n_B \times n_E$ with elements $a_{ki} = 1$ if hotspot i belongs to brace k and $a_{ki} = 0$ otherwise.

The capacity of the frame R at time t_j with respect to the applied load is evaluated in function of the brace conditions at time t_j, $\mathbf{B}_j$, and thus implicitly in function of $\mathbf{X}_R$. Failure of the damaged frame in year j occurs when the annual maximum load $S_{max,j}$ exceeds the frame's capacity $R(\mathbf{B}_j)$. Consequently, the interval failure probability of the frame in function of a certain realization of the brace conditions at time t_j, $\mathbf{B}_j = \mathbf{b}_j$, can be computed as:

$$\Pr(F_j^* | \mathbf{B}_j = \mathbf{b}_j) = \Pr[r(\mathbf{b}_j) \leq S_{max,j}] = 1 - F_{S_{max,j}}[r(\mathbf{b}_j)] \tag{5.33}$$

where $r(\mathbf{b}_j)$ denotes the realization of the frame's capacity when $\mathbf{B}_j$ takes the value $\mathbf{b}_j$. The mean of the annual maximum load $S_{max,j}$ is selected such that the undamaged Zayas frame has an interval failure probability $\Pr(F_j^* | \mathbf{B}_j = \mathbf{0}) = 1.3 \cdot 10^{-6}$, i.e. $\mu_{S_{max,j}} = 62$ kN.

The capacity $r(\mathbf{b}_j)$ is here computed by performing a pushover analysis based on a non-linear finite-element model of the frame with all braces damaged according to $\mathbf{B}_j = \mathbf{b}_j$, i.e. all braces with failed welded connections are removed from the model used in the pushover analysis. Through such an analysis the ultimate capacity of framed steel structures with respect to the applied loads can be quantified. Non-linear effects associated with non-linear material behavior, imperfections, large displacements and deformations (large strains) are modeled explicitly. The analysis captures load redistribution within the structural system resulting from local stiffness changes. Ultimately, it simulates the entire collapse process of the structural system including initial yielding, formation of plastic hinges, member buckling as well as formation of a global system collapse mechanism (see Ultiguide 1999; Skallerud and Amdahl 2002).

In the current study, $2^{13} = 8192$ pushover analyses are carried out using USFOS (2014) to precompute the capacity $r(\mathbf{b}_j)$ for all possible realizations of the brace conditions $\mathbf{B}_j$. This approach is here possible since the material and geometry properties are modeled as deterministic parameters and the number of possible realizations of the brace conditions $\mathbf{B}_j$ is manageable. The corresponding conditional interval failure probabilities $\Pr(F_j^* | \mathbf{B}_j = \mathbf{b}_j)$ are computed according to Equation (5.33) and collected in a data base. These interval failure probabilities have a reference period of one year, but they are independent of year j because the annual maximum loads $S_{max,j}$ are identically distributed. In the subsequent reliability analysis of the deteriorating frame, the computation of $\Pr(F_j^* | \mathbf{X}_R = \mathbf{x}_R)$ corresponds to a lookup operation in which a realization $\mathbf{x}_R$ is matched to a pre-computed interval failure probability $\Pr(F_j^* | \mathbf{B}_j = \mathbf{b}_j)$ at time t_j by combining Equations (5.5) and (5.32), i.e. $\mathbf{b}_j = \mathbf{A} \cdot \mathbf{h}_D(\mathbf{x}_R, t_j)$.

The structural importance of brace k – and thus the structural importance of all hotspots belonging to brace k – is quantified by the single-element importance measure SEI_k (see Equation (5.34)), which is defined as the difference between the interval failure probability of the intact frame and

Table 5.2: Single-element importance (SEI) measure and structural importance category of all braces and hotspots of the Zayas frame.

Brace	Hotspot	SEI	Structural importance category
1, 3	7, 8, 9	1.14×10^{-5}	medium
2, 4	10, 11, 12	1.06×10^{-5}	medium
5, 7	15, 16, 17	1.99×10^{-3}	high
6, 8	18, 19, 20	2.00×10^{-3}	high
9, 10	1, 2, 3, 4	7.25×10^{-7}	low
11	5, 6	8.26×10^{-8}	low
12	13, 14	6.31×10^{-7}	low
13	21, 22	2.27×10^{-7}	low

the interval failure probability of the frame with brace k removed (Straub and Der Kiureghian 2011; Straub 2018b). The single-element importance measures for all braces and hotspots of the Zayas frame are summarized in Table 5.2. The lower X-braces (braces 5 to 8) are the most important braces followed by the X-braces on the level above (braces 1 to 4). The top braces (braces 9 and 10) and the horizontal braces (braces 11 to 13) are the least important braces.

$$SEI_k = \Pr(F_j^* | B_{1,j} = 0, \dots, B_{k-1,j} = 0, B_{k,t} = 1, B_{k+1,j} = 0, \dots, B_{n_B,j} = 0) - $$
$$\Pr(F_j^* | \mathbf{B}_j = \mathbf{0}) \tag{5.34}$$

5.7.1.2 Fatigue model

Fatigue failure of tubular joints typically occurs by initiation and subsequent growth of surface cracks at the weld toe in hotspot regions (Lassen and Recho 2006). For the purpose of illustration, the evolution of the fatigue crack depth A_i at a given hotspot i is described by a simple one-dimensional crack growth model based on Paris' law (Paris and Erdogan 1963):

$$\frac{dA_i(n)}{dn} = C_i \left[\Delta S_i(n) \sqrt{\pi A_i(n)} \right]^{M_i} \tag{5.35}$$

where $dA_i(n)/dn$ is the crack growth rate, n is the number of applied fatigue stress cycles, C_i and M_i are empirical material parameters and $\Delta S_i(n)$ is the varying far-field fatigue stress range as a function of the stress cycles n. The quantity $\Delta K = \Delta S_i(n)\sqrt{\pi A_i(n)}$ is the stress intensity factor (SIF) range. The model can be extended to describe more complex crack shapes, hotspot geometries and stress distributions (e.g. Straub 2004; Maljaars et al. 2012). If desired, the model can be replaced altogether with a more advanced crack growth model (e.g. Altamura and Straub 2014). This will not affect the method as described in this case study.

Fatigue loads are generally random in nature and the load sequence $\{\Delta S_i(n)\}_{n=1}^{\infty}$ is ideally modeled by a stochastic process, i.e. for every stress cycle n there is a random variable $\Delta S_i(n)$. Under the condition that the fatigue stress process is stationary, ergodic and sufficiently mixing, a simplified

approach may be adopted in which the crack growth rate $dA_i(n)/dn$ given by Equations (5.35) is approximated by its expected value with respect to ΔS_i (Altamura and Straub 2014)[8]:

$$\frac{dA_i(n)}{dn} \approx \mathbb{E}_{\Delta S_i}\left[C_i\left[\Delta S_i(n)\sqrt{\pi A_i(n)}\right]^{M_i}\right] = C_i\left[\sqrt{\pi A_i(n)}\right]^{M_i} \cdot \mathbb{E}_{\Delta S_i}[\Delta S_i(n)^{M_i}] \tag{5.36}$$

The fatigue stress process is described by its stationary (long term) distribution $f_{\Delta S_i}(\Delta s_i)$ and an annual stress cycle rate ν_i (e.g. Madsen et al. 1986). The quantity

$$\Delta S_{e,i} = \left(\mathbb{E}_{\Delta S_i}[\Delta S_i(n)^{M_i}]\right)^{1/M_i} \tag{5.37}$$

is interpreted as an equivalent stress range. In the current case study, it is assumed that the stationary distribution of the fatigue stress ranges $f_{\Delta S_i}(\Delta s_i)$ can be modeled by a Weibull distribution. The equivalent stress range is hence given by:

$$\Delta S_{e,i} = K_{\Delta S,i}\Gamma\left(1 + \frac{M_i}{\lambda_{\Delta S,i}}\right)^{1/M_i} \tag{5.38}$$

$\Gamma(\cdot)$ denotes the Gamma function and $K_{\Delta S,i}$ and $\lambda_{\Delta S,i}$ are the Weibull scale and shape parameters. $K_{\Delta S,i}$ is modeled as a lognormal random variable to represent statistical uncertainty in the estimation of the parameters of $f_{\Delta S_i}(\Delta s_i)$. $\lambda_{\Delta S,i}$ is assumed to be deterministic.

The parameters C_i and M_i of Paris' law are modeled as time-invariant random variables to capture uncertainties due to the variability of the material properties and material inhomogeneities. Proper attention must be paid to modeling the correlation among C_i and M_i. They are empirical parameters generally derived from the same experiments and are therefore strongly correlated. To model the dependence among the Paris' law parameters, the linear relationship between $\ln C_i$ and M_i given in (Gurney 1978) is adopted[9]:

$$\ln C_i = -15.84 - 3.34 M_i \tag{5.39}$$

Equation (5.39) is valid if stresses are given in N/mm^2 and the crack growth rate in m/cycle. In the following, C_i is modeled as a lognormally distributed random variable. M_i is thus normal distributed due to the linear relationship between $\ln C_i$ and M_i.

To capture uncertainties in the fabrication quality, the initial crack size $A_{0,i}$ is modeled as a random variable with exponential distribution. Uncertainties in the calculation of the hotspot stress and SIF range are captured by introducing lognormal random bias factors $B_{\Delta S,i}$ and $B_{SIF,i}$, which are

---

[8] In general, fatigue loads are characterized by the a random process $\Delta S(n)$ representing the stress ranges and a random process $R(n) = S_{min}(n)/S_{max}(n)$ representing the corresponding stress ratios, where $S_{min}(n)$ and $S_{max}(n)$ are the minimum and maximum stresses during each stress cycle n (see also Altamura and Straub 2014). Note that Paris' law disregards the effect of the stress ratio.

[9] Equation (5.39) changes to $\ln C_i + (M_i/2 - 1)\ln(1000) = -15.84 - 3.34 M_i$ if stresses are given in N/mm^2 and the crack growth rate in mm/cycle (see Lassen and Recho 2006).

multiplied with the calculated equivalent stress range $\Delta S_{e,i}$. The one-dimensional crack growth model given in Equation (5.35) is rewritten as:

$$\frac{dA_i(n)}{dn} = C_i \left[B_{SIF,i} B_{\Delta S,i} \Delta S_{e,i} \sqrt{\pi A_i(n)} \right]^{M_i} \tag{5.40}$$

Using the initial condition $A_i(n = 0) = A_{0,i}$, an analytical function $A_i(\mathbf{X}_R, t_j)$ can be obtained from Equation (5.40) to predict the fatigue crack size at a given hotpot i at time t_j (see also Madsen et al. 1986):

$$A_i(\mathbf{X}_R, t_j) = \left[\left(1 - \frac{M_i}{2} \right) C_i B_{SIF,i}^{M_i} B_{\Delta S,i}^{M_i} \Delta S_{e,i}^{M_i} \pi^{\frac{M_i}{2}} v_i t_j + A_{0,i}^{\left(1-\frac{M_i}{2}\right)} \right]^{\left(1-\frac{M_i}{2}\right)^{-1}} \tag{5.41}$$

where v_i is the annual stress cycle rate and $v_i t_j$ is the total number of stress cycles applied at a given hotspot i up to time t_j. $\Delta S_{e,i}$ is computed as a function of $K_{\Delta S,i}$, $\lambda_{\Delta S,i}$ and M_i according to Equation (5.38).

The vector of all stochastic parameters describing fatigue deterioration of all n_E hotspots considered in the system reliability analysis is defined as:

$$\mathbf{X}_R = \left[C_1, A_{0,1}, B_{SIF,1}, B_{\Delta S,1}, K_{\Delta S,1}, \dots, C_{n_E}, A_{0,n_E}, B_{SIF,n_E}, B_{\Delta S,n_E}, K_{\Delta S,n_E} \right]^T \tag{5.42}$$

For illustration purposes, the same probabilistic models are applied to describe the crack growth model parameters for all hotspots $i = 1, \dots, n_E$. These models are listed in Table 5.3.

The mean and standard deviation of the equivalent stress range $\Delta S_{e,i}$ are a function of the distributions of $\ln K_{\Delta S,i}$ and $\ln C_i$ through Equations (5.38) and (5.39). They are $\mu_{\Delta S_{e,i}} = 20.1$ N/mm^2 and $\sigma_{\Delta S_{e,i}} = 5.65$ N/mm^2. Note that in real structures, the parameters of the fatigue crack growth model will vary from hotspot to hotspot. This will, however, not affect the methods presented in this thesis.

Table 5.3: Prior probabilistic models of the fatigue crack growth parameters for all hotspots $i = 1, \dots, n_E$.

| Parameter	Dimension	Distribution	Mean	Standard deviation
$\ln K_{\Delta S,i}$	corresponding to N/mm^2	normal	2.0	0.275
$\lambda_{\Delta S,i}$	-	deterministic	0.8	-
v_i	yr^{-1}	deterministic	$5 \cdot 10^6$	-
$A_{0,i}$	mm	exponential	0.11	0.11
$a_{c,i}$	mm	deterministic	20	-
$\ln C_i$	corresponding to N and mm	normal	-29.97	0.514
M_i	-	calculated from Equation (5.39)		
$B_{\Delta S,i}$	-	lognormal	1.0	0.1
$B_{SIF,i}$	-	lognormal	1.0	0.1

Fatigue failure of any hotspot i is described by the limit state function $g_i(\mathbf{x}_R, t_j)$ defined in Equation (5.30). All stochastic input parameters $\mathbf{X}_R$ are time-invariant and $g_i(\mathbf{x}_R, t_j)$ is monotonically decreasing with time t_j. This model thus belongs to model class (a) described in Section 4.2. Based on the prior probabilistic models summarized in Table 5.3, the prior marginal probability of fatigue failure of any hotspot i at time t_j, $\Pr[F_i(t_j)] = \Pr[g_i(\mathbf{X}_R, t_j) \le 0]$, is computed with FORM. The results are shown in Figure 5.5.

Statistical dependence among hotspot fatigue behavior is modeled through correlation coefficients among the fatigue model parameters. In the current example, the fatigue model parameters $A_{0,i}$, C_i, $K_{\Delta S,i}$, $B_{\Delta S,i}$ and $B_{SIF,i}$ are assumed to be equi-correlated among all hotspots $i = 1, \dots, n_E$ with correlation coefficients ρ_{A_0}, $\rho_{\ln C}$, $\rho_{\ln K_{\Delta S}}$, $\rho_{B_{\Delta S}}$ and $\rho_{B_{SIF}}$. The correlation coefficient ρ_{A_0} represents the stochastic dependence due to common fabrication quality; $\rho_{\ln C}$ reflects the stochastic dependence due to common material characteristics; $\rho_{\ln K_{\Delta S}}$ models the stochastic dependence due to common loading characteristics; and $\rho_{B_{\Delta S}}$ and $\rho_{B_{SIF}}$ describe stochastic dependence due to common uncertainties in the calculation of the hotspot fatigue stress and SIF ranges. The joint distribution of all fatigue model parameters is subsequently modeled through a Gaussian copula (Nataf) model (Liu and Der Kiureghian 1986).

To study the influence of different levels of statistical dependence among hotspot fatigue behavior, two different dependence cases are considered (low and high dependence), which are defined in terms of the correlation coefficients ρ_{A_0}, $\rho_{\ln C}$, $\rho_{\ln K_{\Delta S}}$, $\rho_{B_{\Delta S}}$ and $\rho_{B_{SIF}}$ listed in Table 5.4.

5.7.1.3 Inspection model

In the current context, the relevant inspection outcomes are (a) no detection, (b) detection but no measurement, and (c) detection and measurement of a fatigue crack. These inspection outcomes are directly related to the crack size at the inspected hotspot at the time of the inspection. Here, inspection outcomes of the type (a) and (b) are considered. It is assumed that magnetic particle inspection (MPI) is applied to detect a surface crack at a given hotspot (see, for example, Lovejoy 1993). The method applies a magnetic field in the tested component. At the same time, visible iron particles are sprayed onto the tested surface. A surface crack interrupts the magnetic field flowing
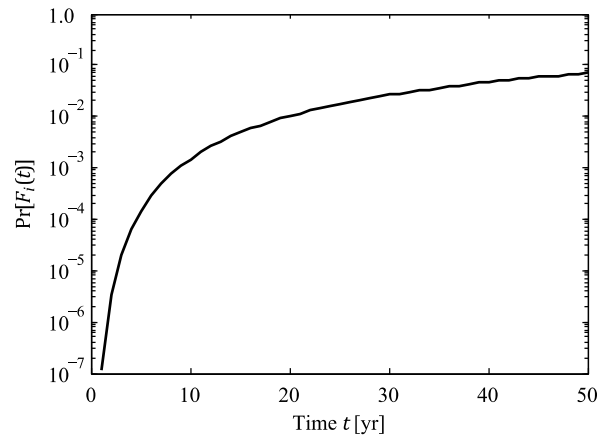
Figure 5.5: Prior marginal probability of fatigue failure $\Pr[F_i(t)]$ of hotspots $i = 1, \dots, n_E$. $\Pr[F_i(t)]$ is approximated by interpolation of the failure probabilities $\Pr[F_i(t_j)] = \Pr[g_i(\mathbf{X}_R, t_j) \le 0]$ for times $t_j = 1, \dots, 50$ yr. Computations of $\Pr[F_i(t_i)]$ are performed with FORM.

Table 5.4: Correlation coefficients modeling stochastic dependence among the parameters of the fatigue crack growth model.

	Low dependence	High dependence
ρ_{A_0}	0.2	0.8
$\rho_{\ln C}$	0.2	0.8
$\rho_{\ln K_{\Delta S}}$	0.2	0.8
$\rho_{B_{\Delta S}}$	0.2	0.8
$\rho_{B_{SIF}}$	0.2	0.8

through the component and a leakage field occurs. The iron particles cluster at the edges of the crack and thus make it visible. The information provided by an inspection using MPI is classified following Section 5.3.1. The classification is summarized in Table 5.5.

The quality of an inspection technique for detecting surface cracks in welds is commonly described by a probability of detection $PoD(a)$, which is defined as:

$$PoD(a) = \Pr(\text{"detection of a fatigue crack with depth } A = a\text{"}) \tag{5.43}$$

The PoD accounts for uncertain factors such as measurement errors, inspector performance and environmental conditions (Straub 2004). To model the performance of MPI, an exponential probability of detection curve is here applied (Moan et al. 2000):

$$PoD(a) = 1 - \exp(-a/\lambda_D) \tag{5.44}$$

with $\lambda_D = 1.95$ mm.

In addition to the PoD, an inspection method for detecting fatigue cracks is characterized by the probability of false indication (PFI), which is the probability of obtaining an indication of a fatigue crack when no fatigue crack is present. It has to be specified relative to a reference weld length (Straub 2004).

During an inspection of a weld, an indication can occur either due to the detection of an existing crack or due to a false indication. The events "detection of a fatigue crack" and "false indication"

Table 5.5: Classification of magnetic particle inspection employed to detect surface cracks at hotspots in tubular joints.

Classification	Categories
Inspected/monitored quantity	An indicator related to an element condition (The observed quantity is the cluster of iron particles at the edges of the surface crack at the inspected hotspot at the time of the inspection.)
Type of information	Inequality information (detection/no detection of a fatigue crack)
Temporal characteristics	Data collection at discrete points in time
Spatial characteristics	Spatially discrete data collection (Only hotspot regions of tubular joints are inspected, which are spatially confined.)

cannot be distinguished when performing an in-service inspection. For this reason, Straub (2004) combines the PoD and the PFI into a single quantity called the probability of indication PoI:

$$PoI(a) = PoD(a) + [1 - PoD(a)] \cdot PFI \tag{5.45}$$

The PoI is also defined with respect to a certain weld length because the PFI is a function of length. According to Straub (2004), the PFI of MPI for tubular joints is 0.298 per meter. Assuming that the inspected weld length is 0.5 m per hotspot and the occurrence of a false indication can be modeled by a Poisson point process, the PFI is 0.138 per hotspot. This value is adopted in the current example.

In the following, an inspection outcome is modeled by a binary random variable $Z_{i,k}$ with states $Z_{i,k} = 0$ (no indication of a fatigue crack at hotspot i in year k) and $Z_{i,k} = 1$ (indication of a fatigue crack at hotspot i in year k). The likelihood functions modeling these inspection outcomes are constructed by combining the PoI model with the fatigue crack growth model described in Section 5.7.1.2. The likelihood function describing the inspection outcome $Z_{i,k} = 1$ is written as:

$$L(\mathbf{x}_R | z_{i,k} = 1) = PoI[a_i(\mathbf{x}_R, t_k)] \tag{5.46}$$

The likelihood function describing the inspection outcome $Z_{i,k} = 0$ is defined as:

$$L(\mathbf{x}_R | z_{i,k} = 0) = 1 - PoI[a_i(\mathbf{x}_R, t_k)] \tag{5.47}$$

In the current example, it is assumed – as commonly done in inspection modeling – that different inspection outcomes $Z_{i,k}$ are stochastically independent for given crack depths $a_i(\mathbf{x}_R, t_k)$. The combined likelihood function $L(\mathbf{x}_R | \mathbf{z}_{1:k})$ of all inspection outcomes $\mathbf{Z}_{1:k} = \mathbf{z}_{1:k}$ up to time t_k is thus given by Equation (5.7).

Note that stochastic dependence in the inspection performance from one location to another often exist due to common influencing factors such as environmental conditions and inspector characteristics. Such dependencies can be captured through modeling the parameters of the PoI models as correlated random variables (see, for example, Straub and Faber 2003; Maljaars and Vrouwenvelder 2014). In this way, the uncertainty in the PoI and the dependence among inspection quality at different locations can be accounted for.

Since indication/no-indication events provide inequality information, the constant c that ensures $cL(\mathbf{x}_R | \mathbf{z}_{1:k}) \leq 1$ for all $\mathbf{x}_R$ can be chosen as $c = 1$.

5.7.1.4 Prior reliability analysis

An estimate of the prior probability of failure $\Pr[F(t)]$ of the Zayas frame is computed for each degree of dependence among hotspot fatigue behavior following Sections 5.4 and 5.6. The problem is solved using SuS with conditional probabilities of each intermediate event of 0.1 and 1000 MCMC samples per subset level, and the statistics of $\Pr[F(t_j)]$ are determined from 500 independent SuS runs. This approach is applied in all numerical examples presented in Section 5.7. The results of the analysis are shown in Figure 5.6. The width of the 95% credible interval indicates the accuracy of the SuS. The interval has 0.95 probability of containing the true value of the
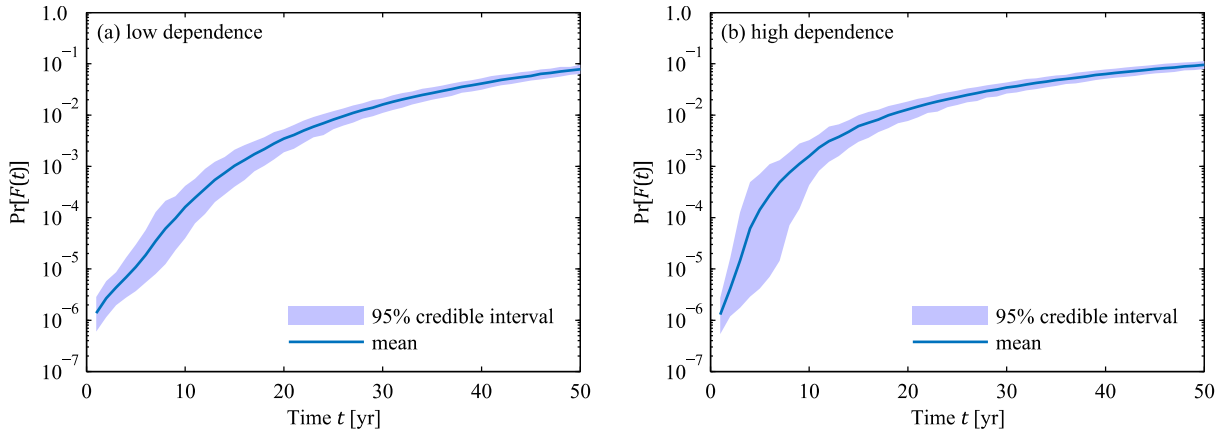
Figure 5.6: Failure probability $\Pr[F(t)]$ of the Zayas frame as a function of different degrees of dependence among hotspot fatigue behavior.

failure probability (within the confines of the model). The accuracy of the computation varies with time t since the number of samples per subset level used in the simulation is the same for all years. Results are less accurate for low values of t, because of the associated smaller failure probability. The accuracy of the SuS can be improved by increasing the number of samples.

Figure 5.7 shows the bounds on the failure probability, which are computed following Equation (4.20). To determine the required interval failure probabilities $\Pr(F_j^*)$, the conditional failure probability $\Pr[F(t_j)|\mathbf{X}_R = \mathbf{x}_R]$ in the limit state function g_F defined in Equation (5.12) is simply replaced by the conditional interval failure probability $\Pr(F_j^*|\mathbf{X}_R = \mathbf{x}_R)$ (see also Schneider et al. 2017). $\Pr(F_j^*)$ is then computed following Equation (5.13). Note that Figure 5.7 only shows the mean of the SuS estimate for $\Pr[F(t)]$ and the mean of the SuS estimate for the corresponding bounds.

At the beginning of the service life – when deterioration has little effect – the failure probability $\Pr[F(t)]$ is close to the upper bound. This behavior is more clearly visible in Figure 5.7(a). Over time, the failure probability converges to the lower bound indicating that the uncertainty on the frame's condition and thus the uncertainty on the frame's capacity dominates the reliability.

Figure 5.7: Best estimate of the bounds on $\Pr[F(t)]$ together with the best estimate of $\Pr[F(t)]$ as a function of the degree of dependence among hotspot fatigue behavior.

Figure 5.8: (a) Failure probability $\Pr[F(t)]$ and (b) failure rate $\lambda(t)$ of the Zayas frame with and without deterioration.

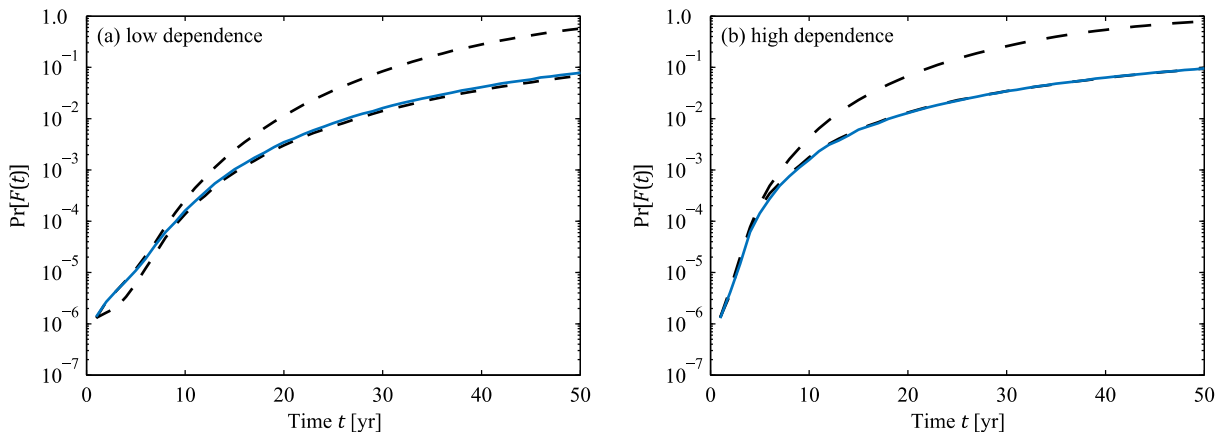Figure 5.8(a) compares the mean of the SuS estimate for the failure probability $\Pr[F(t)]$ of the Zayas frame computed for the different degrees of dependence among hotspot fatigue behavior. It additionally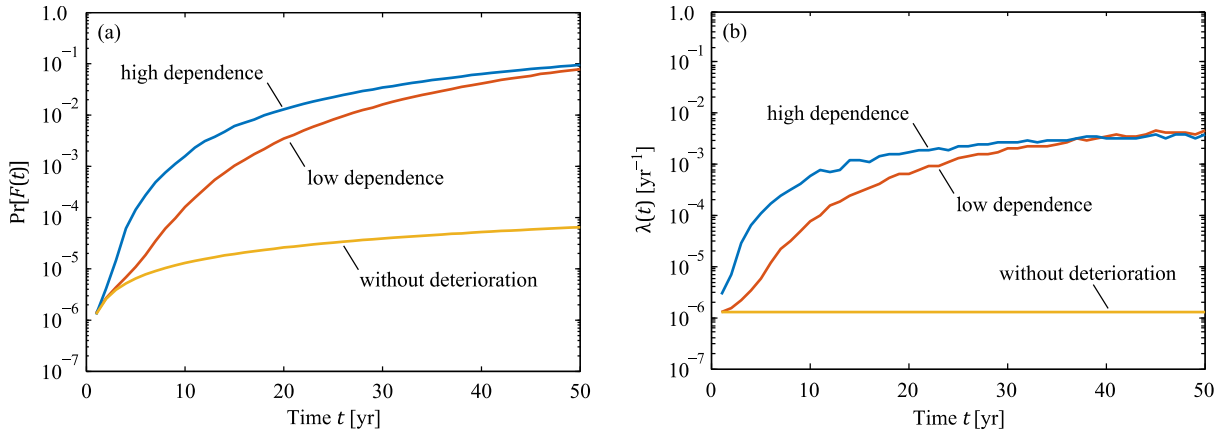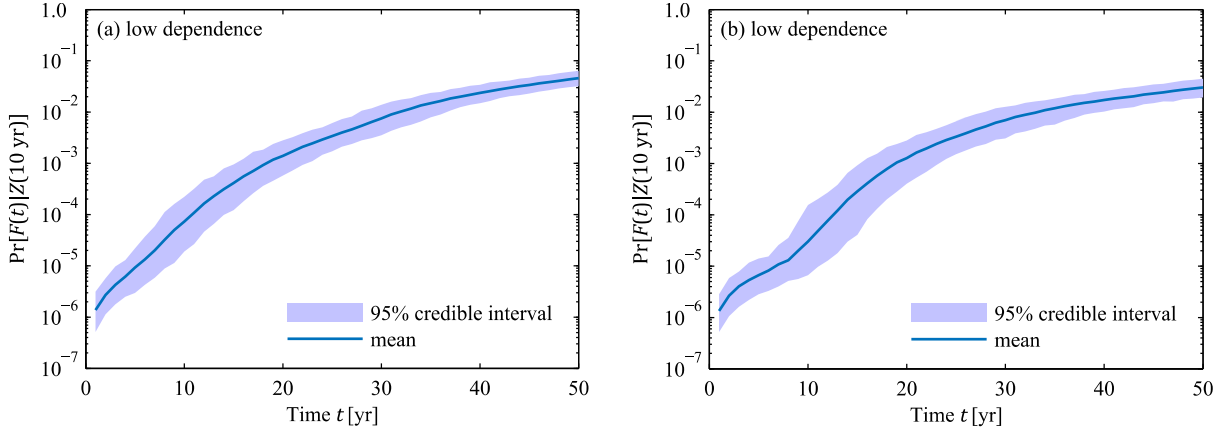 shows the failure probability $\Pr[F(t)]$ of the Zayas frame without deterioration. The corresponding failure rates $\lambda(t)$ are evaluated from $\Pr[F(t)]$ according to Equation (4.9) and shown in Figure 5.8(b). The effect of deterioration on the structural reliability of the frame is clearly visible. In addition, it is evident that a higher dependence among fatigue failures in the structural system leads to a larger system failure probability due to an increased probability of two or more simultaneous fatigue failures. This result is expected for a redundant structural system (Straub and Der Kiureghian 2011).

The net-present value of the service life risk is computed following Equation (4.10) with $\gamma = 2\%$ and $c_F(t) = €10^6$. Without deterioration, the risk is €39.8. With deterioration, it is $€3.76 \cdot 10^4$ when the dependence among hotspot fatigue behavior is small, and $€4.98 \cdot 10^4$ when the dependence is high. The effect of deterioration and dependence among hotspot fatigue behavior is again evident.

5.7.1.5 Posterior reliability analysis

In this section, different inspection scenarios in terms of inspection times, coverage and outcomes are considered to study the effect of inspections on the reliability estimates for the Zayas frame. Firstly, hotspots $\{5, 6, 13, 14, 21, 22\}$ are inspected at time $t = 10$ yr. These hotspots are associated with the least important braces of the frame (see Figure 5.4 and Table 5.2). It is assumed that no fatigue cracks are indicated during the inspection. Figure 5.9 shows the probability of failure of the structure conditional on the inspection outcome as a function of the degree of dependence among hotspot fatigue behavior. At each time t, the failure probability is conditioned on the inspection outcomes available up to time $t = 10$ yr. For times $t < 10$ yr, this corresponds to smoothing (see also Section 4.5). The computation of $\Pr[F(t)|Z(10 \text{ yr})]$ follows Sections 5.5 and 5.6.

Figure 5.10 compares the best estimate of $\Pr[F(t)|Z(10 \text{ yr})]$ with the best estimate of the corresponding bounds. The bounds on $\Pr[F(t_j)|Z(10 \text{ yr})]$ are evaluated by substituting the prior interval failure probabilities $\Pr(F_j^*)$ in Equation (4.20) with the posterior interval failure probabilities $\Pr[F_j^*|Z(10 \text{ yr})]$. The probabilities $\Pr[F_j^*|Z(10 \text{ yr})]$ are in turn determined by substituting

Figure 5.9: Updated failure probability $\Pr[F(t)|Z(10\text{ yr})]$ of the Zayas frame. Hotspots $\{5, 6, 13, 14, 21, 22\}$ are inspected at time $t = 10$ yr. No fatigue cracks are indicated during the inspection.
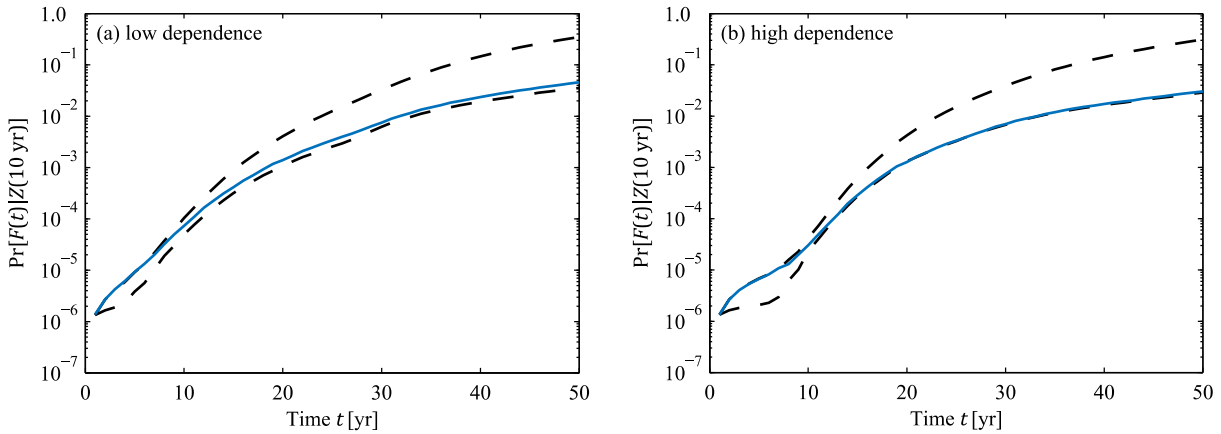
Figure 5.10: Best estimate of the bounds on $\Pr[F(t)|Z(10\text{ yr})]$ together with the best estimate of $\Pr[F(t)|Z(10\text{ yr})]$. Hotspots $\{5, 6, 13, 14, 21, 22\}$ are inspected at time $t = 10$ yr. No fatigue cracks are indicated during the inspection.

$\Pr[F(t_j)|\mathbf{X}_R = \mathbf{x}_R]$ in the limit state function $g_{F \cap Z}$ defined in Equation (5.20) with $\Pr(F_j^* | \mathbf{X}_R = \mathbf{x}_R)$ (see also Schneider et al. 2017). $\Pr[F_j^*|Z(10\text{ yr})]$ is subsequently calculated following Equation (5.22).

The updated failure probability $\Pr[F(t)|Z(10\text{ yr})]$ is closer to the upper bound approximately for the first 10 years. This result implies that in this period, the reliability is dominated by the uncertainty on the time-variant loads. Thereafter, the failure probability approaches again the lower bound as the effect of the inspection decreases with time and the uncertainty on the structural condition dominates again the reliability.

Figure 5.11 shows the best estimate of the failure probability at time t conditional on the information available up to time t, i.e. $\Pr[F(t)|Z(t)]$. This corresponds to filtering (see also Section 4.5). In addition, Figure 5.11 plots the best estimate of the failure probability at time t conditional on the information available up to time $t = 10$ yr, i.e. $\Pr[F(t)|Z(10\text{ yr})]$. It is evident that the failure probability of the frame reduces because of the inspection result. The effect is larger when the dependence among hotspot fatigue failures is high.

Figure 5.11: Best estimate of the failure probability of the Zayas frame at time t conditional the inspection outcome. The solid line is the failure probability at time t conditional on the information available up to time t, i.e. $\Pr[F(t)|Z(t)]$ (filtering). The dashed line is the failure probability at time t conditional on the information available up to time $t = 10$ yr, i.e. $\Pr[F(t)|Z(10 \text{ yr})]$. Hotspots $\{5, 6, 13, 14, 21, 22\}$ are inspected in year 10. No fatigue cracks are indicated during the inspection.

In the second example, hotspots $\{15,16,17,18,19,20\}$ are inspected at time $t = 10$ yr. These hotspots are associated with the most important braces of the Zayas frame (see Figure 5.4 and Table 5.2). It is again assumed that no fatigue cracks are indicated. The corresponding posterior failure probability $\Pr[F(t)|Z(10 \text{ yr})]$ of the structure is shown in Figure 5.12 for both degrees of dependence among hotspot fatigue behavior.

Figure 5.13 shows the best estimate of the bounds on $\Pr[F(t)|Z(10 \text{ yr})]$ together with the best estimate of $\Pr[F(t)|Z(10 \text{ yr})]$. The updated failure probability is close to the upper bound approximately for the first 12 years indicating that deterioration is negligible in this period and the reliability is dominated by the time-variant loads. Over time, when the effect of the inspection outcome diminishes, the uncertainty on the structural condition dominates again the reliability.

Figure 5.14 shows best estimate of the filtered failure probability $\Pr[F(t)|Z(t)]$ together with the best estimate of the failure probability conditional on the information available up to time $t = 10$ yr, i.e. $\Pr[F(t)|Z(10 \text{ yr})]$. In contrast to the first inspection scenario, an inspection of the most

Figure 5.12: Updated failure probability $\Pr[F(t)|Z(10 \text{ yr})]$ of the Zayas frame. Hotspots $\{15,16,17,18,19,20\}$ are inspected at time $t = 10$ yr. No fatigue cracks are indicated during the inspection.
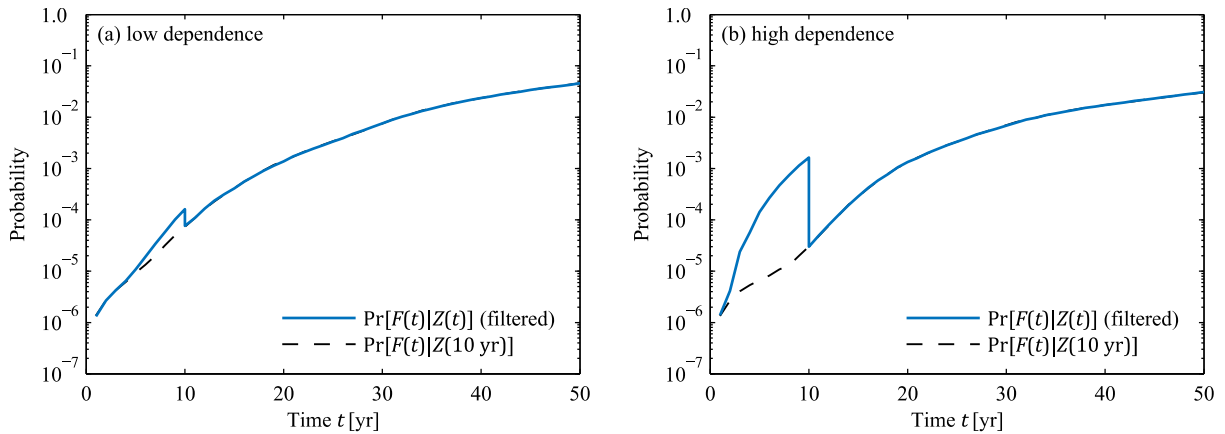
85
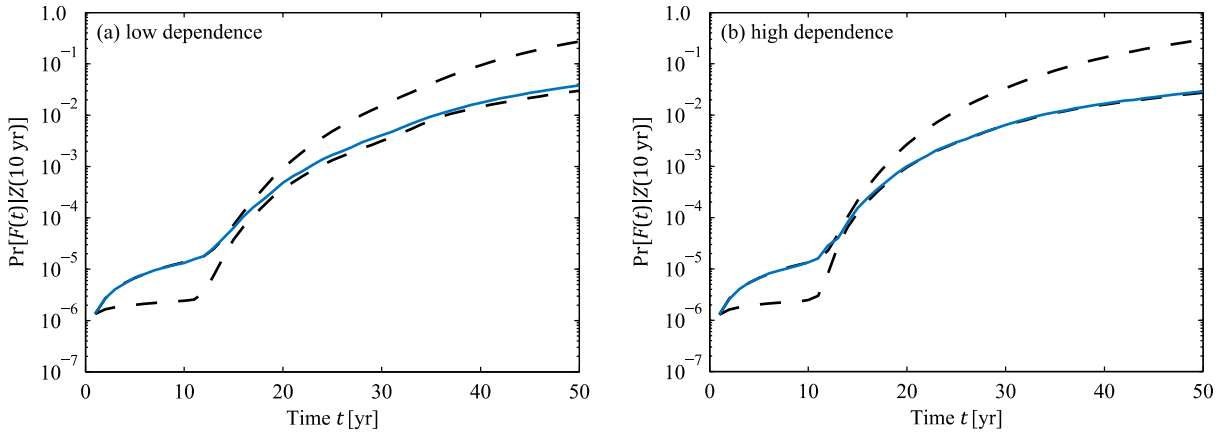
Figure 5.13: Best estimate of the bounds on $\Pr[F(t)|Z(10\ \text{yr})]$ together with the best estimate of $\Pr[F(t)|Z(10\ \text{yr})]$. Hotspots $\{15,16,17,18,19,20\}$ are inspected at time $t = 10$ yr. No fatigue cracks are indicated during the inspection.
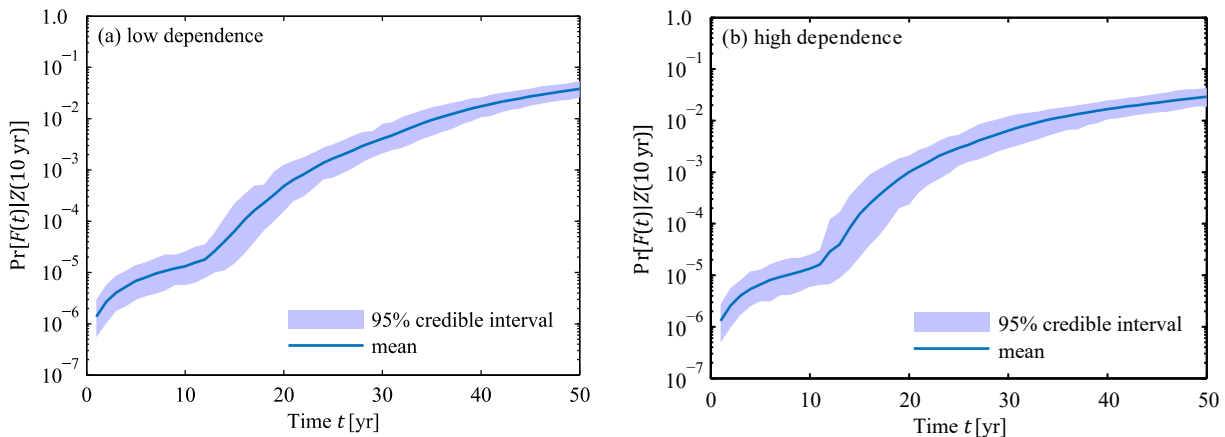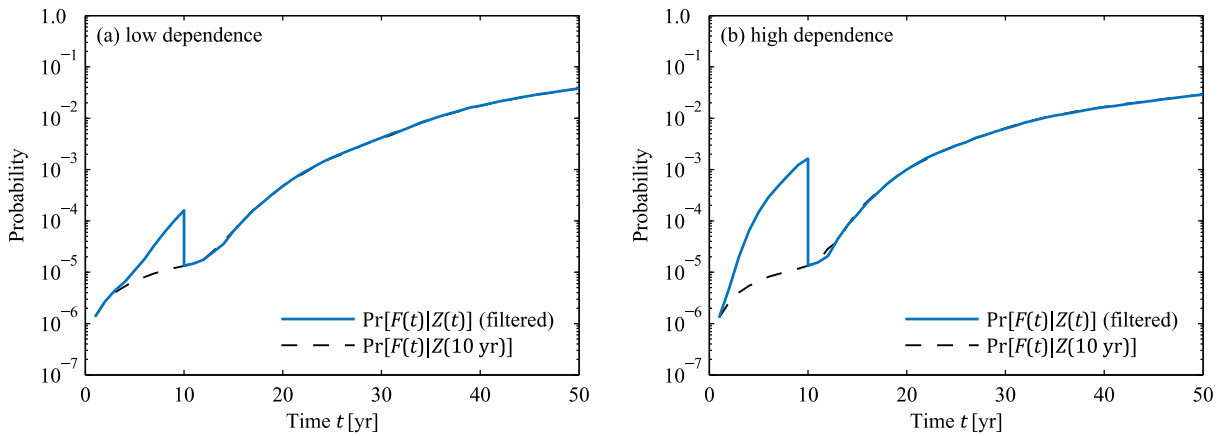

Figure 5.14: Best estimate of the failure probability of the Zayas frame at time t conditional the inspection outcome. The solid line is the failure probability at time t conditional on the information available up to time t, i.e. $\Pr[F(t)|Z(t)]$ (filtering). The dashed line is the failure probability at time t conditional on the information available up to year 10, i.e. $\Pr[F(t)|Z(10\ \text{yr})]$. Hotspots $\{5,6,13,14,21,22\}$ are inspected in year 10. No fatigue cracks are indicated during the inspection.

important structural elements has a significant effect on the failure probability regardless of the degree of dependence among hotspot deterioration.

In the third scenario, hotspots $\{15,16,17,18,19,20\}$ are again inspected in year 10. It is assumed that no fatigue cracks are indicated at hotspots $\{15,16,17,18\}$ and fatigue cracks are indicated at hotspots $\{19,20\}$. The updated failure probability $\Pr[F(t)|Z(10\ \text{yr})]$ is shown in Figure 5.15. The best estimate of the bounds on $\Pr[F(t)|Z(10\ \text{yr})]$ and the best estimate of $\Pr[F(t)|Z(10\ \text{yr})]$ are shown in Figure 5.16. The filtered failure probability $\Pr[F(t)|Z(t)]$ together with the failure probability conditional on the information available up to time $t = 10$ yr, $\Pr[F(t)|Z(10\ \text{yr})]$, are presented in Figure 5.17. In the low dependence case, the no indication and indication outcomes appear to counterbalance each other, and the joint inspection outcome has little effect on the estimated failure probability. In the high dependence case, the joint inspection outcome results in a small reduction in the failure probability estimate.

Figure 5.15: Updated failure probability $\Pr[F(t)|Z(10\,\mathrm{yr})]$ of the Zayas frame. Hotspots $\{15,16,17,18,19,20\}$ are inspected at time $t = 10$ yr. No fatigue cracks are indicated at hotspots $\{15,16,17,18\}$ and fatigue cracks are indicated at hotspots $\{19,20\}$.

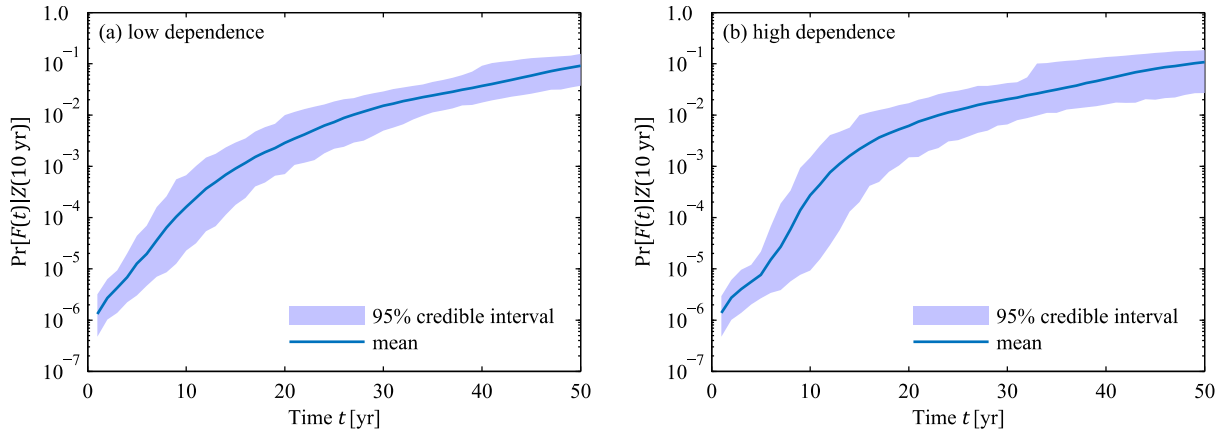**Figure 5.16:** Best estimate of the bounds on $\Pr[F(t)|Z(10\,\mathrm{yr})]$ together with the best estimate of $\Pr[F(t)|Z(10\,\mathrm{yr})]$. Hotspots $\{15,16,17,18,19,20\}$ are inspected at time $t = 10$ year. No fatigue cracks are indicated at hotspots $\{15,16,17,18\}$ and fatigue cracks are indicated at hotspots $\{19,20\}$.
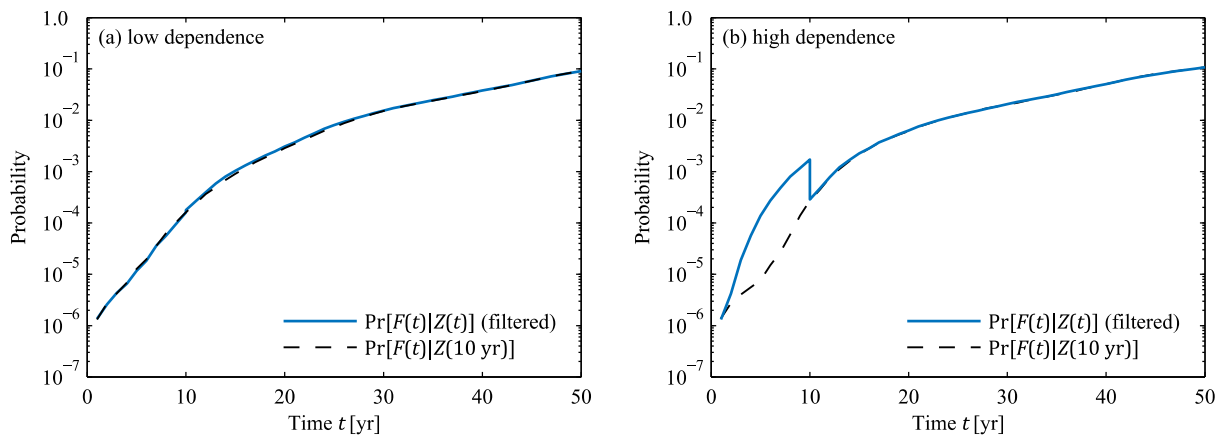
Figure 5.17: Best estimate of the failure probability of the Zayas frame at time t conditional the inspection outcome. The solid line is the failure probability at time t conditional on the information available up to time t, i.e. $\Pr[F(t)|Z(t)]$ (filtering). The dashed line is the failure probability at time t conditional on the information available up to time $t = 10$ yr, i.e. $\Pr[F(t)|Z(10\,\mathrm{yr})]$. Hotspots $\{15,16,17,18,19,20\}$ are inspected at time $t = 10$ year. No fatigue cracks are indicated at hotspots $\{15,16,17,18\}$ and fatigue cracks are indicated at hotspots $\{19,20\}$.

In the last scenario, regular inspections are performed every 10 years. Hotspots {15,16,7,8,5,6} are inspected at time $t = 10$ yr, hotspots {17,18,9,10,13,14} at time $t = 20$ yr, hotspots {19,20,11,12,21,22} at time $t = 30$ yr and hotspots {1,2,3,4} at time $t = 40$ yr. This inspection scheme ensures that (a) each hotspot is inspected at least once during the structure's service life, (b) hotspots associated with braces of each importance category are checked during each inspection, with the exception of the last inspection, in which only hotspots associated with braces of the low importance category are inspected (see Figure 5.4 and Table 5.2). For simplicity, it is again assumed that all inspections result in a "no indication" outcome. The updated failure probability $\Pr[F(t)|Z(40 \text{ yr})]$ is shown in Figure 5.18, The results in Figure 5.18 demonstrate that the inspection outcomes influence the entire lifetime reliability of the frame.

Figure 5.19 shows the best estimate of the bounds on $\Pr[F(t)|Z(40 \text{ yr})]$ and the best estimate of $\Pr[F(t)|Z(40 \text{ yr})]$. The failure probability $\Pr[F(t)|Z(40 \text{ yr})]$ is close to the upper bound for the first 20 years if the dependence among element deterioration is small, and for the first 30 years if the dependence is high. This effect is due to the reduced influence of deterioration on the failure probability in this period.
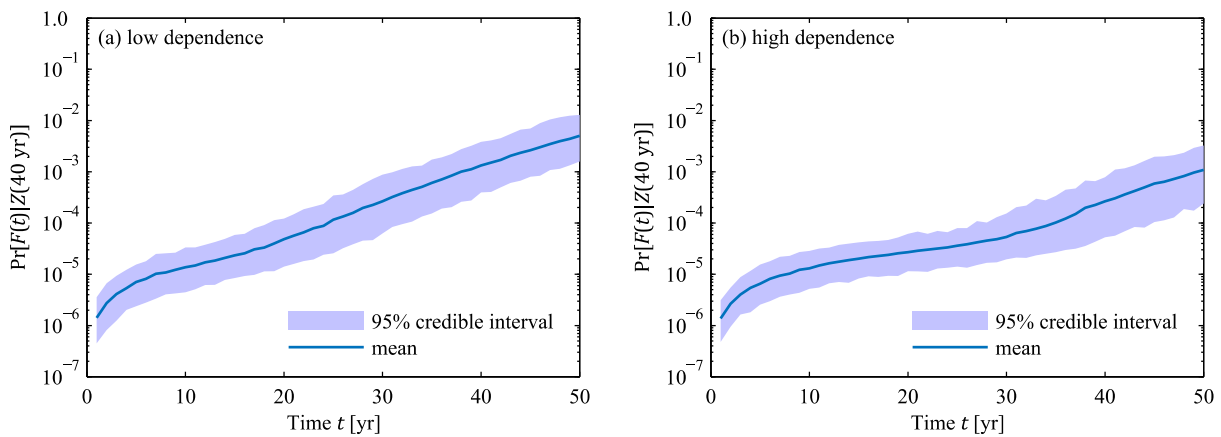
Figure 5.18: Updated failure probability $\Pr[F(t)|Z(40 \text{ yr})]$ of the Zayas frame. Hotspots {15,16,7,8,5,6} are inspected at time $t = 10$ yr, hotspots {17,18,9,10,13,14} at time $t = 20$ yr, hotspots {19,20,11,12,21,22} at time $t = 30$ yr and hotspots {1,2,3,4} at time $t = 40$ yr No fatigue cracks are indicated.

Figure 5.19: Best estimate of the bounds on $\Pr[F(t)|Z(40 \text{ yr})]$ together with the best estimate of $\Pr[F(t)|Z(40 \text{ yr})]$. Hotspots {15,16,7,8,5,6} are inspected at time $t = 10$ yr, hotspots {17,18,9,10,13,14} at time $t = 20$ yr, hotspots {19,20,11,12,21,22} at time $t = 30$ yr and hotspots {1,2,3,4} at time $t = 40$ yr. No fatigue cracks are indicated.
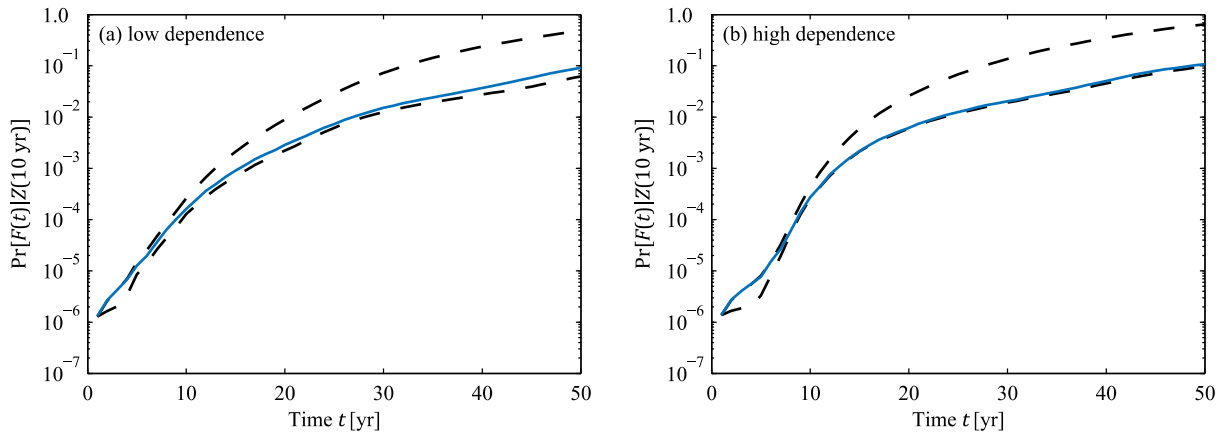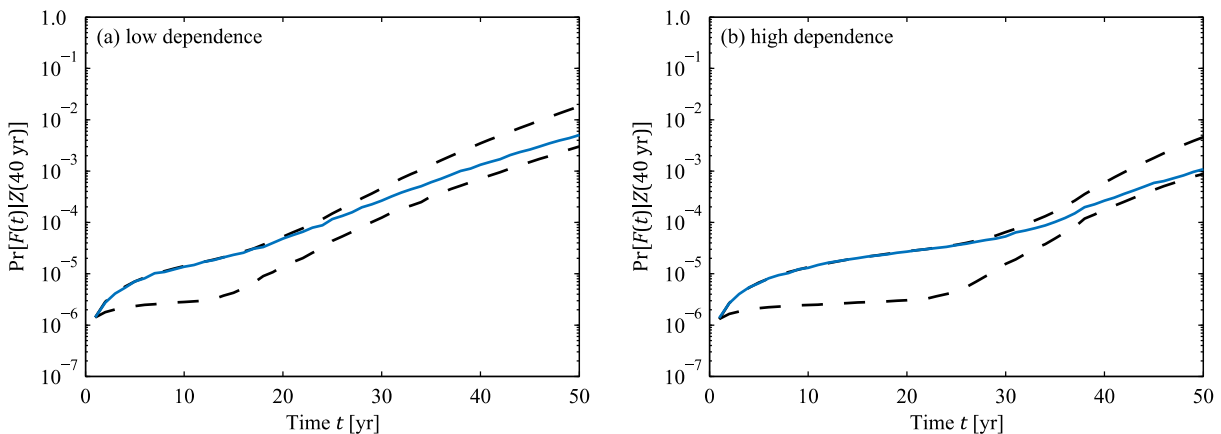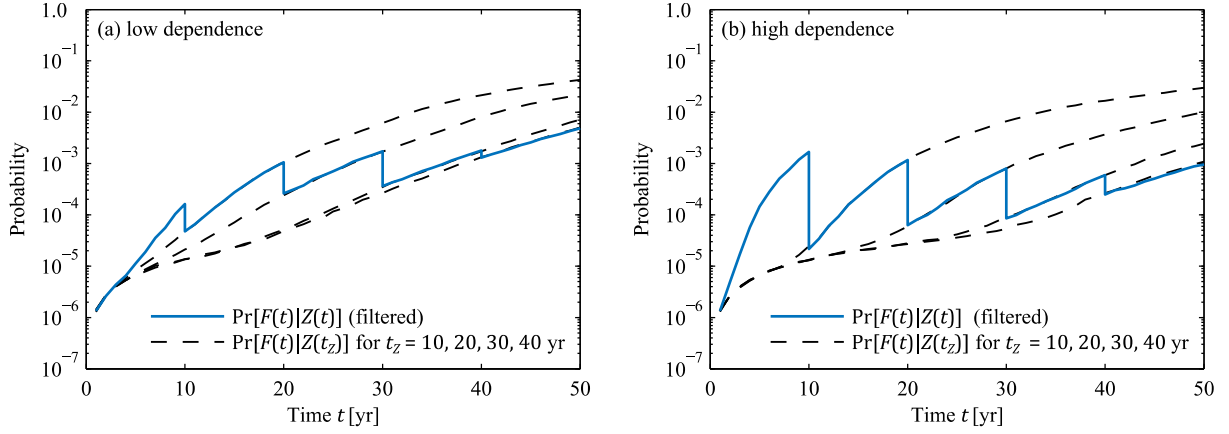
Figure 5.20: Best estimate of the failure probability of the Zayas frame at time t conditional on the inspection outcomes. The solid line is the filtered failure probability $\Pr[F(t)|Z(t)]$. The dashed lines are the conditional failure probabilities $\Pr[F(t)|Z(t_Z)]$ for inspection times $t_Z = 10, 20, 30, 40$ yr. Hotspots $\{15,16,7,8,5,6\}$ are inspected at time $t = 10$ yr, hotspots $\{17,18,9,10,13,14\}$ at time $t = 20$ yr, hotspots $\{19,20,11,12,21,22\}$ at time $t = 30$ yr and hotspots $\{1,2,3,4\}$ are inspected at time $t = 40$ yr. No fatigue cracks are indicated.

Figure 5.20 additionally presents the best estimate of the filtered failure probability $\Pr[F(t)|Z(t)]$ of the frame. It also shows the best estimates of the failure probabilities $\Pr[F(t)|Z(t_Z)]$ conditioned on the information available up to the different inspection times $t_Z = 10, 20, 30, 40$ yr. The inspection outcomes lead to a reduction in the failure probability $\Pr[F(t)|Z(t)]$ after each inspection. The largest reduction is obtained when the dependence among hotspot deterioration is high.

Table 5.6 summarizes 95% credible interval of the SuS estimates for the quantity[10] $c^{-1} \cdot \Pr[Z(t_Z)]$ at times $t_Z = 10, 20, 30, 40$ yr, which is equal to the denominator in Equation (5.14) (Straub and Papaioannou 2015b). It is a measure of the plausibility of the assumed model consisting of (a) the prior stochastic fatigue deterioration model (i.e. the physics-based deterioration model combined with the prior stochastic model of its model parameters) and (b) the inspection model (i.e. the likelihood function). In Bayesian system identification, the quantity $c^{-1} \cdot \Pr[Z(t_Z)]$ is referred to as the evidence of the assumed model and used in Bayesian model class selection (Beck 2010). In the current example, the two assumed models only differ in the degree of dependence among hotspot fatigue behavior. which is defined in terms of the coefficients of correlation specified in Table 5.4. The results in Table 5.6 show that high dependence yields the highest model evidence given the considered inspection data.

Figure 5.21(a) shows the conditional failure probability $\Pr[F(t)|Z(40 \text{ yr})]$ of the Zayas frame for both degrees of dependence among hotspot fatigue behavior, and Figure 5.21(b) shows the corresponding conditional failure rate $\lambda[t|Z(40 \text{ yr})]$. It is calculated from $\Pr[F(t)|Z(T_{SL})]$ as described in Section 4.5. Finally, the risk discounted to time $t = 0$ years is computed based on the posterior PDF $f_{T_F}[t|Z(T_{SL})]$ of the time to failure T_F, which is also determined from $\Pr[F(t)|Z(T_{SL})]$. With $\gamma = 2\%$ and $c_F(t) = €10^6$, the net-present value of the risk is $€2.17 \cdot 10^3$ in the low dependence case and $€4.66 \cdot 10^2$ in the high dependence case. These values are one to two orders of magnitude

---

[10] Note that the constant c is chosen such that $cL(\mathbf{x}_R|\mathbf{z}_{1:k}) \leq 1$ for all $\mathbf{x}_R$. In the current example, it is chosen as $c = 1$ (see Section 5.7.1.3)

Table 5.6: 95% credible interval of the SuS estimate of the model evidence $c^{-1} \cdot \Pr[Z(t_Z)]$ as a function of the different degrees of dependence among hotspot fatigue failures. The statistics of $c^{-1} \cdot \Pr[Z(t_Z)]$ are determined from 500 independent SuS runs.

	$c^{-1} \cdot \Pr[Z(t_Z)]$	
Time t_Z [yr]	Low dependence	High dependence
10	$[2.48; 3.03] \cdot 10^{-1}$	$[2.62; 3.18] \cdot 10^{-1}$
20	$[5.82; 8.28] \cdot 10^{-2}$	$[0.75; 1.03] \cdot 10^{-1}$
30	$[1.28; 2.22] \cdot 10^{-2}$	$[2.13; 3.43] \cdot 10^{-2}$
40	$[4.41; 8.89] \cdot 10^{-3}$	$[0.97; 1.66] \cdot 10^{-2}$
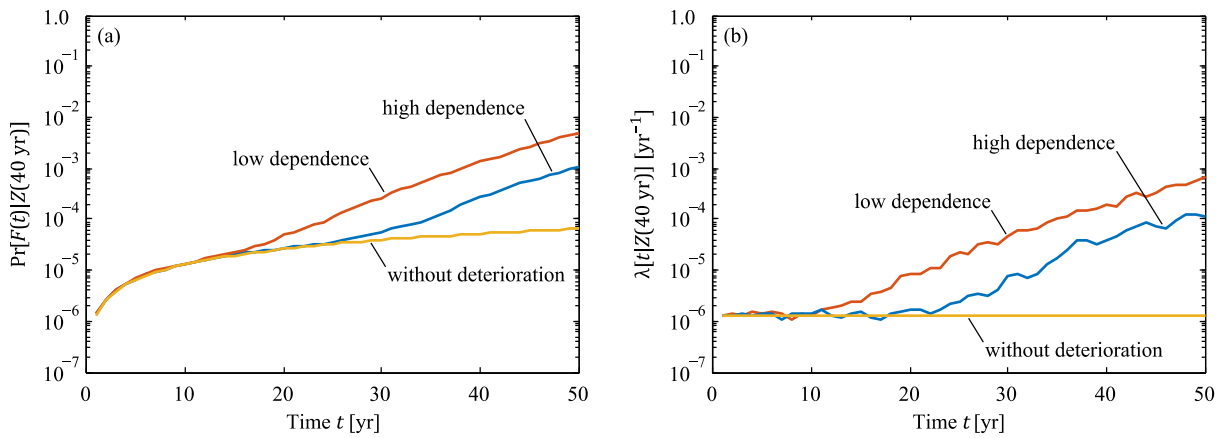
Figure 5.21: Updated (a) failure probability $\Pr[F(t)|Z(40\text{ yr})]$ and (b) failure rate $\lambda[t|Z(40\text{ yr})]$ of the Zayas frame. Hotspots $\{15,16,7,8,5,6\}$ are inspected at time $t = 10$ yr, hotspots $\{17,18,9,10,13,14\}$ at time $t = 20$ yr, hotspots $\{19,20,11,12,21,22\}$ at time $t = 30$ yr and hotspots $\{1,2,3,4\}$ at time $t = 40$ yr. No fatigue cracks are indicated.

smaller than the corresponding values computed for the deteriorating Zayas frame without inspection (see Section 5.7.1.4).

5.7.2 Daniels system

The NRA approach is applied to a Daniels system consisting of welded steel elements with ductile element behavior (see Section 2.4.3). The system is subject to a time-variant load $S(t)$. Additionally, the structural members are subject to fatigue deterioration throughout the system's service life of $T_{SL} = 50$ years. The effect of monitoring results on the reliability of the structural system is studied.

5.7.2.1 System model

The investigated Daniels system has $n_E = 100$ elements with capacities R_i, $i = 1, ..., n_E$. Each structural element is assumed to have one welded connection with one critical hotspot. Fatigue deterioration is again assessed at yearly intervals using the fatigue model presented in Section 5.7.1.2. The random vector $\mathbf{X}_R$ thus contains the capacities R_i, $i = 1, ..., n_E$ and the fatigue model parameters described in Section 5.7.1.2. The joint PDF of $\mathbf{X}_R$ is again represented by the Nataf model.

The condition of an element i at time t_j is modeled by a binary random variable $D_{i,j} = 1$ (element i is fully functioning at time t_j) and $D_{i,j} = 0$ (element i is has completely lost its capacity at time t_j). An element loses its capacity as soon as its welded connection fails. The function $h_{D,i}(\mathbf{X}_R, t_j)$ describing the relation between the capacity parameters $\mathbf{X}_R$ and the element condition $D_{i,j}$ is defined in Equation (5.31). The total capacity of the Daniels system R at time t_j can now be computed as:

$$R(\mathbf{X}_R, t_j) = \sum_{i=1}^{n_E} [1 - D_{i,j}] \cdot R_i \quad \text{with} \quad D_{i,j} = h_{D,i}(\mathbf{X}_R, t_j) \tag{5.48}$$

The element capacities R_i, $i = 1, \dots, n_E$ are modeled as equi-correlated identically normal distributed random variables with c.o.v. $\delta_R = 0.15$ and correlation coefficient $\rho_R = 0.8$. The different annual maxima of the applied load $S_{max,j}, j = 1, \dots, T_{SL}$ are independent and identically lognormal distributed with c.o.v. $\delta_{S_{max,j}} = 0.25$. The ratio of the mean values of $\sum_{i=1}^{n_E} R_i$ and $S_{max,j}$ is calibrated such that the Daniels system without deterioration has an interval failure probability of 1.3×10^{-6}, which corresponds to reliability index of 4.7. The resulting ratio is $n_E \mu_{R_i} / \mu_{S_{max,j}} = 3.97$. The calibration is performed with FORM.

Based on the above, the interval failure probability of the Daniels system in year j as a function of a realization of the capacity parameters $\mathbf{X}_R = \mathbf{x}_R$ can be written as:

$$\Pr(F_j^* | \mathbf{X}_R = \mathbf{x}_R) = \Pr[r(\mathbf{x}_R, t_j) \le S_{max,j}] = 1 - F_{S_{max,j}}[r(\mathbf{x}_R, t_j)] \tag{5.49}$$

where $r(\mathbf{x}_R, t_j)$ denotes the realization of the frame's capacity at time t_j when $\mathbf{X}_R$ takes the value $\mathbf{x}_R$, and $F_{S_{max,j}}(s)$ is the CDF of $S_{max,j}$.

Each element of the Daniels system is equally important due to the perfect load sharing among the structural elements. The single element importance measure of an individual element i of the Daniels system is $\text{SEI}_i = 2.0 \times 10^{-7}$. It follows that the Daniels system is highly redundant with respect to single element failure when compared to the Zayas frame studied in Section 5.7.1 where failure of elements of the highest importance category lead to a significant reduction in system reliability (see Table 5.2).

5.7.2.2 Monitoring model

Consider a monitoring system that periodically measures vibration time history data (e.g. accelerations) from the Daniels system under ambient excitation over finite time windows. Such data can provide information on the condition of the structure and thus indirect information on the capacity parameters $\mathbf{X}_R$. The basic idea is that damages influence the structure's stiffness and, consequently, its dynamic characteristics in terms of its modal parameters (modal frequencies, damping ratios and mode shapes). Changes in the dynamic characteristics of the structure may be an indication of damage. An introduction to vibration-based damage detection is, for example, provided in (Farrar et al. 2001). Following an idea published in (Thöns and Döhler 2012), the current numerical example presents a concept for quantifying the monitoring system's ability to detect fatigue damage in the Daniels system and integrating this type of monitoring information in the reliability analysis.

As described in Section 5.7.2.1, the elements of the Daniels system are modeled as being in a functioning or not functioning state at the end of each interval k as a function of fatigue deterioration. Thus, at any time t_k there are $N_{F,k}$ failed elements and $n_E - N_{F,k}$ elements are available to resist the applied load. Because of the exchangeability of its elements, $N_{F,k}$ represents the overall condition of the Daniels system at time t_k. $N_{F,k}$ is computed as a function h_D of the capacity parameters $\mathbf{X}_R$ as:

$$N_{F,k} = h_D(\mathbf{X}_R, t_k) = \sum_{i=1}^{n_E} \mathbb{I}[g_i(\mathbf{X}_R, t_k) \leq 0] \tag{5.50}$$

The limit state function $g_i(\mathbf{X}_R, t_k)$ describing fatigue failure of element i is defined in Equation (5.30).

Now let the continuous quantity $Y_{i,k}$ be a feature or indicator that is sensitive to fatigue damages in the Daniels system. It is derived from the ith recorded dataset in year k using a suitable algorithm. $Y_{i,k}$ could, for example, be a damage indicator determined by a damage detection algorithm (e.g. Döhler and Mevel 2013). Let $f_{Y_{i,k}|N_{F,j}}(y_{i,k}|n_{F,k})$ be the conditional PDF of $Y_{i,k}$, which represents the probability that the damage indicator is $Y_{i,k} = y_{i,k}$ given that the number of failed elements is $N_{F,k} = n_{F,k}$ at time t_k. It is illustrated Figure 5.22.

To enable an interpretation of the indicator $Y_{i,k}$, a threshold y_T is defined (see Figure 5.22). The Daniels system is assumed to be in the damaged condition if $Y_{i,k}$ is greater than y_T and in the undamaged condition otherwise. Note that (small) defects are always present in the Daniels system even in the undamaged condition, which is here defined as $N_{F,k} = 0$ (see also Section 5.7.1.1).

It is now possible to define the probability of indication $PoI(n_{F,k})$ as (see also Figure 5.22):

$$PoI(n_{F,k}) = \Pr(Y_{i,k} > y_T | N_{F,k} = n_{F,k}) = \int_{y_T}^{\infty} f_{Y_{i,k}|N_{F,k}}(y_{i,k}|n_{F,k}) \, \mathrm{d}y_{i,k} \tag{5.51}$$

The *PoI* can be interpreted as the probability that the monitoring system indicates fatigue damage in the Daniel system when the actual number of failed elements is $N_{F,k} = n_{F,k}$. It depends on the
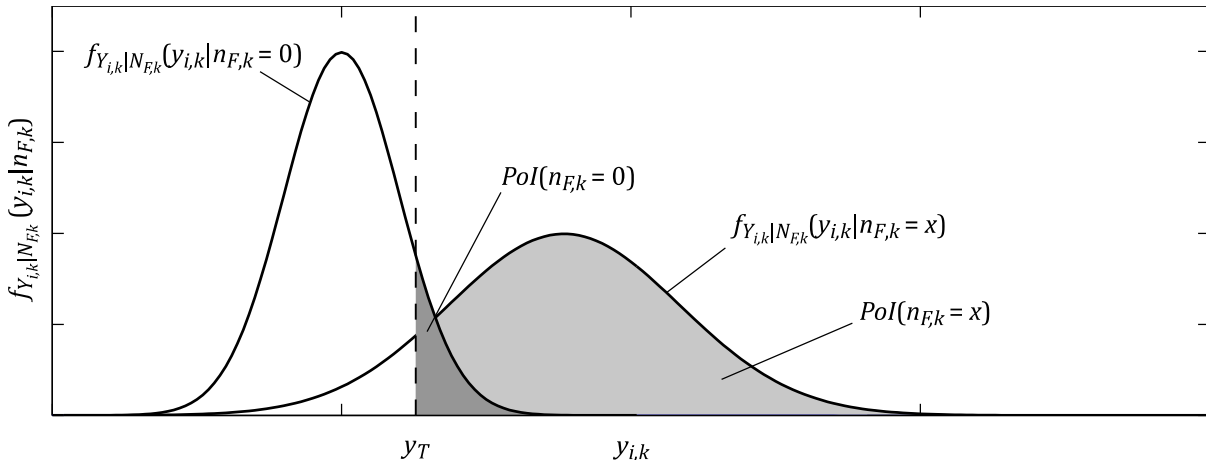
Figure 5.22: Illustration of the conditional PDF $f_{Y_{i,k}|N_{F,j}}(y_{i,k}|n_{F,k})$ of the damage indicator $Y_{i,k}$ and the probability of indication $PoI(n_{F,k})$ for $n_{F,k} = 0$ and $n_{F,k} = x$.

conditional PDF $f_{Y_{i,k}|N_{F,k}}(y_{i,k}|n_{F,k})$ of the indicator $Y_{i,k}$ and the threshold y_T. By varying the number of failed elements $n_{F,k}$ for a fixed threshold y_T, the different values of the PoI can be determined.

To derive the conditional PDF of $Y_{i,k}$, data from the undamaged and damaged structure are required. The acquisition of data from the damaged structure is typically not possible. Thus, the monitoring outcomes associated with various damage states have to be generated based on a stochastic data prediction model, which includes a model of the structural system that relates the observation to the damage states. The model has to account the associated uncertainties largely due to (a) measurement uncertainty, (b) statistical uncertainty due to the limited number of (numerical) trials performed to derive the monitoring model, (c) model uncertainty due to the simplified representation of the structural system, (d) model uncertainty due to the applied data processing method, (e) model uncertainty due to neglecting parameters other than the number of failed elements that also influence the monitoring outcome including material parameters, structural geometry, random defects and varying environmental and operational conditions, and (f) human errors (see also Straub 2004).

To determine the optimal value of the threshold y_T, Bayesian pre-posterior decision analysis could be applied (see, for example, Cottone et al. 2013; Thöns and Lanata 2013). If the monitoring system is employed within the context of managing the structural integrity of the Daniels system, the optimal threshold minimizes the expected value of the service life cost consisting of inspection, monitoring and repair/replacement/retrofitting cost as well as the structural risk.

A derivation of the conditional PDF of the indicator $Y_{i,k}$ and the threshold y_T is beyond the scope of this case study. Instead the assumed PoI model shown in Figure 5.23 is adopted for illustration purposes[11]. Table 5.7 summarizes the classification of the monitoring system, which follows Section 5.3.1.

In the following, the ith monitoring outcome in year k is modeled by a binary random variable $Z_{i,k}$ with states $Z_{i,k} = 0$ (no indication of a fatigue damage in the Daniels system in year k) and $Z_{i,k} = 1$ (indication of a fatigue damage in the Daniels system in year k). To derive the likelihood functions describing these monitoring outcomes, the function $h_D(\mathbf{X}_R, t_k)$ defined in Equation (5.50), which predicts the number of failed elements $N_{F,k}$ at time t_k, is embedded in the PoI model. The likelihood function modeling the monitoring outcome $Z_{i,k} = 1$ is written as:

$$L(\mathbf{x}_R|z_{i,k} = 1) = PoI[h_D(\mathbf{x}_R, t_k)] \tag{5.52}$$

The likelihood function describing the monitoring outcome $Z_{i,k} = 0$ is simply:

$$L(\mathbf{x}_R|z_{i,k} = 0) = 1 - PoI[h_D(\mathbf{x}_R, t_k)] \tag{5.53}$$

---

[11] In the present example, the following logistic model is used to describe the probability of indication: $PoI(n_{F,k}) = p_0 + L/[1 + \exp(-k \cdot (n_{F,k} - x_0))]$ with $p_0 = 0.1$, $L = 0.9$, $k = 1.0$ and $x_0 = 4$.

Table 5.7: Classification of the monitoring system employed to detect fatigue damage in the Daniels system.

Classification	Category
Inspected/monitored quantity	An indicator related to the condition of the system (The observed indicator $Y_{i,k}$ is derived from the recorded data and is related to the number of failed elements $N_{F,k}$ at time t_k.)
Type of information	Inequality information (indication/no indication of fatigue damage in the Daniels system)
Temporal characteristics	Periodic data collection over a certain period
Spatial characteristics	Spatially discrete data collection (Data are collected by different sensors, which are installed at discrete locations in the Daniels system.)
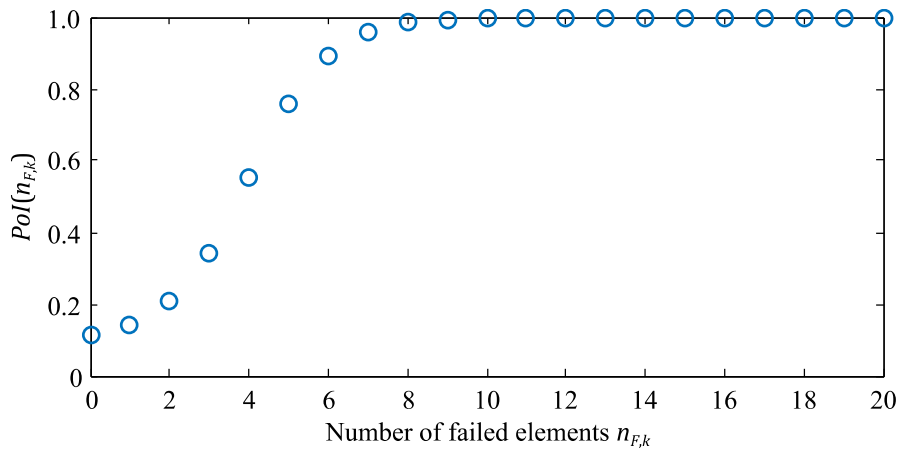
Figure 5.23: Assumed *PoI* model describing the ability of the monitoring system to detect fatigue damage in the Daniels system as a function of the number of failed elements $n_{F,k}$.

In the current example, it is assumed that the different monitoring outcomes $Z_{i,k}$ are statistically independent given the number of failed elements $N_{F,k} = n_{F,k}$. Thus, the combined likelihood function $L(\mathbf{x}_R|\mathbf{z}_{1:k})$ of all monitoring outcomes $\mathbf{Z}_{1:k} = \mathbf{z}_{1:k}$ up to time t_k is given by Equation (5.7).

The constant c that ensures $L(\mathbf{x}_R|\mathbf{z}_{1:k}) \leq 1$ for all $\mathbf{x}_R$ is set to $c = 1$ since indication/no-indication events provide inequality information (see also Section 3.2).

The monitoring model shown in Figure 5.23 has several limitations. Essentially, the model attempts to extract information from the vibration data that is useful for making inference about the capacity parameters $\mathbf{X}_R$. However, in the current (conceptual) formulation, valuable information – which is potentially contained in the measured data – is lost. First, the observation that the (continuous) indicator $Y_{i,k}$ is smaller or greater than the threshold y_T provides less information than the observation that $Y_{i,k}$ is equal to a certain value $y_{i,k}$. Provided that the conditional distribution of $Y_{i,k}$ given $N_{F,k} = n_{F,k}$, $f_{Y_{i,k}|N_{F,k}}(y_{i,k}|n_{F,k})$, is available, the likelihood function describing the relation between the observation $Y_{i,k} = y_{i,k}$ and the deterioration model parameters can be written as $L(\mathbf{x}_R|y_{i,k}) = f_{Y_{i,k}|N_{F,k}}[y_{i,k}|n_{F,k} = h(\mathbf{x}_R, t_j)]$.

Second, the indicator $Y_{i,k}$ is here modeled conditional on the (discrete) number of failed elements $n_{F,k}$. The measured data can, however, provide information about the (continuous) crack sizes at the different hotspots. An improved monitoring model would thus directly describe the relation

between the indicator $Y_{i,k}$ and the crack sizes at the different hotspots, which in turn are a function of the capacity parameters $\mathbf{X}_R$. In this case, the dimension of the monitoring model increases significantly, and a pre-computation of the conditional distribution of $Y_{i,k}$ for all possible combinations of crack sizes (based on a stochastic data prediction model as described above) would be intractable. Instead, the conditional distribution of $Y_{i,k}$ conditional on $\mathbf{X}_R = \mathbf{x}_R$ would have to be constructed on the fly each time the likelihood function $L(\mathbf{x}_R | y_{i,k})$ is evaluated. Obviously, this approach is not suitable for computational purposes.

Third, the monitoring model in Figure 5.23 assumes that monitoring outcomes (i.e. the indicators $Y_{i,k}$) derived from different datasets are independent. This assumption is not necessarily valid as the datasets are recorded by the same permanently installed equipment. Hence, different monitoring outcomes can, for example, be correlated because the underlying datasets are recorded under similar ambient conditions. Correlation among monitoring outcomes should be properly accounted for as it can have a large effect on the posterior distribution of the model parameters (Simoen et al. 2013) and, consequently, on the posterior reliability estimates.

Fourth, the model presented in Figure 5.23 implicitly describes the relation between the indicator $Y_{i,k}$ and the structural condition. The indicator is obtained by pre-processing the vibration data. Thus, the information in the data is condensed and some of the information that is useful for making inference about the capacity parameters is lost. The model could be improved by describing the relation between the data and the capacity parameters directly. A corresponding likelihood function may be formulated based on (a) a stochastic structural response model, which includes a model of the deterioration processes, (b) a prediction-error model describing the relation between the true structural response and the predicted structural response (model uncertainty), and (c) the observation-error model linking the measurement with the true structural response (measurement uncertainty) (e.g. Sedehi et al. 2019). However, it might still be beneficial to pre-process the potentially very large datasets to derive multiple meaningful features (e.g. natural frequencies, mode shapes, damping ratio etc.) instead of only a single feature/indicator as described above. The identified features can subsequently be used to infer the distribution of stochastic parameters defining the problem. This approach is similar to a two-stage Bayesian structural system identification (Au and Zhang 2016).

5.7.2.3 Prior reliability analysis

The prior probability of failure $\Pr[F(t)]$ of the Daniels system is estimated for each degree of dependence among hotspot fatigue behavior following Sections 5.4 and 5.6. The results are shown in Figure 5.24. In general, a large dependence among hotspot fatigue behavior results in a larger probability of joint occurrence of several fatigue failures. Figure 5.24 shows that this behavior severely reduces the reliability of the Daniels system. This outcome is expected for a structural system with a large redundancy (Straub and Der Kiureghian 2011). In contrast, the results computed for the Zayas frame show that the degree of dependence among hotspot fatigue behavior has less influence on the failure probability of structural systems with limited or no redundancy (see Figure 5.6 and Figure 5.8).

Figure 5.25 shows the best estimate of the bounds on the failure probability $\Pr[F(t)]$ together with the best estimate of $\Pr[F(t)]$. The bounds are computed according to Equation (4.20). With a low degree of dependence among hotspot failure behavior, the failure probability $\Pr[F(t)]$ of the Daniels system is close to the upper bound throughout the service life indicating that the reliability is dominated by the uncertainty on the maximum demands $S_{max,j}$. The behavior of the Daniels system with a high degree of dependence among hotspot fatigue behavior differs significantly. In this case, the failure probability $\Pr[F(t)]$ approaches the upper bound only at the beginning of the service life, when the effect of deterioration is negligible. Subsequently, the failure probability $\Pr[F(t)]$ approaches the lower bound indicating that the reliability is dominated by the uncertainty associated with the deterioration process.

Figure 5.26 compares the best estimate of the failure probability $\Pr[F(t)]$ of the Daniels system with and without deterioration. For the Daniels system with a low degree of dependence among hotspot fatigue behavior, deterioration has no effect before year 25. In contrast, a high dependence among hotspot fatigue behavior significantly reduces the system reliability.
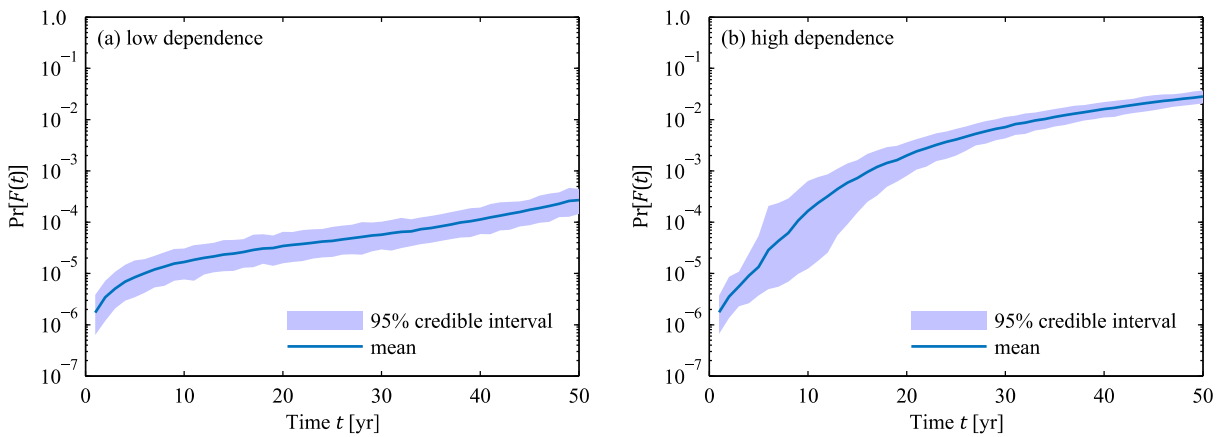
Figure 5.24: Failure probability $\Pr[F(t)]$ of the Daniels system as a function of different degrees of dependence among hotspot fatigue behavior.
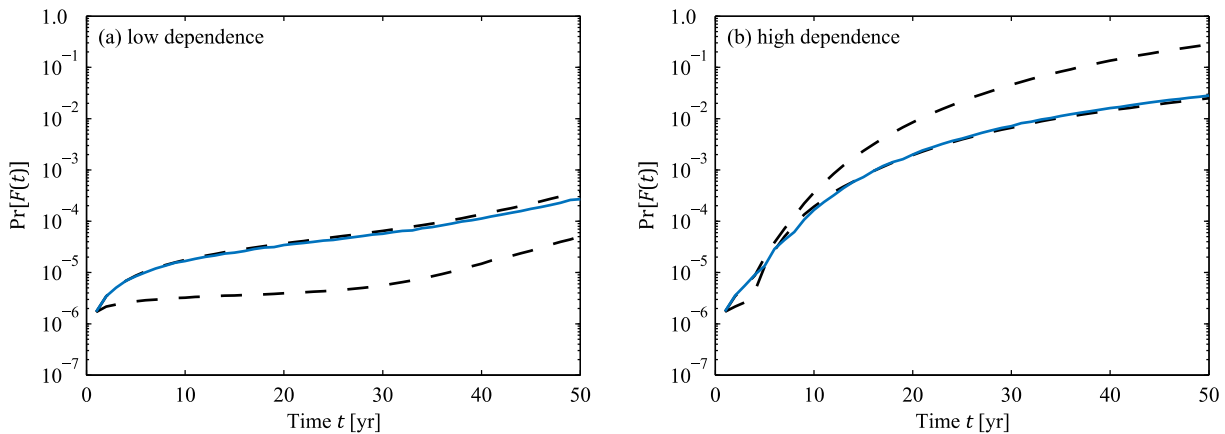
Figure 5.25: Best estimate of the bounds on the failure probability $\Pr[F(t)]$ of the Daniels system together with the best estimate of $\Pr[F(t)]$ as a function of different degrees of dependence among hotspot fatigue behavior.
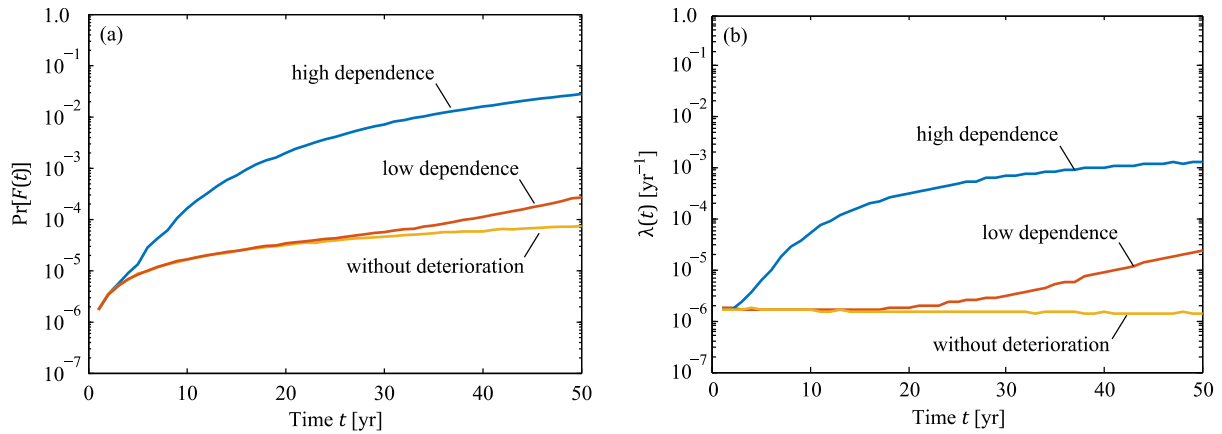
Figure 5.26: (a) Failure probability $\Pr[F(t)]$ and (b) failure rate $\lambda(t)$ of the Daniels system with and without deterioration.

5.7.2.4 Posterior reliability analysis

Different scenarios are considered in the following to study the effect of monitoring on the reliability estimates for the Daniels system. In the first scenario, monitoring is performed in year 10. It is assumed that no damage is indicated. The updated failure probability $\Pr[F(t)|Z(10\,\mathrm{yr})]$ is shown in Figure 5.27. For the Daniels system with low dependence among element deterioration, the monitoring outcome has no effect since deterioration does not have an effect before year 25 (see also Figure 5.26(a)). The monitoring outcome has a larger effect on the failure probability of the Daniels system with large dependence among element fatigue behavior. Figure 5.28 shows the bounds on the posterior failure probability. Figure 5.28(a) confirms that the current monitoring outcome has no effect on the estimated failure probability of the Daniels system with low dependence among element deterioration (see also Figure 5.29). Figure 5.28(b) indicates that the monitoring outcome reduces the uncertainty on the structural condition of the Daniels system with large dependence among element deterioration. Consequently, the reliability is dominated by the uncertainty on the demand and the failure probability approaches the upper bound. Once the uncertainty on the structural condition grows again, the failure probability approaches the lower bound.
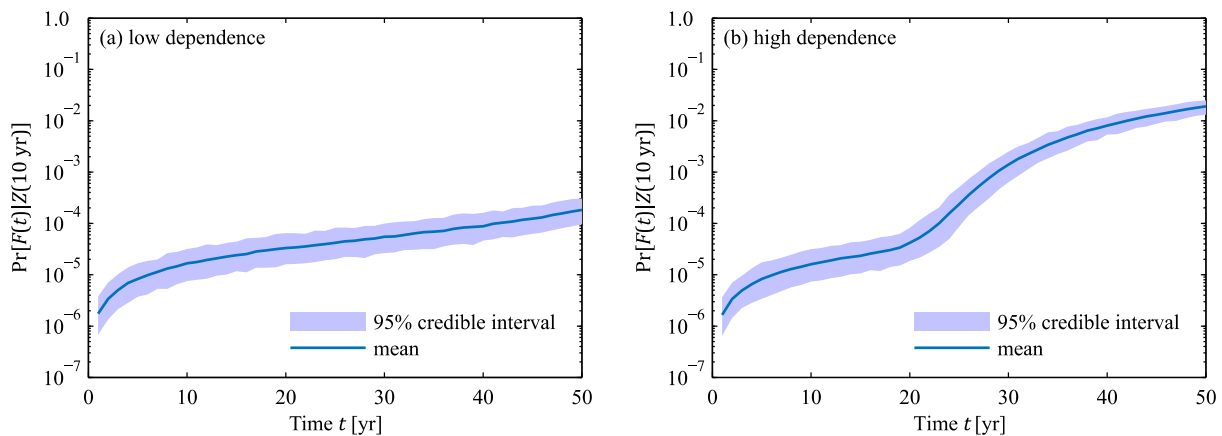
Figure 5.27: Updated failure probability $\Pr[F(t)|Z(10\,\mathrm{yr})]$ of the Daniels system. Monitoring is performed in year 10. No damage is indicated.

The best estimate of the filtered failure probability $\Pr[F(t)|Z(t)]$ together with the failure probability conditional on the information available up to time $t = 10$ yr, $\Pr[F(t)|Z(10 \text{ yr})]$, are presented in Figure 5.30. Both figures demonstrate again that the monitoring outcome has no effect
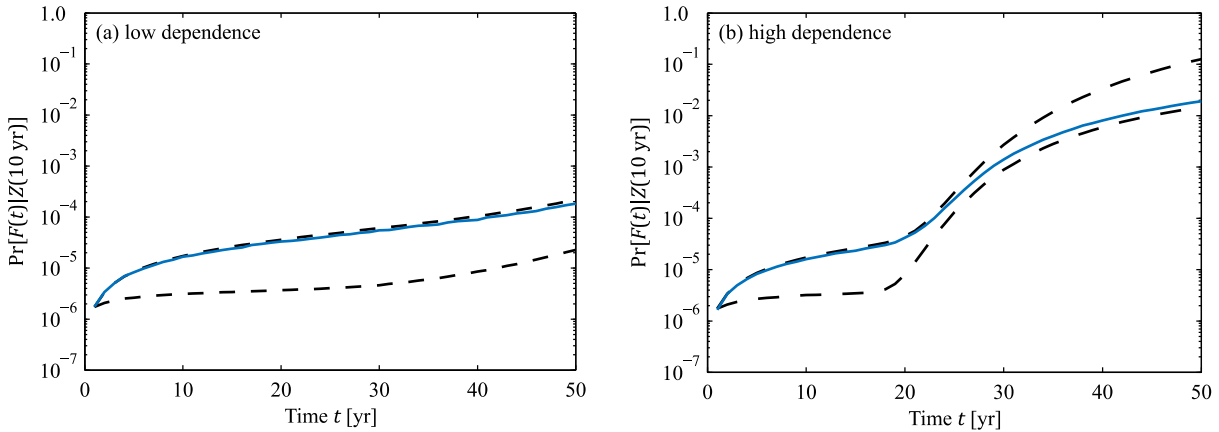
Figure 5.28: Best estimate of the bounds on $\Pr[F(t)|Z(10 \text{ yr})]$ together with the best estimate of $\Pr[F(t)|Z(10 \text{ yr})]$. Monitoring is performed in year 10. No damage is indicated.

Figure 5.29: Best estimates of $\Pr[F(t)]$ and $\Pr[F(t)|Z(10 \text{ yr})]$ of the Daniels system with low dependence among element deterioration. Monitoring is performed in year 10. No damage is indicated.

Figure 5.30: Best estimate of the failure probability of the Daniels system at time t conditional the monitoring outcome. The solid line is the failure probability at time t conditional on the information available up to time t, i.e. $\Pr[F(t)|Z(t)]$ (filtering). The dashed line is the failure probability at time t conditional on the information available up to time $t = 10$ yr, i.e. $\Pr[F(t)|Z(10 \text{ yr})]$. Monitoring is performed in year 10. No damage is indicated.

on the reliability estimate of the Daniels system with small dependence among element deterioration while it has a larger effect on the reliability estimate of the Daniels system with large dependence among element deterioration.

The second scenario assumes that damage is indicated during a monitoring campaign in year 10. The corresponding posterior failure probability $\Pr[F(t)|Z(10\text{ yr})]$ is shown in Figure 5.31. The monitoring result has only a marginal effect on the reliability estimate of the Daniels system with low dependence among hotspot fatigue behavior. In this case, as additionally illustrate din Figure 5.32, a reduction in the overall uncertainty on the structural condition because of the monitoring outcome leads to an initial reduction of the failure probability. Eventually, the posterior estimate of the failure probability exceeds the prior estimate, because the updated deterioration model predicts a faster fatigue crack growth. The effect is, however, limited. In contrast, the monitoring outcome significantly increases the estimate of the failure probability of the Daniels system with large dependence among element deterioration.

The best estimate of the bounds on $\Pr[F(t)|Z(10\text{ yr})]$ and the best estimate of $\Pr[F(t)|Z(10\text{ yr})]$ are shown in Figure 5.33. While the reliability of the Daniels system with low dependence among element deterioration is dominated by the uncertainty in the demand on the structure, the reliability
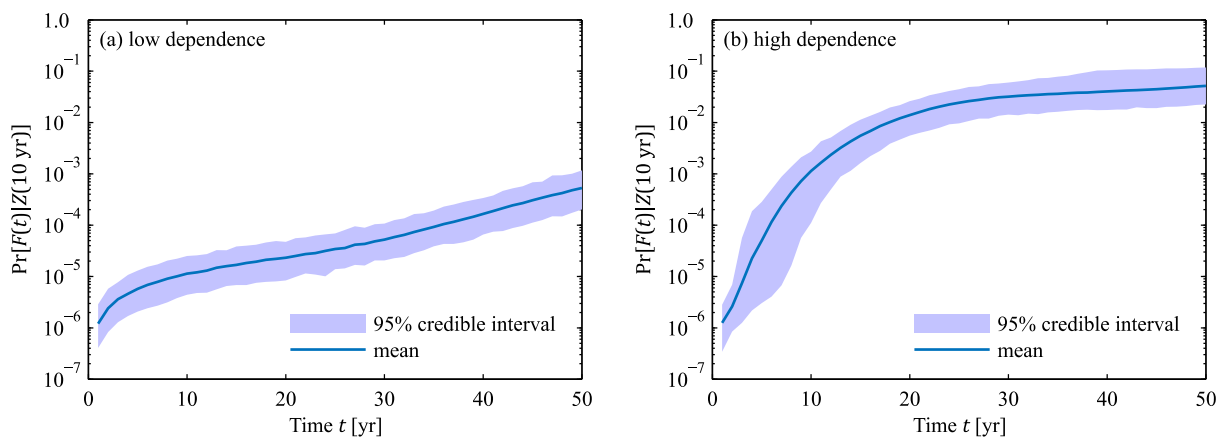
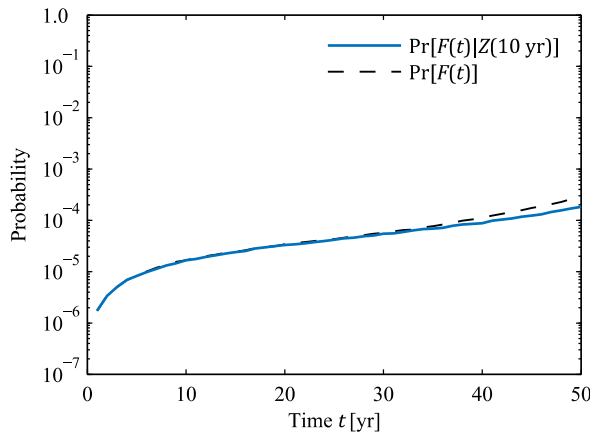

Figure 5.31: Updated failure probability $\Pr[F(t)|Z(10\text{ yr})]$ of the Daniels system. Monitoring is performed in year 10. Damage is indicated.
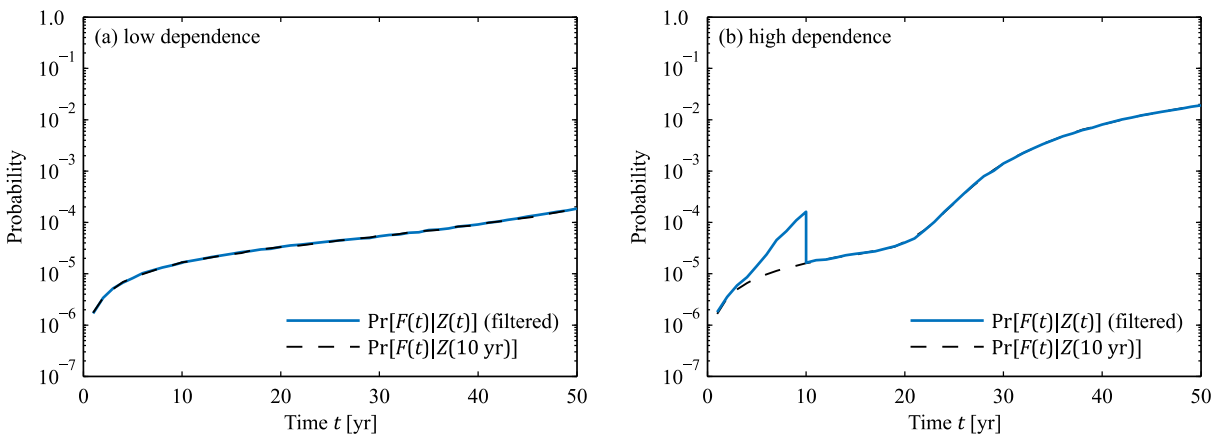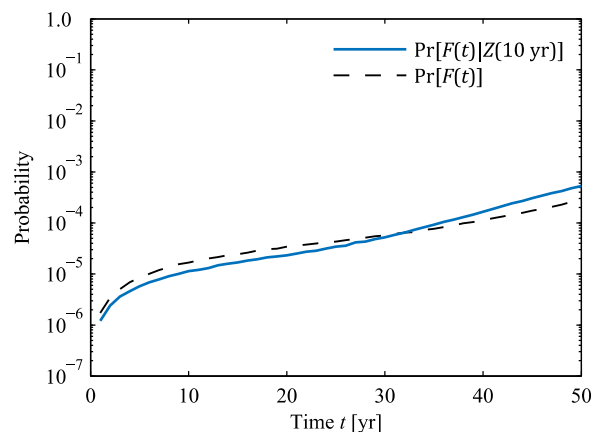

Figure 5.32: Best estimates of $\Pr[F(t)]$ and $\Pr[F(t)|Z(10\text{ yr})]$ of the Daniels system with low dependence among element deterioration. Monitoring is performed in year 10. No damage is indicated.
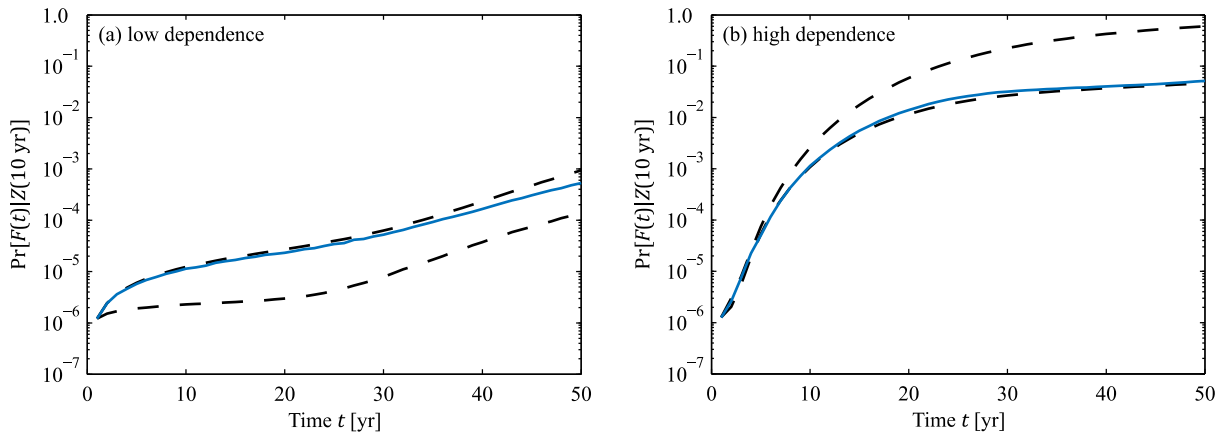
Figure 5.33: Best estimate of the bounds on $\Pr[F(t)|Z(10\text{ yr})]$ together with the best estimate of $\Pr[F(t)|Z(10\text{ yr})]$. Monitoring is performed in year 10. Damage is indicated.
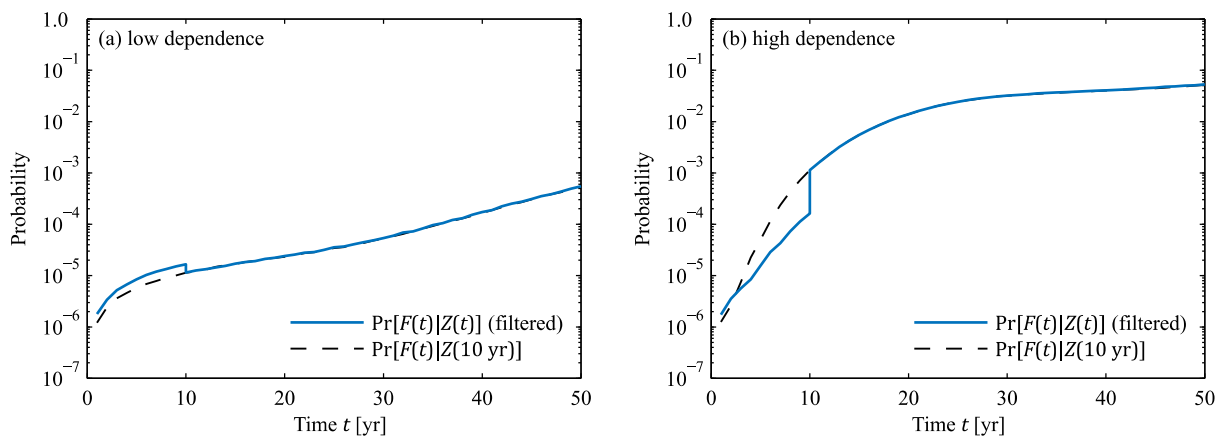
Figure 5.34: Best estimate of the failure probability of the Daniels system at time t conditional the monitoring outcome. The solid line is the failure probability at time t conditional on the information available up to time t, i.e. $\Pr[F(t)|Z(t)]$ (filtering). The dashed line is the failure probability at time t conditional on the information available up to time $t = 10$ yr, i.e. $\Pr[F(t)|Z(10\text{ yr})]$. Monitoring is performed in year 10. Damage is indicated.

of the Daniels system with large dependence among element deterioration is dominated by the uncertainty on the structural condition.

Figure 5.34 additionally shows the best estimate of the filtered failure probability $\Pr[F(t)|Z(t)]$ together with the probability of the failure event $F(t)$ conditional on $Z(10\text{ yr})$. The effect of the degree of dependence among element deterioration on the reliability estimates of the redundant structural system is again evident.

In the third scenario, monitoring is performed once a year throughout the structure's service life. For simplicity, it is assumed that no damage is indicated throughout the service life. Note that this is a monitoring outcome with a low probability of occurrence (see also Figure 5.37). The updated probability of failure $\Pr[F(t)|Z(50\text{ yr})]$ of the Daniels system is shown in Figure 5.35; the best estimate of the corresponding bounds on $\Pr[F(t)|Z(50\text{ yr})]$ together with the best estimate of $\Pr[F(t)|Z(50\text{ yr})]$ are shown in Figure 5.36. In both dependence cases, the positive monitoring results leads to a sustained reduction in the failure probability. The monitored structure behaves like a structure without deterioration due to the positive monitoring outcome.

Figure 5.37 shows 95% credible interval and the mean of the SuS estimate for the model evidence $c^{-1} \cdot \Pr[Z(t_Z)]$ as a function of monitoring time t_Z, where the constant c is also equal to one (see Section 5.7.2.2). The model considering high dependence among hotspot fatigue behavior yields the largest model evidence given the considered monitoring outcome (see also Section 5.7.1.5).
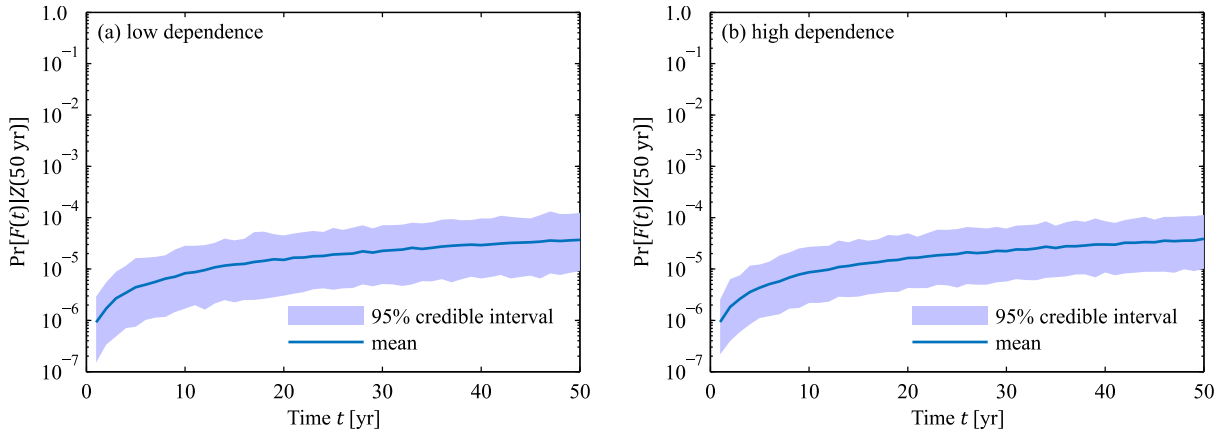
Figure 5.35: Updated failure probability $\Pr[F(t)|Z(50\ \text{yr})]$ of the Daniels system at time t. Monitoring is performed every year. No damage is indicated throughout the service life.
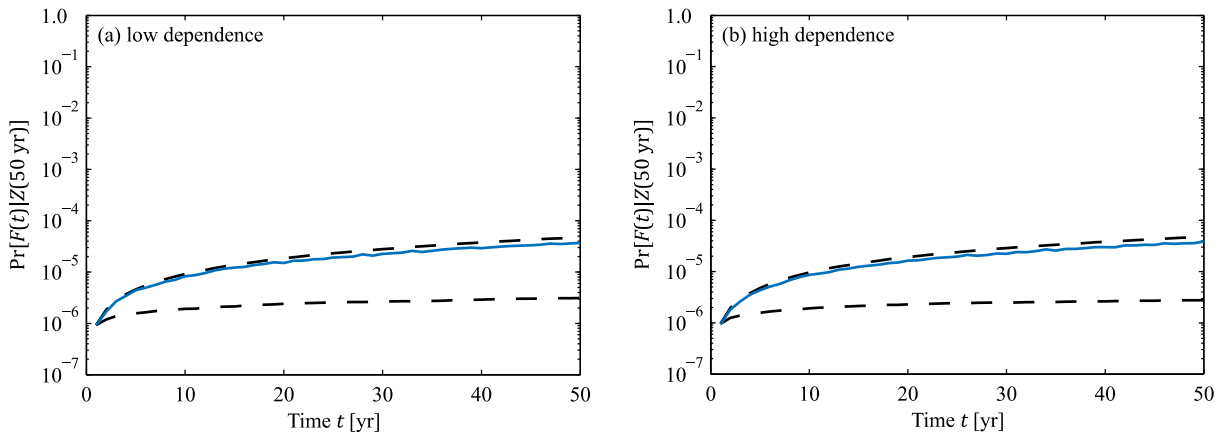
Figure 5.36: Bounds on the updated failure probability $\Pr[F(t)|Z(50\ \text{yr})]$ of the Daniels system at time t. Monitoring is performed every year. No damage is indicated throughout the service life.
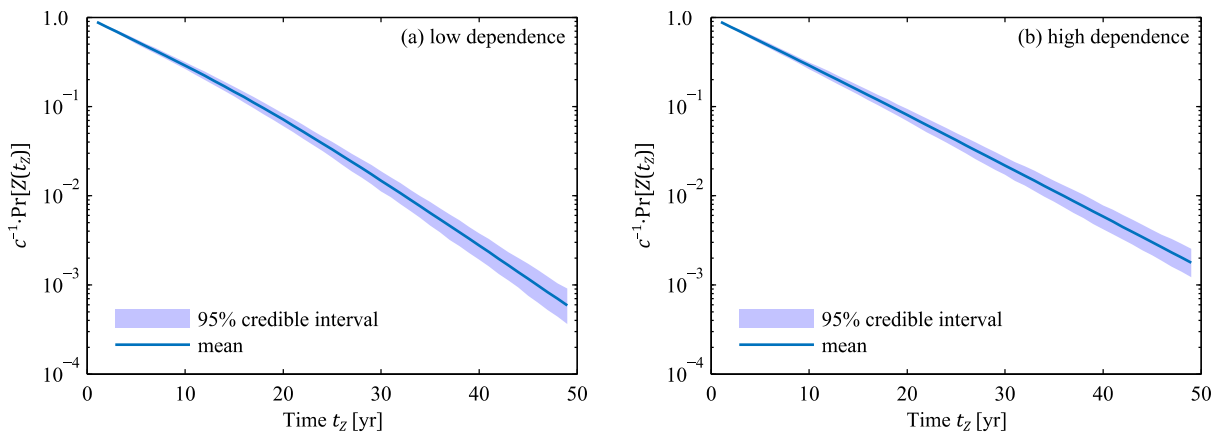
Figure 5.37: 95% credible interval and mean of the SuS estimate for the model evidence $c^{-1} \cdot \Pr[Z(t_Z)]$. Monitoring is performed every year. No damage is indicated throughout the service life.

101

6 Dynamic Bayesian network approach

6.1 Introduction

Bayesian networks (BN) are probabilistic graphical models, which have been developed in the field of artificial intelligence as a tool for reasoning under uncertainty (Russell and Norvig 2010). Over the past two decades, BN have increasingly been applied in engineering reliability and risk analysis (e.g. Friis-Hansen 2000; Faber et al. 2002; Grêt-Regamey and Straub 2006; Langseth and Portinale 2007; Straub and Der Kiureghian 2010b; Bensi et al. 2013; Luque and Straub 2016; Zwirglmaier and Straub 2016; Bismut et al. 2017; Luque and Straub 2019).

A BN is a compact representation of the joint probability distribution of a set of random variables. It consists of a set of nodes and a set of directed links, which together form a directed acyclic graph (DAG). The nodes in the graph represent the random variables, and the links – or rather the lack of links – represent conditional independence assumptions. Each random variable is assigned a local conditional probability distribution, which is defined conditional on its parents in the graph. The independence assumptions encoded in the graphical structure of the BN enable the factorization of the joint probability distribution into the conditional probability distribution of each variable given its parents.

BN are useful for Bayesian updating, i.e. for computing the posterior distribution of a set of random variables given that the values of another set of random variables are observed. This task is called probabilistic inference. Several efficient inference algorithms are available that exploit the conditional independence assumptions encoded in the BN (e.g. Murphy 2001; Jensen and Nielsen 2007).

The following features make BN a useful tool in engineering reliability and risk analysis (see also Straub 2014a; Zwirglmaier 2016)

(a) The graphical format of a BN facilitates the presentation of the model structure and the assumptions implemented in the model. This in turn helps to understand the capabilities and limitations of the model. In addition, the links in the graph often represent causal relations among the random variables. Thus, the dependence structure encoded in a BN can be understood by non-experts.

(b) Data on engineering systems is typically limited. By decomposing the joint probability distribution of the random variables defining the problem into local conditional probability distributions, the number of parameters required to quantify the probabilistic model is reduced. In addition, the modular structure of BN is ideally suited for constructing probabilistic system models required in engineering reliability and risk analysis in which multiple sub-models are typically combined in an overall system model.

(c) Bayesian updating can be performed when new observations of some of the random variables in the model becomes available.

(d)　BN can be extended to decision graphs by including decision and utility nodes (Jensen and Nielsen 2007). Decision graphs can, for example, be utilized to optimize decisions on risk mitigation measures following classical Bayesian decision theory (Raiffa and Schlaifer 1961; Benjamin and Cornell 1970).

In the context of deteriorating structural systems, Straub (2009) has originally modeled stochastic deterioration processes with dynamic Bayesian networks (DBN). Luque and Straub (2016) have extended the DBN model from Straub (2009) to model deteriorating structural systems that can be represented by model class (b) described in Section 4.3. The DBN model couples a model describing the condition of the structural system with a model of the structural system performance, which is defined conditional on the system condition. In its current format, the DBN model enables an evaluation of the interval failure probabilities of the deteriorating structural system conditional on inspection and monitoring outcomes that provide information on the structural condition. This modeling approach is here termed DBN approach and discussed in more detail in the following. First, Section 6.2 provides a more detailed introduction to Bayesian networks. Subsequently, Section 6.3 presents the generic DBN model for deteriorating structural systems. Section 6.4 then discusses some computational aspects related to the inference process. Finally, the DBN approach is applied in Section 6.5 to analyse the reliability of a concrete box girder subject to spatially distributed reinforcement corrosion. Section 6.5 also demonstrates how the model of the box girder can be implemented into a software prototype.

6.2　Bayesian networks

BN can be formulated for discrete and/or continuous random variables. The following introduction is restricted to BN consisting exclusively of discrete random variables. It summarizes the basic concepts and theory required for the remainder of Section 6. Section 6.2.1 presents the basic notions of graph theory following Kjaerulff and Madsen (2013). Subsequently, Section 6.2.2 formally defines discrete BN and explains how the graphical structure of a discrete BN implies the joint PMF of a set of discrete random variables in a compact factorized form. Section 6.2.3 provides an overview on inference in discrete BN and Section 6.2.4 briefly describes DBN. For a detailed introduction to BN, the reader is referred to (Jensen and Nielsen 2007; Russell and Norvig 2010; Murphy 2012; Kjaerulff and Madsen 2013).

6.2.1　Graphs

A graph $G = (V, E)$ consists of a finite set of vertices or nodes V and a set of edges or links $E \subseteq V \times V$. A directed link from node $v \in V$ to node $w \in V$ is designated by an ordered pair $(v, w) \in E$. Often the notation $v \rightarrow w$ is used to denote (v, w). It is assumed that a graph does not contain any directed links of the type (v, v) meaning that there are no self-loops. The sets $pa(v) = \{w : (w, v) \in E\}$ and $ch(v) = \{w : (v, w) \in E\}$ are the parents and children of node v. A node v is a root node if $pa(v) = \emptyset$. A link between nodes v and w is an undirected link if $(v, w) \in E$ and $(w, v) \in E$. An undirected link between v and w is typically denoted by $v - w$. A graph G is a directed graph if E does not contain any undirected links, and a graph G is an undirected graph if E does not contain any directed links.

A path $\langle v_1, \dots, v_n \rangle$ is a sequence of nodes such that $v_i - v_{i+1}$ for each $i = 1, \dots, n-1$. The length of a path is its number of links. A path $\langle v_1, \dots, v_n \rangle$ is a directed path if $v_i \to v_{i+1}$ for each $i = 1, \dots, n-1$. The notation $v \rightsquigarrow w$ is often applied to designate a directed path from node v to node w. The sets $anc(v) = \{w : w \rightsquigarrow v\}$ and $desc(v) = \{w : v \rightsquigarrow w\}$ are the ancestors and the descendants of node v. The set $nd(v) = V \setminus \{v \cup desc(v)\}$ are the non-descendants of node v.

A directed cycle is a directed path $\langle v_1, \dots, v_n \rangle$ of length greater than two in which the start node v_1 is equal to the end node v_n. A directed graph that does not contain any directed cycles is called a directed acyclic graph (DAG). The sequence $(v_1, \dots, v_n)$ is a topological ordering of the nodes in a DAG, if $pa(v_i) \subseteq \{v_1, \dots, v_{i-1}\}$ for all $i = 1, \dots, n$, i.e. parents come before their children in the ordering.

Graphically, nodes are represented as labeled circles and directed links as arrows. Figure 6.1 shows a simple DAG and an undirected graph. Both graphs have five nodes and four links. The graphs in Figure 6.1 belong to the class of singly connected graphs in which there is a maximum of one undirected path between any two nodes (Russell and Norvig 2010). A possible topological ordering of the DAG in Figure 6.1(a) is (b, a, c, d, e).

Figure 6.2 illustrates the parents, ancestors, children, descendants and non-descendants of a node v_i in a more complex DAG.

6.2.2 Discrete Bayesian networks

A discrete BN is a directed acyclic graph $G = (V, E)$, where $V = \{X_1, X_2, \dots, X_n\}$ is a set of discrete random variables and $E \subseteq V \times V$ is a set of directed links connecting pairs of variables. Each variable X_i with parents $pa(X_i)$ is assigned a conditional PMF $p(x_i | pa(x_i))$, where $pa(x_i)$ are the realizations of X_i's parents $pa(X_i)$. Thus, each random variable is defined conditional on its parents. The joint PMF of the random variables in a BN is given by the product of all conditional PMF specified in the BN (e.g. Jensen and Nielsen 2007):

$$p(x_1, \dots, x_n) = \prod_{i=1}^{n} p(x_i | pa(x_i)) \tag{6.1}$$
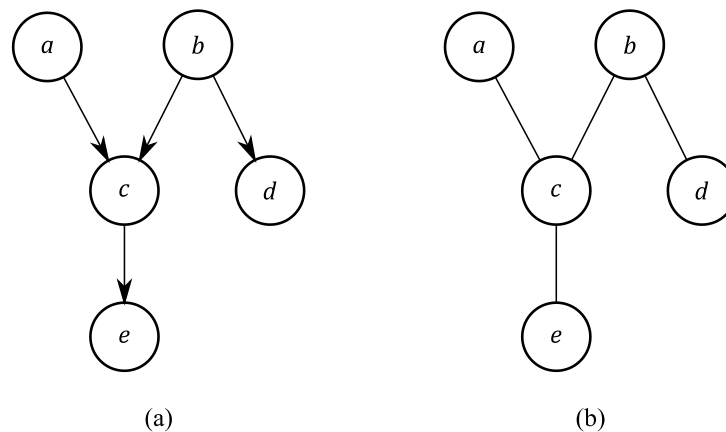
Figure 6.1: (a) A directed acyclic graph (DAG). (b) An undirected graph.
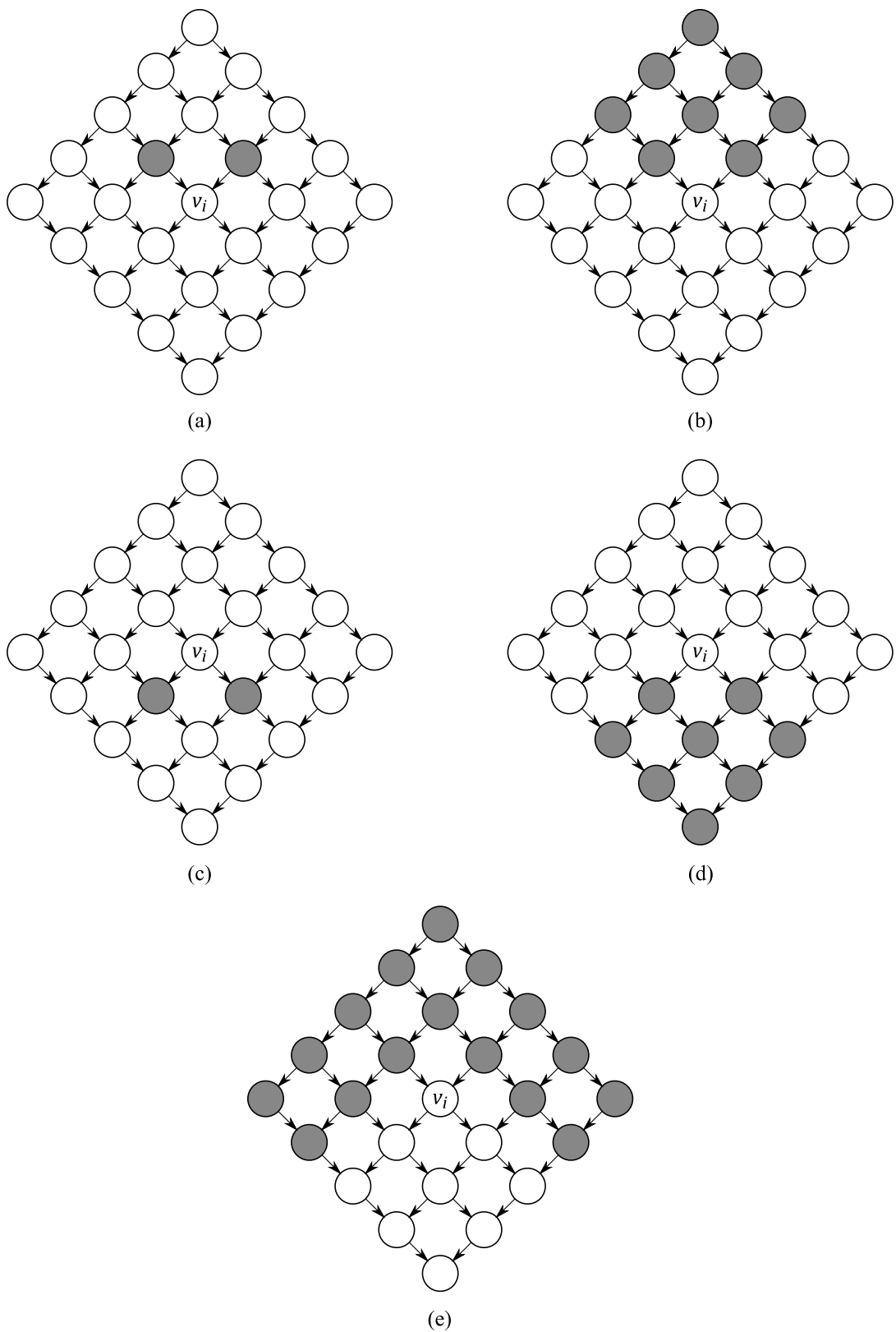
Figure 6.2: DAG with node v_i. The gray nodes respectively indicate v_i's (a) parents $pa(v_i)$, (b) ancestors $anc(v_i)$, (c) children $ch(v_i)$, (d) descendants $desc(v_i)$, and (e) non-descendants $nd(v_i)$.
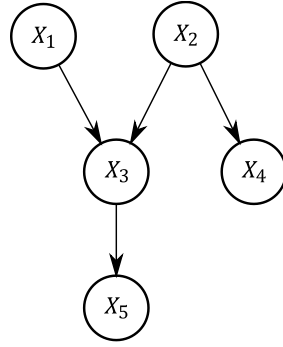
Figure 6.3: A Bayesian network representing the joint probability distribution $p(x_1, \dots, x_5)$ of five discrete random variables $X_1, \dots, X_5$.

The conditional PMF $p(x_i|pa(x_i))$, $i = 1, \dots, n$ are often called conditional probability tables (CPTs) since the numbers defining a PMF can be arranged in tables. As an example, consider the BN in Figure 6.3. The joint PMF of the variables represented by this BN is given by:

$$p(x_1, \dots, x_5) = p(x_5|x_3)p(x_4|x_2)p(x_3|x_2, x_1)p(x_2)p(x_1) \tag{6.2}$$

To demonstrate the validity of Equation (6.1), it is first noted that the conditional independence assumptions encoded in the graphical structure of a BN can be inferred by applying the criteria of d-separation (dependence separation) derived for causal networks (Pearl 1988). In a causal network, a directed link from node A to node B means that node A causes node B. Such networks may be interpreted as a mapping of human reasoning (see Jensen and Nielsen 2007 for more details).

Consider now a path $\pi = \langle X_1, \dots, X_n \rangle$ between nodes X_1 and X_n in a BN. Such a path is said to be d-separated if at least one of the following conditions holds for any $i = 2, \dots, n-1$ (see also Kjaerulff and Madsen 2013):

1. π contains a serial connection $X_{i-1} \to X_i \to X_{i+1}$ or $X_{i-1} \leftarrow X_i \leftarrow X_{i+1}$, and the state of X_i is known (i.e. the value of X_i is observed)
2. π contains a diverging connection $X_{i-1} \leftarrow X_i \to X_{i+1}$, and the state of X_i is known
3. π contains a converging connection $X_{i-1} \to X_i \leftarrow X_{i+1}$, and neither the state of X_i nor the states of any of X_i's descendants is known.

Now let the random vectors **U**, **Y** and **Z** represent three disjoint subsets of the random variables in a BN. The variables **U** and **Y** are said to be d-separated for given values of variables $\mathbf{Z} = \mathbf{z}$ if all paths from **U** to **Y** are d-separated for given $\mathbf{Z} = \mathbf{z}$. In a probabilistic context, d-separation corresponds to conditional independence (e.g. Kjaerulff and Madsen 2013). Hence, if the variables **U** and **Y** in a BN are d-separated for given $\mathbf{Z} = \mathbf{z}$, they are conditionally independent given $\mathbf{Z} = \mathbf{z}$, and the following relationships must hold:

$$p(\mathbf{u}, \mathbf{y}|\mathbf{z}) = p(\mathbf{u}|\mathbf{z})p(\mathbf{y}|\mathbf{z}) \tag{6.3}$$

$$p(\mathbf{u}|\mathbf{y}, \mathbf{z}) = p(\mathbf{u}|\mathbf{z}) \tag{6.4}$$

Note that when constructing BN it is not required that the directed links represent causal relationships among the variables. A BN should, however, not encode any conditional independence properties, which do not actually exist (Jensen and Nielsen 2007).

Now consider the BN in Figure 6.4. From the d-separation criteria it follows that X_i is conditionally independent from all nodes $nd(X_i) \setminus pa(X_i)$ (all gray nodes) if the values of its parents $pa(X_i)$ (black nodes) are known and the values of its descendants $desc(X_i)$ (all white nodes excluding node X_i) are unknown. This property of a BN is also called the directed local Markov property (Murphy 2012).

Finally, consider a BN with n discrete random variables $V = \{X_1, \dots, X_n\}$ and let $(X_1, \dots, X_n)$ be a topological ordering of the variables in the BN. From the directed local Markov property of a BN it can be concluded that each variable X_i is conditionally independent from all nodes $\{X_1, \dots, X_{i-1}\} \setminus pa(X_i)$ given the values of its parents $pa(X_i)$ are known and the values of its descendants $desc(X_i) \subseteq \{X_{i+1}, \dots, X_n\}$ are unknown. This means that for every variable X_i in the BN the conditional PMF $p(x_i|x_{i-1}, \dots, x_1)$ reduces to $p(x_i|pa(x_i))$. Substituting this into the joint PMF

$$p(x_1, \dots, x_n) = p(x_n|x_{n-1}, \dots, x_1)p(x_{n-1}|x_{n-2}, \dots, x_1) \dots p(x_2|x_1)p(x_1) \tag{6.5}$$

constructed using the chain rule of probability yields that the joint PMF of all variables in a BN is simply the product of the conditional PMF of each variable given its parents (see Jensen and Nielsen 2007 for a detailed proof). This demonstrates the validity of Equation (6.1). It follows that the graphical structure of a BN together with the conditional PMF $p(x_i|pa(x_i))$ are sufficient to fully specify the joint PMF of the variables in a BN.

6.2.3 Inference in discrete Bayesian networks

Two classes of inference methods can be distinguished for discrete BN: exact and approximate inference methods. To demonstrate the basic principles of the former, consider a BN with n discrete random variables $\mathbf{X} = [X_1, \dots, X_n]^T$. In the following, the variables are partitioned into $\mathbf{X} =$
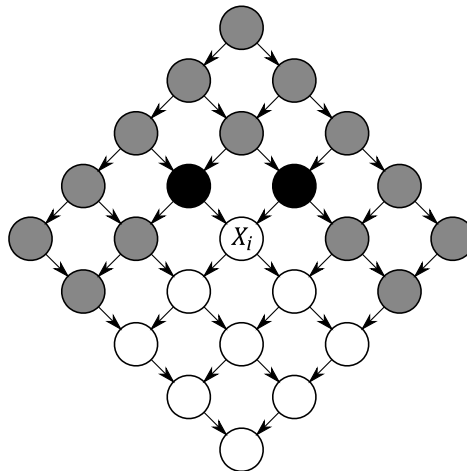
Figure 6.4: Illustration of the local Markov property. X_i is conditionally independent from all gray nodes if the values of its parents (black nodes) are known and the values of its descendants (all white nodes excluding node X_i) are unknown.

$[\mathbf{U}^T, \mathbf{Y}^T, \mathbf{Z}^T]^T$ to represent three disjoint subsets of the variables in the BN. Thus, the BN encodes the joint PMF $p(\mathbf{x}) = p(\mathbf{u}, \mathbf{y}, \mathbf{z})$. Suppose the values $\mathbf{z}$ of the random variables $\mathbf{Z}$ are observed and the posterior PMF of the variables $\mathbf{U}$ given $\mathbf{Z} = \mathbf{z}$ is of interest. It can be computed as follows:

$$p(\mathbf{u}|\mathbf{z}) = \frac{p(\mathbf{u}, \mathbf{z})}{p(\mathbf{z})} = \frac{\sum_{\mathbf{y}} p(\mathbf{u}, \mathbf{y}, \mathbf{z})}{\sum_{\mathbf{u}} \sum_{\mathbf{y}} p(\mathbf{u}, \mathbf{y}, \mathbf{z})} \tag{6.6}$$

Essentially, the variables $\mathbf{Z}$ are fixed at their observed values $\mathbf{z}$, then the variables $\mathbf{Y}$ are marginalized out by summing the distribution $p(\mathbf{u}, \mathbf{y}, \mathbf{z})$ over all states of the variables $\mathbf{Y}$ and finally the distribution $p(\mathbf{u}, \mathbf{z})$ is normalized. The normalizing constant $p(\mathbf{z}) = \Pr(\mathbf{Z} = \mathbf{z})$ is the probability of observing $\mathbf{Z} = \mathbf{z}$.

The summations in Equation (6.6) can be performed directly if the joint distribution $p(\mathbf{u}, \mathbf{y}, \mathbf{z})$ is represented as a multi-dimensional table. The number of entries in the table is equal to the product of the number of states of all random variables. For example, such a table has m^n entries if each of the n variables in the BN has m states. This number grows exponentially as n increases and direct summations quickly become intractable. However, by making use of the factorized form of the joint distribution $p(\mathbf{u}, \mathbf{y}, \mathbf{z})$ implied by the BN, it is possible to sequentially marginalize out the variables that are not of interest. The sizes of the tables over which summations are performed then depend on the order in which the variables are marginalized out. This approach is known as variable elimination (see, for example, Russell and Norvig 2010).

As an example, consider the BN shown in Figure 6.3 representing the joint PMF of variables $X_1, \ldots, X_5$. All variables have m states. Suppose $X_5 = x_5$ is observed and the conditional PMF $p(x_1|x_5)$ is required. The desired posterior distribution is given by $p(x_1|x_5) = p(x_1, x_5)/p(x_5)$. Now consider the problem of computing the normalizing constant $p(x_5)$. By applying the factorized form of the joint PMF encoded in the BN, it can be written as:

$$p(x_5) = \sum_{x_1} \sum_{x_2} \sum_{x_3} \sum_{x_4} p(x_5|x_3) p(x_4|x_2) p(x_3|x_2, x_1) p(x_2) p(x_1) \tag{6.7}$$

The idea of variable elimination is to move the sums inside the products by applying distributive and communitive laws[12]. Equation (6.7) can, for example, be rewritten as:

$$p(x_5) = \sum_{x_3} p(x_5|x_3) \sum_{x_2} p(x_2) \sum_{x_1} p(x_3|x_2, x_1) p(x_1) \sum_{x_4} p(x_4|x_2) \tag{6.8}$$

This expression is evaluated from right to left as shown in Equation (6.9).

---

[12] See Jensen and Nielsen (2007) for an overview on the algebra of potentials.

$$
\begin{aligned}
p(x_5) &= \sum_{x_3} p(x_5|x_3) \sum_{x_2} p(x_2) \sum_{x_1} p(x_3|x_2,x_1)p(x_1) \underbrace{\sum_{x_4} p(x_4|x_2)}_{1} \\
&= \sum_{x_3} p(x_5|x_3) \sum_{x_2} p(x_2) \underbrace{\sum_{x_1} p(x_3|x_2,x_1)p(x_1)}_{\phi_1(x_2,x_3)} \\
&= \sum_{x_3} p(x_5|x_3) \underbrace{\sum_{x_2} p(x_2)\phi_1(x_2,x_3)}_{\phi_2(x_3)} \\
&= \underbrace{\sum_{x_3} p(x_5|x_3)\phi_2(x_3)}_{\phi_3(x_5)}
\end{aligned}
\tag{6.9}
$$

The operations in Equation (6.9) can be interpreted as a series of variable eliminations. First, variable X_4 is eliminated followed by variable X_1, then X_2 and finally X_3. The innermost summation over X_4 can be omitted since $\sum_{x_4} p(x_4|x_2) = 1$. The process thus starts by multiplying together the terms in the scope of the summation operator $\sum_{x_1} \ldots$ to create a temporary table commonly called a potential:

$$
\phi_1'(x_1,x_2,x_3) = p(x_3|x_2,x_1)p(x_1)
\tag{6.10}
$$

Subsequently, X_1 is marginalized out to compute a new potential:

$$
\phi_1(x_2,x_3) = \sum_{x_1} \phi_1'(x_1,x_2,x_3)
\tag{6.11}
$$

In the next step, all terms in the scope of the summation operator $\sum_{x_2} \ldots$ are multiplied together to create a temporary potential:

$$
\phi_2'(x_2,x_3) = p(x_2)\phi_1(x_2,x_3)
\tag{6.12}
$$

X_2 is then marginalized out to obtain a new potential:

$$
\phi_2(x_3) = \sum_{x_2} p(x_2)\phi_2'(x_2,x_3)
\tag{6.13}
$$

This process is continued until all required variables are eliminated. Clearly, eliminating the variables sequentially as shown above is more efficient than enumerating Equation (6.7) directly, because the summations are performed over smaller potentials (or tables). In the current example, the largest created potential is $\phi_1'(x_1,x_2,x_3)$ with m^3 values. This potential is two orders of magnitude smaller than the potential representing the complete joint PMF $p(x_1,\ldots,x_5)$ which has m^5 values.

This example demonstrates that the efficiency of variable elimination depends on the size of the largest potential created during the elimination process. On the one hand, this size is a function of the size of the conditional PMF specified in the BN. On the other hand, it depends on the elimination order and the structure of the BN (Russell and Norvig 2010). Exact inference is typically more efficient in singly connected BN such as the network shown in Figure 6.3 than in multiply connected BN such as the network illustrated in Figure 6.4 (see also Bensi et al. 2013).

Essentially, exact inference algorithms search for an optimal elimination order that minimizes the computational time and/or memory demand. This task is NP-hard[13] and it is thus unlikely to develop an algorithm that finds the optimal elimination order for all types of BN (Cooper 1990). Therefore, existing algorithms apply heuristics to find an efficient elimination order. An overview on available algorithms is, for example, provided in (Murphy 2001; Jensen and Nielsen 2007).

If exact inference becomes inefficient (i.e. in large, multiply connected networks), approximate inference methods may be applied as an alternative. Most approximate inference methods are sampling-based such as likelihood weighting and Markov chain Monte Carlo (MCMC) methods. Essentially, these methods generate samples of a set of variables in a BN given that the values of another set of variables are observed (see, for example, Russell and Norvig 2010 for more details). A significant disadvantage of approximate inference methods is that their efficiency degrades considerably with increasing number of observations and/or decreasing value of the simulated probabilities.

6.2.4 Dynamic Bayesian networks (DBN)

Discrete-time random processes can be modeled with dynamic Bayesian networks (DBN) (see, for example, Murphy 2002; Russell and Norvig 2010). A DBN consists of a sequence of slices $t = 0, 1, \dots, T$, each of which represents a discrete time step in the process. Each slice contains a set of random variables represented by a vector $\mathbf{X}_t$, which are typically divided into $\mathbf{X}_t = [\mathbf{Y}_t^T, \mathbf{Z}_t^T]^T$ to designate unobservable and observable variables. DBN normally encode the first-order Markov assumption (Russell and Norvig 2010)[14], i.e. the variables $\mathbf{X}_t$ in slice t are conditionally independent of all other predecessors $\mathbf{X}_0, \dots, \mathbf{X}_{t-2}$ in slices $0, \dots, t-2$ given its direct predecessors $\mathbf{X}_{t-1}$ in slice $t-1$. It follows that:

$$p(\mathbf{x}_t | \mathbf{x}_{t-1}, \mathbf{x}_{t-2}, \dots, \mathbf{x}_0) = p(\mathbf{x}_t | \mathbf{x}_{t-1}) \tag{6.14}$$

Equation (6.14) implies that the variables $\mathbf{X}_t$ in slice t can have parents in the same slice and in the previous slice $t-1$. Figure 6.5 shows a simple DBN with variables Y_t and Z_t in each slice t.

In accordance with Equation (6.1), the joint PMF $p(\mathbf{x}_{0:T})$ of all variables $\mathbf{X}_{0:T} = [\mathbf{X}_0^T, \mathbf{X}_1^T, \dots, \mathbf{X}_T^T]^T$ in a DBN can be written as:

---

[13] NP-hard stands for non-deterministic polynomial time hard. This is a concept from computational complexity theory (see, for example, Arora and Barak 2009; Wigderson 2019)

[14] Note that this is not a requirement as discussed by Russell and Norvig (2010)
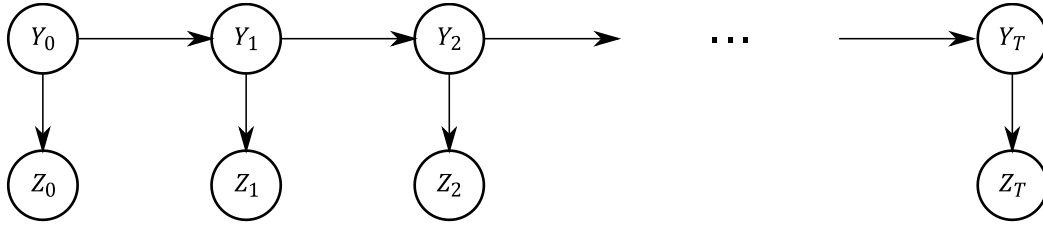
Figure 6.5: A simple dynamic Bayesian network.

$$p(\mathbf{x}_{0:T}) = \prod_{t=0}^{T} \prod_{i=1}^{N} p(x_{i,t}|pa(x_{i,t})) \tag{6.15}$$

where N is the number of random variables in each slice.

Two main inference tasks can be formulated for DBN:

1. Filtering is the task of computing the posterior PMF of all unobservable variables $\mathbf{Y}_t$ in all slice t given the observations $\mathbf{Z}_{0:t} = \mathbf{z}_{0:t}$ up to slice t, i.e. $p(\mathbf{y}_t|\mathbf{z}_{0:t})$.
2. Smoothing is the task of computing the posterior PMF of all unobservable variables $\mathbf{Y}_k$ in any slice k with $0 \le k < t$ given the observations $\mathbf{Z}_{0:t} = \mathbf{z}_{0:t}$ up to slice t, i.e. $p(\mathbf{y}_k|\mathbf{z}_{0:t})$ with $0 \le k < t$.

A number of exact and approximate inference methods are available for solving these inference problems, which exploit the repetitive structure of DBN (see Murphy 2002 for more details).

6.3 Modeling of deteriorating structural systems

6.3.1 Generic DBN model of element deterioration

As discussed in Section 4.3, the reliability of deteriorating structural systems belonging to model class (b) can be approximated using a discrete-time approach. In this approach, the service life of the structure is divided into intervals $(t_{j-1}, t_j]$, $j = 1, ..., m$. Deterioration is modeled at the element level and evaluated at the end of each interval. To this end, the generic DBN model proposed by Straub (2009) is applied. Let $D_{i,j}$ again represent the condition of element i at the end of the jth interval. The framework describes $D_{i,j}$ by a parametric model $h_{D,i}$, which is written in the generic form as:

$$D_{i,j} = h_{D,i}(D_{i,0}, \boldsymbol{\Theta}_i, \boldsymbol{\Omega}_{i,0}, ... \boldsymbol{\Omega}_{i,j}, t_j), \quad j = 1, ..., m \tag{6.16}$$

where $D_{i,0}$ is the initial condition of element i, $\boldsymbol{\Theta}_i$ are the time-invariant model parameters and $\boldsymbol{\Omega}_{i,j}$ are the time-variant model parameters. Additionally, the framework makes two main conditional independence assumptions. First, the framework assumes that the element deterioration state $D_{i,j}$ is conditionally Markovian given $\boldsymbol{\Theta}_i = \boldsymbol{\theta}_i$ and $\boldsymbol{\Omega}_{i,j} = \boldsymbol{\omega}_{i,j}$, i.e.:

$$f(d_{i,j}|d_{i,0}, ..., d_{i,j-1}, \boldsymbol{\theta}_i, \boldsymbol{\omega}_{i,0}, ..., \boldsymbol{\omega}_{i,j}) = f(d_{i,j}|d_{i,j-1}, \boldsymbol{\theta}_i, \boldsymbol{\omega}_{i,j}), \quad j = 1, ..., m \tag{6.17}$$

where $f(d_{i,j}|\cdot)$ is the conditional PDF of $D_{i,j}$. Straub (2009) highlights that the conditional Markov process $D_{i,j}$ is not necessarily homogeneous as the conditional PDF $f(d_{i,j}|d_{i,j-1}, \boldsymbol{\theta}_i, \boldsymbol{\omega}_{i,j})$ may change with each time step j. Secondly, the framework requires that the time-invariant model parameters $\boldsymbol{\Omega}_{i,j}$ are conditionally Markovian given $\boldsymbol{\Theta}_i = \boldsymbol{\theta}_i$ and $D_{i,j-1} = d_{i,j-1}$, i.e.:

$$f(\boldsymbol{\omega}_{i,j}|\boldsymbol{\omega}_{i,0}, \dots, \boldsymbol{\omega}_{i,j-1}, d_{i,0}, \dots d_{i,j-1}, \boldsymbol{\theta}_i) = f(\boldsymbol{\omega}_j|\boldsymbol{\omega}_{j-1}, d_{i,j-1}, \boldsymbol{\theta}_i), \quad j = 1, \dots, m \qquad (6.18)$$

where $f(\boldsymbol{\omega}_{i,j}|\cdot)$ is the conditional PDF of $\boldsymbol{\Omega}_{i,j}$. The assumptions of this model are discussed in (Straub 2009).

Based on the conditional independence assumptions introduced above, it is possible to construct the generic DBN of the element deterioration model shown in Figure 6.6. Each slice j of the DBN represents a discrete time step in the deterioration process. Note that the additional vectors $\boldsymbol{\Theta}_{i,0}, \dots, \boldsymbol{\Theta}_{i,m}$ are introduced so that all slices $j = 1, \dots, m$ are identical. These vectors are deterministically related by the following functions $\boldsymbol{\Theta}_{i,j} = \boldsymbol{\Theta}_{i,j-1}$ for all $j = 1, \dots, m$ and $\boldsymbol{\Theta}_{i,0} = \boldsymbol{\Theta}_i$. This approach simplifies the model building and the graphical representation of the DBN.

As highlighted by Straub (2009), the nodes of the DBN represent vectors of random variables. Depending on the specific implementation of the framework, the variables in these vectors may be included as individual nodes in the DBN. Such a refinement allows encoding further independence assumptions in the DBN and can thus increase the efficiency of the model.

6.3.2 Dependence modeling

Dependence among the parameters of the models describing $D_{i,j}$ can be captured in a BN using a hierarchical approach. As an example, consider the dependent continuous random variables $\mathbf{X} = [X_1, \dots, X_n]^T$ with marginal CDFs $F_{X_i}(x_i)$, $i = 1, \dots, n$ and correlation matrix $\mathbf{R}_X = [\rho_{X,ij}]$. The following presentation demonstrates how such a correlation model can be translated into a hierarchical BN (see Straub and Der Kiureghian 2010a; Luque and Straub 2016 for similar examples).

Given that the joint CDF of $\mathbf{X}$ can be approximated by a Gaussian copula, the Nataf transformation can be used to transform the correlated random variable $\mathbf{X} = [X_1, \dots, X_n]^T$ to correlated standard
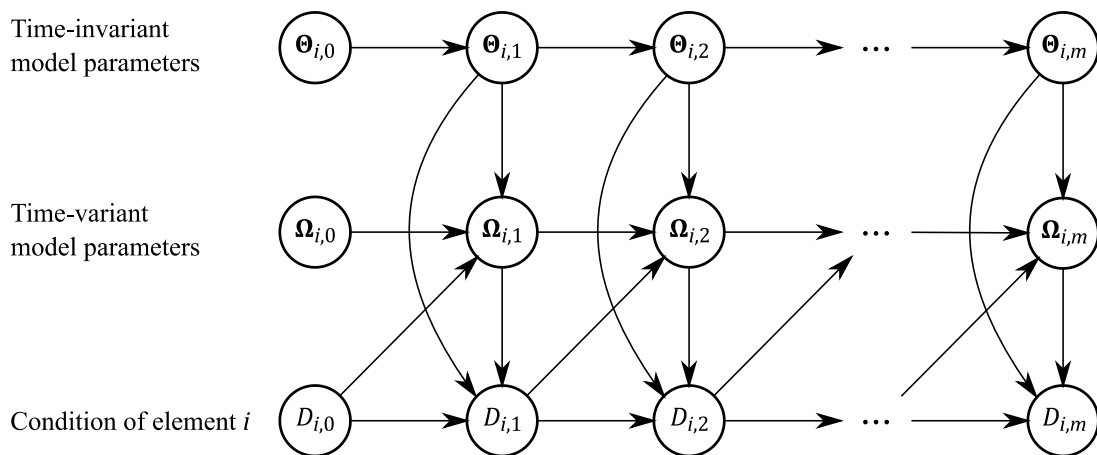
Figure 6.6: Generic DBN model of element deterioration (after Straub 2009).

normal random variables $\mathbf{Y} = [Y_1, \ldots, Y_n]^T$ by applying the following marginal transformations (Liu and Der Kiureghian 1986):

$$Y_i = \Phi^{-1}[F_{X_i}(X_i)], \quad i = 1, \ldots, n \tag{6.19}$$

where $\Phi(\cdot)$ is the standard normal CDF. The random variables $\mathbf{Y}$ are jointly standard normal distributed with correlation matrix $\mathbf{R}_Y = [\rho_{Y,ij}]$, i.e. their joint CDF $F_{\mathbf{Y}}(\mathbf{y})$ is equal to the n-variate standard normal CDF $\Phi_n(\mathbf{y}, \mathbf{R}_Y)$. The elements $\rho_{Y,ij}$ of $\mathbf{R}_Y$ are defined in terms of the corresponding correlation coefficients $\rho_{X,ij}$ through the following relation (Liu and Der Kiureghian 1986; Ditlevsen and Madsen 1996):

$$\rho_{X,ij} = \mathbb{E}[Z_i Z_j] = \int_{-\infty}^{+\infty} \int_{-\infty}^{+\infty} z_i z_j \varphi_2(y_i, y_j, \rho_{Y,ij}) \, \mathrm{d}y_i \, \mathrm{d}y_j \tag{6.20}$$

with

$$z_i = \frac{F_{X_i}^{-1}[\Phi(y_i)] - \mu_{X_i}}{\sigma_{X_i}} \tag{6.21}$$

where μ_{X_i} and σ_{X_i} are the mean and standard deviation of X_i, and $\varphi_2(\cdot)$ is the two-dimensional standard normal PDF. Solutions of Equation (6.20) can be found for most common stochastic distributions in (Liu and Der Kiureghian 1986; Ditlevsen and Madsen 1996; Melchers 1999).

Now suppose the random variables $\mathbf{Y}$ are Dunnet-Sobel class standard normal random variables, i.e. the correlation coefficient between each pair Y_i and Y_j is specified as $\rho_{Y,ij} = r_{Y,i} \cdot r_{Y,j}$ for $i \neq j$ and $\rho_{Y,ij} = 1$ for $i = j$. For such a correlation structure, Dunnett and Sobel (1955) have shown that the joint CDF of the correlated standard normal random variables $F_{\mathbf{Y}}(\mathbf{y}) = \Phi_n(\mathbf{y}, \mathbf{R}_Y)$ can be written as (see also Thoft-Christensen and Murotsu 1986):

$$F_{\mathbf{Y}}(\mathbf{y}) = \Phi_n(\mathbf{y}, \mathbf{R}_Y) = \int_{-\infty}^{+\infty} \left(\prod_{i=1}^{n} F_{Y_i|U}(y_i|u) \right) \varphi(u) \, \mathrm{d}u \tag{6.22}$$

with

$$F_{Y_i|U}(y_i|u) = \Phi\left(\frac{y_i - r_{Y,i} u}{\sqrt{1 - r_{Y,i}^2}} \right), \quad i = 1, \ldots, n \tag{6.23}$$

where U is an independent standard normal random variable with PDF $\varphi(u)$ and $F_{Y_i|U}(y_i|u)$ is the conditional CDF of $Y_i, i, \ldots, n$ given U.

From Equations (6.22) and (6.23) it follows that the correlation among the Dunnet-Sobel class standard normal random variables $Y_1, \ldots, Y_n$ can be modeled through a common parent variable U with standard normal distribution such that $Y_1, \ldots, Y_n$ are conditionally independent given $U = u$ with conditional CDFs $F_{Y_i|U}(y_i|u), i = 1, \ldots, n$. The common parent variable U is in the following
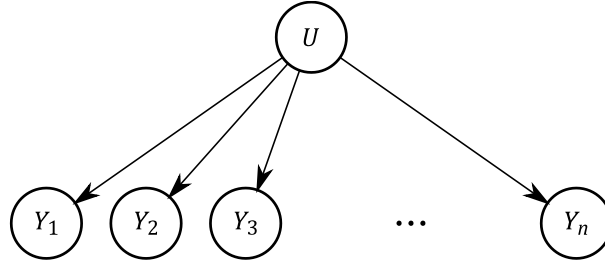
Figure 6.7: Hierarchical BN of correlated standard normal random variables $Y_1, \ldots, Y_n$. U is an independent standard normal random variable.

called a hyper-parameter. This correlation model can be represented by the hierarchical BN shown in Figure 6.7.

Using the marginal transformations given in Equation (6.19), the conditional CDFs given in Equation (6.23) can be expressed in terms of the original random variables $X_1, \ldots, X_n$ as:

$$F_{X_i|U}(x_i|u) = \Phi\left[\frac{\Phi^{-1}[F_{X_i}(x_i)] - r_{Y,i}u}{\sqrt{1 - r_{Y,i}^2}}\right], \quad i = 1, \ldots, n \tag{6.24}$$

Thus, the correlation among the original random variables $X_1, \ldots, X_n$ can be modeled by the hierarchical BN shown in Figure 6.8. The nodes $X_1, \ldots, X_n$ in the hierarchical BN are fully defined by the conditional CDFs $F_{X_i|U}(x_i|u)$, $i = 1, \ldots, n$.

If all X_i's have identical marginal distributions $F_X(x)$ and are equi-correlated with correlation coefficient ρ_X, the conditional PDF $F_{X|U}(x|u)$ reads (see also Luque and Straub 2016):

$$F_{X|U}(x|u) = \Phi\left[\frac{\Phi^{-1}[F_X(x)] - \sqrt{\rho_Y}\,u}{\sqrt{1 - \rho_Y}}\right] \tag{6.25}$$

where ρ_Y is the corresponding correlation coefficient in standard normal space. It can be determined by solving Equation (6.20).

As suggested by Song and Kang (2009), the hierarchical BN shown in Figure 6.8 can be extended by introducing additional hyper-parameters to represent more general correlation structures among the variables $X_1, \ldots, X_n$. This approach can be considered as a generalization of the Dunnet-Sobel
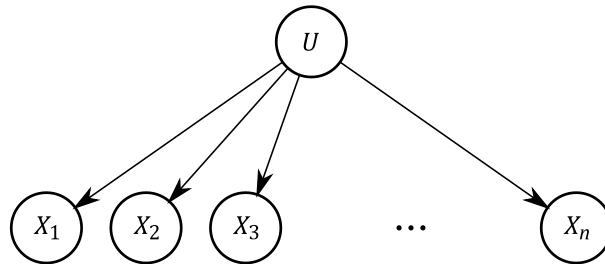
Figure 6.8: Hierarchical BN of correlated random variables $X_1, \ldots, X_n$. U is an independent standard normal random variable.

class standard normal random variables. Adding additional hyper-parameters typically results in a densely connected BN and thus increases the computational costs of inference. Bensi et al. (2011) present methods for reducing the complexity of hierarchical BN representing random fields while minimizing the error in modeling the correlation structure.

As noted in Section 5.2.2, spatial dependence of deterioration in most structural systems mainly exists due to common influencing factors rather than geometrical proximity (Straub 2018b). If these common influencing factors cannot be modeled explicitly, spatial dependence among the deterioration model parameters can be represented by correlation coefficients. Such correlation structures can often be implemented by applying the simple hierarchical BN shown in Figure 6.8, which is based on the Dunnet-Sobel class standard normal random variables.

Section 5.2.2 also notes that probabilistic hierarchical models (e.g. Maes and Dann 2007) are applicable if common features and factors influencing deterioration of different elements in a structural system can be modeled explicitly. Faber et al. (2006) and Straub et al. (2009) apply, for example, probabilistic hierarchical models to describe the spatial variability of reinforcement corrosion in concrete structures. Such correlation models can be readily implemented in a hierarchical BN (see, for example, Qin and Faber 2012; Luque et al. 2017)

6.3.3 Modeling of inspection and monitoring

Inspection and monitoring of deteriorating structural systems typically provide information on the initial condition $D_{i,0}$, the model parameters $\boldsymbol{\Theta}_i$ and $\boldsymbol{\Omega}_{i,0}, \ldots \boldsymbol{\Omega}_{i,j}$, and the element condition $D_{i,j}$. Any measurement or observation is subject to uncertainty. Following Straub (2009), inspection and monitoring outcomes are included in the DBN by introducing additional variables as children of the inspected/monitored variables to account for any uncertainties. As an example, consider the slice j of the generic DBN shown in Figure 6.9. It includes an additional variable $Z_{D,i,j}$ representing an observation of the element deterioration state $D_{i,j}$. Following Section 3, the variable $Z_{D,i,j}$ is described by a likelihood function:

$$L(d_{i,j}|z_{D,i,j}) \propto \Pr(Z_{D,i,j} = z_{D,i,j}|D_{i,j} = d_{i,j}) \tag{6.26}$$

This function is proportional to the probability of observing $Z_{D,ij} = z_{D,i,j}$ when the uncertain element condition $D_{i,j}$ takes a value $d_{i,j}$, and it fully defines the variable $Z_{D,i,j}$ in the DBN. The variable $Z_{D,i,j}$ may, for example, represent the outcome of a measurement of a defect size. In this case, $Z_{D,i,j}$ is a continuous random variable whose outcome space covers all possible defect dimensions. The likelihood function of this measurement is characterized by its measurement error as described in Section 3.2. Note that this model assumes that the observation $Z_{D,i,j}$ is conditionally independent of all other variables in the DBN given $D_{i,j} = d_{i,j}$.

To represent observations of the model parameters $\boldsymbol{\Theta}_i$ and $\boldsymbol{\Omega}_{i,j}$, each slice j of the generic DBN model of element deterioration shown in Figure 6.9 can extended with additional variables as children of these parameters (see Luque and Straub 2016 for more details).
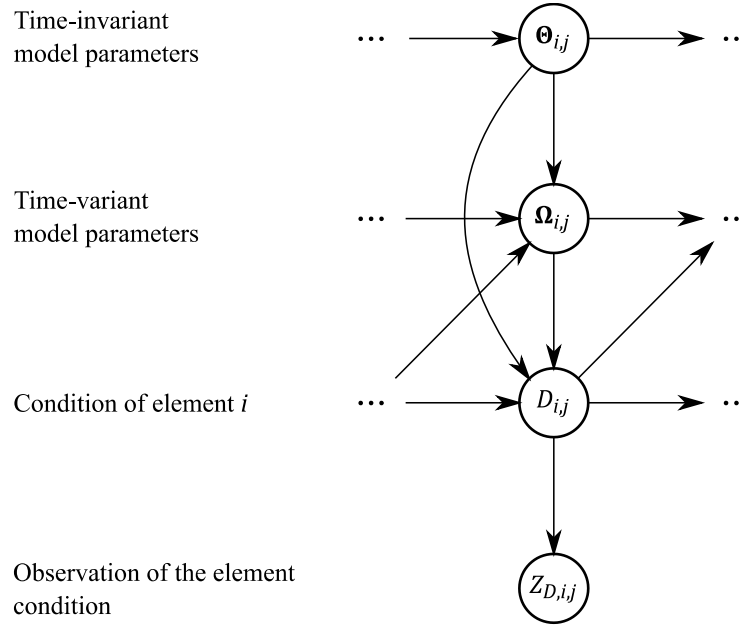
Figure 6.9: Slice j of the generic DBN model of element deterioration including an additional node $Z_{D,i,j}$ representing an observation of the element deterioration state $D_{i,j}$ (after Straub 2009).

6.3.4 Generic DBN model of a deteriorating structural system

The structural system is divided into n_E elements to model its deterioration state. Deterioration of all n_E elements is described with separate DBN models as introduced in Section 6.3.1. Spatial dependence among element deterioration is modeled by applying a hierarchical approach as described in Section 6.3.2. For this purpose, the hyper-parameters $\mathbf{U} = [U_{\boldsymbol{\Theta}}, U_{\boldsymbol{\Omega}}, U_{D_0}]^T$ are introduced, which link the uncertain parameters influencing the condition of the individual elements as illustrated in Figure 6.10.

The hyper-parameters $\mathbf{U} = [U_{\boldsymbol{\Theta}}, U_{\boldsymbol{\Omega}}, U_{D_0}]^T$ explicitly model the correlation among the time-invariant parameters $\boldsymbol{\Theta}_{i,0}$, time-variant parameters $\boldsymbol{\Omega}_{i,0}$ and initial element conditions $D_{i,0}$ at the beginning of the structure's service life. The correlation among the element conditions $D_{i,j}$ in all subsequent time steps $j > 0$ are a function of (a) the correlation among the element conditions in the previous time step $D_{i,j-1}$, (b) the correlation among the time-invariant model parameters $\boldsymbol{\Theta}_{i,j}$, (c) the correlation among the time-variant parameters $\boldsymbol{\Omega}_{i,j}$, and (d) the mathematical relations encoded in the underlying deterioration models $h_{D,i}$. The correlation among the time-invariant parameters $\boldsymbol{\Theta}_{i,j}$ is the same in each time step j whereas the correlation among the time-variant parameters $\boldsymbol{\Omega}_{i,j}$ may vary from time step to time step. The actual cross-correlation among the time-variant parameters $\boldsymbol{\Omega}_{i,j}$ could be modeled explicitly by introducing additional hyper-parameters as their common parents in each slice $j > 0$. However, these additional hyper-parameters are here omitted on purpose as the proposed hierarchical structure shown in Figure 6.10 facilitates the development of efficient inference algorithms, which exploit the conditional independence of the individual element deterioration models given the hyper-parameters $\mathbf{U}$ (see Luque and Straub 2016).

The generic DBN model of a deteriorating structural system shown in Figure 6.10 contains a node S_j in each slice j to represent the system state at the end of interval j, which is a stochastic function
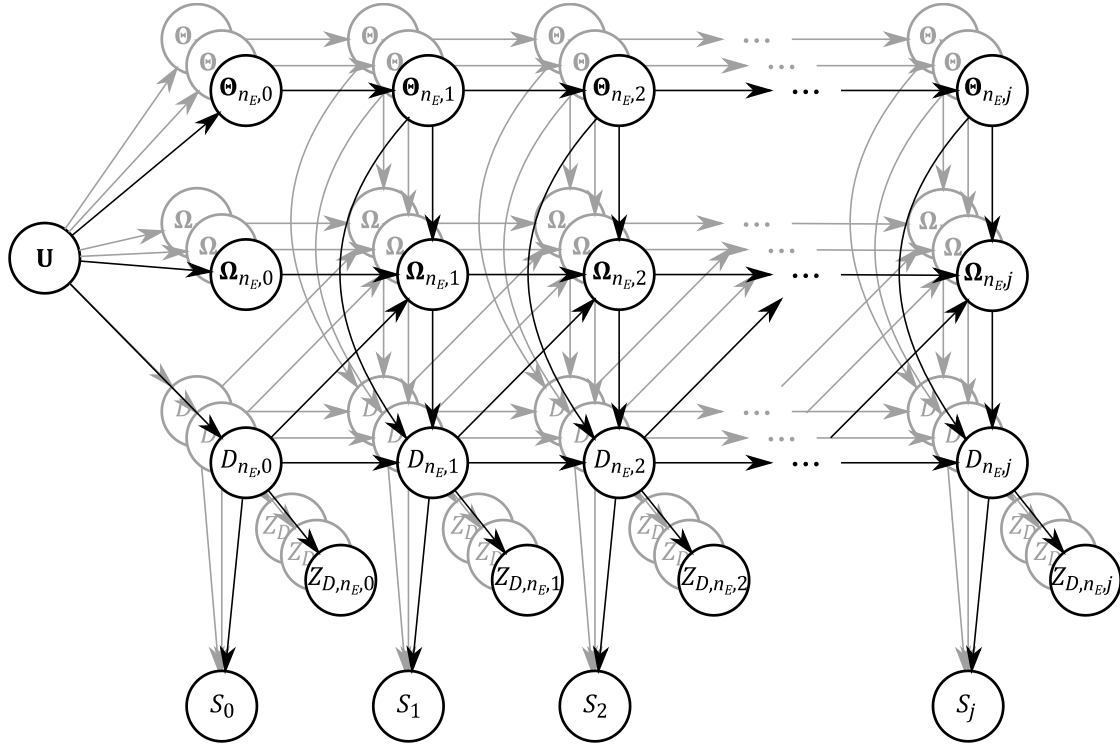
Figure 6.10: Generic DBN model of a deteriorating structural system (adapted from Luque and Straub 2016).
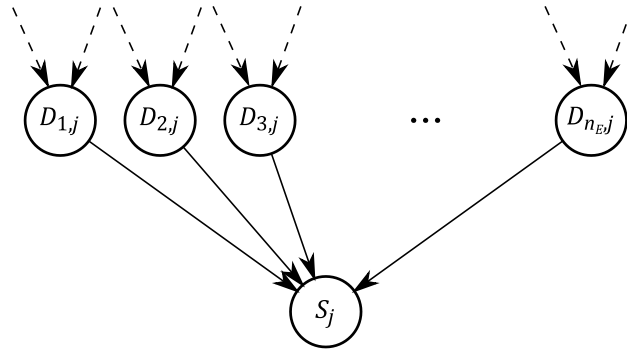
Figure 6.11: Converging connection at node S_j in slice j. Node S_j models the system state conditional on the system condition $\mathbf{D}_j = [D_{1,j}, ..., D_{n_E,j}]^T$ at end of interval j.

of the element conditions. This relation is reflected in the generic DBN model by the directed links pointing from the nodes $D_{i,j}$, $i = 1, ..., n_E$ towards the node S_j as illustrated in Figure 6.11.

In the general case, S_j is a multi-state random variable. In most applications, however, S_j is modeled as a binary random variable, where $F_j^* = \{S_j = 1\}$ is the interval failure event defined in Section 4.3 and $\bar{F}_j^* = \{S_j = 0\}$ is the complement. In this formulation, the node S_j is fully defined by the conditional system failure probability $\Pr(F_j^* | \mathbf{D}_j = \mathbf{d}_j)$, where the vector $\mathbf{D}_j = [D_{1,j}, ..., D_{n_E,j}]^T$ represents the condition of the structural system at end of interval j (see also Section 5.2.1). To determine these probabilities, a probabilistic model of the structural system is defined with element properties modelled according to the system deterioration state $\mathbf{D}_j = \mathbf{d}_j$ and time-invariant structural system reliability analyses are performed (see Sections 2.4 and 4.3). Note that in most cases the number of deteriorating elements is large, and thus the number of possible realizations of the

system condition $\mathbf{d}_j$ is usually intractable. For this reason, more efficient representations of structural systems are often required (see also Luque and Straub 2016).

6.4 Computational aspects

6.4.1 Discretization of continuous random variables

Probabilistic inference in BN can be performed with exact or approximate algorithms. The latter are typically sampling-based, and their performance degrades with increasing number of observations (see also Section 6.2.3). In addition, sampling-based methods are generally inefficient in simulating rare events. In contrast, the performance of exact inference algorithms is not affected by the number of observations considered in the analysis (see also Section 6.2.3). Their performance is also independent of the value of the probabilities to be calculated. For these reasons, exact algorithms are a suitable choice for performing probabilistic inference in BN.

In most applications, DBN models of deteriorating structural systems include continuous and discrete variables. Such networks belong to the class of hybrid BN. Exact inference in hybrid BN is only possible in a few special cases (Langseth et al. 2012): (a) when the model is a conditional linear Gaussian model where the joint distribution of the continuous variables given the discrete variables is the multivariate normal distribution, or (b) when all continuous variables are defined as mixtures of truncated basic functions. A common strategy to overcome this problem is to discretize the continuous variables such that exact inference algorithms available for discrete BN can be applied (Langseth et al. 2012). This approach replaces a continuous variable X by a discrete counterpart $\hat{X}$, which is obtained by dividing the continuous outcome space of X into m_X mutually exclusive, collectively exhaustive intervals. Each interval corresponds to a state of the discrete variable $\hat{X}$. The conditional or marginal PMF of $\hat{X}$ is then computed from the conditional or marginal PDF of X.

A strategy for computing the conditional or marginal of discretized variables is, for example, given in (Straub 2009). To demonstrate some basic principles of this computational task, consider the simple BN shown in Figure 6.12 with four continuous variables. The variables are discretized according to their topological ordering in the BN, e.g. (A, B, C, D).

First, root node A is discretized. Its discrete counterpart is $\hat{A}$ with m_A states denoted by $\hat{a}_i$, $i = 1, \dots, m_A$. The marginal PMF of $\hat{A}$ is simply given by:

$$p(\hat{a}_i) = \Pr(\hat{a}_i^L < A \le \hat{a}_i^U) = F_A(\hat{a}_i^U) - F_A(\hat{a}_i^L) \tag{6.27}$$

where $F_A(\cdot)$ is the CDF of A, and $\hat{a}_i^U$ and $\hat{a}_i^L$ are the upper and lower boundaries of the interval corresponding to state $\hat{a}_i$.

Next, variable B is replaced by the discrete variable $\hat{B}$ with m_B states, which are denoted by $\hat{b}_j$, $j = 1, \dots, m_B$. The conditional PMF of $\hat{B}$ is computed as:

$$p(\hat{b}_j | \hat{a}_i) = F_B(\hat{b}_j^U | \hat{a}_i) - F_B(\hat{b}_j^L | \hat{a}_i) \tag{6.28}$$
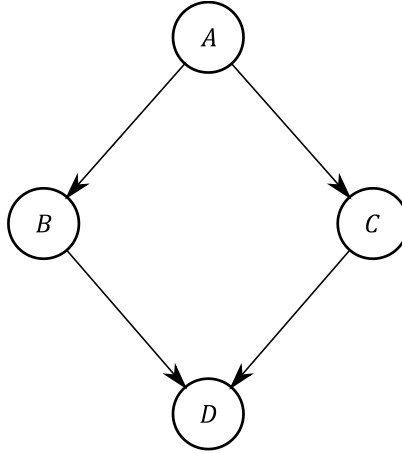
Figure 6.12: A simple BN with four continuous variables.

where $F_B(\cdot|\hat{a}_i)$ is the CDF of B conditional on $\hat{A} = \hat{a}_i$, and $\hat{b}_j^U$ and $\hat{b}_j^L$ are the upper and lower boundaries of the interval corresponding to state $\hat{b}_j$. The CDF of B conditional on $\hat{A} = \hat{a}_i$ is computed as:

$$F_B(b|\hat{a}_i) = \int_{\hat{a}_i^L}^{\hat{a}_i^U} F_B(b|a)\, f_A(a|\hat{a}_i)\, da \tag{6.29}$$

where $f_A(a|\hat{a}_i)$ is the PDF of A truncated in the range $\hat{a}_i^L < a \le \hat{a}_i^U$. To evaluate the integral in Equation (6.29), MCS may, for example, be applied if no closed-form solution exists. Variable C is substituted by the discrete variable $\hat{C}$ with states $\hat{c}_k$, $k = 1, \ldots, m_C$, and the conditional PMF of $\hat{C}$ is computed in the same way as the conditional PMF of $\hat{B}$.

Now suppose variable D is a deterministic function of B and C such that $D = h(B, C)$. D's discrete counterpart is $\hat{D}$ with states $\hat{d}_m$, $m = 1, \ldots, m_D$. To obtain the conditional PMF of $\hat{D}$, MCS can also be applied. Consider the computation of $\hat{D}$'s conditional PMF for a given combination of its parents' states $\hat{B} = \hat{b}_j$ and $\hat{C} = \hat{c}_k$. For this combination, N samples $(b^{(n)}, c^{(n)})$, $n = 1, \ldots, N$ are generated from the conditional PDFs $f_B(b|\hat{b}_j)$ and $f_C(c|\hat{c}_k)$. Subsequently, the corresponding samples $d^{(n)}$, $n = 1, \ldots, N$ are computed by evaluating h for each generated pair $(b^{(n)}, c^{(n)})$, $n = 1, \ldots, N$. Finally, a normalized histogram is constructed based on the samples $d^{(n)}$, $n = 1, \ldots, N$ to approximate the values of the PMF $p(\hat{d}_m|\hat{b}_j, \hat{c}_k)$, $m = 1, \ldots, m_D$. The bins of the histogram are defined in accordance with the intervals defining the states $\hat{d}_m$, $m = 1, \ldots, m_D$. This process is repeated for each of the $m_B \cdot m_C$ combinations of $\hat{D}$'s parents.

The approach presented above is based on two approximations: (a) the joint PDF of B and C given $\hat{B} = \hat{b}_j$ and $\hat{C} = \hat{c}_k$ is approximated by $f_{BC}(b, c|\hat{b}_j, \hat{c}_k) = f_B(b|\hat{b}_j) \cdot f_C(c|\hat{c}_k)$, and (b) the conditional PDFs $f_B(b|\hat{b}_j)$ and $f_C(c|\hat{c}_k)$ have to be assumed since $f_B(b)$ and $f_C(c)$ are here unknown. To this end, a uniform distribution on the discretization intervals corresponding to the states $\hat{b}_j$ and $\hat{c}_k$ may be applied as an approximation of $f_B(b|\hat{b}_j)$ and $f_C(c|\hat{c}_k)$ if these intervals are bounded on both sides, and an exponential PDF may be used if a discretization interval is unbounded on one side (see Straub 2009 for mode details).

The choice of the intervals influences the accuracy and the computational efficiency of exact inference algorithms. If the number of discrete intervals is small, the discretization may introduce a large error as the conditional or marginal PMF of $\hat{X}$ can be a poor approximation of the conditional or marginal PDF of X. This error can be reduced by increasing the number of intervals. However, introducing too many states has an adverse effect on the performance of exact inference algorithms. As highlighted in Section 6.2.3, their efficiency depends on the size of the largest potential handled during the elimination process, which grows approximately exponentially with the number of states of the involved variables. To achieve an optimal balance between accuracy and computation time, several discretization strategies have been proposed in the context of reliability analysis (see, for example, Neil et al. 2007; Straub 2009; Straub and Der Kiureghian 2010b; Zwirglmaier and Straub 2016).

In the context of modeling deterioration processes, the heuristics proposed in (Straub 2009) have proven to be effective. The model is kept simple by defining the same discretization scheme for all time slices. The discretization scheme of the random deterioration model parameters accounts for their influence on the element deterioration state. To this end, the intervals are selected for each parameter such that after applying the deterioration model they result in approximately equally spaced intervals in the outcome space of the element deterioration state.

6.4.2 Inference algorithm

Luque and Straub (2016) propose an exact inference algorithm tailored to evaluate the hierarchical DBN of a deteriorating structural system shown in Figure 6.10. The algorithm solves the filtering task and hence computes the posterior distribution of all unobserved variables in slice t of the DBN conditional on the values of all observed variables up to slice j (see also Section 6.2.4)[15]. By exploiting the conditional independence of the individual element deterioration models given the hyper-parameters $\mathbf{U}$, the algorithm computes the posterior distribution of all variables except of the system state S_j with nearly linear computational complexity with respect to the number of elements and time steps. The computation time is not affected by the number of observations considered in the analysis. However, the evaluation of the posterior distribution of the system state S_j is the computational bottleneck of the algorithm. This task requires operating with the conditional PMF $p(s_j | \mathbf{d}_j)$, which grows exponentially with the number of elements. Therefore, computing the posterior distribution of S_j can quickly become intractable as the number of elements grows unless a more efficient representation of the relation among system and element conditions than the converging connection shown in Figure 6.11 can be identified (Luque and Straub 2016).

An implementation of the exact inference algorithm proposed in (Luque and Straub 2016) is beyond the scope of this thesis. Instead, probabilistic inference is performed using likelihood weighting (Fung and Chang 1989; Schachter and Poet 1989). This is a simple approximate method that generates samples of the variables in a BN, which are consistent with the values of all observed variables in the network. To this end, likelihood weighting fixes the values of all observed variables and samples all other variables in topological order. The distribution from which an unobserved random variable's value is sampled is conditional on the values already assigned to its parents. The

---

[15] The algorithm has been adapted by Bismut and Straub (2018) to solve the smoothing task.

samples are, however, not equally important. Each generated sample is weighted by the likelihood that the sample explains the observed values. The likelihood corresponds to the product of the conditional probabilities of each observed variable's value given the values assigned to its parents. This guarantees that samples in which the observations are unlikely are given less weight.

An advantage of approximate inference algorithms including likelihood weighting is that they can be applied to perform inference in BN with continuous random variables. Nevertheless, the continuous variables are in this thesis discretized with a view to implementing an exact inference algorithm in future applications.

Likelihood weighting is implemented as summarized in Algorithm 6.1. This implementation exploits the repetitive structure of the DBN and generates K weighted samples of the variables $\mathbf{X}_j = [\mathbf{Y}_j^T, \mathbf{Z}_j^T]^T$ in slice j of the DBN given $\mathbf{Z}_j = \mathbf{z}_j$ is observed and K samples of the variables $\mathbf{X}_{j-1}$ in slice $j-1$ are available. $\mathbf{Y}_j$ and $\mathbf{Z}_j$ denote the unobservable and observable variables in slice j.

The weighted samples $(\mathbf{x}_0^{(k)}, w_0^{(k)}), ..., (\mathbf{x}_m^{(k)}, w_m^{(k)})$, $k = 1, ..., K$ are used to solve the filtering, prediction and smoothing task as follows (see Section 6.2.4):

Filtering: The posterior PMF $p(y_{i,j}|\mathbf{z}_{0:j})$ of any unobserved variable $Y_{i,j}$ in slice j conditional on the values of all observed variables $\mathbf{Z}_{0:j} = \mathbf{z}_{0:j}$ up to slice j is computed as (see, for example, Fung and Chang 1989):

Algorithm 6.1: Likelihood weighting for generating K weighted samples of the variables $\mathbf{X}_j = [\mathbf{Y}_j^T, \mathbf{Z}_j^T]^T$ in slice j of the DBN given $\mathbf{Z}_j = \mathbf{z}_j$ is observed and K samples of the variables $\mathbf{X}_{j-1}$ in slice $j-1$ are available.

Input: DBN encoding the joint PMF $p(\mathbf{x}_{0:m})$ of variables $\mathbf{X}_{0:m} = [\mathbf{X}_0^T, \mathbf{X}_1^T, ..., \mathbf{X}_m^T]^T$, $\mathbf{z}_j$ (observed values of variables $\mathbf{Z}_j$ in slice j of the DBN), K (number of samples to be generated) and $\mathbf{x}_{j-1}^{(k)}$, $k = 1, ..., K$ (K samples of the variables $\mathbf{X}_{j-1}$ in slice $j-1$ of the DBN)

1. Let $(X_{1,j}, ..., X_{n,j})$ be a topological ordering of $\mathbf{X}_j$.

2. For $k = 1, ..., K$:

    a. Initialize weight $w_j^{(k)} = 1$.

    b. Generate a sample $\mathbf{x}_j^{(k)} = [x_{1,j}^{(k)}, ..., x_{n,j}^{(k)}]^T$:

        For $i = 1, ..., n$:

            Let $\mathbf{p}_{i,j}^{(k)}$ be the values of $X_{i,j}$'s parents $pa(X_{i,j})$ in $(\mathbf{x}_{j-1}^{(k)}, \mathbf{x}_j^{(k)})$

            If $X_{i,j}$ is an observed variable:

$$x_{i,j}^{(k)} = \text{observed value of } X_{i,j} \text{ in } \mathbf{z}_j$$
$$w_j^{(k)} = w_j^{(k)} \cdot p(x_{i,j}^{(k)}|\mathbf{p}_{i,j}^{(k)})$$

            Else:

$$x_{i,j}^{(k)} = \text{a random sample from } p(x_{i,j}|\mathbf{p}_{i,j}^{(k)})$$

3. Return $(\mathbf{x}_j^{(k)}, w_j^{(k)})$, $k = 1, ..., K$.

$$p(y_{i,j}|\mathbf{z}_{0:j}) = \Pr(Y_{i,j} = y_{i,j}|\mathbf{Z}_{0:j} = \mathbf{z}_{0:j}) \approx \frac{\sum_{k=1}^{K} \mathbb{I}[y_{i,j}^{(k)} = y_{i,j}]\, w_{0:j}^{(k)}}{\sum_{k=1}^{K} w_{0:j}^{(k)}} \tag{6.30}$$

where $\mathbb{I}(\cdot)$ is the indicator function, $y_{i,j}^{(k)}$ is the kth sample of $Y_{i,j}$ and $w_{0:j}^{(k)} = \prod_{i=0}^{j} w_i^{(k)}$ is the weight representing the joint likelihood of all observed values $\mathbf{z}_{0:j} = [\mathbf{z}_0^T, \mathbf{z}_1^T, ..., \mathbf{z}_j^T]^T$ in the kth sample of variables $\mathbf{X}_{0:j} = [\mathbf{X}_0^T, \mathbf{X}_1^T, ..., \mathbf{X}_j^T]^T$. Equation (6.30) simply divides the weight of all samples $\mathbf{x}_j^{(k)}$ with $y_{i,j}^{(k)} = y_{i,j}$ by the total weight of all samples.

Smoothing: The posterior PMF $p(y_{i,l}|\mathbf{z}_{0:j})$ of any unobserved variable $Y_{i,l}$ in slice l with $0 \leq l < j$ conditional on $\mathbf{Z}_{0:j} = \mathbf{z}_{0:j}$ is approximated as:

$$p(y_{i,l}|\mathbf{z}_{0:j}) = \Pr(Y_{i,l} = y_{i,l}|\mathbf{Z}_{0:j} = \mathbf{z}_{0:j}) \approx \frac{\sum_{k=1}^{K} \mathbb{I}[y_{i,l}^{(k)} = y_{i,l}]\, w_{0:j}^{(k)}}{\sum_{k=1}^{K} w_{0:j}^{(k)}} \tag{6.31}$$

where $y_{i,l}^{(k)}$ is the kth sample of $Y_{i,l}$.

When computing the posterior distribution of the system state S_j, two situations can be distinguished: (a) the number of states of the system condition $\mathbf{D}_j$ is limited and the conditional PMF $p(s_j|\mathbf{d}_j)$ can be pre-computed, and (b) the number of states of $\mathbf{D}_j$ is too large to enable pre-computations. In case (a), the posterior PMF $p(s_j|\mathbf{z}_{0:j})$ is approximated by simply generating weighted samples of S_j and applying Equation (6.30) (smoothing is performed by applying Equation (6.31)). In case (b), weighted samples of the system condition $\mathbf{D}_j$ are generated and the posterior probabilities of the different states of S_j are evaluated based on the weighted samples of $\mathbf{D}_j$ in a post-processing step, in which the conditional probabilities $p(s_j|\mathbf{d}_j)$ are computed as required on the fly. As an example, consider the case in which the system state S_j is modeled as a binary random variable and the posterior probability of the interval failure event $F_j^* = \{S_j = 1\}$ in any interval j given the observation event $\mathbf{Z}_{0:j} = \mathbf{z}_{0:j}$ is of interest (this corresponds to filtering). This probability is approximated in a post-processing step as follows:

$$\Pr(F_j^*|\mathbf{Z}_{0:j} = \mathbf{z}_{0:j}) = \sum_{\mathbf{d}_j} \Pr(F_j^*|\mathbf{D}_j = \mathbf{d}_j)\, p(\mathbf{d}_j|\mathbf{z}_{0:j}) \approx \frac{\sum_{k=1}^{K} \Pr[F_j^*|\mathbf{D}_j = \mathbf{d}_j^{(k)}]\, w_{0:j}^{(k)}}{\sum_{k=1}^{K} w_{0:j}^{(k)}} \tag{6.32}$$

where $\mathbf{d}_j^{(k)}$ is the kth sample of the system condition $\mathbf{D}_j$, $w_{0:j}^{(k)} = \prod_{i=0}^{j} w_i^{(k)}$ is the corresponding weight (see also Equation (6.30)), and $\Pr(F_j^*|\mathbf{D}_j = \mathbf{d}_j)$ is the conditional interval failure probability conditional on $\mathbf{D}_j = \mathbf{d}_j$. Note that this approach assumes that the computations of $\Pr(F_j^*|\mathbf{D}_j = \mathbf{d}_j)$ are relatively inexpensive. Prediction and smoothing of the probabilities of the interval events F_j^* are performed in analogy to Equation (6.31).

6.5 Numerical example: concrete box girder subject to corrosion

This section revises and updates material originally published in Schneider, R., Fischer, J., Bügler, M., Nowak, M., Thöns, S., Borrmann, A. and Straub, D. (2015). Assessing and updating the reliability of concrete bridges subjected to spatial deterioration - principles and software implementation. *Structural Concrete* **16**(3): 356–365. Some passages and figures are directly taken from this reference.

For illustration purposes, the DBN approach presented in Section 6.3 is applied to analyze the reliability of an existing highway bridge shown in Figure 6.13. The bridge was commissioned in 1974 and consists of two separate structures; one for each driving direction. Both bridge super-structures consist of a continuous single-cell prestressed concrete box girder with six spans ranging from 46 m to 70 m (see Figure 6.13(a)). Each box girder is 352 m long and 24.5 m wide; their cross-sections at mid-span and above the columns are shown in Figure 6.13(b).

The current case study only considers the north eastern box girder (see Figure 6.13(a)). To assess the reliability of the box girder, several assumptions are made, and simplifications introduced. First, the box girder is assumed to be subject only to chloride-induced reinforcement corrosion throughout its service life. A physics-based stochastic model of the initiation phase of this deterioration process is readily available (see, for example, fib Bulletin No. 34 2006). Secondly, the initiation model is extended by a highly-simplified propagation model to predict the loss of reinforcement steel after corrosion initiation. Thirdly, a simple structural model is applied to compute the conditional interval failure probability of the corroded structure under traffic loading. The structural model is developed based on design drawings and considers only global bending failure.

Section 6.5.1 presents a DBN model that describes the progress of reinforcement corrosion in the box girder. The model is motivated by the work of Qin and Faber (2012). It considers the spatial correlation of the corrosion process and includes random variables to represent the outcome of half-cell potential measurements, which can be performed to detect corroding reinforcement in concrete structures.

The deterioration model underlying the DBN model considers gradual degradation of the box girder's reinforcement after corrosion initiation. The uncertain condition of the box girder is thus described by a set of continuous random variables representing the loss of reinforcement cross-section throughout the structure. Although these variables are discretized as discussed in Section 6.4.1, the number of possible realizations of the condition is still too large to allow direct modeling of the structural system performance (failed/not failed) in the DBN. This is, however, not problematic, because probabilistic inference in the DBN is performed with likelihood weighting. The posterior system failure probability of the box girder can, therefore, be evaluated in a post-processing step based on the weighted samples of the system deterioration state as described in Section 6.4.2. This post-processing step includes the evaluation of the interval failure probability conditional on each generated sample of the system condition. A structural model that enables the evaluation of the conditional interval failure probability is described in Section 6.5.1.4.

(a)

(b)
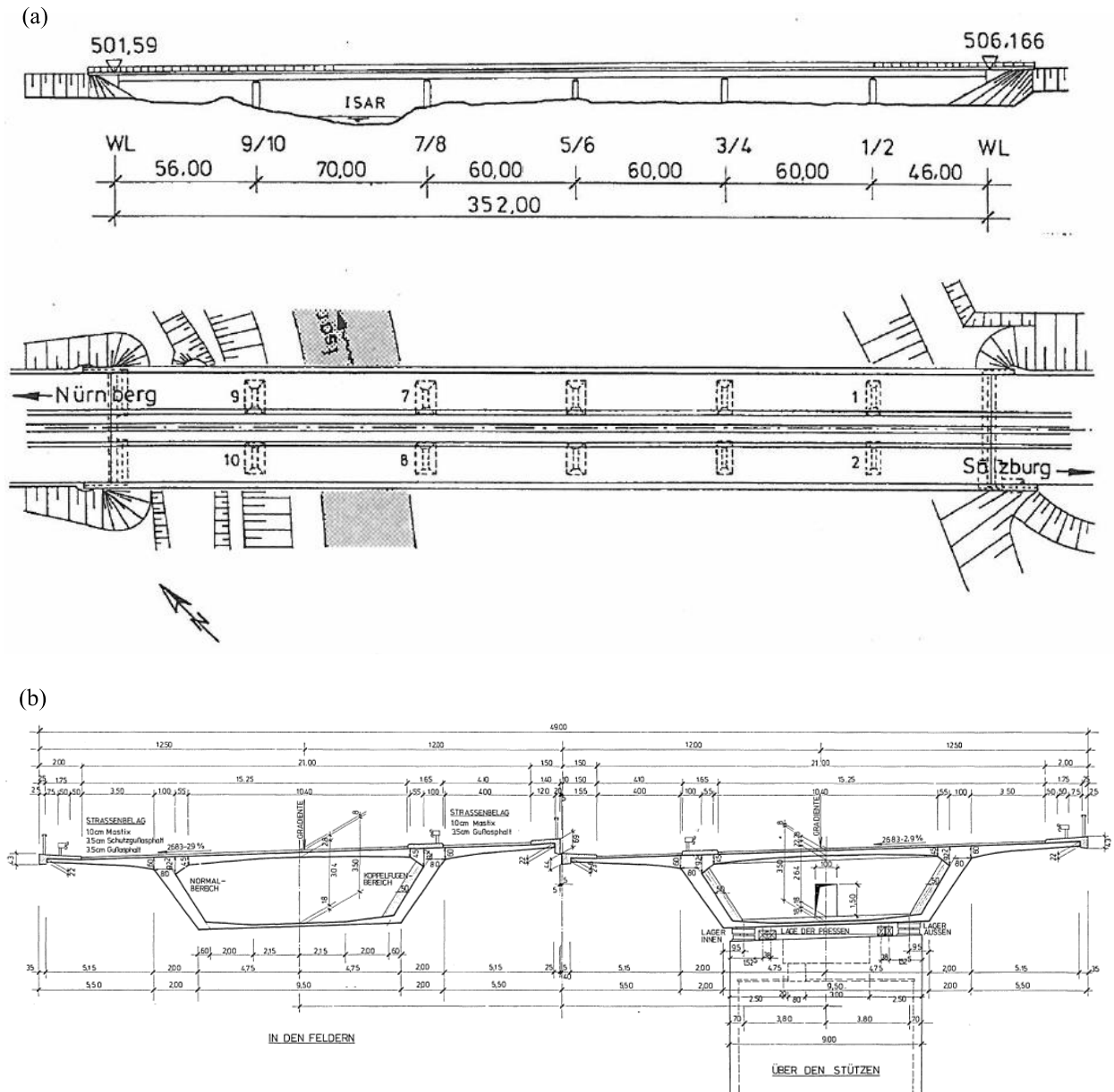
Figure 6.13: (a) Elevation and plan view of the highway bridge. (b) Cross-sections of the box girders at mid-span and above the columns

To proof the concept, the models presented in Section 6.5.1 are implemented in a software proto-type, which is described in Section 6.5.2. The prototype is applied to analyze the prior and posterior reliability of the deteriorating box girder. These analyses are summarized in Sections 6.5.3 and 6.5.4.

6.5.1 DBN model of the deteriorating box girder

6.5.1.1 DBN model of chloride-induced reinforcement corrosion

The box girder is exposed to chloride attack throughout its service life due to, for example, the application of de-icing salt. Over time the chlorides migrate from the concrete surface into the concrete. This process is commonly described by a diffusion model. Corrosion of the outer layer

125

of reinforcement at depth W starts when the concentration of chlorides exceeds a critical value C_{cr} and the passive layer protecting the reinforcement is broken down. Applying a simplified variant of the diffusion model given in (fib Bulletin No. 34 2006), the time to initiation of reinforcement corrosion T_I is given by:

$$T_I = X_I \cdot \frac{W^2}{4D} \left(\text{erf}^{-1} \left(1 - \frac{C_{cr}}{C_s} \right) \right)^{-2} \tag{6.33}$$

where D is the diffusion coefficient, C_s is the chloride concentration on the concrete surface, X_I is a random variable representing the model uncertainty associated with T_I and $\text{erf}(\cdot)$ is the Gaussian error function. Following Straub et al. (2009) and Qin and Faber (2012), all parameters W, D, C_{cr}, C_s and X_I are modeled as lognormal random variables.

The state of corrosion initiation at time t_j is modeled by a binary random variable CI_j, where $CI_j = 0$ is the event of no corrosion initiation and $CI_j = 1$ is the event of corrosion initiation. Both events are described by the limit state function $g_{CI}(t_j)$:

$$g_{CI}(t_j) = T_I - t_j \tag{6.34}$$

The event $CI_j = 1$ occurs if $g_{CI}(t_j) \leq 0$, and $CI_j = 0$ otherwise.

The chlorides continue to migrate into the concrete resulting in the de-passivation of the next reinforcement layers. At the same time, the various stages of corrosion propagation take place. First, corrosion products start to build up on the surface of the reinforcement. Once the volume of the corrosion product is sufficiently large, small cracks appear in the concrete cover. The corrosion products then disperse through the cracks and become visible on the concrete surface after some time[16]. The concrete cover may spall when the corrosion products continue to accumulate on the surface of the reinforcement. Spalling of the concrete cover exposes the structure even further to the environment and thus accelerates the corrosion process. Eventually, reinforcement corrosion reduces the structure's serviceability and load carrying capacity beyond acceptable limits.

Reinforcement corrosion reduces the load carrying capacity of reinforced concrete structures mainly because of two effects (Osterminski and Schießl 2012): (a) loss of the cross-sectional area of the reinforcement due to uniform and/or pitting corrosion, and (b) loss of bond between the reinforcement and the concrete due to spalling and/or delamination. In the current case study – for illustration purposes – only the effect of the loss of reinforcement cross-sectional area is considered and the propagation phase of chloride-induced reinforcement corrosion is modeled by a simple linear model as illustrated in Figure 6.14.

The state of corrosion propagation at time t_j is here described in terms of the relative corrosion progress Δ_j ranging from 0 to 1. Given Δ_j, the remaining cross-sectional area of the reinforcement A_j at time t_j is computed as:

---

[16] Cracking of the concrete cover and visible coloring of the concrete surface are thus an observable indicator of progressed reinforcement corrosion in concrete structures (see, for example, Faber et al. 2006).
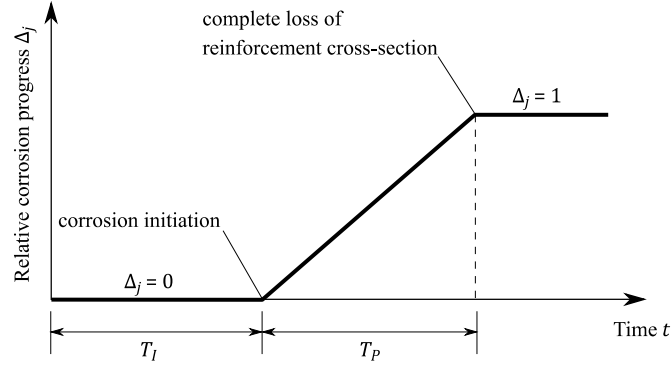
Figure 6.14: Initiation and propagation phase of chloride-induced reinforcement corrosion. The propagation phase is here described by a simple linear model.

$$A_j = (1 - \Delta_j)\, A_0 \tag{6.35}$$

where A_0 is the initial cross-sectional area of the reinforcement. Δ_j is a function of the time to corrosion initiation T_I and the time between corrosion initiation and complete loss of reinforcement cross-section T_p (see Figure 6.14). A deterioration model h_D describing Δ_j can now be written as:

$$\Delta_j = h_D(t_j, T_I, T_p) = \begin{cases} 0, & t_j \le T_I \\ \dfrac{1}{T_P}(t_j - T_I), & T_I < t_j \le T_P + T_I \\ 1, & t_j > T_P + T_I \end{cases} \tag{6.36}$$

For the sake of demonstration, T_P is modeled as a lognormal variable. Note that the propagation model can be replaced by a more detailed, physics-based model (see, for example, Vu and Stewart 2000; Osterminski and Schießl 2012).

The deterioration model h_D contains only time-invariant parameters. These are, in terms of the generic model described in Section 6.3.1, $\Theta = [T_I, T_p]^T$, where T_I is a function of the variables W, D, C_{cr}, C_s and X_I as defined by Equation (6.33). The deterioration state is, in terms of the generic model, $D_j = \Delta_j$. The resulting DBN model of chloride-induced reinforcement corrosion is shown in Figure 6.15.

The DBN model describes the corrosion process as a discrete time process. In the current example, each slice j of the DBN represents the state of the corrosion process at end of year j, and the last slice m corresponds to the service life of the structure (expressed in years).

As discussed in Section 6.4, the continuous random variables W, D, C_s, C_{cr}, X_I, $T_{I,j}$, $T_{P,j}$ and Δ_j are discretized according to their topological ordering in the DBN. First, variable W is discretized by dividing its continuous outcome space into m_W intervals. These intervals are defined in terms of $m_W + 1$ interval boundaries $(w_0, w_1, \dots, w_{m_W})$, which are chosen as follows. The boundaries w_0 and w_{m_W} are set equal to the lower and upper boundaries of W's outcome space. The boundaries w_1 and w_{m_W-1} are defined such that the probability of W taking a value outside the range $w_1 < w \le w_{m_W-1}$ is smaller than a value p. All remaining boundaries $(w_2, \dots, w_{m_W-2})$ are selected such that the intervals within the range $w_1 < w \le w_{m_W-1}$ have equal lengths. The marginal

127
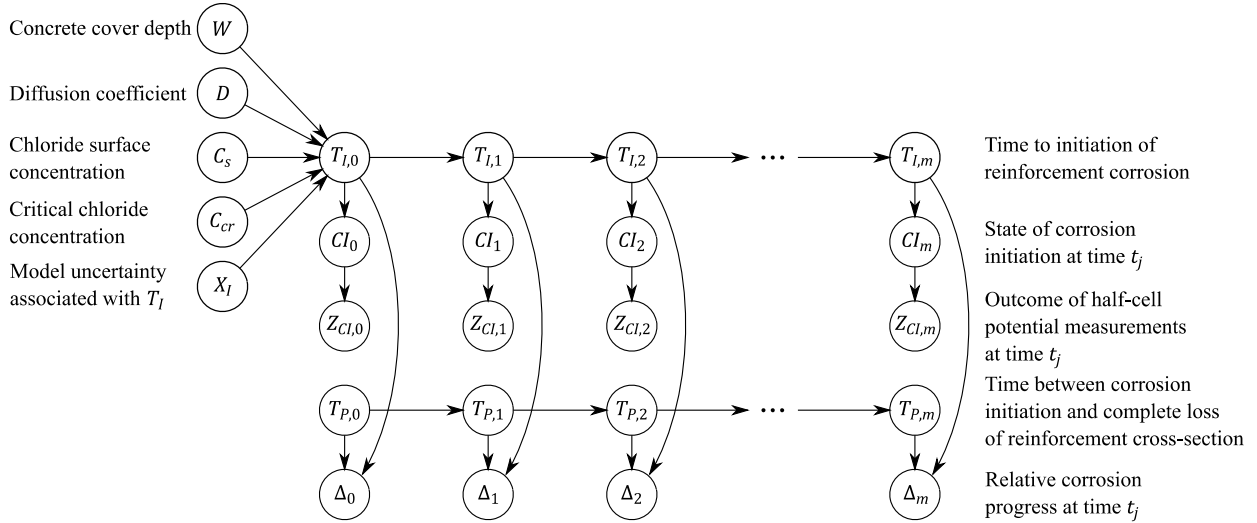
Figure 6.15: DBN model of chloride-induced reinforcement corrosion.

PMF $p(w)$ is computed following Equation (6.27). Variables D, C_s, C_{cr} and X_I are discretized in the same way as W.

Next, variables $T_{I,j}$ and $T_{P,j}$ are discretized. Their outcome spaces are divided into $m_T = m + 1$ intervals. The corresponding interval boundaries are defined as $(0, 1, 2, \ldots, T, \infty)$. The same discretization scheme in applied for all slices j. The marginal PMF of $p(t_{P,0})$ is obtained analytically following Equation (6.27). As described in the example in Section 6.4.1, MSC is applied to compute the conditional PMF $p(t_{I,0}|w, d, c_s, c_{cr}, x_I)$ based on Equation (6.33). The conditional PMF $p(t_{I,j}|t_{I,j-1})$ and $p(t_{P,j}|t_{P,j-1})$, $j = 1, \ldots, m$ are unit matrices since $T_{I,j}$ and $T_{P,j}$ are time-invariant.

Finally, the m_Δ states of variable Δ_j are defined. The first and last state correspond to the events $\Delta_j = 0$ and $\Delta_j = 1$. All remaining states are defined by dividing the outcome space of Δ_j into $m_\Delta - 2$ intervals with equal lengths. It follows that the second state corresponds to the event $0 < \Delta_j \leq 1/(m_\Delta - 2)$, the third state is equal to the event $1/(m_\Delta - 2) < \Delta_j \leq 2/(m_\Delta - 2)$ and so on. Note that the penultimate state of Δ_j corresponds to the event $(m_\Delta - 3)/(m_\Delta - 2) < \Delta_j < 1$. The same discretization scheme is applied for all slices j. The conditional PMF $p(\delta_j|t_{I,j}, t_{P,j})$ is constructed as a function of year j based on Equation (6.36). It follows that $p(\delta_j|t_{I,j}, t_{P,j})$ changes with each slice j.

The discrete random variable CI_j is characterized by the conditional PMF $p(ci_j|t_{I,j})$, which is determined as a function of year j based on the limit state function $g_{CI}(t_j)$ defined in Equation (6.34). Thus, $p(ci_j|t_{I,j})$ also changes with each slice j.

6.5.1.2 Modeling the outcome of half-cell potential measurements

Half-cell potential measurements determine the potential difference between an external reference electrode and the reinforcement. The measurements are performed on a grid over large concrete surfaces. A low potential difference indicates reinforcement corrosion (see, for example, Elsener et al. 2003). This inspection method thus provides information on the state of corrosion initiation CI_j at time t_j. Let U_j be the uncertain potential difference determined with a half-cell potential measurement at a given location on a concrete surface at time t_j. Furthermore, let

$f_{U_j|CI_j}(u_j|ci_j = 0)$ be the conditional PDF representing the probability that the measured potential difference is $U_j = u_j$ given that the state of corrosion initiation is $CI_j = 0$ (no corrosion initiation). Similarly, $f_{U_j|CI_j}(u_j|ci_j = 1)$ indicates the probability that the measurement results in $U_j = u_j$ given that the state of corrosion initiation is $CI_j = 1$ (corrosion initiation). The conditional density functions $f_{U_j|CI_j}(u_j|ci_j = 0)$ and $f_{U_j|CI_j}(u_j|ci_j = 1)$ can be derived from experiments (see, for example, Lentz 2001; Johnsen et al. 2003; Keßler et al. 2014). They are illustrated in Figure 6.16.

A threshold potential u_T is defined to enable an interpretation of the measurement outcome as illustrated in Figure 6.16. By definition, the inspection indicates reinforcement corrosion if the measured potential difference is smaller than the threshold potential u_T. A probability of indication $PoI(ci_j)$ can thus be determined as:

$$PoI(ci_j) = \Pr(U_j \leq u_T|CI_j = ci_j) = \int_{-\infty}^{u_T} f_{U_j|CI_j}(u_j|ci_j)\,du_j \tag{6.37}$$

The PoI models the quality of half-cell potential measurements. The inspection method would be perfect if the probability of indication given that corrosion has started is $PoI(ci_j = 1) = 1$ and the probability of indication given that corrosion has not started is $PoI(ci_j = 0) = 0$.

The threshold u_T is typically selected to achieve a high probability of indication given that the state of corrosion initiation is $CI_j = 1$, e.g. $PoI(ci_j = 1) = 0.9$ (see, for example, Lentz 2001). With a fixed threshold u_T, the probability of indication given that the state of corrosion initiation is $CI_t = 0$ is then computed based on Equation (6.37).

Half-cell potential measurements can now be classified following Section 5.3.1. The classification is summarized in Table 6.1.
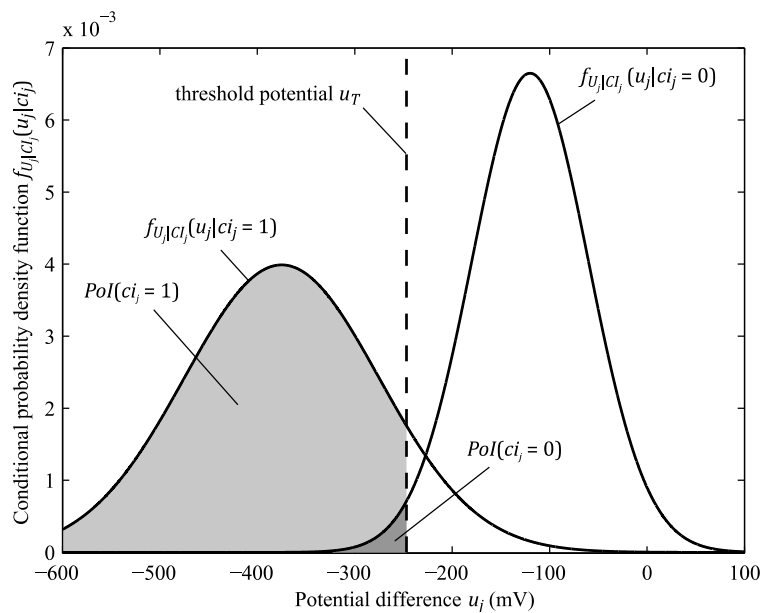
Figure 6.16: Illustration of the conditional PDF $f_{U_j|CI_j}(u_j|ci_j)$ of the potential difference U_j and the probability of indication $PoI(ci_j)$ for $CI_j = 0$ (no corrosion initiation) and $CI_j = 1$ (corrosion initiation).

Table 6.1: Classification of half-cell potential measurements.

Classification	Categories
Inspected/monitored quantity	Indicator related to the output of the deterioration model (The measured indicator is the potential difference which is related to the state of corrosion initiation)
Type of information	Inequality information (indication/no indication of corrosion initiation)
Temporal characteristics	Data collection at discrete points in time
Spatial characteristics	Spatially (quasi) continuous data collection (The measurements are performed on a grid over the entire concrete surfaces.)

Table 6.2: Likelihood $p(z_{CI,t}|ci_t) = \Pr(Z_{CI,t} = z_{CI,t}|CI_t = ci_t)$ of half-cell potential measurements.

	$CI_j = 0$ (no initiation)	$CI_j = 1$ (initiation)
$Z_{CI,j} = 0$ (no indication)	$1 - PoI(ci_j = 0)$	$1 - PoI(ci_j = 1)$
$Z_{CI,j} = 1$ (indication)	$PoI(ci_j = 0)$	$PoI(ci_j = 1)$

To represent the outcome of half-cell potential measurements, the DBN model shown Figure 6.15 includes a binary random variable $Z_{CI,j}$ as child of variable CI_j in each slice j, where $Z_{CI,j} = 0$ is the event of no indication of corrosion and $Z_{CI,j} = 1$ is the complement. The variable $Z_{CI,j}$ is described by the likelihood $p(z_{CI,j}|ci_j) = \Pr(Z_{CI,j} = z_{CI,j}|CI_j = ci_j)$. The likelihood $p(z_{CI,j}|ci_j)$ is fully characterized by the probability of indication $PoI(ci_j)$ as shown in Table 6.2. As an example, the probability of no indication of corrosion given that corrosion has started, is $\Pr(Z_{CI,j} = 0|CI_j = 1) = 1 - PoI(ci_j = 1)$.

6.5.1.3 DBN model of system deterioration

Chloride-induced reinforcement corrosion varies randomly throughout the structure due to the spatial correlation among the parameters influencing the progress of corrosion such as concrete cover depth, chloride surface concentration and concrete properties. To account for the spatial variability of the corrosion process, the box girder is divided into n_S sections as indicated in Figure 6.17. Each section is further divided into four elements (area segments): deck plate, bottom flange and two webs. Thus, there are $n_E = 4 \cdot n_S$ elements.

The progress of chloride-induced reinforcement corrosion is modeled at the element level using separate DBN models as introduced in Sections 6.5.1.1 and 6.5.1.2. Within an element, the deterioration state at time t_j is assumed to be uniform, i.e. a relative corrosion progress of 0.05 represents an average 5% reduction in the overall cross-sectional area of the reinforcement in the associated element. Note that the current discretization scheme does not consider the spatial variability of the corrosion process around the circumference of the box girder. To account for this aspect properly, each element should be further divided in the direction perpendicular to the longitudinal axis of the box girder.

Following Section 6.3.4, a hierarchical model is applied to represent spatial dependence among element deterioration. To this end, the hyper-parameters U_W, U_D, U_{C_s}, $U_{C_{cr}}$, U_{X_I} and U_{T_P} are in-
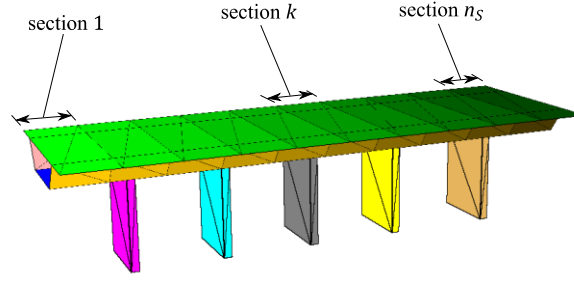
Figure 6.17: Sections defining the element sizes of the deterioration model of the box girder. Each section consists of four elements: deck plate, bottom flange and two webs.

troduced. In the system model, all element deterioration models are connected through these hyper-parameters as illustrated in Figure 6.18. In accordance with the notation introduced in Section 6.3, all random variables in the DBN model are indexed by the element number i and the slice j.

The conditional CDFs of variables W_i, D_i, $C_{s,i}$, $C_{cr,i}$, $X_{I,i}$ and $T_{P,i,0}$, $i = 1, \ldots, n_E$ are determined as a function of the specified correlation coefficients using Equation (6.24). Subsequently, the hyper-parameters U_W, U_D, U_{C_s}, $U_{C_{cr}}$, U_{X_I} and U_{T_P} are discretized following the same scheme as described for variable W in Section 6.5.1.1. The conditional PMF of variables W_i, D_i, $C_{s,i}$, $C_{cr,i}$, $X_{I,i}$ and $T_{P,i,0}$, $i = 1, \ldots, n_E$ are then computed following Equation (6.28).

The DBN model describes the progress of chloride-induced reinforcement corrosion throughout the box girder at yearly intervals. The system condition at the end of year j is, in terms of the generic model presented in Section 6.3.4, defined as follows:

$$\mathbf{D}_j = [\Delta_{1,j}, \ldots, \Delta_{n_E,j}]^T \tag{6.38}$$

In the current example, $\mathbf{D}_j$ has $m_\Delta^{n_E}$ distinct states.

In contrast to the generic system model described in Section 6.3.4, the system model shown in Figure 6.18 does not contain a variable S_j as a child of variables $\Delta_{i,j}$, $i = 1, \ldots, n_E$ in each slice j to represent system state at the end of year j. This is because the number of realizations of the system deterioration state $\mathbf{D}_j$ is here too large to enable pre-computation of the conditional PMF $p(s_j|\mathbf{d}_j)$. Instead, the DBN model is applied to generate weighted samples of $\mathbf{D}_j$ with likelihood weighting as summarized in Algorithm 6.1. These samples are subsequently used to approximate the posterior interval failure probability of the box girder as described in Section 6.4.2. This post-processing step includes the computation of the conditional interval failure probability $\Pr(F_j^*|\mathbf{D}_j = \mathbf{d}_j)$ of the box girder for each generated sample of $\mathbf{D}_j$. A model that enables the evaluation of $\Pr(F_j^*|\mathbf{D}_j = \mathbf{d}_j)$ is described in the following section.

6.5.1.4 Conditional interval failure probability

The box girder is modeled at mechanism level to determine the conditional interval failure probability $\Pr(F_j^*|\mathbf{D}_j = \mathbf{d}_j)$ (see Section 2.4.2). To this end, a simple beam model is applied that only considers global bending failure. The ultimate capacity of the damaged box girder is estimated using plastic limit analysis. The damaged box girder is assumed to fail when sufficient plastic
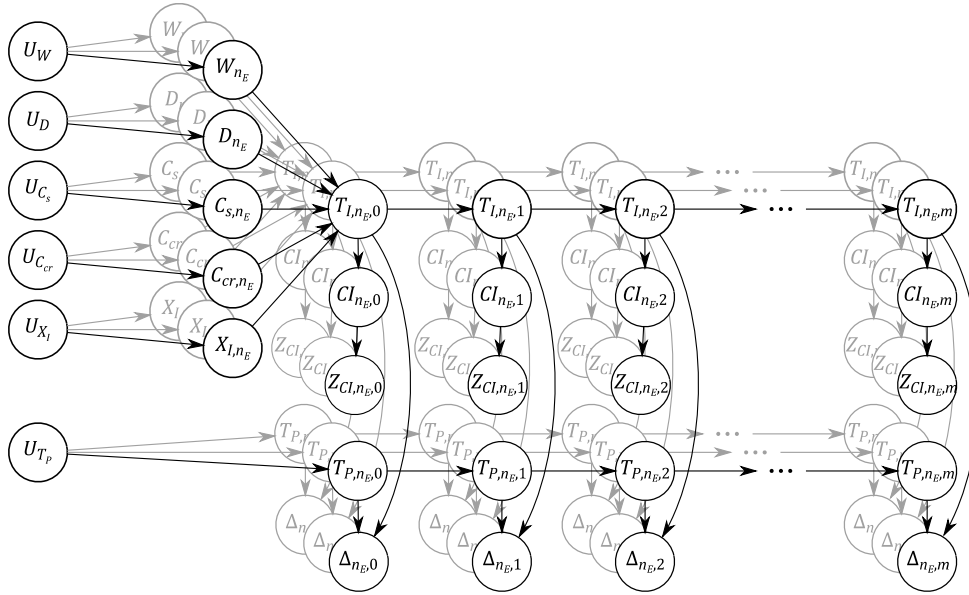
Figure 6.18: DBN model of the deteriorating box girder.

hinges develop under the applied loads such that a collapse mechanism forms. This approach accounts for structural redundancies due to the plastic cross-sectional capacity and static indeterminacy of the box girder. It allows for inelastic moment redistribution along the box girder following the formation of plastic hinges.

The box girder is subject to a traffic load. In the current study, the traffic load is represented by a spanwise uniformly distributed load whose maximum in year j is denoted by $S_{max,j}$. The different $S_{max,j}$ are model as independent and identically distributed random variables with CDF $F_{S_{max,j}}(s)$. Different load cases are defined such that the bending moments along each span and at each column are maximized (see Figure 6.19).

Dead and prestressing loads, including losses in prestressing due to creep and shrinkage, are modeled as deterministic parameters, likewise the material and geometrical properties of the box girder. Therefore, it is possible to calculate a deterministic maximum plastic bending resistance for each cross-section along the box girder as a function of a given system condition $\mathbf{D}_j = \mathbf{d}_j$. In the context of reinforcement corrosion, the cross-sectional area of the reinforcement associated with each element of the deterioration model is reduced according to $\mathbf{D}_j = \mathbf{d}_j$ by applying Equation (6.35). Note that in the current example a realization of the system condition $\mathbf{D}_j = \mathbf{d}_j$ defines a combination of discrete states of variables $\Delta_{i,j}$, $i = 1, \ldots, n_E$. As described in Section 6.5.1.1, a discrete state of variable $\Delta_{i,j}$ corresponds to an interval of its continuous outcome space, which ranges from 0 to 1. To enable the evaluation of $\Pr(F_j^* | \mathbf{D}_j = \mathbf{d}_j)$, a discrete state of variable $\Delta_{i,j}$ is here represented by the midpoint of the corresponding interval.

Figure 6.20 shows the plastic bending resistance of the undamaged box girder as a function of position x along the girder. The plastic bending resistance of each cross-section depends on the area of the reinforcement and prestressing tendons, their yield strengths and internal lever arm as well as the resistance of the compression zone. The amount and location of the reinforcement and the number and locations of the prestressing tendons in the deck plate, webs and bottom flange
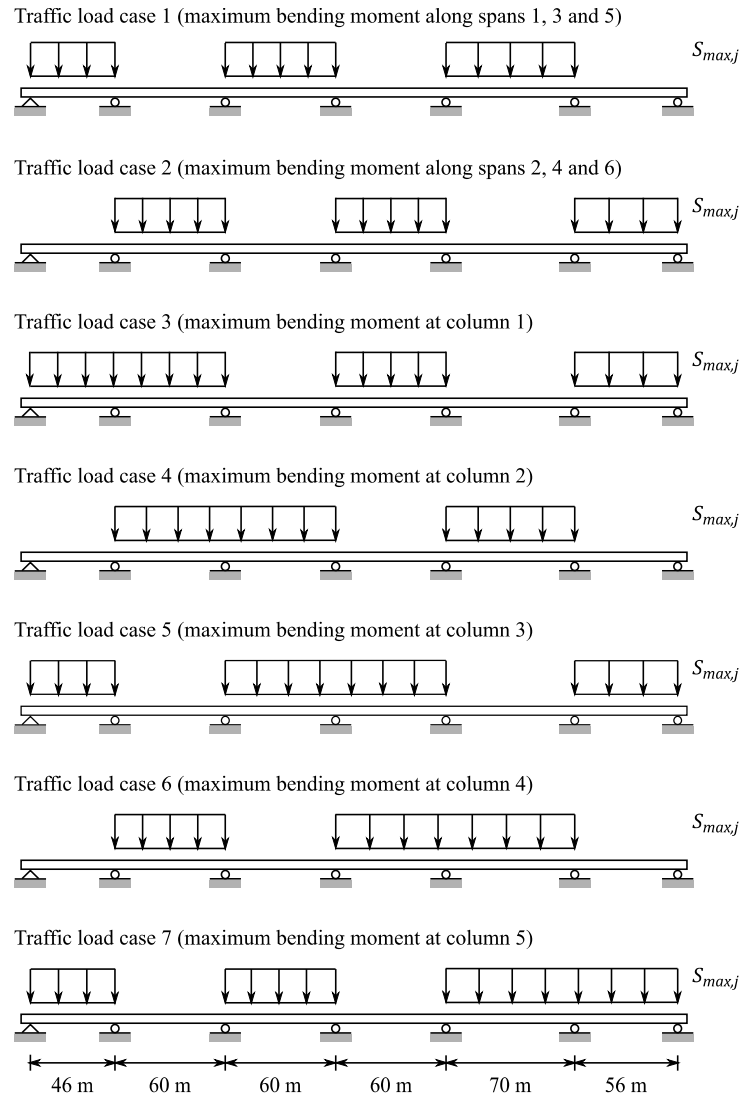
Figure 6.19: Traffic load cases. They are defined such that the bending moments along each span and at each column are maximized.

varies along the girder. This explains the steps in the bending resistance shown in Figure 6.20. Note that the statically indeterminate part of the prestressing-induced bending moments is applied as a structural load in the analysis.

Dead and prestressing loads as well as material and geometrical properties are modeled deterministically, because the uncertainties associated with these quantities are here estimated to be significantly lower than the uncertainties associated with the progress of reinforcement corrosion and the traffic load.

The damaged box girder can fail by forming a collapse mechanism under any of the applied traffic load cases defined in Figure 6.19. Let $F_{k,j}^*$ denote the event of forming a collapse mechanism in year j under traffic load case k. A limit state function g_k describing this event can be written as:

$$g_k(\mathbf{d}_j, s_{max,j}) = r_k(\mathbf{d}_j) - s_{max,j} \tag{6.39}$$

133
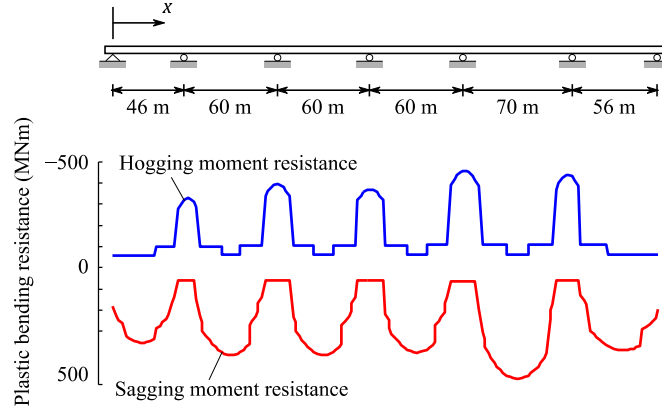
Figure 6.20: Initial plastic bending resistance of the box girder as function of position x along the girder.

where $s_{max,j}$ is a realization of the annual maximum of the traffic load and $r_k(\mathbf{d}_j)$ is the realization of the box girder's capacity with respect to traffic load case k given $\mathbf{D}_j = \mathbf{d}_j$. With the structural model modified according to the deterioration state $\mathbf{D}_j = \mathbf{d}_j$, the deterministic capacity $r_k(\mathbf{d}_j)$ is here computed using plastic limit analysis based on a finite element (FE) beam model.

Overall system failure of the damaged box girder in year j occurs as soon as the weakest collapse mechanisms forms. From system reliability theory, it follows that the conditional interval failure probability $\Pr(F_j^* | \mathbf{D}_j = \mathbf{d}_j)$ is defined as:

$$
\begin{aligned}
\Pr(F_j^* | \mathbf{D}_j = \mathbf{d}_j) &= \Pr\left(F_{1,j}^* \cup \ldots \cup F_{7,j}^* | \mathbf{D}_j = \mathbf{d}_j\right) \\
&= \Pr\left[g_1(\mathbf{d}_j, S_{max,j}) \leq 0 \cup \ldots \cup g_7(\mathbf{d}_j, S_{max,j}) \leq 0\right]
\end{aligned}
\tag{6.40}
$$

Following Section 2.2, an equivalent limit state function describing the event F_t can now be written as:

$$
\begin{aligned}
g(\mathbf{d}_j, s_{max,j}) &= \min\left[g_1(\mathbf{d}_j, s_{max,j}), \ldots, g_7(\mathbf{d}_j, s_{max,j})\right] \\
&= \min\left[r_1(\mathbf{d}_j) - s_{max,j}, \ldots, r_7(\mathbf{d}_j) - s_{max,j}\right] \\
&= \min\left[r_1(\mathbf{d}_j), \ldots, r_7(\mathbf{d}_j)\right] - s_{max,j} \\
&= r(\mathbf{d}_j) - s_{max,j}
\end{aligned}
\tag{6.41}
$$

where $r(\mathbf{d}_j) = \min[r_1(\mathbf{d}_j), \ldots, r_7(\mathbf{d}_j)]$ can be interpreted as the minimum capacity of the box girder. Once $r(\mathbf{d}_j)$ is known, the conditional interval failure probability of the box girder can be calculated as:

$$
\begin{aligned}
\Pr(F_j^* | \mathbf{D}_j = \mathbf{d}_j) &= \Pr[g(\mathbf{d}_j, S_{max,j}) \leq 0] \\
&= \Pr[r(\mathbf{d}_j) \leq S_{max,j}] \\
&= 1 - F_{S_{max,j}}[r(\mathbf{d}_j)]
\end{aligned}
\tag{6.42}
$$

6.5.2 Software prototype

To prove the concept, the models presented in Section 6.5.1 are implemented in a software prototype. It consists of two parts: a front end with a graphical user interface (GUI) implemented in Java, and a back end implemented in Matlab. The front end provides the functionality required for defining the DBN model of the deteriorating box girder, entering inspection data and visualizing results. The back end is the computational engine of the software prototype. This part of the prototype has mainly been implemented by the author of this thesis. The architecture of the software prototype is illustrated in Figure 6.21.

The GUI is divided into two panels as shown in Figure 6.22. The upper panel displays a rotatable 3D model of the box girder. The data required for the 3D representation is stored in a text file in XML (eXtensible Markup Language) format and called the "structural model data base" (see Figure 6.21). This file also contains information on the sizes and locations of the individual sections of the girder. The lower panel consists of different tabs for entering and visualizing model data.

The user may assign the relevant deterioration models to each element if the "assign damage models" tab is active. The default data of possible deterioration models is defined in a "deterioration model data base" (see Figure 6.21)[17]. The "assign damage groups" tab provides a table that allows the user to define groups of correlated elements. There is no interdependence among elements belonging to different groups. The user may set the parameters of the deterioration models in a
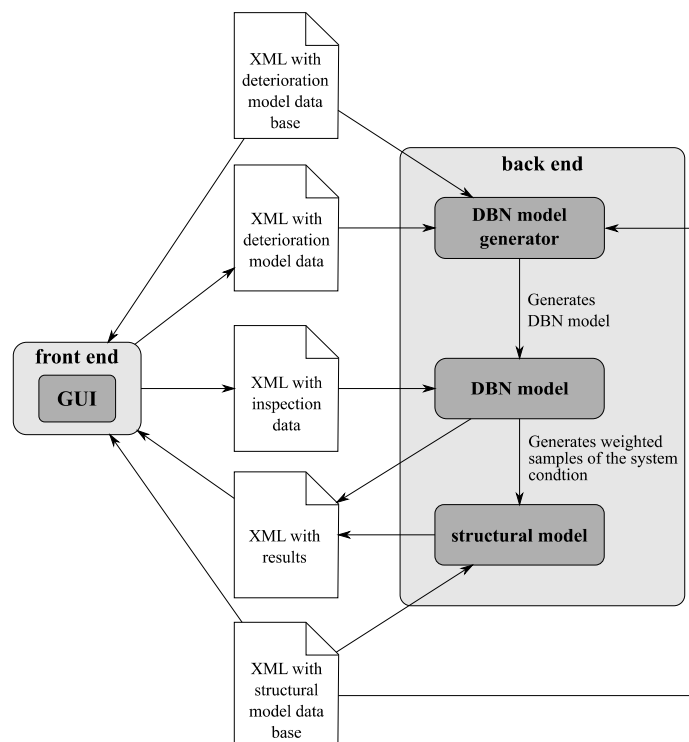
Figure 6.21: Architecture of the software prototype.

---

[17] Currently, only chloride-induced reinforcement corrosion is available. The software can be extended in the future to include additional deterioration processes.

135
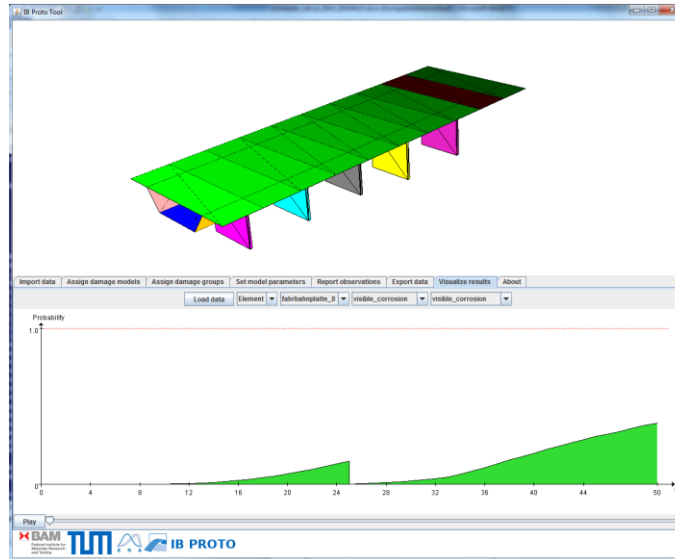
Figure 6.22: Screenshot of the GUI (front end).

table provided in the "set model parameters" tab. The data for the DBN model of system deterioration (deterioration model assignments, group definitions and parameter data) can be exported to an XML file as indicated in Figure 6.21. Inspection results providing information on the condition of any element can be entered if the "report observations" tab is active. The inspection results can also be exported to an XML file (see Figure 6.21).

The back end consists of three main modules as indicated in Figure 6.21. The first module generates a DBN model of the deteriorating box girder as described in Section 6.5.1 based on the "deterioration model data" (deterioration model assignments, group definitions and parameter data) and the "deterioration model data base" (default deterioration model data) and the "structural model data base" (service life). The second module provides the data structure for the DBN model and implements the likelihood weighting algorithm as described in Algorithm 6.1. The third module implements the structural capacity model of the box girder as described in 6.5.1.4. The data required to initialize the structural model is contained in the "structural model data base" (geometry, material and load data). The module computes the posterior interval failure probabilities of the box girder for each interval j based on the weighted samples of the system deterioration state $\mathbf{D}_j$ following Section 6.4.2. The conditional interval failure probabilities $\Pr(F_j^* | \mathbf{D}_j = \mathbf{d}_j)$ are computed as a function of the ultimate capacity of the damaged box girder $r(\mathbf{d}_j)$ following Equation (6.42). To determine $r(\mathbf{d}_j)$, the third module implements an FE beam model, which forms the basis for performing the plastic limit analysis of the damaged box girder. The analysis results (probabilities of element deterioration states and system failure probability) are exported to an XML file (see Figure 6.21). These results can be imported and visualized in the "visualize results" tab of the GUI as shown in Figure 6.22.

6.5.3 Prior reliability analysis

The software prototype is applied to analyze the prior system condition and reliability of the corroding box girder. The box girder is assumed to have a service life $T_{SL} = 50$ years. The maximum

of the traffic load in any year j, $S_{max,j}$, is assumed to have the Gumbel distribution with a coefficient of variation $\delta_{S_{max,j}} = 0.3$. The parameters of the Gumbel distribution are calibrated such that the undamaged box girder has an interval failure probability $\Pr(F_j^* | \mathbf{D}_j = \mathbf{0}) = 1.3 \cdot 10^{-6}$.

To model the system condition, the box girder is divided into $n_S = 176$ sections. Therefore, the model has $n_E = 4 \cdot n_S = 704$ elements. Each section is 2 m long. The lengths of the beam elements are also chosen to be 2 m. The deck plate of the box girder is assumed to be exposed to a higher chloride surface concentration than the webs and bottom flange. The prior probabilistic models of the corrosion model parameters for all elements of the system deterioration model are listed in Table 6.3.

The corrosion model parameters W_i, D_i, $C_{s,i}$, $C_{cr,i}$, $X_{I,i}$ and $T_{P,i,0}$ are modeled as partially correlated among all elements $i = 1, \dots, n_E$. To study the influence of different levels of statistical dependence among element corrosion behavior, two different dependence cases are considered (low and high). These cases are defined in terms of the correlation coefficients $\rho_{\ln W}$, $\rho_{\ln D}$, $\rho_{\ln C_s}$, $\rho_{\ln C_{cr}}$, $\rho_{\ln X_I}$ and $\rho_{\ln T_P}$ listed in Table 6.4.

Table 6.5 summarizes the applied discretization scheme for the hyper and corrosion model parameters.

Table 6.3: Prior probabilistic models of the corrosion model parameters for all elements $i = 1, \dots, n_E$.

Parameter	Dimension	Distribution	Mean	Standard deviation
W_i	mm	lognormal	40.0	8.0
D_i	mm²/year	lognormal	20.0	10.0
$C_{s,i}$[a]	wt.%[c]	lognormal	1.5	0.6
$C_{s,i}$[b]	wt.%	lognormal	1.0	0.4
C_{cr}	wt.%	lognormal	0.8	0.1
$X_{I,i}$	-	lognormal	1.0	0.05
$T_{P,i,0}$	year	lognormal	20.0	6.0

[a] deck plate

[b] webs and bottom flange

[c] percentage by weight of cement

Table 6.4: Correlation coefficients modeling stochastic dependence among the parameters of the corrosion model.

	Low dependence	High dependence
$\rho_{\ln W}$	0.2	0.8
$\rho_{\ln D}$	0.2	0.8
$\rho_{\ln C_s}$	0.2	0.8
$\rho_{\ln C_{cr}}$	0.2	0.8
$\rho_{\ln X_I}$	0.2	0.8
$\rho_{\ln T_P}$	0.2	0.8

Table 6.5: Discretization scheme for the hyper-parameters and corrosion model parameters.

Parameter	Number of states	Interval boundaries
$U_W, U_D, U_{C_s}, U_{C_{cr}}, U_{X_I}, U_{T_P}$	20	$0, -3.1: (3.1 - (-3.1))/18: 3.1, \infty$
W_i	12	$0, 21.3: (72.3 - 21.3)/10: 72.3, \infty$
D_i	12	$0, 4.2: (77 - 4.2)/10: 77, \infty$
$C_{s,i}$[a]	12	$0, 0.42: (4.6 - 0.42)/10: 4.6, \infty$
$C_{s,i}$[b]	12	$0, 0.28: (3.1 - 0.28)/10: 3.1, \infty$
C_{cr}	12	$0, 0.54: (1.17 - 0.54)/10: 1.17, \infty$
$X_{I,i}$	12	$0, 0.86: (1.16 - 0.86)/10: 1.16, \infty$
$T_{I,i,j}, T_{P,i,j}$	51	$0: 1: 50, \infty$
$\Delta_{i,j}$	22	$0: 1/20: 1$[c]

[a] deck plate

[b] webs and bottom flange

[c] these interval boundaries define states 2 to 21 of variable $\Delta_{i,j}$ (see Section 6.5.1.1)

Based on the model data summarized above, prior probabilities of the element conditions and the prior interval failure probabilities of the box girder are computed by simulating 10^5 weighted samples of the system condition. Figure 6.23(a) shows the prior (marginal) probability of corrosion initiation up to time t, $\Pr[CI_i(t) = 1]$, for all deck plate, web and bottom flange elements. In addition – to illustrate the progress of corrosion – Figure 6.23(b) shows the prior (marginal) probability that the relative corrosion progress Δ_i in the deck plate elements, and web and bottom flange elements exceeds 0.2 at any time up to time t, $\Pr[\Delta_i(t) \geq 0.2]$. This probability is equal to the probability that on average more than 20% of the overall cross-sectional area of the reinforcement in the associated elements is lost due to corrosion. The probabilities $\Pr[CI_i(t) = 1]$ and $\Pr[\Delta_i(t) \geq 0.2]$ are determined by interpolating the different probabilities $\Pr(CI_{i,j} = 1)$ and $\Pr(\Delta_{i,j} \geq 0.2)$ computed with the DBN model.

The results in Figure 6.23 illustrate that the probabilities $\Pr[CI_i(t) = 1]$ and $\Pr[\Delta_i(t) \geq 0.2]$ estimated for all deck plate elements are higher than the corresponding probabilities calculated for all web and bottom flange elements. These results are expected since the deck plate elements are exposed to a higher surface concentration of chlorides.

Note that the corrosion initiation model presented in Section 6.5.1.1 belongs to model class (a) described in Section 4.2. Thus, the probability $\Pr(CI_{i,j} = 1) = \Pr[g_{CI}(t_j) \leq 0]$ corresponds to the probability of corrosion initiation up to time t_j. The same holds for the overall corrosion model, which combines the initiation model with the propagation model. It follows that the probability $\Pr(\Delta_{i,j} \geq 0.2) = \Pr(0.2 - \Delta_{i,j} \leq 0)$ is equal to the probability that the relative corrosion progress in element i exceeds 0.2 up to time t_j.

Also note that the prior marginal PMF of variables $CI_{i,j}$ and $\Delta_{i,j}, j = 1, \dots, T_{SL}$ are identical for all deck plate elements irrespective of the degree of dependence among element corrosion behavior. This is because the same prior probabilistic models are here applied to describe the corrosion
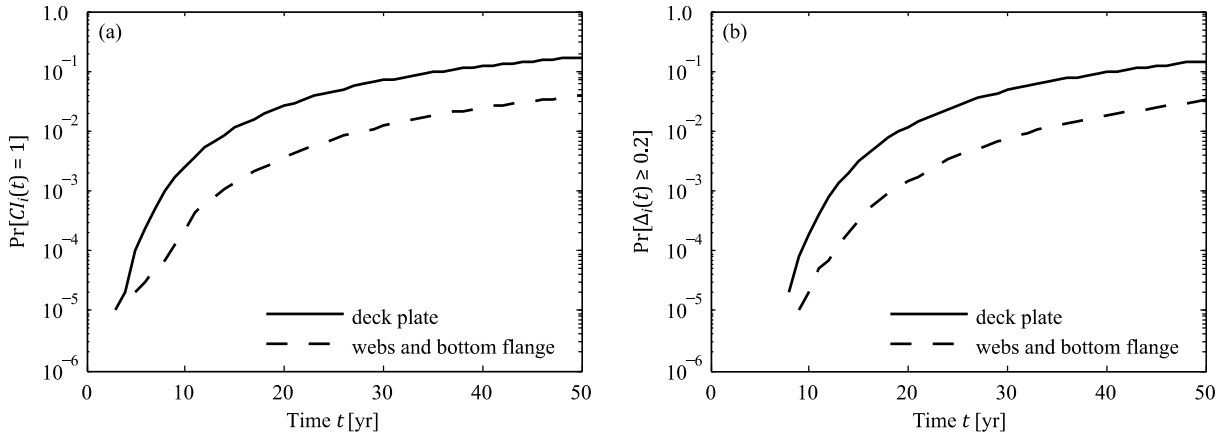
Figure 6.23: (a) Prior marginal probability of corrosion initiation $\Pr[CI_i(t) = 1]$ of all deck plate, web and bottom flange elements. (b) Prior marginal probability that the relative corrosion progress Δ_i in the deck plate elements, and web and bottom flange elements exceeds 0.2 at any time up to time t, $\Pr[\Delta_i(t) \geq 0.2]$.

model parameters of each deck plate element (see Table 6.3). The same applies to the web and bottom flange elements.

The corrosion initiation state and the relative corrosion progress of two different elements are correlated. To study the correlation among element deterioration, the correlation coefficient between the corrosion initiation state $\rho[CI_i(t), CI_j(t)]$ and the correlation coefficient among the relative corrosion progresses $\rho[\Delta_i(t), \Delta_j(t)]$ of two deck plate elements i and j are computed from the simulated samples. The results are shown in Figure 6.24. The correlations are low at the beginning of the service life because of the small probabilities of corrosion initiation. However, they increase with time. As expected, the correlation coefficients strongly depend on the correlation among the parameters influencing the element deterioration state.

Figure 6.25 shows the prior estimate of the interval failure probabilities $\Pr(F_j^*)$ for each degree of dependence among element corrosion behavior. At the beginning of the service life, when the probability of corrosion initiation is low, the interval failure probability remains close to its lower
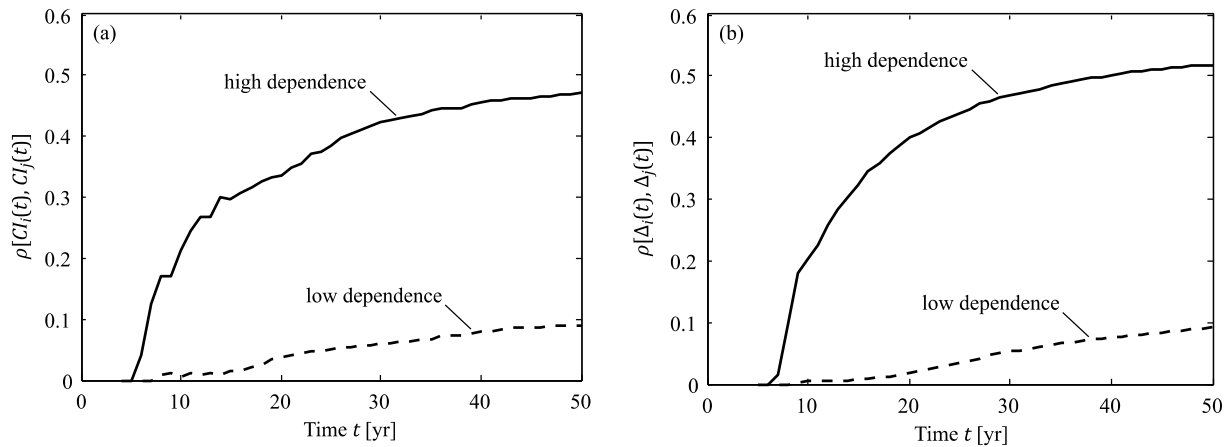
Figure 6.24: (a) Correlation coefficient among corrosion initiation states $\rho[CI_i(t), CI_j(t)]$ and (b) correlation coefficient among the relative corrosion progresses $\rho[\Delta_i(t), \Delta_j(t)]$ of two deck plate elements i and j as a function of time t and degree of dependence among element corrosion behavior.
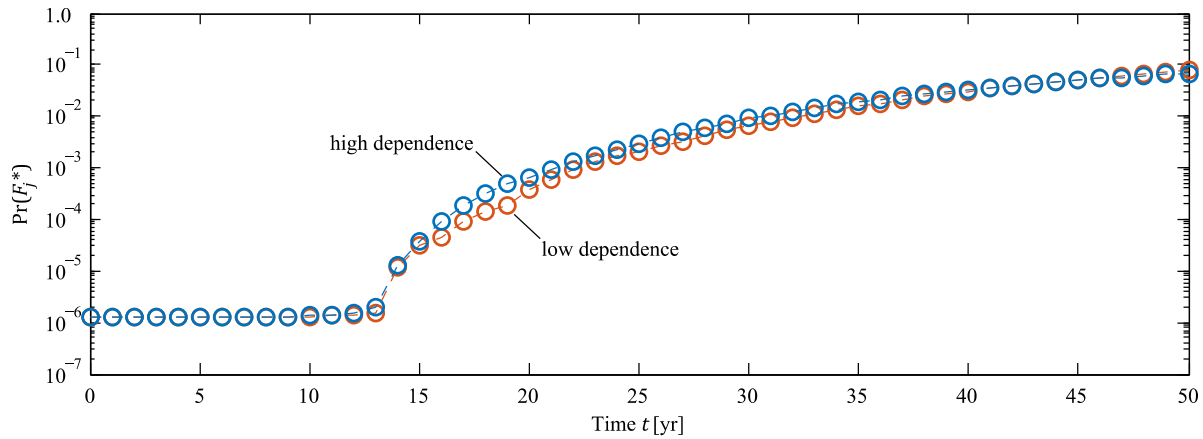
Figure 6.25: Prior interval failure probability $\Pr(F_j^*)$ of the box girder as a function of the degree of dependence among element corrosion behavior.

limit. Thereafter, the system failure probability increases noticeably because deterioration increasingly influences the reliability of the structural system.

The results in Figure 6.25 show that the degree of dependence among element deterioration behavior has little influence on the prior estimate of the interval failure probability indicating that box girder has limited redundancy. As demonstrated by Straub and Der Kiureghian (2011), correlation among element deterioration has less effect on the reliability of structural systems with limited or no redundancy.

Note that the computed interval failure probabilities below approximately 10^{-4} have a low accuracy with the applied importance sampling scheme. The interval failure probability is approximated following Equation (6.32) based on 10^5 weighted samples of the system condition. Whereas the computation of $\Pr(F_j^* | \mathbf{D}_j = \mathbf{d}_j)$ is exact within the confines of the applied model, the sampling approach cannot accurately represent extreme deterioration states that might influence the reliability at the beginning of the service life. Nevertheless, this error is not critical, because the interest is typically in the higher failure probabilities occurring later during the service life. Furthermore, the lower limit of the interval failure probability, which corresponds to the interval failure probability of the undamaged box girder, is exact within the confines of the applied model.
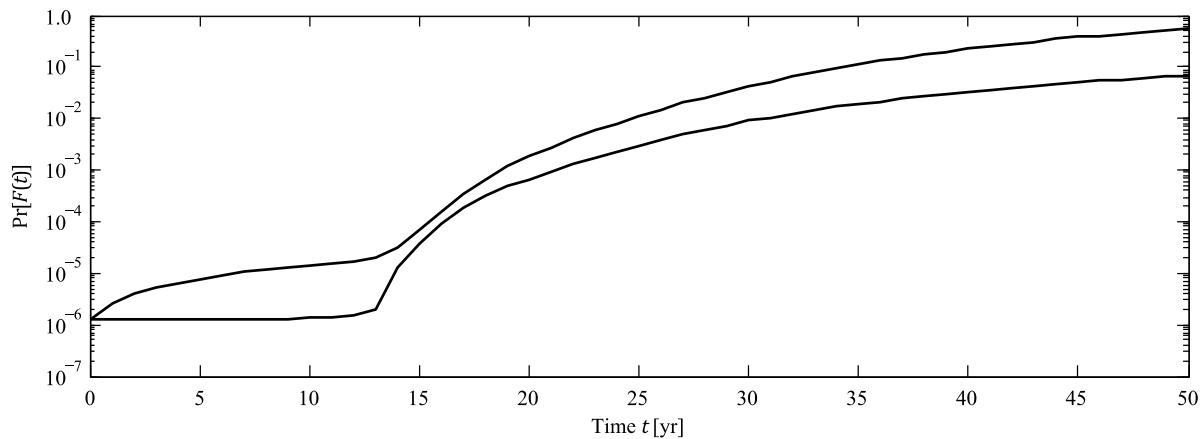
Figure 6.26: Bounds on the prior failure probability $\Pr[F(t)]$ of the box girder with high dependence among element deterioration.

Figure 6.26 shows the bounds on the failure probability $\Pr[F(t)]$ of the box girder with high dependence among element deterioration, which are computed following Equation (4.20). The bounds on the failure probability of the box girder with low dependence among element deterioration are similar because the interval failure probabilities $\Pr(F_j^*)$ are similar in both dependence cases (see Figure 6.25).

6.5.4 Posterior reliability analysis

A 20 m long section of the deck plate between $x = 210$ m and $x = 230$ m as indicated in Figure 6.27 is inspected in year 25 using half-cell potential measurements.

To model the quality of half-cell potential measurements, the probability of indication given that reinforcement corrosion has started is defined as $PoI(ci_j = 1) = 0.9$ and the probability of indication given that the reinforcement is still passive is chosen as $PoI(ci_j = 0) = 0.29$ (see also Faber and Sørensen 2002). For the numerical evaluations shown in this section, the measurements are assumed to result in no indication of corrosion initiation for each inspected element.

Posterior probabilities of the element conditions and the posterior interval failure probabilities of the box girder are computed from 10^5 weighted samples of the system condition as described in Section 6.4.2. Figure 6.28 shows the posterior probabilities of corrosion initiation $\Pr[CI_i(t) = 1|\mathbf{Z}_{0:t} = \mathbf{z}_{0:t}]$ for all deck plate, web and bottom flange elements. At any time t, the probability of corrosion initiation is shown conditional on all inspection outcomes available up time t. This process is known as filtering (see also Section 4.5). The corrosion probability of the inspected deck plate elements reduces after the inspection due to the positive inspection result. The inspection
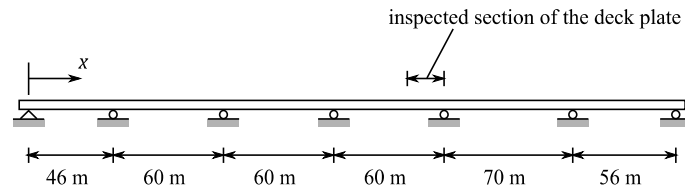
Figure 6.27: Inspected section of the deck plate between $x = 210$ m and $x = 230$ m.

Figure 6.28: Posterior probability of corrosion initiation $\Pr[CI_i(t) = 1|Z_{0:t} = z_{0:t}]$ for all deck plate elements, and web and bottom flange elements as a function of different degrees of dependence among element corrosion behavior. A 20 m long section of the deck plate between $x = 210$ m and $x = 230$ m is inspected using half-cell potential measurements at time $t = 25$ year. No corrosion is indicated. At any time t, the probability of corrosion initiation is shown conditional on all information available up time t (filtering).
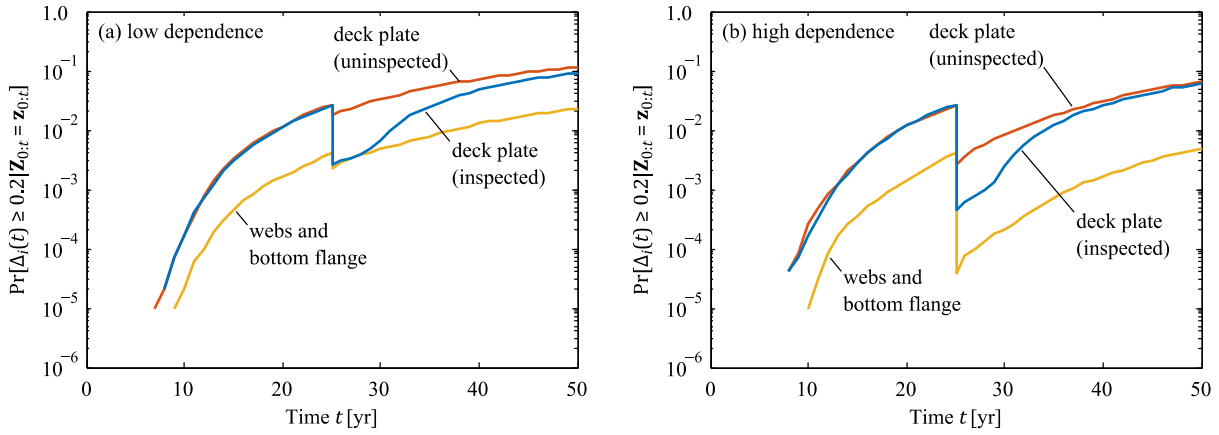
Figure 6.29: Posterior probability that the relative corrosion progress $\Delta_i(t)$ in the deck plate elements, and web and bottom flange elements exceeds 0.2, i.e. $\Pr[\Delta_i(t) \geq 0.2 | \mathbf{Z}_{0:t} = \mathbf{z}_{0:t}]$. The probability is presented as a function of different degrees of dependence among element corrosion behavior. A 20 m long section of the deck plate between $x = 210$ m and $x = 230$ m is inspected using half-cell potential measurements at time $t = 25$ year. No corrosion initiation is detected. At any time t, the probability of the event $\Delta_i(t) \geq 0.2$ is shown conditional on all information available up time t (filtering).

outcome has also a positive effect on the corrosion probabilities of the uninspected elements. This effect is larger when the degree of dependence among element corrosion behavior is high.

Figure 6.29 shows the posterior probability that the relative corrosion progress $\Delta_i(t)$ in the deck plate elements, and web and bottom flange elements exceeds 0.2. The results confirm that the indirect effect of the inspection results on the condition of the uninspected elements increases with increasing correlation among element deterioration behavior.

The posterior interval failure probabilities $\Pr(F_j^* | \mathbf{Z}_{0:m} = \mathbf{z}_{0:m})$ of the box girder are shown in Figure 6.30 as a function of the degree of dependence among element deterioration. For any interval j, the interval failure probability is shown conditional on all inspection results available up to the end of the structure's service life. This corresponds to smoothing (see also Sections 6.2.4 and 6.4.2). The interval failure probabilities reduce due to the positive inspection result. As expected, the effect is larger when the dependence among element deterioration is high.

Figure 6.31 shows the bounds on the posterior failure probability $\Pr[F(t) | \mathbf{Z}_{0:t} = \mathbf{z}_{0:t}]$ of the box girder in function of the level of dependence among element corrosion behavior. They are computed by substituting the prior interval failure probabilities $\Pr(F_j^*)$ in Equation (4.20) with the posterior interval failure probabilities $\Pr(F_j^* | \mathbf{Z}_{0:m} = \mathbf{z}_{0:m})$. At any time t, the bounds on the failure probability are shown conditional on the information available up to time t (filtering). The influence of the positive inspection result and the degree of dependence among element deterioration is evident.
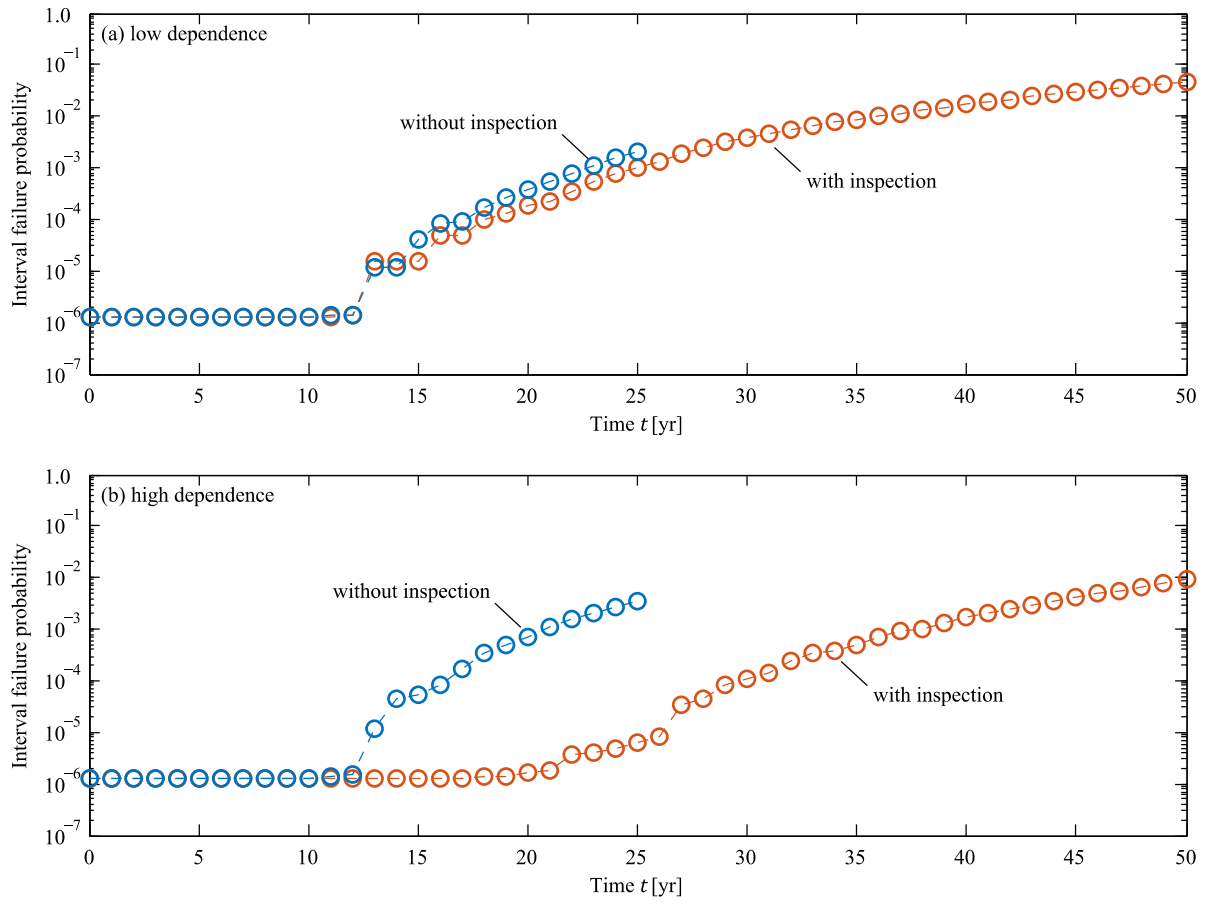
Figure 6.30: Interval failure probability of the box girder with and without inspection. The probability is shown as a function of different degrees of dependence among element corrosion behavior.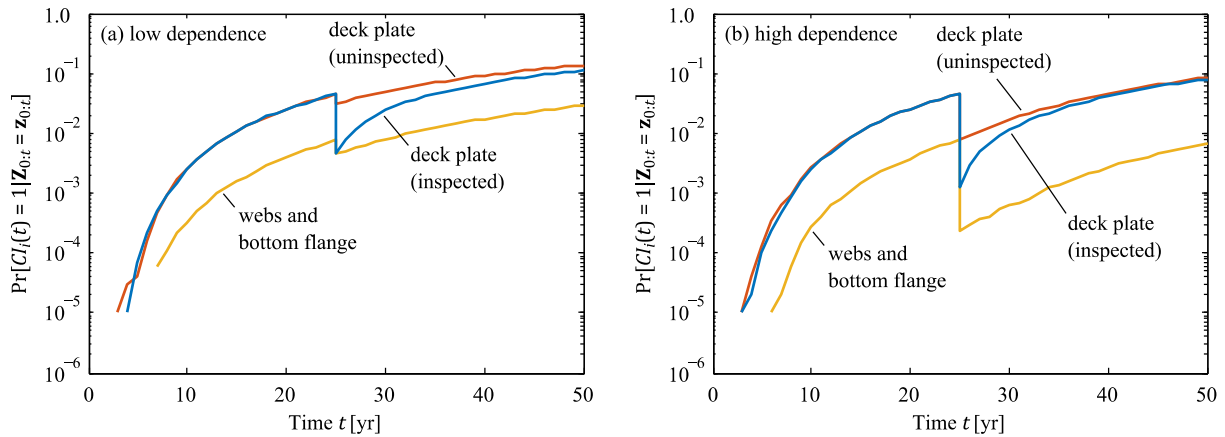 A 20 m long section of the deck plate between $x = 210$ m and $x = 230$ m is inspected using half-cell potential measurements at time $t = 25$ years. No corrosion initiation is detected. For any interval j, the posterior interval failure probability is shown conditional on all information available up the end of the service life (smoothing).
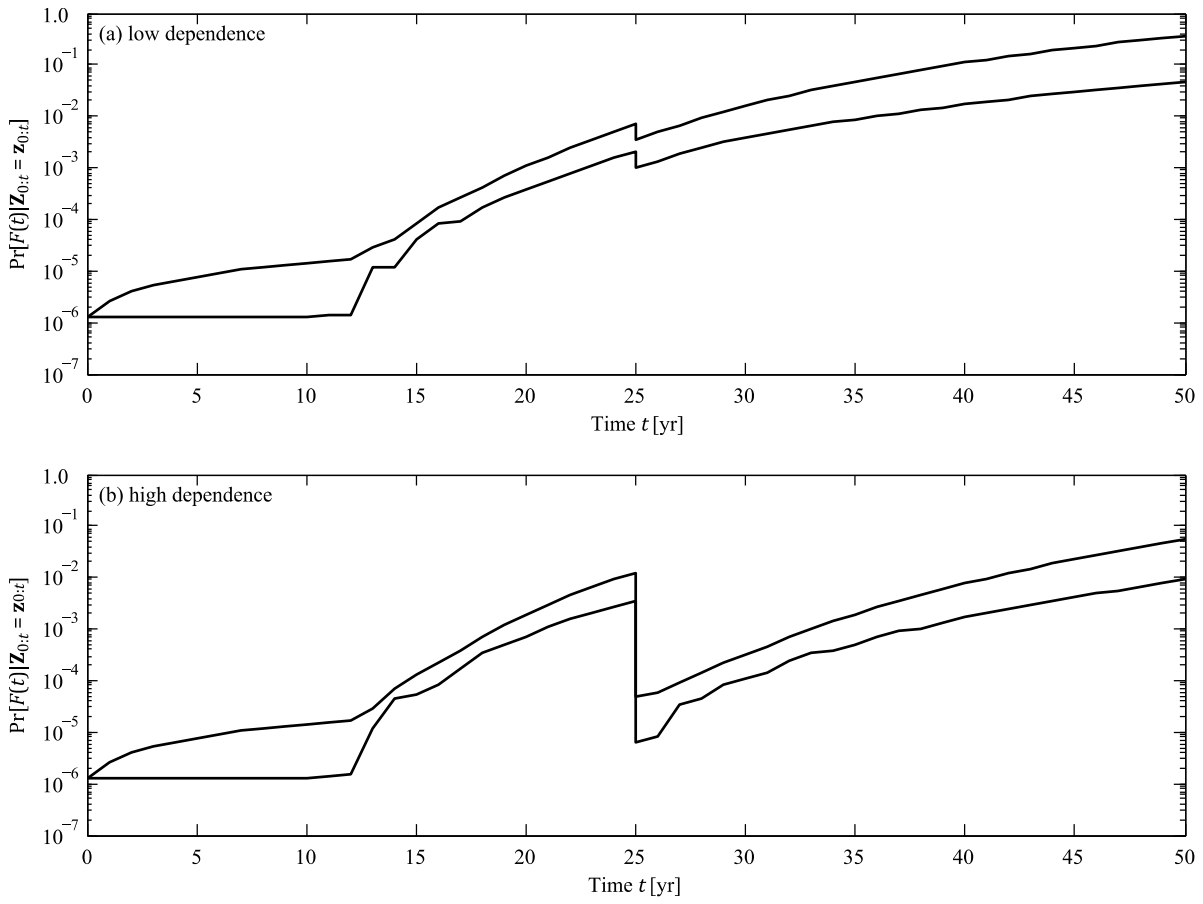
Figure 6.31: Bounds on the posterior system failure probability $\Pr[F(t)|\mathbf{Z}_{0:t} = \mathbf{z}_{0:t}]$ of the box girder as a function of different degrees of dependence among element corrosion behavior. A 20 m long section of the deck plate between $x = 210$ m and $x = 230$ m is inspected using half-cell potential measurements at time $t = 25$ years. No corrosion is indicated. At any time t, the bounds are shown conditional on all information available up to time t (filtering).

7 Discussion

7.1 General

Structural reliability analysis is the most systematic and consistent approach to analyze the condition and performance of deteriorating structural systems for which inspection and monitoring data are available. The application of this approach hinges upon the availability of (a) stochastic system deterioration models, (b) structural system reliability models, (c) models of inspection and monitoring, and (f) robust and efficient computational procedures. Stochastic deterioration models are only available for a few common phenomena including fatigue crack propagation in metallic structures (e.g. Lin and Yang 1985; Madsen 1997) and reinforcement corrosion in concrete structures (e.g. DuraCrete 1998; Stewart and Rosowsky 1998a). In general, predictions of deterioration based on quantitative models are associated with large uncertainties as they are only simplified representations of the actual phenomena and often do not include all relevant influencing parameters. In addition, the parameters influencing deterioration are subject to variability and generally there is only limited data available on those parameters. Bayesian methods can, however, be applied to improve and develop new deterioration models based on in-service inspection and monitoring data (e.g. Tran et al. 2016; Luque et al. 2017).

In addition, structures are typically subject to several deterioration processes at the same time. Modeling the interaction among different deterioration processes is an additional challenge. Only a limited number of cases exist, in which the interaction between different deterioration processes can be captured. For example, the effect of pitting corrosion on the fatigue behavior of aluminum structures can be quantified (e.g. Harlow and Wei 1994). Models are also available to describe the coupled effect of carbonation and chloride penetration on the condition of reinforced concrete structures (e.g. Hackl and Köhler 2016).

Deterioration in structural systems is typically modeled at the structural element level. Thus, models of the structural systems are required to assess the effect of deteriorating element capacities on the structural reliability. An overview on available structural system reliability models can be found in (Shao and Murotsu 1999). Because of their complexity, existing models are rarely applied in practice. With advances in computer capacities, it will be increasingly feasible to couple standard finite element codes with structural reliability methods as the basis for assessing the reliability of deteriorating structural systems (e.g. Sudret and Der Kiureghian 2000; Papaioannou 2013).

Deterioration processes at different locations in a structure are dependent because of spatial variability and common influencing factors. This dependence reduces the reliability of redundant structural systems and determines how much information on the condition of the entire structure is obtained from a single observation or measurement. Spatial dependence of deterioration processes is typically modeled by introducing correlations among the parameters of the models describing deterioration of the structural elements. Hierarchical and random field models can be applied to describe these correlations. Since only a few studies on stochastic dependence among

deterioration effects can be found in the literature (e.g. Li et al. 2004; Vrouwenvelder 2004; Malioka 2009; Luque et al. 2017), the parameters of the spatial deterioration models generally have to be estimated based on engineering judgement. However, Bayesian methods can be applied to improve spatial deterioration models with in-service inspection and monitoring results (e.g. Luque et al. 2017).

Models of inspection and monitoring that provide information on the structural condition are highly developed in some areas. For example, performance models are available for various inspection methods used to detect fatigue cracks in steel structures (e.g. Visser 2002) and for half-cell potential measurements performed to detect corroding reinforcement in concrete structures (e.g. Lentz et al. 2002; Johnsen et al. 2003; Keßler 2015). In other areas, such models are still lacking or incomplete. This includes, for example, performance models for monitoring systems employed to identify damage in structures based on vibration response data. In this area, significant contributions have been made in the field of Bayesian structural system identification (e.g. Beck and Katafygiotis 1998; Beck 2010; Papadimitriou and Lombaert 2012; Au and Zhang 2016; Huang et al. 2017). One challenge here is to explicitly account for the influence of varying operational and environmental conditions on the performance of such systems (Sohn et al. 2004). In general, challenges associated with the modeling of inspection and monitoring are related to identifying a model that connects the observation or measurement with the quantity of interest, and modeling the dependence among the observations or measurements (Straub 2018b).

The above discussion highlights that challenges associated with the modeling of deteriorating structures, and inspection and monitoring remain. Additional challenges arise in computing the time-variant reliability of deteriorating structural systems. This thesis contributes to the development of robust and efficient approaches to solve these computational challenges.

7.2 Nested reliability analysis approach

Section 5 proposes a generic framework for (a) computing the failure probability $\Pr[F(t_j)]$ of deteriorating structures whose deteriorating capacity can be modeled as statistically independent of the demand, and (b) updating $\Pr[F(t_j)]$ with information on the structural condition. The framework can be applied when the performance of the structural system is described by the conditional interval failure probability given the structural condition, i.e. $\Pr(F_i^*|\mathbf{X}_R = \mathbf{x}_R)$. The proposed framework enables the application of state-of-the-art deterioration models to describe deterioration at the structural element level. It considers stochastic dependence among the parameters of the element deterioration models, and accounts for the relation between deterioration of the structural elements and failure of the structural system. As demonstrated in the numerical examples, the framework is particularly suitable for structural systems with discrete structural elements, whose deterioration state can be represented by a binary model (functioning/not functioning) at the system level (i.e. at the system level a structural element has either its full capacity prior to deterioration failure or it has completely lost its capacity because of deterioration failure).

Information on the structural condition is included in the reliability estimation through Bayesian updating of the deterioration models describing the condition of the different structural elements.

By modeling the dependence among deterioration effects at different locations in a structure, the condition of the entire system can be inferred from observations of the condition of parts of the system. The proposed framework can handle any type of information on the system condition if a corresponding likelihood function is formulated (i.e. a stochastic model connecting the observation to the stochastic deterioration model parameters). In particular, the framework can also include information from monitoring systems. For monitoring systems, which potentially provide a large amount of data, it might be beneficial to pre-process the data. In such a pre-processing step (e.g. a modal system identification), the probability of the observed data given a certain value of the model parameters is determined. This probability is the likelihood function that is inputted into Equations (5.20) and (5.21). Such an approach is similar to a two-stage Bayesian structural system identification (Au and Zhang 2016).

The problem of computing the failure probability conditional on inspection and monitoring data is formulated such that it can be solved with any structural reliability method. The resulting component reliability problems are here evaluated with subset simulation, which is computationally robust since it provides reasonably accurate results without a need for tailoring the algorithm to specific applications. It is also considerably more efficient than crude Monte Carlo simulation (Au and Beck 2001; Straub et al. 2016). In most cases, the modeling of deterioration in structural systems leads to many random variables. Subset simulation does not restrict the number of random variables that can be included in the analysis since it can handle high dimensional reliability problems. In addition, it is also flexible with regards to the dependence structure of the random variables defining the problem. It enables an implementation of a variety of models to represent their spatial and temporal dependence, including hierarchical and random field/process models.

In the numerical examples, the number of samples per subset level was chosen such that the results have reasonable accuracy. The accuracy can always be improved by increasing the number of samples per subset level. It is, however, important to highlight that the number of subsets increases with decreasing value of (a) the failure probability and (b) the probability of the observation event $Z(t)$. As shown in the numerical examples, the probability of the observation event $Z(t)$ reduces with the number of inspection and monitoring outcomes. In this case, the difference between the prior distribution of the model parameters and the likelihood increases. Simulating smaller probabilities requires more subsets and thus more model evaluations. The efficiency of the subset simulation in terms of the number of model evaluations is proportional to the logarithm of simulated probabilities (see also Section 2.2.3).

The current implementation of the proposed framework computes the failure probabilities $\Pr[F(t_j)]$ with separate subset simulation runs for different time t_j. The efficiency of this approach can be significantly improved by exploiting the fact that the failure event $F(t_{j-1})$ is a subset of the failure event $F(t_j)$, i.e. $F(t_{j-1}) \subseteq F(t_j)$ (Kim and Straub 2019; Straub et al. 2020). This implies that the following sequential procedure can be applied to compute $\Pr[F(t_j)]$ with subset simulation. First, the probability of failure up to the end of the last interval j, $\Pr[F(t_j)]$, is computed with subset simulation. Subsequently, the conditional failure probability $\Pr[F(t_{j-1})|F(t_j)]$ is estimated with a new subset simulation run, which starts with samples conditional on $F(t_j)$. These samples

are available from the final step in the estimation of $\Pr[F(t_j)]$ with subset simulation. The probability of failure up to time t_{j-1} is then computed as $\Pr[F(t_{j-1})] = \Pr[F(t_{j-1})|F(t_j)]\Pr[F(t_j)]$. The procedure is continued for $\Pr[F(t_{j-2})]$, $\Pr[F(t_{j-3})]$ and so on. Similarly, the posterior failure probabilities $\Pr[F(t_j)|Z(t_k)]$ can be computed with subset simulation in reverse chronological order following the estimation of $\Pr[Z(t_k)]$ (see also Section 5.6).

The proposed framework relies on the efficient computation of the conditional interval failure probability $\Pr(F_i^*|\mathbf{X}_R = \mathbf{x}_R)$. As demonstrated in the numerical example considering the Zayas frame, applications in which (a) the uncertainties in the permanent loads and time-invariant structural properties are negligible and (b) the number of distinct system deterioration states $\mathbf{D}_i = \mathbf{h}_D(\mathbf{X}_R, t_i)$ is limited, the conditional probability $\Pr(F_i^*|\mathbf{D}_i = \mathbf{d}_i)$ can be pre-computed. If the system reliability analysis is demanding, it might take some time to establish a data base with all values of $\Pr(F_i^*|\mathbf{D}_i = \mathbf{d}_i)$, but this is typically not critical, as this computation must be carried out only once and the data base can be used in all subsequent reliability calculations. In all remaining applications, $\Pr(F_i^*|\mathbf{X}_R = \mathbf{x}_R)$ must be computed on the fly. If such calculations are inexpensive, as demonstrated in the numerical example considering the Daniels system, the representation of the structural system performance by the conditional interval failure probability $\Pr(F_i^*|\mathbf{X}_R = \mathbf{x}_R)$ is still beneficial. In cases in which it is infeasible to compute $\Pr(F_i^*|\mathbf{X}_R = \mathbf{x}_R)$ on the fly, two possible strategies exist: (a) one can investigate the possibility of developing a response surface for $\Pr(F_i^*|\mathbf{X}_R = \mathbf{x}_R)$. Note, however, that many of the classical response surface techniques used in structural reliability will not be applicable since the system condition $\mathbf{D}_i$ is usually described by a discrete model. This is an area of future research. (b) Alternatively, the failure probability $\Pr[F(t_j)]$ can be computed by explicitly solving the series system problem $\Pr[F(t_j)] = \Pr(F_1^* \cup F_2^* \cup \ldots \cup F_j^*)$. An efficient solution to solving this problem is presented in Straub et al. (2020). It computes the interval failure probabilities $\Pr(F_i^*)$ in inverse chronological order using subset simulation, and subsequently evaluates the failure probability $\Pr[F(t_j)]$ based on a FORM approximation of the series system reliability problem. In this case, however, the advantages of the separating the computation of the system condition and the system reliability conditional on the system condition are lost.

The proposed procedure is here formulated and implemented to compute and update the probability of the failure event $F(t_j)$. It can, however, be extended to enable learning of the posterior distribution of the deterioration model parameters contained in $\mathbf{X}_R$ and the system condition $\mathbf{D}_i$ at the end of each interval i. Any property of the posterior distributions of $\mathbf{X}_R$ and $\mathbf{D}_i$ can be approximated by applying Monte Carlo techniques based on samples conditional on the observation event $Z(t)$. These samples are a by-product of estimating $\Pr[Z(t)]$ with subset simulation. This corresponds to an application of the BUS with subset simulation (see Section 3.3.4).

When applying the proposed framework, one should keep in mind that it introduces three approximations errors. The first approximation error is introduced in the definition of the interval failure probability $\Pr(F_i^*)$ in Equation (4.14) or (4.16). It depends on the choice of the time interval and on how well the time-dependent demands can be represented by time-invariant random variables (see also Straub et al. 2020). This error can be evaluated by considering the non-deteriorating structure. Note that the discrete-time approach presented in Section 4.3 is always conservative if

the structure is subject to only one time-variant load (Straub et al. 2020). The second approximation error is introduced in the computation of the conditional interval failure probability $\Pr(F_i^* | \mathbf{X}_R = \mathbf{x}_R)$ defined in Equation (5.8). The third approximation error is introduced in the evaluation of the reliability problems in Equations (5.13) and (5.22). The last two approximation errors are a function of the structural reliability method applied in the analysis (see also Section 2.2).

7.3 Dynamic Bayesian network approach

In Section 6, a generic DBN model for probabilistically representing deteriorating structural systems with separable demand and capacity parameters is presented, which is based on work published by Straub (2009) and Luque and Straub (2016). Deterioration is modeled at the structural element level and dependence among the parameters influencing the element conditions is described by defining a hierarchical structure. The model describing the correlated element conditions is coupled with a model of the structural system performance, which is defined conditional on the element conditions. In this way, the DBN model accounts for the dependence among the element conditions, and the relation among the element conditions and the structural system reliability. Combined with inference algorithms that exploit the conditional independence assumptions encoded in the DBN, the condition of the system elements and the system reliability can be assessed and updated with (partial) observations of the element conditions or the parameters influencing the element conditions. In addition, the DBN model visualizes the dependence among the random variables defining the problem. In this way, it facilitates the communication of the model to non-experts. This is an important feature that makes the DBN approach highly useful for practical applications.

The generic DBN presented in Section 6 enables the computation of the interval failure probabilities conditional on inspection and monitoring data. Based on the interval failure probabilities, an upper bound on the system failure probability is then found following Equations (4.20). The DBN can be adapted to directly compute system failure probability. To this end, links from nodes S_j to nodes S_{j+1} have to be introduced to capture the situation in which a structure is in the failed state at time t_{j+1} if it has failed at time t_j. However, the advantages of the hierarchical structure of the DBN described in Section 6.3 will be lost if these links are introduced. As discussed further below, the hierarchical structure enables the development of efficient exact inference algorithms.

This thesis focuses on applying the DBN approach in a numerical example considering a concrete box girder subject to chloride-induced reinforcement corrosion. In the numerical example, a DBN model describing initiation and propagation of the corrosion process is developed. The DBN model includes random variables to represent the outcome of half-cell potential measurements, which provide spatial information on corrosion initiation. Direct modeling of the structural system state, which is represented by a random variable S_j in the generic DBN model, is here not possible since the number of realizations of the system deterioration state $\mathbf{D}_j$ is too large to enable pre-computation of the conditional PMF $p(s_j | \mathbf{d}_j)$. To overcome this problem, probabilistic inference is here performed using likelihood weighting, which is a simple sampling-based inference algorithm. The

algorithm is applied to generate weighted samples of $\mathbf{D}_j$ based on the DBN model. Subsequently, these samples are applied to approximate the posterior distribution of $\mathbf{D}_j$ and the posterior probability of the interval failure event $F_j^* = \{S_j = 1\}$. The latter step includes the computation of the conditional interval failure probability $\Pr(F_j^*|\mathbf{D}_j = \mathbf{d}_j)$ for each generated sample of $\mathbf{D}_j$. This approach is computationally robust but inefficient for two reasons: (a) likelihood weighting is inefficient in simulating rare events and (b) its performance degrades considerably with increasing number of observations (Russell and Norvig 2010).

As an alternative[18], probabilistic inference can be performed using Gibbs sampling, which is a MCMC method that exploits the independence assumptions encoded in a BN (Russell and Norvig 2010). Nevertheless, MCMC methods are also sampling-based and their efficiency is a function of the number of observations included in the analysis as well as the value of the event probabilities of interest. In addition, MCMC algorithms do not necessarily converge, and the convergence of the results must always be carefully checked. In contrast, exact inference in discrete DBN does not suffer from these limitations, and, consequently, it is a promising strategy for performing probabilistic inference in BN. Motivated by this, Luque and Straub (2016) developed an exact inference algorithm tailored to evaluating the hierarchical DBN of deteriorating structural systems presented in Section 6.3. They show that the proposed exact inference algorithm is orders of magnitude faster in evaluating the system deterioration model than standard MCMC algorithms. Most importantly, its performance does not depend on the number of observations included in the analysis. However, Luque and Straub (2016) found that the evaluation of the posterior distribution of the system state S_j quickly becomes intractable as the number of elements grows. They discuss three options to overcome this problem: (a) in some applications, a more efficient representation of the relationship between system and element conditions than the converging connection at node S_j can be identified (see also Bensi et al. 2013). (b) Approximate system models may be applied that require as input only the marginal effect of element failure on the system failure probability (Straub and Der Kiureghian 2011). (c) The exact inference algorithm may be combined with sampling-based algorithms. In this case, the posterior distribution of the element deterioration states may be determined using the exact inference algorithm. Subsequently, samples of the correlated element deterioration states may be generated from their posterior distribution to estimate the system failure probability. This is an area of future research.

While discrete DBN with exact inference algorithms can be powerful, their implementation is rather demanding. Firstly, the identification and implementation of an efficient discretization scheme increases the pre-processing effort (see, for example, Neil et al. 2007; Zwirglmaier and Straub 2016). Secondly, the number of random variables that can be included in the model is limited when considering exact inference (Luque and Straub 2016). However, it is generally possible to reduce the number of random variables by a-priori identifying the most influential variables, but this process also increases the pre-processing effort. As noted by Luque and Straub (2016), the increased pre-processing effort is justified if the model is applied to perform repetitive computations to solve optimization problems such as planning of inspections, monitoring and maintenance activities

---

[18] Note that Zwirglmaier et al. (2017) recently introduced a subset simulation strategy for BN to enhance sampling-based inference of rare event probabilities in BN.

within the framework of pre-posterior analysis from classical Bayesian decision theory (see also Luque and Straub 2019).

Stochastic dependence among element deterioration is included in the DBN model by applying a hierarchical approach. While the hierarchical structure of the DBN model enables the development of efficient exact inference algorithms (see Luque and Straub 2016), it imposes restrictions on the dependence structure. This represents a limitation, which is not critical, because dependence among element deterioration is, in most applications, caused by common influencing factors, which can be represented by hierarchical models (see also Sections 5.2.2 and 6.3.2).

An important outcome of the numerical example is a software prototype implementing the model of the deteriorating box girder presented in Section 6.5.1. The prototype consists of a graphical user interface (front end) and a computational engine (back end), and can be applied to assess the reliability of the box girder and update it with outcomes of half-cell potential measurements. The prototype is computationally robust since it does not require input from an expert in structural reliability analysis to perform reliability updating of the aging box girder. It is, thus, a first step towards developing a software tool that can be used by engineering practitioners to perform reliability assessments of deteriorating concrete bridges and update their reliability with inspection and monitoring results.

7.4 Numerical results

As expected, the numerical results in this thesis confirm that deterioration reduces the reliability of structural systems. The results additionally demonstrate the importance of considering the dependence among deterioration effects at different locations in the structure when evaluating the reliability of redundant structures. The effect of dependence is stronger as the system redundancy increases (from the box girder to the Daniels system). Neglecting dependence among element capacities can thus result in a (substantial) underestimation of the failure probability of redundant structural systems and, consequently, of the risk associated with operating such systems (see also Gollwitzer and Rackwitz 1990). The numerical example considering the box girder also shows that the correlation among element deterioration is a function of time. As expected, this correlation strongly depends on the degree of correlation among the parameters influencing the condition of the structural elements.

The numerical examples considering the Zayas frame and the box girder show that dependence among element deterioration enables learning of the condition of all system elements from inspecting a subset of the elements (i.e. the condition of non-inspected elements can be inferred from samples taken at selected locations). The largest learning effect is achieved if elements with large uncertainty in their condition and thus high probability of deterioration failure are inspected (Straub and Faber 2005). In addition, the example considering the Zayas frame shows that an inspection of an element with a large single element importance measure has a larger impact on the system reliability than an inspection of an element with a small single element importance measure. Based on this, Bismut et al. (2017) propose a prioritization index as a function of the probability of element deterioration failure and the single element importance measure to select elements

for inspection. In principle, elements can be selected for inspection according to the value of information (VoI) of the inspections. The VoI of an inspection quantifies its benefit prior to performing it (Raiffa and Schlaifer 1961; Straub and Faber 2005). Exact computation of the VoI of an inspection is challenging. Therefore, proxies that provide a similar ranking as the VoI such as the prioritization index introduced by Bismut et al. (2017) are applied in a recently proposed heuristic approach to optimizing inspections at the structural system level (Luque and Straub 2019).

The numerical example considering the (highly redundant) Daniels system demonstrates – at least conceptually – how information on the system condition obtained from a global damage detection system can be integrated into a system reliability analysis. The example applies a hypothetical probability of indication model to describe the monitoring system's ability to detect structural damage. The results clearly show that the monitoring information has only a small effect on the reliability estimates for the Daniels system with low dependence among element deterioration. In this situation, there is little benefit in applying such a monitoring system. Again, the value of information analysis from classical Bayesian decision theory can be utilized to quantify the benefit of a monitoring system prior to installing it (Pozzi and Der Kiureghian 2011; Thöns and Faber 2013; Straub et al. 2017; Thöns 2018).

8 Concluding remarks and outlook

8.1 Concluding remarks

Structural reliability analysis is a consistent approach to assess deteriorating structures. In structural reliability, a physics-based engineering model consisting of deterioration and structural models is combined with a probabilistic model of the input parameters to account for the relevant uncertainties. Based on the probabilistic engineering model, an initial prediction of the structural condition and reliability is made. On many structures, inspection and monitoring are employed to reduce the uncertainty on the structural condition. In a probabilistic setting, the information contained in the inspection and monitoring data can be consistently integrated in the prediction of the system's condition and reliability using Bayesian analysis.

The reliability of deteriorating structures should be analyzed at the structural system level to account for (a) the effect of deterioration at different structural elements on the system reliability, and (b) the influence of inspection and monitoring data on the system reliability. The correlation among the deterioration states of different structural elements must be properly modeled since it reduces the reliability of redundant structural systems and has an effect on what can be learned from inspecting and monitoring individual elements.

The reliability analysis of deteriorating structural systems requires the solution of time-variant reliability problems. Solving such problems is challenging. However, as discussed in Section 4.3, the time-variant reliability problem can be approximated through a series of time-invariant reliability problems if the deteriorating structural system can be described by a stochastic model with separable demand and capacity parameters. In most applications, this assumption holds at least approximately. The reliability analysis based on the simplified formulation of the problem is still computationally demanding since the reliability has to be computed at multiple points in time. In addition, the analysis has to be repeated from the beginning of the structure's service life each time new information on the structural system becomes available.

This thesis explores two novel solution strategies for computing the time-variant reliability of deteriorating structural systems conditional on inspection and monitoring data. Both strategies are based on the transformation of the time-variant reliability problem into a series of time-invariant reliability problems. Firstly, the problem is formulated as a nested reliability problem in which the computation of the system condition is separated from the computation of the system reliability conditional on the system condition. This approach is termed nested reliability analysis (NRA) approach. Secondly, hierarchical dynamic Bayesian networks (DBN) are employed to probabilistically represent deteriorating structural systems. The DBN can be evaluated with inference algorithms that exploit the conditional independence assumptions encoded in the DBN. This approach is termed DBN approach.

Both approaches describe deterioration at the structural element level and thus enable the implementation of state-of-the-art deterioration models. Stochastic dependence among deterioration states of different elements is modeled by introducing correlations among the parameters of the deterioration models. To account for the relation between deterioration of structural elements and the structural system reliability, the model describing the condition of the structure is coupled with a stochastic structural model, which describes the system performance by the conditional probability of structural system failure given the condition of the structure. Based on the coupled deterioration and structural model, the time-variant reliability of deteriorating structural systems is estimated. Information on the structural condition provided by inspection and monitoring is included in the reliability analysis through Bayesian updating of the element deterioration models. Any type of information on the structural condition can be included if the corresponding likelihood function is available.

The NRA approach has the advantage that it can be implemented with established structural reliability methods (SRM) that work in high dimensions. In this thesis, it is implemented with subset simulation, which is a robust and efficient sampling-based SRM. The NRA approach with subset simulation does not restrict the number of random variables that can be included in the analysis and enables an implementation of a variety of correlation models to represent their spatial and temporal dependence. Nevertheless, it is still sampling-based. Its efficiency is hence a function of the number of inspection and monitoring outcomes, as well as the value of the simulated event probabilities.

Representing deteriorating structural systems with DBN has the advantage that problem can be visualized and communicated to stakeholders who are not experts in structural reliability analysis. In addition, a DBN enables the application of exact and approximate inference algorithms to perform Bayesian analysis of deteriorating structural systems. In this thesis, probabilistic inference is performed with likelihood weighting, which is a simple sampling-based inference algorithm. The DBN approach with likelihood weighting is computationally robust, and – as a proof of concept – it is implemented in a software prototype that can be used by engineers who are not experts in structural reliability analysis to assess the reliability of a corroding concrete box girder conditional on half-cell potential measurements. Nonetheless, likelihood weighting is inefficient as its performance rapidly degrades with increasing number of observations and/or decreasing value of the event probabilities of interest. In future applications, the exact inference algorithm proposed by Luque and Straub (2016) may be applied to evaluate the DBN of deteriorating structures. This algorithm exploits the hierarchical structure of the DBN and is computationally efficient and robust. Its performance does neither depend on the number of observations included in the analysis nor on the magnitude of the event probabilities to be calculated. Nevertheless, the algorithm imposes restrictions on the dependence structure and the number of random variables that can be included in the model. An additional limitation of the exact inference algorithm is the increased pre-processing effort since an efficient discretization scheme must be identified and implemented before the algorithm can be applied. The increased modeling effort is, however, justified when the model is applied to perform repetitive computations to solve optimization problems such as planning of inspections, monitoring and maintenance.

8.2 Outlook

8.2.1 Modeling and computational challenges

Some challenges associated with the computation the time-variant reliability of deteriorating structural systems conditional on information provided by inspection and monitoring data are addressed in this thesis. However, numerous open issues remain. In the following, some potential areas for future research are presented.

Dependence among deterioration processes at different locations in structural systems has a significant influence on the reliability of redundant structural systems and is relevant when determining the required inspection and monitoring coverage and times. Such dependencies exist due variability and common influencing factors. Hierarchical and random field models are available to represent spatial dependence among these influencing parameters (see Section 5.2.2). The effect of different model choices should be systematically studied. In addition, further research should be conducted to learn the parameters of such dependence models from experiments and in-service data. Finally, recommendations for engineering practice should be derived.

More and more deteriorating structures are equipped with monitoring systems that continuously capture static and dynamic response data. Methods of Bayesian system identification are a foundation to determine the probability of the measured data conditional on the structural condition (e.g. Zhang and Au 2016; Huang et al. 2017), i.e. the likelihood function of the monitoring data. This likelihood function describes the performance of the monitoring system and is required to include the data in the system reliability analysis (see also Section 5.7.2). One challenge is to consider the effect of varying operational and environmental conditions in the modeling of the performance of such monitoring systems (e.g. Behmanesh and Moaveni 2016; Simon et al. 2020; Simon et al. 2021). This is an area of future research.

The exact inference algorithm for evaluating the DBN model of deteriorating structures proposed by Luque and Straub (2016) is efficient and robust. In most applications, direct modeling of the structural system state is, however, not possible, because the number of different system configurations is typically too large (see also Section 6.4.2). Recently, Zwirglmaier et al. (2017) have proposed a novel sampling-based inference algorithm suitable for estimating rare event probabilities with BN. The algorithm employs a subset simulation strategy. Future research could explore the possibility of coupling this algorithm with the exact inference algorithm proposed by Luque and Straub (2016) to update the structural system condition.

8.2.2 Risk-based planning of operation and maintenance

Apart from addressing the remaining modeling and computational challenges related to the reliability analysis of deteriorating structural systems, future research should also continue to develop methods for optimizing operation and maintenance strategies for deteriorating structural systems.

Over the past 40 years, substantial efforts were made towards developing risk-based methods for optimizing inspection and repair strategies for deteriorating structural systems (e.g. Thoft-Christensen and Sørensen 1987; Madsen et al. 1989; Sørensen and Faber 1991; Straub and Faber 2005). Risk-based inspection planning identifies the inspection and repair strategy that minimizes

the expected total service life cost consisting of (a) the expected service life cost of inspections and repairs and (b) the service life cost associate with structural failure (risk). In risk-based inspection planning, structural reliability analysis is mainly applied to compute the probability of structural failure over the service life conditional on potential inspection outcomes, which is required in the estimation of the service life risk (see also Section 4.1).

The inspection planning problem is a special instance of a sequential decision problem under uncertainty, because decisions on inspections and repairs are made at multiple points in time, at which different amounts of information are available (Raiffa and Schlaifer 1961; Russell and Norvig 2010; Kochenderfer 2015). Each decision on performing new inspections and repairs must consider all past and all potential future observations and decisions. The complexity of the problem grows exponentially with the number of decision times and the number of system elements . In the past, a heuristic approach has been successfully applied to derive practical solutions to the problem at the structural element level (Faber et al. 2000; Straub 2004; Nielsen and Sørensen 2011). In this approach, inspections are planned, and repairs are performed based on parameterized decision rules. As an example, an element is inspected at fixed intervals and repaired when the measured size of an indicated defect exceeds a threshold. In this case, the optimization reduces to finding the combination of the inspection interval and repair threshold that minimizes the expected total service life cost.

Recently, Luque and Straub (2019), Bismut et al. (2017), Bismut and Straub (2018) and Schneider et al. (2018) have extended the heuristic approach to optimize inspection and repair strategies at the structural system level. They also define strategies at the system level in terms of parameterized decision rules which deterministically prescribe when, what and how to inspect and repair conditional on all available information at the different decision times. In this way, the search space of possible strategies is reduced. For each defined strategy, the expected total service life cost is computed using Monte Carlo simulation based on sampled inspection and repair histories. The strategy that minimizes the expected total service life cost is the optimal one in the set of pre-selected strategies.

Within the Monte Carlo simulation, the probability of system failure over the service life must be computed many times for different potential inspection and repair histories. This is a challenging problem as discussed in this thesis. Luque and Straub (2019), Bismut et al. (2017) and Bismut and Straub (2018) apply the DBN approach with the exact inference algorithm described in (Luque and Straub 2016) for this task. Schneider et al. (2018) and Schneider (2019) perform these computations using the NRA approach with subset simulation described in Section 5.

The proposed methodology is a pragmatic and efficient solution to risk-based planning of inspection and repair at the structural system level and has significant potential to enhance the management of deteriorating structures. It accounts for the dependence among all system elements, the relation between element deterioration and system failure, and the effect of partial inspections on the system reliability. It is relatively easy to communicate this approach to stakeholders who are not experts in risk-based planning of operation and maintenance. The heuristics can incorporate various operational constraints. In this way, impractical strategies can be excluded from the set of

possible strategies. Note that the strategy identified with this method is not necessarily the global optimum, but it can be easily compared to any other strategy proposed as an alternative.

To demonstrate the benefit of risk-based planning of operation and maintenance at the structural system level, future research should focus on applying the proposed methodology to real structural systems. The heuristics can be adapted to include the experience and preferences of asset owners and operators. Furthermore, it would be highly valuable to consider applications involving global damage detection systems. Such an application requires explicit modeling of the performance of such monitoring systems and rules that guide decisions based on the potential monitoring outcomes. This would ultimately facilitate an evaluation of the value of information (VoI) of global damage detection systems, in which the expected total service life cost with and without monitoring system are compared (Pozzi and Der Kiureghian 2011; Thöns and Faber 2013; Straub et al. 2017; Thöns 2018).

A Markov chain Monte Carlo sampling for subset simulation

A.1 Markov chains

Consider a sequence of random vectors $\mathbf{U}_1, \mathbf{U}_2, \dots, \mathbf{U}_T$ of arbitrary length T. Such a sequence forms a Markov chain if its joint PDF $p(\mathbf{u}_1, \mathbf{u}_2, \dots, \mathbf{u}_T)$ can be written in the following factorized form:

$$p(\mathbf{u}_1, \mathbf{u}_2, \dots, \mathbf{u}_T) = p(\mathbf{u}_1)p(\mathbf{u}_2|\mathbf{u}_1) \dots p(\mathbf{u}_T|\mathbf{u}_{T-1}) = p(\mathbf{u}_1) \prod_{t=2}^{T} p(\mathbf{u}_t|\mathbf{u}_{t-1}) \qquad \text{(A.1)}$$

Equation (A.1) implies the Markov assumption according to which $\mathbf{U}_t$ is conditionally independent of all other predecessors $\mathbf{U}_1, \dots, \mathbf{U}_{t-2}$ given its direct predecessor $\mathbf{U}_{t-1}$. The marginal PDF of $\mathbf{U}_t$ can be written as:

$$p(\mathbf{u}_t) = \int_{\mathbf{U}_{t-1}} p(\mathbf{u}_t|\mathbf{u}_{t-1})\, p(\mathbf{u}_{t-1})\, \mathrm{d}\mathbf{u}_{t-1} \qquad \text{(A.2)}$$

where $p(\mathbf{u}_{t-1})$ is the marginal PDF of $\mathbf{U}_{t-1}$. The conditional PDF $p(\mathbf{u}_t|\mathbf{u}_{t-1})$ is the transition PDF of the Markov chain representing the probability of moving from $\mathbf{u}_{t-1}$ to any state in the state space of $\mathbf{U}_t$. A Markov chain is homogeneous if the transition PDF $p(\mathbf{u}_t|\mathbf{u}_{t-1})$ is independent of t, i.e. $p(\mathbf{u}_{t+1}|\mathbf{u}_t) = p(\mathbf{u}_t|\mathbf{u}_{t-1})$ for all $t = 2, \dots, T-1$. Provided that a homogenous Markov chain is irreducible and aperiodic, the marginal PDF of $\mathbf{U}_t$ will asymptotically converge to a unique stationary PDF, denoted by $\pi(\mathbf{u})$, as $t \to \infty$ (see, for example, Tierney 1994), which satisfies:

$$\pi(\mathbf{u}_t) = \int_{\mathbf{U}_{t-1}} p(\mathbf{u}_t|\mathbf{u}_{t-1})\, \pi(\mathbf{u}_{t-1})\, \mathrm{d}\mathbf{u}_{t-1} \qquad \text{(A.3)}$$

Irreducibility and aperiodicity are relatively general regularity conditions. Irreducibility is fulfilled if, for any initial state $\mathbf{u}_1$, there is a non-zero probability of reaching any set of the chain's state space in a finite number of steps, and aperiodicity is satisfied if there is a non-zero probability that the chain will remain at the same state (see, for example, Tierney 1994). A Markov chain that has a unique stationary PDF is called ergodic.

A.2 MCMC sampling for subset simulation

Markov chain Monte Carlo (MCMC) sampling algorithms simulate states of an ergodic Markov chain, which has the target distribution, from which samples are desired, as its unique stationary distribution. The simulation process is generally started at an arbitrary vector $\mathbf{u}_1$. New samples are then generated by successively simulating the transition of the Markov chain from its current state

$\mathbf{u}_t$ to its next state $\mathbf{u}_{t+1}$. The number of iterations that are required until the marginal distribution of the constructed Markov chain is sufficiently close to its unique stationary distribution is called the burn-in period. The samples generated following the burn-in period are identically distributed according to the desired target distribution. They are, however, correlated since each sample depends directly on its predecessor.

As described in Section 2.2.3, subset simulation applies MCMC sampling at subset levels $i = 2, \ldots, M$ to generate samples from $\varphi_n(\mathbf{u}|E_{i-1})$ by simulating states of Markov chains starting from the samples conditional on the event E_{i-2} for which $G(\mathbf{u}) \leq b_{i-1}$. Therefore, the starting vectors or seeds of the Markov chains are already distributed according to the desired target distribution $\varphi_n(\mathbf{u}|E_{i-1})$ and in the context of subset simulation the Markov chains do not require a burn-in period to reach their stationary state (see also Au et al. 2012).

The main component of MCMC sampling algorithms is the transition of the Markov chain from its current state $\mathbf{u}_t$ to its next state $\mathbf{u}_{t+1}$. A standard implementation of this transition is the Metropolis-Hastings algorithm (Metropolis et al. 1953; Hastings 1970). To sample from $\varphi_n(\mathbf{u}|E_{i-1})$, this algorithm performs the transition in two steps. If the current state of the Markov chain is $\mathbf{u}_t$, a candidate state $\mathbf{u}'$ is sampled from an arbitrary proposal distribution $q(\mathbf{u}'|\mathbf{u}_t)$, which is an n-dimensional PDF dependent on $\mathbf{u}_t$. This candidate is accepted with a certain acceptance probability $a(\mathbf{u}_t, \mathbf{u}')$ and the chain moves to $\mathbf{u}_{t+1} = \mathbf{u}'$. If the candidate state $\mathbf{u}'$ is rejected, the chain remains at $\mathbf{u}_{t+1} = \mathbf{u}_t$. The acceptance probability $a(\mathbf{u}_t, \mathbf{u}')$ is defined as:

$$a(\mathbf{u}_t, \mathbf{u}') = \min\left\{1, \frac{\varphi_n(\mathbf{u}'|E_{i-1})}{\varphi_n(\mathbf{u}_t|E_{i-1})} \frac{q(\mathbf{u}_t|\mathbf{u}')}{q(\mathbf{u}'|\mathbf{u}_t)}\right\} \tag{A.4}$$

Hastings (1970) and Tierney (1994) show that this transition procedure leaves the target distribution $\varphi_n(\mathbf{u}|E_{i-1})$ invariant independent of the choice of the proposal distribution, i.e. if $\mathbf{u}_t$ is distributed according to $\varphi_n(\mathbf{u}|E_{i-1})$ then $\mathbf{u}_{t+1}$ is distributed according to $\varphi_n(\mathbf{u}|E_{i-1})$. This property of the Metropolis-Hastings algorithm ensures that $\varphi_n(\mathbf{u}|E_{i-1})$ is the unique stationary PDF of the simulated Markov chain. Inserting Equation (2.18) into Equation (A.4) gives:

$$a(\mathbf{u}_t, \mathbf{u}') = \min\left\{1, \frac{\varphi_n(\mathbf{u}') \, \mathbb{I}[G(\mathbf{u}') \leq b_{i-1}]}{\varphi_n(\mathbf{u}_t) \, \mathbb{I}[G(\mathbf{u}_t) \leq b_{i-1}]} \frac{q(\mathbf{u}_t|\mathbf{u}')}{q(\mathbf{u}'|\mathbf{u}_t)}\right\} \tag{A.5}$$

As mentioned above, in the context of subset simulation, the current state of the Markov chain $\mathbf{u}_t$ is always distributed according to $\varphi_n(\mathbf{u}|E_{i-1})$. Therefore, $\mathbb{I}[G(\mathbf{u}_t) \leq b_{i-1}] = 1$ and Equation (A.5) simplifies as follows (Papaioannou et al. 2015):

$$\begin{aligned} a(\mathbf{u}_t, \mathbf{u}') &= \min\left\{1, \frac{\varphi_n(\mathbf{u}')}{\varphi_n(\mathbf{u}_t)} \frac{q(\mathbf{u}_t|\mathbf{u}')}{q(\mathbf{u}'|\mathbf{u}_t)} \mathbb{I}[G(\mathbf{u}') \leq b_{i-1}]\right\} \\ &= \min\left\{1, \frac{\varphi_n(\mathbf{u}')}{\varphi_n(\mathbf{u}_t)} \frac{q(\mathbf{u}_t|\mathbf{u}')}{q(\mathbf{u}'|\mathbf{u}_t)}\right\} \mathbb{I}[G(\mathbf{u}') \leq b_{i-1}] \\ &= \tilde{a}(\mathbf{u}_t, \mathbf{u}') \, \mathbb{I}[G(\mathbf{u}') \leq b_{i-1}] \end{aligned} \tag{A.6}$$

It follows that a Metropolis-Hastings-type transition for sampling from $\varphi_n(\mathbf{u}|E_{i-1})$ can be performed in two steps. First, a normal Metropolis-Hastings transition with stationary distribution $\varphi_n(\mathbf{u})$ is carried out with acceptance probability $\tilde{a}(\mathbf{u}_t, \mathbf{u}')$, which is a function of the proposal PDF $q(\mathbf{u}_{t+1}|\mathbf{u}_t)$. This transition generates a sample $\mathbf{u}'$ from $\varphi_n(\mathbf{u})$. Subsequently, the sample $\mathbf{u}'$ is accepted if it lies in the domain describing the event E_{i-1}, i.e. if $G(\mathbf{u}') \leq b_{i-1}$, otherwise the sample $\mathbf{u}'$ is rejected and the chain remains in its current state. The Metropolis-Hastings transition for sampling from $\varphi_n(\mathbf{u}|E_{i-1})$ at subset level i of the subset simulation is summarized in Algorithm A.1.

Au and Beck (2001) found that the probability of rejecting the candidate in step 1 is close to one when the number of random variables n is large. This leads to many repeated samples and, ultimately, to an increased correlation among the generated samples, which reduces the efficiency and accuracy of subset simulation (see also Katafygiotis and Zuev 2008; Papaioannou et al. 2015). To overcome this problem, several modified variants of the original Metropolis-Hastings algorithm have been proposed. This includes the component-wise Metropolis-Hastings algorithm (Au and Beck 2001), the Metropolis-Hastings algorithm with repeated generation of pre-candidates (Santoso et al. 2011), component-wise Metropolis-Hastings algorithm with delayed rejection of the candidate state (Miao and Ghosn 2011) and a Metropolis-Hastings-type algorithm for sampling in standard normal space recently proposed by Papaioannou et al. (2015). The latter algorithm is simpler than existing algorithms but equally accurate and efficient. For these reasons, it has been implemented in this thesis.

The algorithm proposed by Papaioannou et al. (2015) applies a proposal PDF $q(\mathbf{u}'|\mathbf{u}_t)$ such that the acceptance probability of the candidate state $\mathbf{u}'$ in step 1 of Algorithm A.1 is $\tilde{a}(\mathbf{u}_t, \mathbf{u}') = 1$, i.e.

Algorithm A.1: Metropolis-Hastings algorithm for generating N samples from $\varphi_n(\mathbf{u}|E_{i-1})$ at subset level i of the subset simulation

---

Input: $\mathbf{u}_1$ (seed), N (number of states to be simulated), $G(\mathbf{u})$ (limit state function) and
$\quad\quad b_{i-1}$ (threshold)

For $t = 1, \dots, N$:

1. Generate a candidate $\mathbf{u}'$ from $\varphi_n(\cdot)$:

   a. Generate a pre-candidate $\mathbf{u}''$ through sampling from $q(\cdot\,|\mathbf{u}_t)$.

   b. Accept or reject $\mathbf{u}''$ by setting

   $$\mathbf{u}' = \begin{cases} \mathbf{u}'', & \text{with probability } \tilde{a}(\mathbf{u}_t, \mathbf{u}'') \\ \mathbf{u}_t, & \text{with probability } 1 - \tilde{a}(\mathbf{u}_t, \mathbf{u}'') \end{cases}$$

   where

   $$\tilde{a}(\mathbf{u}_t, \mathbf{u}'') = \min\left\{1, \frac{\varphi_n(\mathbf{u}'')}{\varphi_n(\mathbf{u}_t)} \frac{q(\mathbf{u}_t|\mathbf{u}'')}{q(\mathbf{u}''|\mathbf{u}_t)}\right\}$$

2. Accept or reject $\mathbf{u}'$ by setting

   $$\mathbf{u}_{t+1} = \begin{cases} \mathbf{u}', & \text{if } G(\mathbf{u}') \leq b_{i-1} \\ \mathbf{u}_t, & \text{otherwise} \end{cases}$$

---

the proposed candidate state $\mathbf{u}'$ is always accepted. Let the random vectors $\mathbf{U}_t = [U_{t,1}, \ldots, U_{t,n}]^T$ and $\mathbf{U}' = [U'_1, \ldots, U'_n]^T$ respectively represent the uncertain current and candidate state of the Markov chain. Both $\mathbf{U}_t$ and $\mathbf{U}'$ have the n-variate standard normal PDF $\varphi_n(\cdot)$ as marginal PDF. Papaioannou et al. (2015) impose that $\mathbf{U}_t$ and $\mathbf{U}'$ are jointly standard normal distributed with component-wise cross-correlation coefficient ρ_k. In addition, the algorithm assumes that each component $U_{t,k}$ is independent of the components U'_l for all $k \neq l$. It follows that the $2n$-dimensional standard normal random vector $\mathbf{U} = [\mathbf{U}_t^T, \mathbf{U}'^T]^T$ has zero mean vector and covariance matrix $\mathbf{\Sigma} \in \mathbb{R}^{2n \times 2n}$ given by:

$$\mathbf{\Sigma} = \begin{bmatrix} \mathbf{I} & \mathbf{R} \\ \mathbf{R}^T & \mathbf{I} \end{bmatrix} \tag{A.7}$$

where $\mathbf{I}$ is the unity matrix of size n and $\mathbf{R} \in \mathbb{R}^{n \times n}$ is a diagonal matrix with the kth diagonal element equal to ρ_k. It follows that (a) the joint PDF of $\mathbf{U}$ is the $2n$-variate standard normal PDF $\varphi_{2n}(\mathbf{u}; \mathbf{\Sigma})$, (b) the marginal PDF of $\mathbf{U}_t$ and $\mathbf{U}'$ is the n-variate standard normal PDF $\varphi_n(\cdot)$, (c) the conditional PDF of $\mathbf{U}_t$ given $\mathbf{U}' = \mathbf{u}'$ is the n-variate standard normal PDF $\varphi_n(\mathbf{u}_t - \mathbf{R}\mathbf{u}'; \mathbf{I} - \mathbf{R}\mathbf{R}^T)$, and (d) the conditional PDF of $\mathbf{U}'$ given $\mathbf{U}_t = \mathbf{u}_t$ is the n-variate standard normal PDF $\varphi_n(\mathbf{u}' - \mathbf{R}^T\mathbf{u}_t; \mathbf{I} - \mathbf{R}^T\mathbf{R})$ (see, for example, Petersen and Pedersen 2012). The following identity holds:

$$\varphi_n(\mathbf{u}' - \mathbf{R}^T\mathbf{u}_t; \mathbf{I} - \mathbf{R}^T\mathbf{R}) = \varphi_n(\mathbf{u}' - \mathbf{R}\mathbf{u}_t; \mathbf{I} - \mathbf{R}\mathbf{R}^T) \tag{A.8}$$

since $\mathbf{R}$ is symmetric (see also Au 2016). Therefore, the joint PDF of $\mathbf{U}$ can be written as:

$$\varphi_{2n}(\mathbf{u}; \mathbf{\Sigma}) = \varphi_n(\mathbf{u}_t - \mathbf{R}\mathbf{u}'; \mathbf{I} - \mathbf{R}\mathbf{R}^T)\varphi_n(\mathbf{u}') = \varphi_n(\mathbf{u}' - \mathbf{R}\mathbf{u}_t; \mathbf{I} - \mathbf{R}\mathbf{R}^T)\varphi_n(\mathbf{u}_t) \tag{A.9}$$

It can now be shown that $\tilde{a}(\mathbf{u}_t, \mathbf{u}') = 1$ when $q(\mathbf{u}'|\mathbf{u}_t) = \varphi_n(\mathbf{u}' - \mathbf{R}\mathbf{u}_t; \mathbf{I} - \mathbf{R}\mathbf{R}^T)$ is used as proposal PDF:

$$
\begin{aligned}
\tilde{a}(\mathbf{u}_t, \mathbf{u}') &= \min\left\{1, \frac{\varphi_n(\mathbf{u}')}{\varphi_n(\mathbf{u}_t)}\frac{q(\mathbf{u}_t|\mathbf{u}')}{q(\mathbf{u}'|\mathbf{u}_t)}\right\} \\
&= \min\left\{1, \frac{\varphi_n(\mathbf{u}')}{\varphi_n(\mathbf{u}_t)}\frac{\varphi_n(\mathbf{u}_t - \mathbf{R}\mathbf{u}'; \mathbf{I} - \mathbf{R}\mathbf{R}^T)}{\varphi_n(\mathbf{u}' - \mathbf{R}\mathbf{u}_t; \mathbf{I} - \mathbf{R}\mathbf{R}^T)}\right\} \\
&= \min\left\{1, \frac{\varphi_{2n}(\mathbf{u}; \mathbf{\Sigma})}{\varphi_{2n}(\mathbf{u}; \mathbf{\Sigma})}\right\} \\
&= 1
\end{aligned}
\tag{A.10}
$$

It also follows that given $\mathbf{U}_t$ each component k of $\mathbf{U}'$ is an independent normal random variable with mean value $\rho_k u_{t,k}$ and variance $1 - \rho_k^2$. The Metropolis-Hastings algorithm summarized in Algorithm A.1 can thus be rewritten as summarized Algorithm A.2. Papaioannou et al. (2015) proof that this updating scheme leaves the target distribution $\varphi_n(\mathbf{u}|E_{i-1})$ invariant (see also Au 2016).

The stochastic dependence among successive states of the Markov chains is controlled by the choice of the correlation coefficient ρ_k. On the one hand, a small ρ_k will result in many rejected candidates in step 2 and it will thus lead to a high correlation among the generated samples. On the other hand, a large ρ_k will increase the acceptance rate of the candidates in step 2 but it will also lead to a high correlation among the generated samples. A common choice of the correlation coefficient is $\rho_k = 0.8$ (Papaioannou et al. 2015). The correlation coefficient ρ_k can also be chosen adaptively during the simulation such that the acceptance rate in step 2 remains close to an optimal value (see Papaioannou et al. 2015 for more details). This approach ensures that the samples have low correlation and enhances the efficiency of subset simulation as the conditional probabilities $\Pr(E_i|E_{i-1})$ can be estimated with a smaller number of samples.

Algorithm A.2: Conditional sampling in **U**-space for generating N samples from $\varphi_n(\mathbf{u}|E_{i-1})$ at subset level i of the subset simulation (Papaioannou et al. 2015)

Input: $\mathbf{u}_1$ (seed), N (number of states to be simulated), $G(\mathbf{u})$ (limit state function),
$\quad\quad b_{i-1}$ (threshold), ρ_k, $k = 1, \ldots, n$ (correlation coefficients)

For $t = 1, \ldots, N$:

1. Generate a candidate $\mathbf{u}' = [u_1', \ldots, u_n']^T$ from $\varphi_n(\cdot)$:

   For $k = 1, \ldots, n$:

   Generate u_k' from the normal distribution with mean $\rho_k u_{t,k}$ and variance $1 - \rho_k^2$.

2. Accept or reject $\mathbf{u}'$ by setting

   $$\mathbf{u}_{t+1} = \begin{cases} \mathbf{u}', & \text{if } G(\mathbf{u}') \leq b_{i-1} \\ \mathbf{u}_t, & \text{otherwise} \end{cases}$$

Bibliography

Altamura, A. and Straub, D. (2014). Reliability assessment of high cycle fatigue under variable amplitude loading: review and solutions. *Engineering Fracture Mechanics* **121**: 40-66

Andrieu-Renaud, C., Sudret, B. and Lemaire, M. (2004). The PHI2 method: a way to compute time-variant reliability. *Reliability Engineering & System Safety* **84**(1): 75-86

Arora, S. and Barak, B. (2009). *Computational Complexity: A Modern Approach*. Cambridge University Press

Au, S.-K. (2016). On MCMC algorithm for Subset Simulation. *Probabilistic Engineering Mechanics* **43**: 117-120

Au, S.-K. and Beck, J. L. (2001). Estimation of small failure probabilities in high dimensions by subset simulation. *Probabilistic Engineering Mechanics* **16**(4): 263-277

Au, S.-K., Beck, J. L., Zuev, K. M. and Katafygiotis, L. S. (2012). Discussion of paper by F. Miao and M. Ghosn "Modified subset simulation method for reliability analysis of structural systems", Structural Safety, 33:251–260, 2011. *Structural Safety* **34**(1): 379-380

Au, S.-K. and Zhang, F.-L. (2016). Fundamental two-stage formulation for Bayesian system identification, Part I: General theory. *Mechanical Systems and Signal Processing* **66–67**: 31-42

Au, S. K. and Beck, J. L. (1999). A new adaptive importance sampling scheme for reliability calculations. *Structural Safety* **21**(2): 135-158

Barone, G. and Frangopol, D. M. (2014). Reliability, risk and lifetime distributions as performance indicators for life-cycle maintenance of deteriorating structures. *Reliability Engineering & System Safety* **123**: 21-37

Bastidas-Arteaga, E., Bressolette, P., Chateauneuf, A. and Sánchez-Silva, M. (2009). Probabilistic lifetime assessment of RC structures under coupled corrosion–fatigue deterioration processes. *Structural Safety* **31**(1): 84-96

Beck, A. T. and Melchers, R. E. (2004). Overload failure of structural components under random crack propagation and loading – a random process approach. *Structural Safety* **26**(4): 471-488

Beck, J. L. (2010). Bayesian system identification based on probability logic. *Structural Control and Health Monitoring* **17**(7): 825-847

Beck, J. L. and Katafygiotis, L. S. (1998). Updating Models and Their Uncertainties. I: Bayesian Statistical Framework. *Journal of Engineering Mechanics* **124**(4): 455-461

Behmanesh, I. and Moaveni, B. (2016). Accounting for environmental variability, modeling errors, and parameter estimation uncertainties in structural identification. *Journal of Sound and Vibration* **374**: 92-110

Benjamin, J. R. and Cornell, C. A. (1970). *Probability, Statistics and Decision for Civil Engineers*. Mc Graw Hill Book Company

Bensi, M., Der Kiureghian, A. and Straub, D. (2013). Efficient Bayesian network modeling of systems. *Reliability Engineering & System Safety* **112**(0): 200-213

Bensi, M., Kiureghian, A. D. and Straub, D. (2011). Bayesian network modeling of correlated random variables drawn from a Gaussian random field. *Structural Safety* **33**(6): 317-332

Betz, W. (2017). *Bayesian inference of engineering models*. PhD thesis, Technische Universität München, Germany

Betz, W., Beck, J. L., Papaioannou, I. and Straub, D. (2018a). Bayesian inference with reliability methods without knowing the maximum of the likelihood function. *Probabilistic Engineering Mechanics* **53**: 14-22

Betz, W., Papaioannou, I., Beck, J. L. and Straub, D. (2018b). Bayesian inference with Subset Simulation: Strategies and improvements. *Computer Methods in Applied Mechanics and Engineering* **331**: 72-93

Betz, W., Papaioannou, I. and Straub, D. (2014). Numerical methods for the discretization of random fields by means of the Karhunen–Loève expansion. *Computer Methods in Applied Mechanics and Engineering* **271**: 109–129

Bismut, E., Luque, J. and Straub, D. (2017). Optimal priorization of inspections in structural systems considering component interactions and interdependence. *12th International Conference on Structural Safety & Reliability (ICOSSAR 2017)*, Vienna, Austria

Bismut, E. and Straub, D. (2018). Adaptive direct policy search for inspection and maintenance planning in structural systems. *6th International Symposium on Life-Cycle Civil Engineering (IALCCE 2018)*, Ghent, Belgium

BMVI (2018). *Verkehrsinvestitionsbericht für das Berichtsjahr 2016*. Bundesministerium für Verkehr und digitale Infrastruktur (BMVI), Germany. [in German].

Bolotin, V. V. (1981). *Wahrscheinlichkeitsmethoden zur Berechnung von Konstruktionen*. VEB-Verlag für das Bauwesen, Berlin [in German].

Breitung, K. (1984). Asymptotic approximation for multinormal integrals. *Journal of Engineering Mechanics* **110**(3): 357–366

Bucher, C. (1988). Adaptive sampling - an iterative fast Monte Carlo procedure. *Structural Safety* **5**(2): 119-126

Bucher, C. (2009). Asymptotic sampling for high-dimensional reliability analysis. *Probabilistic Engineering Mechanics* **24**(4): 504-510

Chopin, N. (2012). Fast simulation of truncated Gaussian distributions. *Statistics and Computing* **21**(2): 275-288

Cooper, G. F. (1990). The computational complexity of probabilistic inference using Bayesian belief networks (research note). *Artif. Intell.* **42**(2-3): 393-405

Corotis, R. and Nafday, A. (1989). Structural System Reliability Using Linear Programming and Simulation. *Journal of Structural Engineering* **115**(10): 2435-2447

Cottone, G., Gollwitzer, S., Heckenberger, U. and Straub, D. (2013). Reliability-oriented optimization of replacement strategies for monitored composite panels for aircraft structures. *9th International Workshop on Structural Health Monitoring (IWSHM 2013)*, Stanford, California, USA

Daniels, H. E. (1945). The statistical theory of the strength of bundles of threads. I. *Proceedings of the Royal Society of London*: 405-435

DiazDelaO, F. A., Garbuno-Inigo, A., Au, S. K. and Yoshida, I. (2017). Bayesian updating and model class selection with Subset Simulation. *Computer Methods in Applied Mechanics and Engineering* **317**: 1102-1121

Ditlevsen, O. (1982). Model uncertainty in structural reliability. *Structural Safety* **1**(1): 73-86

Ditlevsen, O. (2002). Stochastic model for joint wave and wind loads on offshore structures. *Structural Safety* **24**(2): 139-163

Ditlevsen, O. and Bjerager, P. (1989). Plastic Reliability Analysis By Directional Simulation. *Journal of Engineering Mechanics* **115**(6): 1347-1362

Ditlevsen, O. and Madsen, H. O. (1996). *Structural Reliability Methods*. John Wiley & Sons Ltd

Döhler, M. and Mevel, L. (2013). Subspace-based fault detection robust to changes in the noise covariances. *Automatica* **49**(9): 2734-2743

Doucet, A., Freitas, N. d. and Gordon, N. (2001). *Sequential Monte Carlo Methods in Practice.* Springer, New York

Dunnett, C. W. and Sobel, M. (1955). Approximations to the probability integral and certain percentage points of a multivariate analogue of Student's t-distribution. *Biometrika* **42**(1-2): 258-260

DuraCrete (1998). Modelling of Degradation. In. DuraCrete: Probabilistic Performance Based Durability Design of Concrete Structures, The European Union – Brite EuRam III (Project BE95-1347/R4-5).

Elsener, B., Andrade, C., Gulikers, J., Polder, R. and Raupach, M. (2003). Hall-cell potential measurements - Potential mapping on reinforced concrete structures. *Materials and Structures* **36**(7): 461-471

Enevoldsen, I. and Sørensen, J. (1993). Reliability-Based Optimization of Series Systems of Parallel Systems. *Journal of Structural Engineering* **119**(4): 1069-1084

Enevoldsen, I. and Sørensen, J. D. (1992). Optimization algorithms for calculation of the joint design point in parallel systems. *Structural optimization* **4**(2): 121-127

Enright, M. P. and Frangopol, D. M. (1999). Reliability-based condition assessment of deteriorating concrete bridges considering load redistribution. *Structural Safety* **21**(2): 159-195

Faber, M. H. (2009). *Risk and Safety in Engineering*. ETH Zürich, Switzerland

Faber, M. H., Engelund, S., Sørensen, J. D. and Bloch, A. (2000). Simplified and Generic Risk Based Inspection Planning. *19th Conference on Offshore Mechanics and Arctic Engineering (OMAE)*, New Orleans, Louisiana, USA.

Faber, M. H., Kroon, I. B., Kragh, E. K., Bayly, D. and Decosemaeker, P. (2002). Risk assessment of decommissioning options using Bayesian networks. *Journal of Offshore Mechanics and Arctic Engineering* **124**(4): 231-238

Faber, M. H. and Sørensen, J. D. (2002). Indicators for inspection and maintenance planning of concrete structures. *Structural Safety* **24**(2–4): 377-396

Faber, M. H., Straub, D. and Maes, M. A. (2006). A computational framework for risk assessment of RC structures using indicators. *Computer-Aided Civil and Infrastructure Engineering* **21**(3): 216-230

Farrar, C. R., Doebling, S. W. and Nix, D. A. (2001). Vibration–based structural damage identification. *Philosophical Transactions of the Royal Society of London A: Mathematical, Physical and Engineering Sciences* **359**(1778): 131-149

fib Bulletin No. 34 (2006). Model Code for Service Life Design. Switzerland, The International Federation for Structural Concrete (fib - fédération internationale du béton).

Fischer, J., Straub, D., Schneider, R., Thöns, S. and Rücker, W. (2014). *Intelligente Brücke – Zuverlässigkeitsbasierte Bewertung von Brückenbauwerken unter Berücksichtigung von Inspektions- und Überwachungsergebnissen*. Berichte der Bundesanstalt für Straßenwesen, Reihe B: Brücken- und Ingenieurbau, Heft B 99, Bundesanstalt für Straßenwesen (BASt), Bergisch Gladbach, Germany. [in German].

Fricke, W. (2003). Fatigue analysis of welded joints: state of development. *Marine Structures* **16**(3): 185-200

Friis-Hansen, A. (2000). *Bayesian networks as a decision support tool in marine applications*, Technical University of Denmark

Fung, R. and Chang, K.-C. (1989). Weighing and Integrating Evidence for Stochastic Simulation in Bayesian Networks. *Fifth Conference on Uncertainty in Artificial Intelligence (UAI1989)*, Ontario, Canada

Gelman, A., Carlin, J. B., Stern, H. S. and Rubin, D. B. (2004). *Bayesian data analysis*. Chapman and Hall/CRC, Boca Raton, Florida

Gilks, W. R., Richardson, S. and Spiegelhalter, D. J. (1996). *Markov Chain Monte Carlo in Practice*. Chapman & Hall

Giovanis, D. G., Papaioannou, I., Straub, D. and Papadopoulos, V. (2017). Bayesian updating with subset simulation using artificial neural networks. *Computer Methods in Applied Mechanics and Engineering* **319**: 124-145

Gollwitzer, S. and Rackwitz, R. (1988). An efficient numerical solution to the multinormal integral. *Probabilistic Engineering Mechanics* **3**(2): 98-101

Gollwitzer, S. and Rackwitz, R. (1990). On the reliability of Daniels systems. *Structural Safety* **7**(2-4): 229–243

Grêt-Regamey, A. and Straub, D. (2006). Spatially explicit avalanche risk assessment linking Bayesian networks to a GIS. *Natural Hazards Earth System Sciences* **6**(6): 911-926

Gurney, T. R. (1978). *An analysis of some recent fatigue crack propagation data for steels subjected to pulsating tension loading*. Report 1978E, The Welding Institute TWI, UK

Haardt, P. (1999). *Algorithmen zur Zustandsbewertung von Ingenieurbauwerken*. Berichte der Bundesanstalt für Straßenwesen, Reihe B: Brücken- und Ingenieurbau, Heft B 22. Bundesanstalt für Straßenwesen (BASt), Bergisch Gladbach [in German].

Hackl, J. and Köhler, J. (2016). Reliability assessment of deteriorating reinforced concrete structures by representing the coupled effect of corrosion initiation and progression by Bayesian networks. *Structural Safety* **62**: 12-23

Harlow, D. G. and Wei, R. P. (1994). Probability approach for prediction of corrosion and corrosion fatigue life. *AIAA Journal* **32**(10): 2073-2079

Hasofer, A. M. and Lind, N. C. (1974). An exact and invariant first order reliability format. *Journal of Engineering Mechanics* **100**(EM1): 111-121

Hastings, W. K. (1970). Monte Carlo sampling methods using Markov chains and their applications. *Biometrika* **57**(1): 97-109

Hergenröder, M. and Rackwitz, R. (1992). Zur statistischen Instandhaltungsplanung für bestehende Betonbauwerke. *Bauingenieur* **67**: 491-497 [in German].

Hohenbichler, M. and Rackwitz, R. (1981). Non-Normal Dependent Vectors in Structural Safety. *Journal of the Engineering Mechanics Division* **107**(6): 1227-1238

Hohenbichler, M. and Rackwitz, R. (1983). First-order concepts in system reliability. *Structural Safety* **1**(3): 177-188

Hohenbichler, M. and Rackwitz, R. (1988). Improvement Of Second-Order Reliability Estimates by Importance Sampling. *Journal of Engineering Mechanics* **114**(12): 2195-2199

Huang, Y., Beck, J. L. and Li, H. (2017). Hierarchical sparse Bayesian learning for structural damage detection: Theory, computation and application. *Structural Safety* **64**: 37-53

ISO 2394 (2015). General principles on reliability for structures. International Organization for Standardization. Switzerland.

JCSS (2001). Probabilistic Model Code, Joint Committee on Structural Safety (JCSS).

Jensen, F. V. and Nielsen, T. D. (2007). *Bayesian Networks and Decision Graphs*. Springer Publishing Company

Johnsen, T. H., Geiker, M. R. and Faber, M. H. (2003). Quantifying condition indicators for concrete structures. *Concrete International* **25**(12): 47-54

Kang, W.-H. and Song, J. (2010). Evaluation of multivariate normal integrals for general systems by sequential compounding. *Structural Safety* **32**(1): 35-41

Kang, W.-H., Song, J. and Gardoni, P. (2008). Matrix-based system reliability method and applications to bridge networks. *Reliability Engineering & System Safety* **93**(11): 1584-1593

Katafygiotis, L. S. and Zuev, K. M. (2008). Geometric insight into the challenges of solving high-dimensional reliability problems. *Probabilistic Engineering Mechanics* **23**(2–3): 208-218

Keßler, S. (2015). *Zur Verwertbarkeit von Potentialfeldmessungen für die Zustandserfassung und -prognose von Stahlbetonbauteilen – Validierung und Einsatz im Lebensdauermanagement*. PhD thesis, Technischen Universität München, Germany. [in German].

Keßler, S., Fischer, J., Straub, D. and Gehlen, C. (2014). Updating of service-life prediction of reinforced concrete structures with potential mapping. *Cement and Concrete Composites* **47**: 47-52

Kim, D.-S., Ok, S.-Y., Song, J. and Koh, H.-M. (2013). System reliability analysis using dominant failure modes identified by selective searching technique. *Reliability Engineering & System Safety* **119**(0): 316-331

Kim, H.-J. and Straub, D. (2019). Efficient computation of the lifetime reliability of deteriorating structures. *13th International Conference on Applications of Statistics and Probability in Civil Engineering (ICASP 13)*, Seoul, Korea

Kjaerulff, U. B. and Madsen, A. L. (2013). *Bayesian Networks and Influence Diagrams: A Guide to Construction and Analysis*. Springer

Kochenderfer, M. J. (2015). *Decision Making Under Uncertainty: Theory and Application* MIT Lincoln Laboratory Series. The MIT Press, Cambridge, Massachusetts

Koutsourelakis, P. S., Pradlwarter, H. J. and Schuëller, G. I. (2004). Reliability of structures in high dimensions, part I: algorithms and applications. *Probabilistic Engineering Mechanics* **19**(4): 409-417

Kurtz, N. and Song, J. (2013). Cross-entropy-based adaptive importance sampling using Gaussian mixture. *Structural Safety* **42**: 35-44

Langseth, H., Nielsen, T. D., Rumí, R. and Salmerón, A. (2012). Mixtures of truncated basis functions. *International Journal of Approximate Reasoning* **53**(2): 212-227

Langseth, H. and Portinale, L. (2007). Bayesian networks in reliability. *Reliability Engineering & System Safety* **92**(1): 92-108

Lassen, T. and Recho, N. (2006). *Fatigue Life Analyses of Welded Structures*. ISTE Ltd., London

Lentz, A. (2001). *Potentialmessungen zur Unterhaltsplanung bei Stahlbetonbauwerken* Diplom Thesis, ETH Zurich, Switzerland

Lentz, A., Johnsen, T. H. and Faber, M. H. (2002). Half-cell potential measurements for condition assessment. *1st International Conference on Bridge Maintenance, Safety and Management (IABMAS'02)*, Barcelona, Spain

Li, Q., Wang, C. and Ellingwood, B. R. (2015). Time-dependent reliability of aging structures in the presence of non-stationary loads and degradation. *Structural Safety* **52, Part A**: 132-141

Li, Y., Vrouwenvelder, T., Wijnants, G. H. and Walraven, J. (2004). Spatial variability of concrete deterioration and repair strategies. *Structural Concrete* **5**(3): 121-129

Lin, Y. K. and Yang, J. N. (1985). A stochastic theory of fatigue crack propagation. *AIAA Journal* **23**(1): 117-124

Liu, P.-L. and Der Kiureghian, A. (1986). Multivariate distribution models with prescribed marginals and covariances. *Probabilistic Engineering Mechanics* **1**(2): 105-112

Lovejoy, D. (1993). *Magnetic Particle Inspection: A practical guide*. Springer, Netherlands

Luque, J., Hamann, R. and Straub, D. (2017). Spatial probabilistic modeling of corrosion in ship structures. *ASCE-ASME Journal of Risk and Uncertainty in Engineering Systems, Part B: Mechanical Engineering* **3**(3): 031001

Luque, J. and Straub, D. (2016). Reliability analysis and updating of deteriorating systems with dynamic Bayesian networks. *Structural Safety* **62**: 34-46

Luque, J. and Straub, D. (2019). Risk-based optimal inspection strategies for structural systems using dynamic Bayesian networks. *Structural Safety* **76**: 68-80

Madsen, H. O. (1987). Model updating in reliability theory. *5th International Conference on Applications of Statistics and Probability in Civil Engineering (ICASP 5)*, Vancouver, Canada

Madsen, H. O. (1997). Stochastic modeling of fatigue crack growth and inspection. In: Guedes Soares, C. Probabilistic Methods for Structural Design. Netherlands, Kluwer Accademic Publishers.

Madsen, H. O., Krenk, S. and Lind, N. C. (1986). *Methods of Structural Safety*. Prentice Hall

Madsen, H. O., Sørensen, J. D. and Olesen, R. (1989). Optimal inspection planning for fatigue damage of offshore structures. *5th International Conference on Structural Safety and Reliability (ICOSSAR 1989)*, San Francisco, California

Madsen, H. O., Torhaug, R. and Cramer, E. H. (1991). Probability-based cost benefit analysis of fatigue design, inspection and maintenance. *Marine Structural Inspection, Maintenance and Monitoring Symposium*, Arlington, Virginia

Maes, M. A. and Dann, M. (2007). Hierarchical Bayes methods for systems with spatially varying condition states. *Canadian Journal of Civil Engineering* **34**(10): 1289-1298

Malioka, V. (2009). *Condition Indicators for the Assessment of Local and Spatial Deterioration of Concrete Structures*. PhD Thesis, ETH Zurich, Switzerland

Maljaars, J., Steenbergen, H. M. G. M. and Vrouwenvelder, A. C. W. M. (2012). Probabilistic model for fatigue crack growth and fracture of welded joints in civil engineering structures. *International Journal of Fatigue* **38**: 108-117

Maljaars, J. and Vrouwenvelder, A. C. W. M. (2014). Probabilistic fatigue life updating accounting for inspections of multiple critical locations. *International Journal of Fatigue* **68**: 24-37

Melchers, R. E. (1994). Structural system reliability assessment using directional simulation. *Structural Safety* **16**(1–2): 23-37

Melchers, R. E. (1999). *Structural Reliability Analysis and Prediction*. John Wiley and Sons Ltd.

Metropolis, N., Rosenbluth, A. W., Rosenbluth, M. N., Teller, A. H. and Teller, E. (1953). Equation of state calculations by fast computing machines. *The Journal of Chemical Physics* **21**(6): 1087-1092

Miao, F. and Ghosn, M. (2011). Modified subset simulation method for reliability analysis of structural systems. *Structural Safety* **33**(4–5): 251-260

Moan, T. and Song, R. (2000). Implications of Inspection Updating on System Fatigue Reliability of Offshore Structures. *Journal of Offshore Mechanics and Arctic Engineering* **122**(3): 173-180

Moan, T., Vardal, O. T., Hellevig, N. C. and Skjoldli, K. (2000). Initial crack depth and PoD values inferred from in-service observations of cracks in North Sea jackets. *Journal of Offshore Mechanics and Arctic Engineering* **122**: 157-162

Mori, Y. and Ellingwood, B. (1993). Reliability-Based Service-Life Assessment of Aging Concrete Structures. *Journal of Structural Engineering* **119**(5): 1600-1621

Moses, F. (1982). System reliability developments in structural engineering. *Structural Safety* **1**(1): 3-13

Murotsu, Y., Okada, H., Taguchi, K., Grimmelt, M. and Yonezawa, M. (1984). Automatic generation of stochastically dominant failure modes of frame structures. *Structural Safety* **2**(1): 17-25

Murphy, K. P. (2001). The Bayes Net Toolbox for Matlab. *Computing Science and Statistics* **33**: 1-20

Murphy, K. P. (2002). *Dynamic Bayesian Networks: Representation, Inference and Learning*. PhD Thesis, University of California, Berkley

Murphy, K. P. (2012). *Machine Learning: A Probabilistic Perspective*. The MIT Press

Neil, M., Tailor, M. and Marquez, D. (2007). Inference in hybrid Bayesian networks using dynamic discretization. *Statistics and Computing* **17**(3): 219-233

Nielsen, J. J. and Sørensen, J. D. (2011). On risk-based operation and maintenance of offshore wind turbine components. *Reliability Engineering & System Safety* **96**(1): 218-229

Osterminski, K. and Schießl, P. (2012). Design model for reinforcement corrosion. *Structural Concrete* **13**(3): 156-165

Papadimitriou, C. and Lombaert, G. (2012). The effect of prediction error correlation on optimal sensor placement in structural dynamics. *Mechanical Systems and Signal Processing* **28**: 105-127

Papaioannou, I. (2013). *Non-intrusive finite element reliability analysis: Structural reliability analysis with 'black box' finite element programs*. SVH-Verlag

Papaioannou, I., Betz, W., Zwirgelmaier, K. and Straub, D. (2015). MCMC Algorithms for Subset Simulation. *Probabilistic Engineering Mechanics* **41**: 89-103

Papaioannou, I., Papadimitriou, C. and Straub, D. (2016). Sequential importance sampling for structural reliability analysis. *Structural Safety* **62**: 66-75

Papakonstantinou, K. G. and Shinozuka, M. (2013). Spatial stochastic direct and inverse analysis for the extent of damage in deteriorated RC structures. *Computers & Structures* **128**: 286-296

Paris, P. C. and Erdogan, F. A. (1963). A critical analysis of crack propagation laws. *Journal of Basic Engineering* **85**: 528-534

Pearl, J. (1988). *Probabilistic reasoning in intelligent systems: networks of plausible inference*. The Morgan series in representation and reasoning. Morgan Kaufmann Publishers, San Francisco, USA

Petersen, K. B. and Pedersen, M. S. (2012). *The Matrix Cookbook*. Technical University of Denmark

Phares, B. M., Rolander, D. D., Graybeal, B. A. and Washer, G. A. (2001). Reliability of Visual Bridge Inspection. *Public Roads* **64**(5)

Plummer, M., Best, N., Cowles, K. and Vines, K. (2006). CODA: convergence diagnosis and output analysis for MCMC. *R News* **6**(6): 7–11

Pozzi, M. and Der Kiureghian, A. (2011). Assessing the value of information for long-term structural health monitoring. *Health Monitoring of Structural and Biological Systems 2011*, San Diego, California, USA

Qin, J. and Faber, M. H. (2012). Risk Management of Large RC Structures within a Spatial Information System. *Computer-Aided Civil and Infrastructure Engineering* **27**: 385–405

Rackwitz, R. (2000). Optimization - the basis of code-making and reliability verification. *Structural Safety* **22**: 22-60

Rackwitz, R. (2001). Reliability analysis - a review and some perspectives. *Structural Safety* **23**(4): 365–395

Rackwitz, R. (2006). *Zuverlässigkeit und Lasten im konstruktiven Ingenieurbau. Teil I: Zuverlässigkeitstheoretische Grundlagen* Technische Universität München [in German].

Rackwitz, R. and Fiessler, B. (1978). Structural reliability under combined load sequences. *Computers and Structures* **9**(5): 489-494

Raiffa, H. and Schlaifer, R. (1961). *Applied statistical decision theory*. Division of Research, Harvard Business School, Harvard University

Rausand, M. and Høyland, A. (2004). *System Reliability Theory: Models, Statistical Methods, and Applications*. Wiley Series in Probability and Statistics. John Wiley & Sons, Inc.

RILEM (2001). *Probabilistic Assessment of Existing Structures - JCSS Report*. The International Union of Laboratories and Experts in Construction Materials, Systems and Structures (RILEM)

Russell, S. J. and Norvig, P. (2010). *Artificial Intelligence - A Modern Approach*. Prentice Hall

Santoso, A. M., Phoon, K. K. and Quek, S. T. (2011). Modified Metropolis–Hastings algorithm with reduced chain correlation for efficient subset simulation. *Probabilistic Engineering Mechanics* **26**(2): 331-341

Sarveswaran, V. and Roberts, M. B. (1999). Reliability analysis of deteriorating structures — the experience and needs of practising engineers. *Structural Safety* **21**(4): 357-372

Schachter, R. D. and Poet, M. A. (1989). Simulation Approaches to General Probabilistic Inference on Belief Networks. *Fifth Conference on Uncertainty in Artificial Intelligence (UAI1989)*, Ontario, Canada

Schall, G., Faber, M. and Rackwitz, R. (1991). The Ergodicity Assumption for Sea States in the Reliability Estimation of Offshore Structures. *Journal of Offshore Mechanics and Arctic Engineering* **113**(3)

Schneider, R. (2019). Effect of repair models on risk-based optimal inspection strategies for support structures of offshore wind turbines. *5th Conference on Smart Monitoring, Assessment und Rehabilitation of Civil Structures (SMAR 2019)*, Potsdam, Germany

Schneider, R., Fischer, J., Bügler, M., Nowak, M., Thöns, S., Borrmann, A. and Straub, D. (2015a). Assessing and updating the reliability of concrete bridges subjected to spatial deterioration - principles and software implementation. *Structural Concrete* **16**(3): 356–365

Schneider, R., Fischer, J., Straub, D., Thöns, S., Bügler, M. and Borrmann, A. (2015b). *Intelligente Brücke – Prototyp zur Ermittlung der Schadens- und Zustandsentwicklung für Elemente des Brückenmodells*. Berichte der Bundesanstalt für Straßenwesen, Reihe B: Brücken- und Ingenieurbau, Heft B 117, Bundesanstalt für Straßenwesen (BASt), Bergisch Gladbach, Germany. [in German].

Schneider, R. and Straub, D. (2020). Cumulative failure probability of deteriorating structures: Can it drop? *18th International Probabilistic Workshop (IPW2020)*, Guimarães, Portugal

Schneider, R., Thöns, S., Fischer, J., Bügler, M., Borrmann, A. and Straub, D. (2014). A software prototype for assessing the reliability of a concrete bridge superstructure subjected to chloride-

induced reinforcement corrosion. *4th International Symposium on Life-Cycle Civil Engineering (IALCCE 2014)*, Tokyo, Japan

Schneider, R., Thöns, S., Rogge, A., Bismut, E. and Straub, D. (2018). A sampling-based approach to identifying optimal inspection and repair strategies for offshore jacket structures. *6th International Symposium on Life-Cycle Civil Engineering (IALCCE 2018)*, Ghent, Belgium

Schneider, R., Thöns, S., Rücker, W. and Straub, D. (2013). Effect of different inspection strategies on the reliability of Daniels systems subjected to fatigue. *11th International Conference on Structural Safety & Reliability (ICOSSAR 2013)*, New York, USA

Schneider, R., Thöns, S. and Straub, D. (2017). Reliability analysis and updating of deteriorating systems with subset simulation. *Structural Safety* **64**: 20-36

Schuëller, G. I., Pradlwarter, H. J. and Koutsourelakis, P. S. (2004). A critical appraisal of reliability estimation procedures for high dimensions. *Probabilistic Engineering Mechanics* **19**(4): 463-474 [in eng].

Schuëller, G. I. and Stix, R. (1987). A critical appraisal of methods to determine failure probabilities. *Structural Safety* **4**(4): 293-309

Sedehi, O., Papadimitriou, C. and Katafygiotis, L. S. (2019). Probabilistic hierarchical Bayesian framework for time-domain model updating and robust predictions. *Mechanical Systems and Signal Processing* **123**: 648-673

Shao, S. and Murotsu, Y. (1999). Approach to failure mode analysis of large structures. *Probabilistic Engineering Mechanics* **14**(1–2): 169-177

Shetty, N. K. (1994). Selective enumeration method for identification of dominant failure paths of large structures. *13th International Conference on Offshore Mechanics and Arctic Engineering (OMAE-13)*, Houston, Texas

Shinozuka, M. (1964). Probability of failure under random loading. *Journal of the Engineering Mechanics Division* **90**(5): 147-170

Simoen, E., Papadimitriou, C. and Lombaert, G. (2013). On prediction error correlation in Bayesian model updating. *Journal of Sound and Vibration* **332**(18): 4136-4152

Simon, P., Schneider, R. and Baeßler, M. (2021). Bayesian system identification of a reinforced concrete beam subject to temperature variations based on static response data. *10th International Conference on Bridge Maintenance, Safety and Management (IABMAS 2020)*, Sapporo, Japan

Simon, P., Schneider, R., Viefhues, E., Said, S., Herrmann, R. and Baeßler, M. (2020). Vibration-based structural health monitoring of a reinforced concrete beam subject to varying ambient temperatures using Bayesian methods. *XI International Conference on Structural Dynamics (EURODYN 2020)*, Athens, Greece

Sindel, R. and Rackwitz, R. (1998). Problems and solution strategies in reliability updating. *Journal of Offshore Mechanics and Arctic Engineering* **120**(2): 109-114

Skallerud, B. and Amdahl, J. (2002). *Nonlinear analysis of offshore structures*. Reasearch Studies Press Ltd., UK

Smith, A. F. M. and Gelfand, A. E. (1992). Bayesian Statistics without Tears: A Sampling-Resampling Perspective. *The American Statistician* **46**(2): 84-88

Sohn, H., Farrar, C. R., Hemez, F. M., Shunk, D. D., Stinemates, D. W. and Nadler, B. R. (2004). *A Review of structural health monitoring literature: 1996–2001*. LA-13976-MS, Los Alamos National Laboratory, USA

Song, J. and Der Kiureghian, A. (2003). Bounds on System Reliability by Linear Programming. *Journal of Engineering Mechanics* **129**(6): 627-636

Song, J. and Kang, W.-H. (2009). System reliability and sensitivity under statistical dependence by matrix-based system reliability method. *Structural Safety* **31**(2): 148–156

Sørensen, J. D. (2009). Framework for risk-based planning of operation and maintenance for offshore wind turbines. *Wind Energy* **12**(5): 493-506

Sørensen, J. D. and Faber, M. H. (1991). Optimal Inspection and Repair Strategies for Structural Systems. *Proceedings of the 4th IFIP WG 7.5 Working Conference*, Munich, Germany.

Stewart, M. G. and Al-Harthy, A. (2008). Pitting corrosion and structural reliability of corroding RC structures: Experimental data and probabilistic analysis. *Reliability Engineering & System Safety* **93**(3): 373-382

Stewart, M. G. and Mullard, J. A. (2007). Spatial time-dependent reliability analysis of corrosion damage and the timing of first repair for RC structures. *Engineering Structures* **29**(7): 1457-1464

Stewart, M. G. and Rosowsky, D. V. (1998a). Structural Safety and Serviceability of Concrete Bridges Subject to Corrosion. *Journal of Infrastructure Systems* **4**(4): 146-155

Stewart, M. G. and Rosowsky, D. V. (1998b). Time-dependent reliability of deteriorating reinforced concrete bridge decks. *Structural Safety* **20**(1): 91-109

Straub, D. (2004). *Generic Approaches to Risk Based Inspection Planning for Steel Structures*. PhD thesis, ETH Zürich, Switzerland

Straub, D. (2009). Stochastic modeling of deterioration processes through dynamic Bayesian networks. *Journal of Engineering Mechanics* **135**(10): 1089-1099

Straub, D. (2011a). Reliability updating with equality information. *Probabilistic Engineering Mechanics* **26**(2): 254–258

Straub, D. (2011b). Reliability updating with inspection and monitoring data in deteriorating reinforced concrete slabs. *11th International Conference on Applications of Statistics and Probability in Civil Engineering (ICASP11)*, Zurich, Switzerland

Straub, D. (2012). *Lecture notes in structural reliability*. Engineering Risk Analysis Group, Technische Universität München

Straub, D. (2014a). Engineering Risk Assessment. In: Klüppelberg, C., Straub, D. and Welpe, I. M. Risk – A Multidisciplinary Introduction, Springer International Publishing.

Straub, D. (2014b). Value of Information Analysis with Structural Reliability Methods. *Structural Safety* **49**: 75-85

Straub, D. (2018a). *Lecture notes in engineering risk analysis*. Engineering Risk Analysis Group, Technische Universität München

Straub, D. (2018b). Reliability assessment of deteriorating structures: challenges and (some) solutions. *6th International Symposium on Life-Cycle Civil Engineering (IALCCE 2018)*, Ghent, Belgium

Straub, D., Chatzi, E., Bismut, E., Courage, W. M. G., Döhler, M., Faber, M. H., Köhler, J., Lombaert, G., Omenzetter, P., Pozzi, M., Thöns, S., Val, D. and Zonta, D. (2017). Value of information: A roadmap to quantifying the benefit of structural health monitoring. *12th International Conference on Structural Safety & Reliability (ICOSSAR 2017)*, Vienna, Austria

Straub, D. and Der Kiureghian, A. (2010a). Bayesian network enhanced with structural reliability methods: Application. *Journal of Engineering Mechanics* **136**(10): 1259-1270

Straub, D. and Der Kiureghian, A. (2010b). Bayesian network enhanced with structural reliability methods: Methodology. *Journal of Engineering Mechanics* **136**(10): 1248-1258

Straub, D. and Der Kiureghian, A. (2011). Reliability acceptance criteria for deteriorating elements of structural systems. *Journal of Structural Engineering* **137**(12): 1573-1582

Straub, D. and Faber, M. H. (2003). Modeling Dependency in Inspection Performance. *9th International Conference on Applications of Statistics and Probability in Civil Engineering (ICASP9)*, San Francisco, California

Straub, D. and Faber, M. H. (2005). Risk based inspection planning for structural systems. *Structural Safety* **27**: 335–355

Straub, D. and Faber, M. H. (2006). Computational Aspects of Generic Risk Based Inspection Planning. *Computer-Aided Civil and Infrastructure Engineering* **21**: 179–192

Straub, D. and Faber, M. H. (2007). Temporal Variability in Corrosion Modeling and Reliability Updating. *Journal of Offshore Mechanics and Arctic Engineering* **129**(4): 265-272

Straub, D., Malioka, V. and Faber, M. H. (2009). A framework for the asset integrity management of large deteriorating concrete structures. *Structure and Infrastructure Engineering* **5**(3): 199-213

Straub, D. and Papaioannou, I. (2015a). Bayesian analysis for learning and updating geotechnical parameters and models with measurements. In: Phoon, K.-K. and Ching, J. Risk and reliability in geotechnical engineering, CRC Press.

Straub, D. and Papaioannou, I. (2015b). Bayesian updating with structural reliability methods. *Journal of Engineering Mechanics* **141**(3)

Straub, D., Papaioannou, I. and Betz, W. (2016). Bayesian analysis of rare events. *Journal of Computational Physics* **314**: 538-556

Straub, D., Schneider, R., Bismut, E. and Kim, H.-J. (2020). Reliability analysis of deteriorating structural systems. *Structural Safety* **82**: 101877

Sudret, B. (2008). Analytical derivation of the outcrossing rate in time-variant reliability problems. *Structure and Infrastructure Engineering* **4**(5): 353-362

Sudret, B. and Der Kiureghian, A. (2000). *Stochastic Finite Element Methods and Reliability: A State-of-the-Art Report*. UCB/SEMM-2000/08, University of California, Berkley, USA

Tang, W. H. (1973). Probabilistic updating of flaw information. *Journal of Testing and Evaluation* **1**(6): 459-467

Thoft-Christensen, P. and Murotsu, Y. (1986). *Application of Structural Systems Reliability Theory*. Springer-Verlag

Thoft-Christensen, P. and Sørensen, J. D. (1987). Optimal strategy for inspection and repair of structural systems. *Civil Engineering Systems* **4**: 94-100

Thöns, S. (2018). On the Value of Monitoring Information for the Structural Integrity and Risk Management. *Computer-Aided Civil and Infrastructure Engineering* **33**(1): 79-94

Thöns, S. and Döhler, M. (2012). Structural reliability updating with stochastic subspace damage detection information. *5th European Conference on Structural Control (EACS 2012)*, Genoa, Italy

Thöns, S. and Faber, M. H. (2013). Assessing the Value of Structural Health Monitoring. *11th International Conference on Structural Safety & Reliability (ICOSSAR 2013)*, New York, USA

Thöns, S. and Lanata, F. (2013). Risk and Operation Optimised Damage Detection and Inspection Systems. *11th International Conference on Structural Safety & Reliability (ICOSSAR 2013)*, New York, USA

Tierney, L. (1994). Markov chains for exploring posterior distributions. *The Annals of Statistics* **22**(4): 1701-1762

Tran, T.-B., Bastidas-Arteaga, E. and Schoefs, F. (2016). Improved Bayesian network configurations for random variable identification of concrete chlorination models. *Materials and Structures* **49**(11): 4705-4718

Turkstra, C. J. and Madsen, H. O. (1980). Load Combinations in Codified Structural Design *Journal of the Structural Division* **106**(12): 2527-2543

Ultiguide (1999). *Best practice guidelines for use of non-linear methods in documentation of ultimate limit states for jacket type offshore structures*. Det Norske Veritas (DNV), Norway

USFOS (2014). *Ultimate Strength of Framed Offshore Structures*. Version 8-7, USFOS A/S, Norway

Val, D. V., Stewart, M. G. and Melchers, R. E. (2000). Life-Cycle Performance of RC Bridges: Probabilistic Approach. *Computer-Aided Civil and Infrastructure Engineering* **15**(1): 14-25

van Noortwijk, J. M. (2009). A survey of the application of gamma processes in maintenance. *Reliability Engineering & System Safety* **94**(1): 2-21

Visser, W. (2002). *POD/POS curves for non-destructive examination*. Offshore Technology Report 2000/18. Health & Safety Executive (HSE), UK

Vollrath, F. and Tathoff, H. (2002). *Handbuch der Brückeninstandhaltung*. Verlag Bau+Technik, Düsseldorf, Germany [in German].

Vrouwenvelder, A. C. W. M. (2004). Spatial correlation aspects in deterioration models. *2nd International Conference on Lifetime-Oriented Design Concepts*, Bochum, Germany

Vu, K. A. T. and Stewart, M. G. (2000). Structural reliability of concrete bridges including improved chloride-induced corrosion models. *Structural Safety* **22**(4): 313-333

Wang, C., Zhang, H. and Li, Q. (2017). Time-dependent reliability assessment of aging series systems subjected to non-stationary loads. *Structure and Infrastructure Engineering* **13**(12): 1513-1522

Wen, Y. K. and Chen, H.-C. (1987). On fast integration for time variant structural reliability. *Probabilistic Engineering Mechanics* **2**(3): 156-162

Wigderson, A. (2019). *Mathematics and Computation - Ideas Revolutionizing Technology and Science*. Princeton University Press, Princeton, New Jersey

Xiao, Q. and Mahadevan, S. (1994). Fast failure mode identification for ductile structural system reliability. *Structural Safety* **13**(4): 207-226

Ying, L. and Vrouwenvelder, A. C. W. M. (2007). Service life prediction and repair of concrete structures with spatial variability. *Heron* **52**(4)

Zayas, V. A., Mahin, S. A. and Popov, E. P. (1980). *Cyclic inelastic behavior of steel offshore structures*. UCB/EERC-80/27, University of California, Berkley, USA

Zhang, F.-L. and Au, S.-K. (2016). Fundamental two-stage formulation for Bayesian system identification, Part II: Application to ambient vibration data. *Mechanical Systems and Signal Processing* **66–67**: 43-61

Zwirglmaier, K., Papaioannou, I. and Straub, D. (2017). Enhancing sampling based inference in hybrid BNs for reliability assessment. *12th International Conference on Structural Safety & Reliability (ICOSSAR 2017)*, Vienna, Austria

Zwirglmaier, K. and Straub, D. (2016). A discretization procedure for rare events in Bayesian networks. *Reliability Engineering & System Safety* **153**: 96-109

Zwirglmaier, K. M. (2016). *Reliability analysis with Bayesian networks*. PhD thesis, Technische Universität München